



Evaluation of Gusset-less Truss Connection to Aid Bridge Inspection and Condition Assessment

Final Report

Prepared by University of New Hampshire Department of Civil and Environmental Engineering, College of Engineering and Physical Sciences, in cooperation with the U.S. Department of Transportation, Federal Highway Administration

Technical Report Documentation Page

1. Report No. FHWA-NH-RD-26962M		2. Gov. Accession No.	3. Recipient's Catalog No.
4. Title and Subtitle Evaluation of Gusset-less Truss Connection to Aid Bridge Inspection and Condition Assessment		5. Report Date February 2019	
		6. Performing Organization Code	
7. Author(s) Erin S. Bell, Ph.D., P.E., and Ricardo A. Medina, Ph.D., P.E.		8. Performing Organization Report No.	
9. Performing Organization Name and Address University of New Hampshire Department of Civil and Environmental Engineering College of Engineering and Physical Sciences Kingsbury Hall 33 Academic Way Durham, New Hampshire 03824		10. Work Unit No. (TRAIS)	
		11. Contract or Grant No. 26962M, A004(530)	
12. Sponsoring Agency Name and Address New Hampshire Department of Transportation Bureau of Materials & Research Box 483, 5 Hazen Drive Concord, New Hampshire 03302-0483		13. Type of Report and Period Covered FINAL REPORT	
		14. Sponsoring Agency Code	
15. Supplementary Notes Conducted in cooperation with the U.S. DEPARTMENT OF TRANSPORTATION, FEDERAL HIGHWAY ADMINISTRATION			
16. Abstract In 2013, the newly designed Memorial Bridge, located between Portsmouth, NH, and Kittery, ME, was opened to traffic. The structural system of the bridge is composed of truss elements with a unique "gusset-less" connection which utilizes curved steel to transition from the chords to the diagonals where splice plates join the members. In this study, the fatigue performance of the gusset-less connection is primarily investigated through an experimental fatigue test of a scale model of the connection, tested with a pulsating (tension-only) fatigue loading at the UNH Structural Engineering Laboratory. Finite Element Models (FEM) of the connection were developed to assist with the specimen's design and also to validate the testing results. The numerical models were used to estimate maximum stresses in the region of interest near the radiused fillet weld of the connection, determine a suitable scale for the experimental specimens, and inform the design of the experimental setup. A monitoring protocol was developed to systematically monitor the structural response of the test setup. The experimental results showed that the design assumptions were reasonable and that, in the absence of significant defects, the radiused fillet welds in the Memorial Bridge are expected to have infinite fatigue life.			
17. Key Words Gusset, gusset-less, truss, bridge, inspection, condition, weld, finite, element		18. Distribution Statement No Restrictions. This document is available to the public through the National Technical Information Service (NTIS), Springfield, Virginia, 22161.	
19. Security Classif. (of this report) UNCLASSIFIED	20. Security Classif. (of this page) UNCLASSIFIED	21. No. of Pages 171	22. Price

Evaluation of a Gusset-less Truss Connection to Aid Bridge Inspection and Condition Assessment

Erin S. Bell, Ph.D., P.E.

Ricardo A. Medina, Ph.D., P.E.

University of New Hampshire
Department of Civil and Environmental Engineering
College of Engineering and Physical Science
Kingsbury Hall
33 Academic Way
Durham, New Hampshire 03824

DISCLAIMER

This document is disseminated under the sponsorship of the New Hampshire Department of Transportation (NHDOT) and the Federal Highway Administration (FHWA) in the interest of information exchange. It does not constitute a standard, specification, or regulation. The NHDOT and FHWA assume no liability for the use of information contained in this document.

The State of New Hampshire and the Federal Highway Administration do not endorse products, manufacturers, engineering firms, or software. Products, manufacturers, engineering firms, software, and/or proprietary trade names appearing in this report are included only because they are considered essential to the objectives of the document.

Evaluation of Gusset-less Truss Connection to Aid Bridge Inspection and Condition Assessment

Submitted by:

Erin S. Bell, Ph.D., P.E.

Ricardo A. Medina, Ph.D., P.E.

Researchers:

Fernanda Fischer, M.S. Thesis Project

Duncan W. McGeehan, M.S. Thesis Project

Shokoufeh Zargar, Doctoral Candidate

Andrew Lanza, Undergraduate Researcher

January 2019



**University of
New Hampshire**

DEPARTMENT OF CIVIL AND ENVIRONMENTAL ENGINEERING

COLLEGE OF ENGINEERING & PHYSICAL SCIENCES

University of New Hampshire

TABLE OF CONTENT

TABLE OF CONTENT.....	II
LIST OF FIGURES	IV
LIST OF TABLES	VII
EXECUTIVE SUMMARY	VIII
1. INTRODUCTION.....	1
1.1 PROJECT OVERVIEW.....	1
1.2 BACKGROUND INFORMATION AND LITERATURE REVIEW.....	2
1.2.1 INSTRUMENTATION.....	2
1.2.2 TEST MONITORING	3
1.2.3 FINITE ELEMENT MODEL.....	3
1.2.4 FATIGUE.....	4
2. DESIGN AND FABRICATION OF GUSSET-LESS BRIDGE CONNECTION SPECIMENS FOR FATIGUE ASSESSMENT	8
2.1 DESIGN AND ANALYSIS METHODS	8
2.1.1 PRELIMINARY DESIGN CONSIDERATIONS.....	8
2.1.2 SPECIMEN DESIGN AND FABRICATION	9
2.2 SPECIMEN PHOTOS, INSTRUMENTATION PLAN AND FINAL MODEL.....	15
3. DESIGN OF EXPERIMENTAL SETUP FOR FATIGUE TESTING AT THE UNH STRUCTURAL ENGINEERING LABORATORY	19
3.1 DESIGN CONSTRAINTS	19
3.2 EXPERIMENTAL SETUP FOR FATIGUE OF GUSSET-LESS CONNECTION SPECIMEN	21
3.3 ACTUATOR AND MOUNTING BOLTS SPECIFICATIONS.....	23
3.4 ADDITIONAL MODIFICATIONS OF THE TEST SPECIMEN.....	25
3.5 INSTRUMENTATION.....	31
4. FATIGUE TEST MONITORING	35
4.1 FATIGUE TEST MONITORING PROTOCOL	35
4.2 SYSTEM IDENTIFICATION	39
4.3 REPRESENTATIVE MEASUREMENT	44
4.4 SUMMARY	50
5. FINITE ELEMENT MODELING	51
5.1 FINITE ELEMENT MODELING.....	51
5.2 FATIGUE TEST SPECIMEN FINITE ELEMENT MODEL.....	51
5.3 RESULTS FROM THE FINITE ELEMENT MODEL OF THE FATIGUE SPECIMEN AND TEST SETUP	54
5.4 RECOMMENDATION FOR GUSSET-LESS CONNECTION INSPECTION	60
5.5 SUMMARY	60
6. FATIGUE TESTING RESULTS	61

6.1	INTRODUCTION.....	61
6.2	STRAIN GAUGE RESULTS.....	61
6.3	DIGITAL IMAGE CORRELATION DISPLACEMENT MEASUREMENTS.....	68
6.4	MEASUREMENT COMPARISON.....	71
6.5	SUMMARY AND DISCUSSION.....	73
7.	SUMMARY, CONCLUSIONS, AND FUTURE WORK.....	74
7.1	SUMMARY.....	74
7.2	OBSERVATIONS.....	75
7.3	CONCLUSIONS.....	75
7.4	FUTURE WORK.....	76
	REFERENCES.....	77
	APPENDICES.....	A1
	APPENDIX A – SETUP DESIGN CALCULATIONS.....	A2
	APPENDIX B – SHOP DRAWINGS.....	A46
	APPENDIX C – INSTRUMENTATION.....	A54
	APPENDIX D – TEST TRACKING.....	A57
	APPENDIX E – SYSTEM ID.....	A63
	APPENDIX F – FATIGUE RESULTS.....	A70

LIST OF FIGURES

Figure 1 - Gusset-less Connections at the Memorial Bridge, Portsmouth NH.....	1
Figure 2 - Welded Steel S-N Curves [16].....	4
Figure 3 - Sample Fatigue Categories [19].....	5
Figure 4 - Fatigue Mean-Stress Effect [26].....	6
Figure 5 - Goodman Line [27].....	6
Figure 6 - Typical Lower-chord Gusset-less Connection.....	9
Figure 7 - Specimen Geometry.....	10
Figure 8 - Specimen Nomenclature Explanation.....	13
Figure 9 - Graphical Representation of Abaqus® Model.....	13
Figure 10 - Strain Rates for Different Loading Conditions [32].....	14
Figure 11 - Simplified Specimen Shop Drawings.....	14
Figure 12 - Fabricated Specimen of the Gusset-less Connection.....	16
Figure 13 - Memorial Bridge Instrumentation Plan – Lower chord connection [37].....	16
Figure 14 - Instrumentation of North Side of the Scale Model of the Gusset-less Connection ...	17
Figure 15 - Absolute Maximum Principal Stresses.....	17
Figure 16 - Simulated Strain Rate Histories.....	18
Figure 17 - Front view of Green Frame from the University of New Hampshire’s Structural High Bay, Kingsbury S106.....	19
Figure 18 - University of New Hampshire Structural High Bay, Kingsbury S106, Strong Floor Tie-down Hole Pattern with General Dimensions and Location of Experimental Setup.....	20
Figure 19 - MTS Actuator Model 244.41 Drawing [39].....	21
Figure 20 - Reaction Block Options During Fatigue Testing Setup Design Process.....	22
Figure 21 - Fatigue Testing Setup Drawing From South View.....	22
Figure 22 - Structural Supports.....	22
Figure 23 - Assembled Experimental Setup (without concrete poured on the reaction block)	23
Figure 24 - Schematic of the MTS actuator Used for the Fatigue Testing [40].....	23
Figure 25 - MTS Actuator Swivel Operation Specifications [41].....	24
Figure 26 - MTS Recommended Bolts Specification for Actuator Attachment [39].....	25
Figure 27 - Location of Shim Support at Specimen Tip for the Fatigue Test.....	26
Figure 28 - Reaction Block Reinforcement and Reaction Block with Concrete.....	27
Figure 29 - System Components - Overall Test Setup, Reaction Block (a), Bracket Support (b), Specimen (c), and Shim Support (d).....	28
Figure 30 - Cyclic Loading Sample.....	29
Figure 31 - Sample Loading Protocol.....	30
Figure 32 - Loading Schematic.....	30
Figure 33 - Instrumentation of Gusset-less Fatigue Specimen.....	33
Figure 34 - DIC Schematic and Setup for the Fatigue Testing.....	34
Figure 35 - Sample Speckle Pattern.....	35
Figure 36 - Monitoring Protocol Flowchart.....	37
Figure 37 - Shim Support Movement.....	38
Figure 38 - System Identification - DIC Measurement Locations.....	40
Figure 39 - Force Time-History of the Fatigue Specimen Collected on July 24, 2018.....	41
Figure 40 - Force Time-History of the Fatigue Specimen Collected on October 23, 2018.....	41
Figure 41 - DIC and LVDT Verification of the Fatigue Testing Collected on July 24, 2018.....	42

Figure 42 - Reaction Block (Right) - Horizontal Displacement Comparison between July 24, 2018 and October 23, 2018.....	42
Figure 43 - Hysteresis Loop Recorded During Fatigue Testing on June 20, 2018 and July 10, 2018.....	45
Figure 44 - Hysteresis Loop Recorded During Fatigue Testing on July 11, 2018 and July 18, 2018.....	45
Figure 45 - Hysteresis Loop Recorded During Fatigue Testing on July 19, 2018 and August 16, 2018.....	46
Figure 46 - Hysteresis Loop Recorded During Fatigue Testing on August 17, 2018 and October 1, 2018.....	46
Figure 47 - Hysteresis Loop Recorded During Fatigue Testing on October 11, 2018 and October 30, 2018.....	47
Figure 48 - Hysteresis Loop Recorded During Fatigue Testing on June 20, 2018 and June 27, 2018.....	48
Figure 49 - Hysteresis Loop Recorded During Fatigue Testing on June 27, 2018 and July 3, 2018.....	49
Figure 50 - Hysteresis Loop Recorded During Fatigue Testing on July 3, 2018 and July 10, 2018.....	49
Figure 51 - Close up View of Hysteresis Loop Recorded During Fatigue Testing on July 3, 2018 and July 10, 2018.....	50
Figure 52 - Finite Element Model of Experimental Test Setup in Abaqus.....	52
Figure 53 - Meshing of Entire Model in Abaqus.....	54
Figure 54 - Predicted Deflected Shape of the fatigue specimen and test set-up.....	55
Figure 55 - Predicted Specimen Deflected Shape of the Fatigue Specimen.....	55
Figure 56 - Design Stress Contour for the Gusset-less Connection at the Memorial Bridge from HNTB Corporation.....	56
Figure 57 - Predicted Web Max Principal Stress (Absolute) for the Gusset-less Connection at the Memorial Bridge.....	56
Figure 58 - Predicted Specimen Max Principal Stress (Absolute) Under Laboratory Loading Conditions of the Fatigue Specimen.....	57
Figure 59 - Predicted AOI Max Principal Stress (Absolute) Under Laboratory Loading Conditions of the Fatigue Specimen.....	57
Figure 60 - Predicted Specimen Horizontal Strain Under Laboratory Loading Conditions of the Fatigue Specimen.....	58
Figure 61 - Predicted AOI Horizontal Strain Under Laboratory Loading Conditions of the Fatigue Specimen.....	58
Figure 62 - Predicted Specimen Vertical Strain Under Laboratory Loading Conditions of the Fatigue Specimen.....	59
Figure 63 - Predicted AOI Vertical Strain Under Laboratory Loading Conditions of the Fatigue Specimen.....	59
Figure 64 - Horizontal Strain Pattern Along Weld Toe.....	62
Figure 65 - Horizontal Strain Pattern Recorded Away from Weld Toe from the Fatigue Specimen on October 30, 2018.....	63
Figure 66 - Horizontal Strain Recorded at the Web of Both Faces of the Fatigue Specimen on October 30, 2018.....	64

Figure 67 - Horizontal Strain Comparison Recorded from the Fatigue Specimen on July 17, 2018, August 29, 2018 and October 30, 2018	65
Figure 68 - Vertical Strain Comparison Recorded from the Fatigue Specimen on July 17, 2018, August 29, 2018 and October 30, 2018.	65
Figure 69 - Analysis Area of Interest – DIC on the Fatigue Specimen	69
Figure 70 - Horizontal Displacement Contour Recorded Via Digital Image Correlation During Fatigue Testing.....	70
Figure 71 - StrainResponse Recorded Via Digital Image Correlation at Locations Shown in Figure 72 from the Fatigue Specimen	70
Figure 72 - Locations of Recorded Digital Image Correlation Data	71
Figure 73 - Strain Rosette Data Sheet.....	A54
Figure 74 - Uniaxial Strain Gauge Data Sheet [40].....	A55
Figure 75 - DIC Correlation [41].....	A56
Figure 76 - Lagrange Strain Equations [42]	A56
Figure 77 - Test Tracking Data Sheet - Front.....	A61
Figure 78 - Test Tracking Data Sheet - Back	A62
Figure 79 - Horizontal Displacements - All Locations.....	A63
Figure 80 - Reaction Block Right - Vertical Displacement.....	A63
Figure 81 - Reaction Block Right - Horizontal Displacement.....	A64
Figure 82 - Reaction Block Left - Horizontal Displacement.....	A64
Figure 83 - Reaction Block Left - Vertical Displacement	A65
Figure 84 - Actuator - Horizontal Displacement	A65
Figure 85 - Actuator Tip - Horizontal Displacement.....	A66
Figure 86 - Actuator - Vertical Displacement.....	A66
Figure 87 - Specimen Tip - Horizontal Displacement.....	A67
Figure 88 - Actuator Tip - Vertical Displacement	A67
Figure 89 - Bracket - Vertical Displacement	A68
Figure 90 - Specimen Tip - Vertical Displacement	A68
Figure 91 - Bracket - Horizontal Displacement.....	A69
Figure 92 - NRW1 - Vertical	A70
Figure 93 - NRW1 - Horizontal.....	A70
Figure 94 - NRW1 - Diagonal	A71
Figure 95 - NRW2 - Horizontal.....	A71
Figure 96 - NRW2 - Vertical	A72
Figure 97 - NRW2 - Diagonal	A72
Figure 98 - NRW3 - Vertical	A73
Figure 99 - NRW3 – Horizontal	A73
Figure 100 - NRW3 – Diagonal.....	A74
Figure 101 - NRW4 - Horizontal.....	A74
Figure 102 - NRW4 - Vertical	A75
Figure 103 - NRW4 - Diagonal	A75
Figure 104 - NRW5 - Horizontal.....	A76
Figure 105 - NRW5 - Vertical	A76
Figure 106 - NRW5 - Diagonal	A77

LIST OF TABLES

Table 1 - Scaling Options	11
Table 2 - Summary of Main Differences and Similarities of Prototype and Model.....	11
Table 3 - Summary of Models Created in Abaqus®	12
Table 4 - Fatigue Specimen System Identification Comparison from July 24, 2018 and October 23, 2018.....	43
Table 5 - NRW1 – Test Interval Comparison.....	66
Table 6 - NRW2 - Test Interval Comparison.....	66
Table 7 - NRW3 - Test Interval Comparison.....	67
Table 8 - NRW4 - Test Interval Comparison.....	67
Table 9 - NRW5 - Test Interval Comparison.....	68
Table 10 - Structural Response Comparison between Digital Image Correlation and Strain Gauge Measurements	71
Table 11 - Structural Response Comparison between Strain Gauge Measurements and Model Predictions.....	72
Table 12 - Structural Response Comparison between Digital Image Correlation and Model Predictions.....	73
Table 13 - Test Tracking History.....	A57

Executive Summary

In 2013, the newly designed Memorial Bridge, located between Portsmouth, NH, and Kittery, ME, was opened to traffic. The structural system of the bridge is composed of truss elements with a unique “gusset-less” connection which utilizes curved steel to transition from the chords to the diagonals where splice plates join the members. With such a unique connection, it is important to verify the design assumptions and assess its performance. In this study, the fatigue performance of the gusset-less connection is primarily investigated through an experimental fatigue test of a scale model of the connection. More specifically, the focus of this study is on the fatigue performance of the radiused fillet weld at a typical bottom chord gusset-less connection. To successfully accomplish this goal, two identically scaled versions of the gusset-less connection were designed and fabricated. These specimens were tested with a pulsating (tension-only) fatigue loading at the UNH Structural Engineering Laboratory. Finite Element Models (FEM) of the connection were developed to assist with the specimen’s design and also validate the testing results. The numerical models were used to estimate maximum stresses in the region of interest near the radiused fillet weld of the connection, determine a suitable scale for the experimental specimens, and inform the design of the experimental setup.

In a high-cycle fatigue test, it is critical to ensure that consistency is maintained across all testing periods. This is especially challenging when the test setup is not standardized, and the laboratory infrastructure is limited. In this work, a monitoring protocol was developed to systematically monitor the structural response of the test setup. Using this protocol, for a total of 1,600,000 fatigue load cycles, the average difference in structural response was found to be limited by 5%. Adopting the most conservative assumptions, using a hot-spot stress of 14 ksi at the toe of the weld, the AASHTO S-N curve, and a category C fatigue detail, experimental results showed that the design assumptions were reasonable. Therefore, in the absence of significant defects, the radiused fillet welds in the Memorial Bridge are indeed expected to have infinite fatigue life.

The presented work benefited from the collaboration of other interested parties, which provided valuable input during the design, fabrication and construction of the specimen and experimental setup. These parties include the New Hampshire Department of Transportation (NHDOT), which were the project sponsors, and HNTB Corporation, which were responsible for the design of the bridge.

Research Goals and Activities

The overall objective of this research is to evaluate the fatigue performance of the gusset-less truss connection. In this report, work in support of this evaluation is presented. The focus of this report is on the experimental fatigue testing, which is used to evaluate the fatigue life prediction of the gusset-less connection. Additionally, documentation is provided for a test monitoring protocol that was developed to ensure consistency across testing periods. The layout of this report is presented below;

Chapter 1 – Introduction; This chapter provides background information on the project, an overview of the objectives of this work, and a summary of relevant literature.

Chapter 2 – Design and Fabrication of Gusset-Less Bridge Connection Specimens for Fatigue Assessment; This chapter describes the design process and fabrication of the specimen.

Chapter 3 – Design of Experimental Setup for Fatigue Testing at the UNH Structural Engineering Laboratory; This chapter introduces the experimental fatigue testing, specifically the physical test setup, the loading protocol and the instrumentation plan for the fatigue test.

Chapter 4 – Fatigue Test Monitoring; This chapter discusses the importance, and the development, of a monitoring protocol for high-cycle fatigue testing performed across multiple testing intervals.

Chapter 5 – Finite Element Monitoring; This chapter discusses the use of finite element modeling as a tool for understanding and evaluating the fatigue test specimen and setup.

Chapter 6 – Fatigue Testing Results; This chapter introduces the results of the fatigue testing and the implications of those results.

Chapter 7 – Summary, Conclusions, and Future Work; This chapter presents an overall summary of the work, including conclusions, and future work for this project.

In addition to these chapters, this report includes six appendices;

- A. Setup design and calculations
- B. Shop drawings of the specimen
- C. Instrumentation – Strain gauge data sheets, DIC background and additional info
- D. Fatigue Test Tracking – Data sheets from testing
- E. System ID – Additional plots from system IDs
- F. Additional fatigue test results

Goals and Outcomes

- Create two specimen pairs (A and B) of a scale model of a gusset-less connection from the Memorial Bridge. Specimen pair A will be tested to failure in a quasi-static testing protocol and Specimen pair B will be tested for fatigue performance. **Completed.**
- Conduct quasi-static set of tests on each member of Specimen pair A to determine stress distribution in the connection and failure mode. **Removed from this project as determined at the March 28th, 2017 NHDOT-UNH Technical Advisory Group meeting.**
- Evaluate these results in conjunction with field collected data and analytical models that are the work product of a complimentary FHWA-AID DEMO project to: (i) further understand and quantify the structural performance of the gusset-less connection, and (ii) validate analytical models. **Data collected from the October 2017 load test was used to validate the numerical model of the gusset-less connection.**
- Conduct fatigue testing on Specimen pair B and collect performance data to determine the stress pattern and predict fatigue failure mode. **Not completed due to delays and challenges associated with testing Specimen A. The information gained during the testing of Specimen A, including the impact of residual stresses and weld defects, will be included in the testing of Specimen B during the proposed Phase 2.**
- Compare the findings of this project with the FHWA guideline for connection assessment to facilitate the development of an evaluation protocol for inspection and structural condition assessment. **The fatigue design category C was used to design the fatigue testing and the fatigue testing results show that this selection was conservative. The fatigue testing of Specimen A was used to validate the structural model, along with field collected data from the Memorial Bridge. This structural model predicts the hot spot stress locations for focus during bridge visual inspection.**

It should be noted that at the completion of this project, fatigue testing on Specimen B was not completed due to delays and challenges associated with testing Specimen A. The information gained during the testing of Specimen A, including the impact of residual stresses and weld defects, will be included in the testing of Specimen B during the proposed Phase 2.

Project Tasks and Activities

Task 1: Literature Review and Finalize Testing Plan

A comprehensive literature review on connection load rating and fatigue assessment will be performed to inform the development of the final testing plan. The research team will work with NHDOT to finalize the testing plan and the specimen sizes to be evaluated in this project.

Activities: Detail the importance of the fatigue assessment of the gusset-less connection (Chapter 1)

Task-2: Design and Construction of Small-scale Physical Models

Small-scale physical models of a gusset-less truss connection (four specimens or two pairs: A and B) will be designed, detailed, and constructed for laboratory testing under quasi-static and fatigue (cyclic) loading at the UNH structural laboratory. The connection type will be modeled after an instrumented gusset-less truss connection of the Memorial Bridge. Half of the specimens will be used for quasi-static testing and the other half for fatigue testing. Specimens will be designed to cover two bend ratios (i.e., one bend ratio per specimen pair) in order to have both quasi-static and a fatigue testing for each bend ratio. One bend ratio will correspond to the bend ratio of the Memorial Bridge connection. Specimen sizes will be consistent with the largest possible scale model to be accommodated at the UNH structural laboratory.

Activities: Design and construction of small-scale physical models (Chapters 2 and 3 Appendices A to C). Develop analytical models of small-scale physical specimens (Chapter 5).

Task-3: Analytical Models of Small-scale Physical Specimens

Modify the physics-based analytical models of the gusset-less truss connection developed as part of the NSF-funded Living Bridge Project to reflect the small-scale physical models constructed in Task 2. These analytical models will be used to design the laboratory experiments to quantify the structural behavior and performance of the connection. This design process will incorporate the estimation of the distribution of loading demands on the connection as well as the characterization of appropriate boundary conditions for testing.

Activities: Develop analytical models of small-scale physical specimens (Chapter 5).

Task 4: Validation of Structural Connection Analytical Model

Validate the structural connection model with available field data and laboratory data obtained in Task 4. Special attention will be placed on the implementation of appropriate structural similitude and scaling laws to effectively utilize both field and laboratory data. Use the validated structural model to design the set of fatigue tests by estimating appropriate traffic-induced stress/load levels and number of cycles to represent representative demands experienced by the Memorial Bridge connection. Provide an interim report and presentation to the State on project results.

Activities: Validate structural connection analytical model (Chapter 5).

Task-5: Fatigue Testing

Use digital image correlation, photoelastic coatings, and strain gauges to measure and visualize the stress distribution across the connection, specifically in the heat-affected zone of the welds during the fatigue experiments. Bridge inspectors will be invited to view and examine the connection before and at a maximum of three different stages during the fatigue tests.

Activities: Fatigue Testing (Chapters 4 and 6 and Appendices D to F).

Task-7: Data Analysis and Interpretation of Laboratory Testing

Experimental data will be analyzed to identify structural parameters and visual indicators of reduced structural performance. Then, statistical analysis of the data collected from field data together with quasi-static and fatigue testing will be used to identify, with a higher degree of confidence, the significant factors that impact structural performance and prediction of remaining service life.

Activities: Data analysis and interpretation of laboratory testing (Chapter 5 and Appendices D to F).

Task-8: Evaluation Protocol for Inspection and Condition Assessment

The research team will develop an evaluation protocol for inspection and structural condition assessment for gusset-less connections. Once the evaluation protocol is designed for the Memorial Bridge connection, a general procedure will be implemented to develop similar protocols for other future innovative structural elements using the results from Tasks 2 through 7. In addition, the team will also develop a foundational information for load rating of the gusset-less connection of the Memorial Bridge.

Activities: Evaluation protocol for inspection and condition assessment (Chapter 5 and Appendix D).

Task-9: Final Report and Presentation

A final report and a presentation will be prepared to the State. Videos and images from each test useful for bridge inspection and condition assessment will be available to the State as part of the final project report.

1. INTRODUCTION

This chapter provides background information on the project. An overview of the project objective and background information on fatigue testing, measurement methods used, fatigue test monitoring, Finite Element Modeling (FEM), as well as a literature review are included.

1.1 Project Overview

The Memorial Bridge spans the Piscataqua River between Portsmouth, NH, and Kittery, ME. The original Memorial Bridge was in operation since 1923, when it was originally opened to traffic, making it over 89 years old when it was officially closed in 2012 due to structural deficiencies. The original design was a vertical lift bridge utilizing a traditional steel truss structural system, where the center span of the three-span bridge was the vertical lift span. In 2013, the new Memorial Bridge, designed by HNTB Corp., was opened to traffic. The new bridge utilized a similar design with a lift-span in the center and a steel truss structural system. One of the major changes was the innovate connection designed for the members of the truss system.

In most bridges that use a steel truss structural system, the connections between the members are made using gusset plates. When using gusset plate connections, there are multiple structural members framing into one joint, where the gusset plates are bolted and/or welded to each side of the members. Although widely used and studied, the gusset plate connections have a few major drawbacks, such as the following;

- Gusset plates make inspections more difficult. Specifically, the plates will cover the structural members that are being connected.
- The members framing into the connection location cause stress concentrations.

On the new Memorial Bridge, these issues are mitigated through the use of a “gusset-less” truss connection, shown in Figure 1.



Figure 1 - Gusset-less Connections at the Memorial Bridge, Portsmouth NH

This connection aims to have a smooth transition of forces from the diagonal truss members to the top and bottom chords of the truss system. This is accomplished using cold-bent steel flanges and a unique geometric approach. Since connections are incorporated into the chords of the bridge, the diagonal members are connected individually using bolted splice plates. Some of the main benefits of using this connection are as follows [1];

- Reduction in number of bolts needed on the bridge, compared to a traditional gusseted connection.
- The connections are much easier to inspect than a gusseted connection since nothing is shrouded behind a large plate.
- The spliced connections can be partially replaced while the bridge is under load.

Although this connection has many benefits, it has not been as widely used or studied as a traditional gusseted connection. One aim of this research is to investigate the structural performance of this connection through laboratory testing. More specifically, the aim of the overall study is to evaluate the fatigue performance of the gusset-less truss connection. In addition to the structural performance, it is important to understand the connection and the critical locations for inspections. The overall project also intends to use the laboratory data to aid in the development of an inspection protocol for the Memorial Bridge.

1.2 Background Information and Literature Review

In order to achieve the goals of this project, a literature review was needed to provide background information on the work to be performed. In this literature review, there are five main topics investigated; instrumentation, test monitoring, finite element modeling, and fatigue. The background information needed for this study is provided in the following sub-sections.

1.2.1 Instrumentation

Structural performance prediction of innovative connection details requires both advanced design tools and analysis models that are verified through experimental data. For most civil structures field or full-scale tests to failure are not feasible, therefore scale-model laboratory experiments are critical to advancing the state-of-the-art for structural design. Scale-model laboratory experiments must be carefully designed to provide information on specific structural behaviors. In order to isolate the target behavior, all behaviors, including influences of boundary conditions and members interactions, must be controlled and accurately accounted for in the associated structural models.

Characterization of the structural response of a laboratory experiment can be challenging depending on multiple factors including the experimental objectives, specimen geometry, available laboratory resources and infrastructure, experimental setup, and loading conditions. These factors will have a large influence on the selection of what type of measurements can be made and the method used to obtain those measurements. The typical types of measurements used to characterize a structure are the displacement, the strain, the acceleration, or any combination thereof, in the directions of interest. Obtaining these measurements is not always a trivial task depending on the experiment and the level of characterization desired. Therefore, it is important to choose the appropriate measurement method that will provide the best characterization of the system to achieve the goals of the experiments. The measurement methods used in this study include: 2-Dimensional Digital Image Correlation (DIC), strain gauges (uniaxial and rosettes), and

Linear Variable Differential Transformers (LVDTs). Each of these measurement methods are used to characterize a specific behavior in the system and create redundancy in data collection.

Resistance based strain gauges have been used extensively to measure the strain response of civil engineering structures. The gauges work by forming a circuit in which there is a known electrical resistance, and as the specimen is deformed, the gauge is also deformed, and a change in resistance is induced. Based on the gauge geometry and the circuit, this change in resistance results in a change in voltage, which is converted to a strain measurement [2]. In a fatigue test, it is important to ensure that the gauge is not susceptible to failure due to repeated loadings [3].

LVDTs have also been used extensively [4] to measure the displacement response of civil engineering structures. The LVDTs work by associating the position of the LVDT core with a signal value. As the position of the core changes, the magnitude and sign of the signal changes, allowing the LVDT to measure the magnitude and direction of the displaced core [5].

Finally, 2-D DIC has also been used frequently and has been gaining popularity as imaging technology has advanced. Generally, in civil engineering applications, DIC is used to measure full-field surface displacements and strains. This is accomplished by identifying and tracking the movement of groups of pixels, through a series of digital images, captured via a speckle pattern on the area of interest. Using a correlation algorithm, as the specimen is deformed, the translation vectors for each pixel grouping are calculated and the movement is computed relative to the location of the pixel groupings of an undeformed reference image [6].

1.2.2 Test Monitoring

The instrumentation generally serves the purpose of measuring the structural response of the test specimen, but in specialized testing fixtures, it is important to understand the behavior and influence of the different components of the entire test setup. Since the consistency, reliability, and performance of the experiment are vital, it is important to monitor the response to ensure the behavior is as expected using a systematic approach. Research has been performed on characterization of structural systems and the interaction between experimental and numerical models considering field conditions and errors [7-9].

1.2.3 Finite Element Model

In civil engineering applications, finite element models (FEMs) are often used as an analytical tool to aid in design as well as the analysis of local and global behavior of engineering structures. The key to using a FEM as a tool in engineering is understanding the assumptions that go into the analysis being performed and being able to distinguish between a good estimation and a bad estimation of reality in terms of results. This requires experience and engineering judgement when creating the FEM as well as interpreting the results.

Often FE modeling is an iterative process in which models are created and refined until reasonable results are obtained. Within these iterations, adjustments are made in the form of element type, element geometry, load applications and boundary conditions, to name a few. One of the most common sources of variation in FEM results is the mesh used, in terms of geometry and type [10]. In most software, there are a wide variety of element types to choose from depending on the model geometry. Some of the common elements used are beam elements (1-D), quadrilateral or triangular (2-D), and tetrahedral or hexahedral (3-D) [11]. In addition to the element-type, the size of the elements is of great importance. Many previous research studies [10, 12, 13] have shown that the

size of the elements have a large impact on the accuracy and resolution of the analysis. Unfortunately, as the element size decreases, more elements are required for a model of the same size, and with more elements the computations become much more time consuming. For this reason, it is important to refine a mesh, typically through a sensitivity analysis, until any further changes in mesh size do not greatly influence the results. The ideal mesh will minimize computation time while maximizing the accuracy in the model. As previously mentioned, the acceptance of the model is dependent on experience and engineering judgement, so great care must be taken to ensure that the model is representative of reality.

1.2.4 Fatigue

Fatigue, in terms of engineering materials, is the degradation of material due to repeated loading and unloading. The cyclic loading causes cumulative damage in the material which causes microscopic cracks to form and propagate. Fatigue failures occur when these microscopic cracks reach a critical size and then they propagate very quickly [14]. The fatigue life of a structural component is generally defined as the number of cycles, with an applied stress range, before the crack reaches this critical size.

In most cases fatigue can be categorized as high-cycle or low-cycle fatigue. High-cycle fatigue is characterized by a low applied stress range and results in a high number of load cycles to failure, typically greater than 10^5 cycles [15]. Low-cycle fatigue is the opposite, with a high applied stress range which results in a low number of load cycles to failure [14]. This relationship between cycles to failure and the applied stress range is typically documented in terms of an S-N curve [14]. The S-N curves use a log-log scale with the y-axis showing the applied stress range and the x-axis showing the expected cycles to failure. A sample high-cycle fatigue S-N curve for welded steel fatigue details is shown in Figure 2 [16].

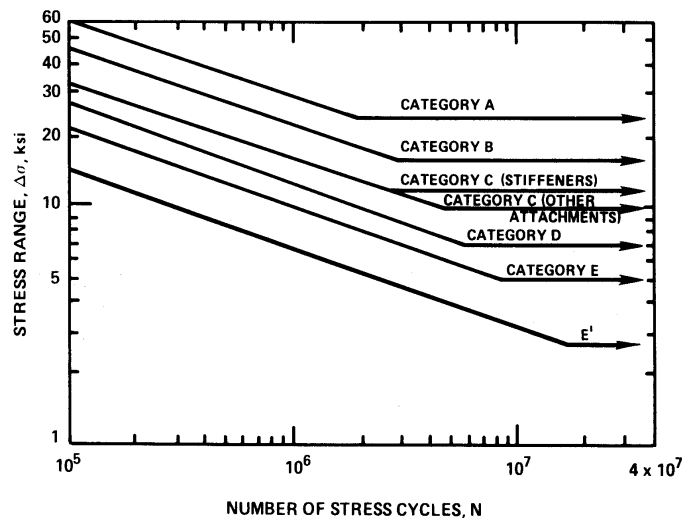


Figure 2 - Welded Steel S-N Curves [16]

As Figure 2 shows, there are two distinct portions of the S-N curve. The first portion shows the relationship between the applied stress and the expected cycles to failure, but at a certain threshold the slope flattens, and the cycles to failure increase indefinitely. This threshold is commonly referred to as the endurance limit and it signifies the maximum applied stress range at which fatigue

failure would not occur. This means that any applied stress equal to or lower than the endurance limit will not result in any fatigue damage [14]. These relationships are derived experimentally with many inputs such as material, geometry, and loading conditions. These inputs are the most influential factors in terms of fatigue performance and for this reason, S-N curves exist for many different materials and geometries.

The fatigue performance of welded structures has been studied extensively [17-19]. From these previous studies typical welded steel details have been categorized according to loading and geometry, and S-N curves have been developed to characterize the fatigue performance. Figure 3 is a schematic defining the fatigue categories shown based on the geometry and loading [19]. Some of the important issues to note about these experimentally derived relationships are that the test was performed and nominal stress were measured and used, the loading was a fully-reversed loading, and the residual stresses were not measured, but were assumed to be the same for each weld configuration [20].

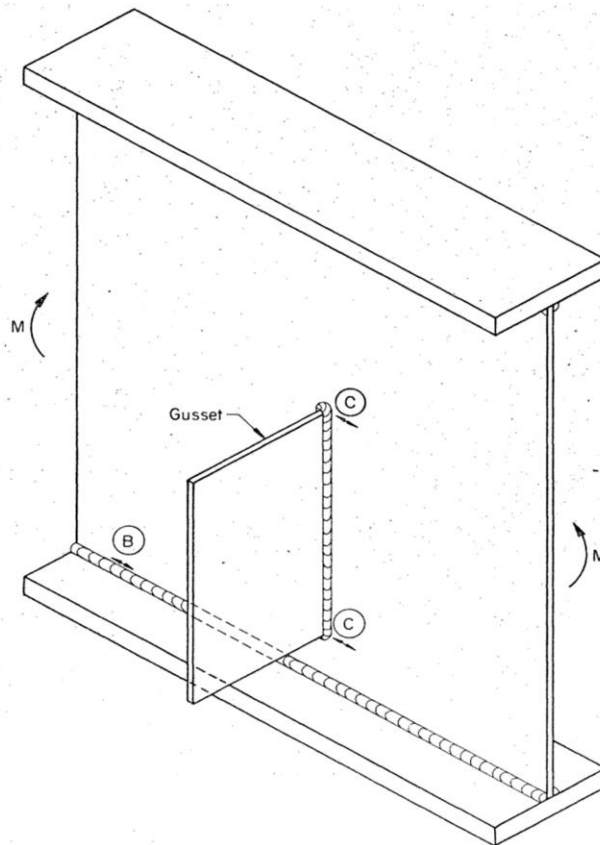


Figure 3 - Sample Fatigue Categories [19]

Nominal stress refers to the stress at some distance from the weld, but that distance is not explicitly defined. This stress is essentially the stress close to the weld without any effect from local concentrations due to the weld geometry or a notch [21]. Another approach that can be used is the structural stress, or hot-spot stress. This is a method in which stresses are measured close to the weld and extrapolated to incorporate the stress concentration effect of the weld geometry [21].

In terms of loading there are a few variables which have a large impact on the fatigue performance. The most influential factor is the applied stress range, in which the higher the applied stress range, the lower the expected cycles to failure. Another important variable that has more of a secondary effect is the mean applied stress. Generally, there are two common loading scenarios for a fatigue test; a fully-reversed loading or a pulsating-tensile loading. The fully-reversed case is when the cyclic stress range is centered about zero stress, meaning that the specimen experiences an equal magnitude of compressive and tensile stresses. The pulsating-tensile loading is when the cyclic stress range is limited to tensile stress only, meaning that the mean stress is tensile, and the specimen is never loaded in compression. The effect of mean-stress has been studied extensively [22-25], to summarize, a tensile mean-stress is detrimental to fatigue performance and a compressive mean-stress is beneficial. The theoretical relationship is shown graphically in Figure 4 [26], where S_m is the mean stress.

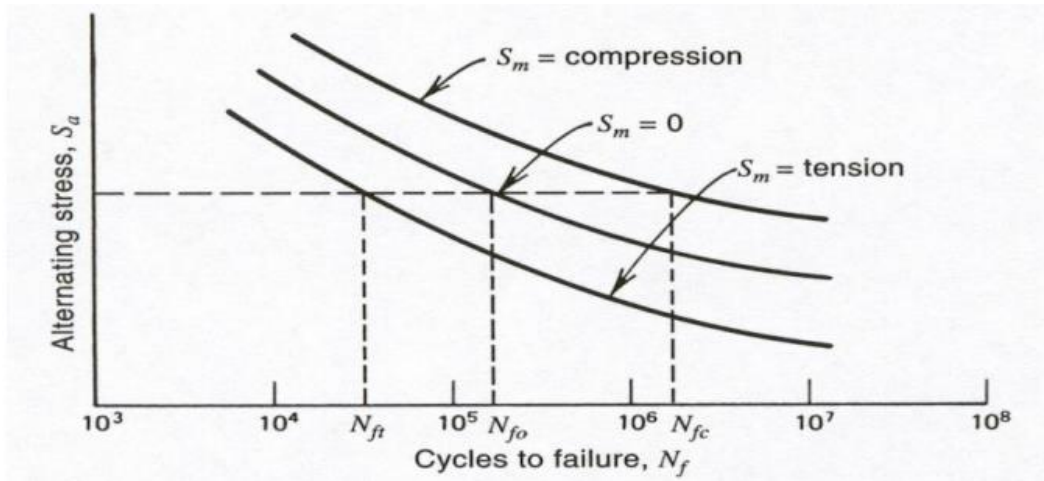


Figure 4 - Fatigue Mean-Stress Effect [26]

Methods have been developed to convert the different types of tests to the fully reversed case in order to compare the results to standardized S-N curves. The most commonly used relationship is the Goodman line shown in Figure 5 [27]. This line uses a combination of alternating stress (σ_a), along the y-axis, and mean-stress (σ_m) along the x-axis to identify an equivalent alternating stress (σ'_e) that would provide the same fatigue life, in terms of cycles, when the mean stress is zero.

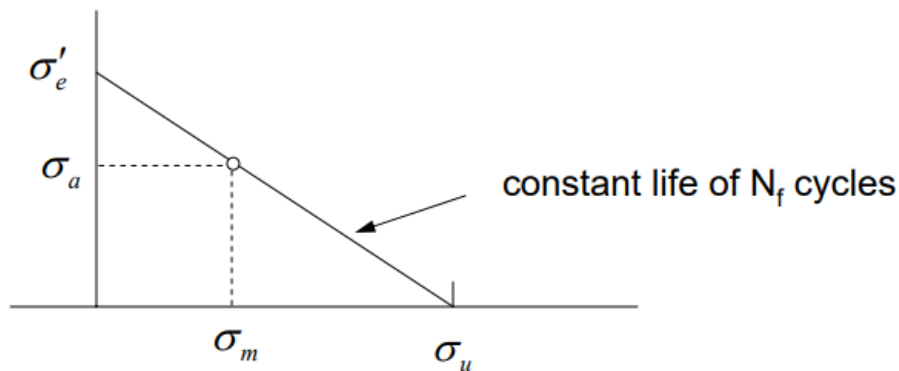


Figure 5 - Goodman Line [27]

In addition to the mean-stress effect, the residual stress state of the specimen will have a secondary effect on the fatigue performance. The behavior is similar to the mean-stress effect where tensile stresses are detrimental and compressive stresses are beneficial to fatigue performance [28]. Often times the residual stresses are not accounted for in civil engineering applications but their effects are assumed to be implicitly included in S-N curves for design.

2. DESIGN AND FABRICATION OF GUSSET-LESS BRIDGE CONNECTION SPECIMENS FOR FATIGUE ASSESSMENT

The gusset-less truss connection, used in place of typical gusseted connection on the previously mentioned Memorial Bridge, has a unique geometry which incorporates prominent bends in the steel to create a transition from the chord to the diagonals. In addition to this, the connection has large, multiple-pass welds connecting the flanges to the web. In the design of this connection, the critical fatigue location was identified as the curved weld of the gusset-less connection on the bottom chord of the bridge. Additionally, this area was assumed by the designer to be a category C weld fatigue detail.

This chapter will discuss the design of the scale gusset-less truss connection fatigue specimen, with the limitation of the structural laboratory as a main design constraint.

2.1 Design and Analysis Methods

This section documents preliminary design considerations and main decisions made during the design and fabrication of the specimens to be tested, including the use of a finite element (FE) model and similitude scaling.

2.1.1 Preliminary Design Considerations

Under ideal conditions, any experiment aimed at characterizing the response of a prototype should be representative of the geometry and properties of the prototype as well as the field conditions it is exposed to. However, the reality is that laboratory conditions provide significant limitations and compromises need to be made when designing and fabricating specimens and test setups able to provide valuable information on the field performance of the prototype. Focusing on the main goal of this study and considering test limitations, this experimental program was designed with the primary objective of comparing the magnitude and distribution of stresses under the curved flange to those obtained from a FE analysis of the connection. The minimum target stress level used for specimen design was 10 ksi: the stress range corresponding to the endurance limit of a Category C weld. If the specimen does not fail, stress ranges can be further increased until failure is imminent. This requires a cyclic loading protocol with increasing amplitudes.

The test limitations include the availability of a single fatigue-rated actuator and its loading capacity. Moreover, the load can only be applied in a unidirectional manner, which means that the load will only act on a single plane as opposed to the loading conditions experienced by the connection in the field where loads are applied from four different members (Figure 6). Also, the possibility of using a loading ram, which would keep a constant established force at the specimen, was studied. This option was rejected because it would increase the costs of the setup. In order to address these limitations, FE models were developed in Abaqus® [29] to determine the most appropriate geometry and sizes for the specimens. Similitude scaling was used due to the inability to design and fabricate specimens whose sizes were identical to those of the prototype given laboratory loading and boundary condition constraints.

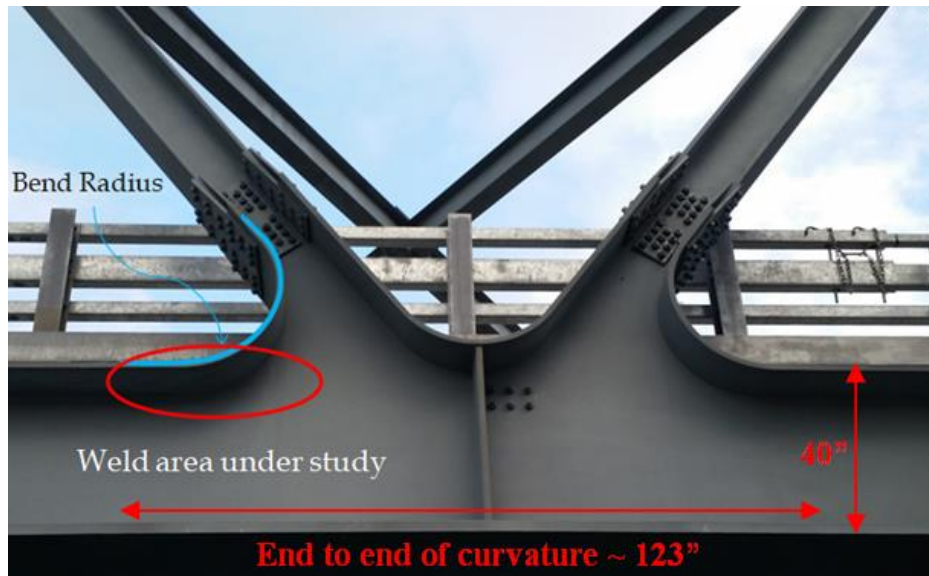


Figure 6 - Typical Lower-chord Gusset-less Connection

2.1.2 Specimen Design and Fabrication

The process of designing and fabricating the specimen required careful consideration of the goals and needs of the bridge owner, who is the project sponsor, which includes understanding the behavior of the gusset-less connection when fatigue load is applied, specifically at the radiused fillet weld area. Moreover, the project sponsor is interested in developing an inspection protocol for maintenance of the gusset-less connection. Another interest is from the designers, who have been serving as project consultants along the way, which also consist of analyzing the behavior of the weld and implementation of the gusset-less connections in future bridges.

Thus, the research team and representatives of the NHDOT participated in several technical advisory group meetings throughout this project to report on progress and solicit input, as well as conference calls and meetings with HNTB Corporation, the bridge designers and CANAM Bridges, INC, the bridge fabricators. The purpose of meeting with all interested parties was to incorporate as much input as possible into the design and fabrication of specimens to not only fulfill the needs of the project sponsor but to provide information useful for the potential application of the gusset-less connection design into future bridge designs. This interaction proved to be critical to determine the general geometry and size of the specimen, the influence of the weld size, and consideration of residual stresses. This latter issue is outside of the scope of this report.

2.1.2.1 *Specimen Geometry*

The main challenge with designing a test specimen for the gusset-less connection is determining its geometry and size. Preference was giving to fabricating a “full-scale” specimen. In many instances, “full-scale” is considered as a specimen with a geometric scaling of at least 50%. The Memorial Bridge has different dimensions for its top and bottom chord connections; therefore, the first decision was to determine which connection to evaluate. Because the focus of this study is fatigue performance, the fatigue limit state is deemed to be a more critical issue for connection elements along the bottom chord of the truss bridge, due to the tensile loading at the bottom chord. If a crack initiates, it tends to propagate during tensile loading, while a compressive loading tends

to close a crack. Hence, a typical bottom chord connection was selected as the prototype connection to be tested (Figure 6).

In order to maximize the specimen size in the laboratory, given the properties of the connection, a decision was made to take advantage of symmetry and design a specimen that was only half of the prototype connection (Figure 7). FE analysis of the specimen demonstrated that the full height of the web of the bottom chord was not needed to represent the target magnitude and distribution of the stresses close to the radiused fillet weld in the region of interest. Therefore, the height of the web was reduced to $2/3$ of its original size (Figure 7). In the FE analysis, the load from a single actuator was applied on the bottom chord parallel to its longitudinal axis, as explained in the following sections.

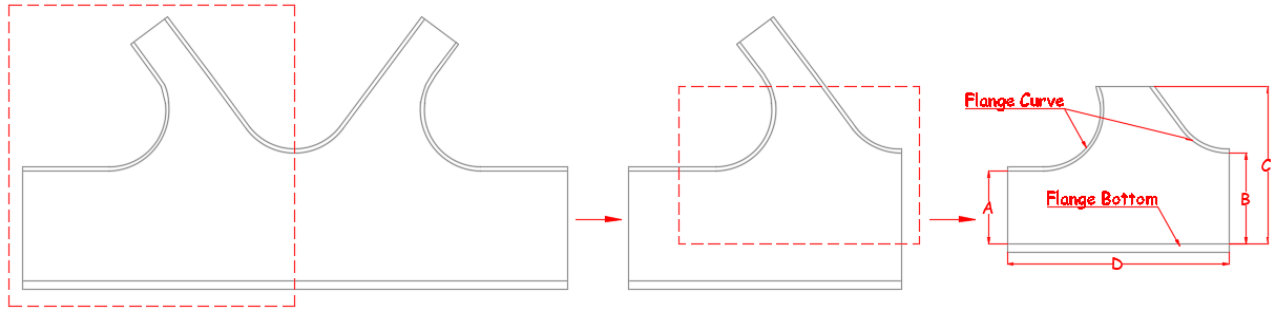


Figure 7 - Specimen Geometry

2.1.2.2 Similitude Scaling

The scaling process was conducted considering a desired maximum load to be applied to the specimen equal to 90 kips, which is about 81% of the load capacity of the fatigue-rated actuator (110 kips) that is available for this test. Similitude scaling was used based on scaling two basic parameters: length and load [30]. The focus on length and load was warranted because the specimens were fabricated with the same material used to fabricate the prototype (ASTM A709 Grade 50) using an identical fabrication process. Applying the similitude method, where S_L is the geometric scale factor for length, S_A is the scale factor for area, S_F is the scale factor for force, and S_s is the scale factor for stress; the following equations are used:

$$S_A = S_L^2 \quad (1)$$

When the stress is kept constant between the model and prototype, which is the case herein,

$$S_F = S_A * S_s = S_L^2 \quad (2)$$

Therefore,

$$\sqrt{S_F} = S_L \quad (3)$$

Hence, the ratio of the force, F , in the prototype (p) to the force in the model or specimen (m), as well as the ratio of the length, L , of the prototype (p) to length of the model or specimen (m) is given by:

$$\sqrt{\frac{F_p}{F_m}} = L_p / L_m \quad (4)$$

Equation 4 was used to generate the values depicted in Table 1, which shows the various iterations involved to determine the final specimen scale. For each iteration presented in this table, the basic

criterion was to obtain a stress distribution in the region of interest consistent with the target stress distribution, as detailed in section FE Modeling of the Specimen. The dimensions shown in the table are described in Figure 7.

Table 1 - Scaling Options

Scale	Fm/Fp	Force Prototype (kips)	Force Model (kips)	Overall dimension								t_web and t_flange_curve		t_flange_bottom		w_flange_curve		w_flange_bottom		welds	
				A		B		C		D		Exact	Rounded	Exact	Rounded	Exact	Rounded	Exact	Rounded	Exact	Rounded
				Exact	Rounded*	Exact	Rounded	Exact	Rounded	Exact	Rounded										
1.000	1.000	90	90	23.960	24.000	29.960	30.000	52.310	52.250	73.370	73.375	1.250	1.250	2.750	2.750	26.000	26.000	36.000	36.000	0.625	0.625
1.059	0.944	90	85	23.285	23.250	29.116	29.125	50.836	50.875	71.303	71.250	1.215	1.250	2.673	2.625	25.267	25.250	34.986	35.000	0.607	0.625
1.125	0.889	90	80	22.590	22.625	28.247	28.250	49.318	49.375	69.174	69.125	1.179	1.125	2.593	2.625	24.513	24.500	33.941	34.000	0.589	0.625
1.200	0.833	90	75	21.872	21.875	27.350	27.375	47.752	47.750	66.977	67.000	1.141	1.125	2.510	2.500	23.735	23.750	32.863	32.875	0.571	0.625
1.286	0.778	90	70	21.131	21.125	26.422	26.375	46.133	46.125	64.706	64.750	1.102	1.125	2.425	2.375	22.930	22.875	31.749	31.750	0.551	0.500
1.385	0.722	90	65	20.362	20.375	25.461	25.500	44.455	44.500	62.353	62.375	1.062	1.000	2.337	2.375	22.096	22.125	30.594	30.625	0.531	0.500
1.500	0.667	90	60	19.563	19.625	24.462	24.500	42.711	42.750	59.906	59.875	1.021	1.000	2.245	2.250	21.229	21.250	29.394	29.375	0.510	0.500
1.636	0.611	90	55	18.730	18.750	23.421	23.375	40.893	40.875	57.356	57.375	0.977	1.000	2.150	2.125	20.325	20.375	28.142	28.125	0.489	0.500
1.800	0.556	90	50	17.859	17.875	22.331	22.375	38.990	39.000	54.687	54.625	0.932	0.875	2.050	2.000	19.379	19.375	26.833	26.875	0.466	0.500
2.000	0.500	90	45	16.942	17.000	21.185	21.125	36.989	37.000	51.880	51.875	0.884	0.875	1.945	2.000	18.385	18.375	25.456	25.500	0.442	0.500
2.250	0.444	90	40	15.973	16.000	19.973	20.000	34.873	34.875	48.913	48.875	0.833	0.875	1.833	1.875	17.333	17.375	24.000	24.000	0.417	0.375
2.571	0.389	90	35	14.942	15.000	18.683	18.625	32.621	32.625	45.754	45.750	0.780	0.750	1.715	1.750	16.214	16.250	22.450	22.500	0.390	0.375
3.000	0.333	90	30	13.833	13.875	17.297	17.250	30.201	30.250	42.360	42.375	0.722	0.750	1.588	1.625	15.011	15.000	20.785	20.750	0.361	0.375

t= thickness
w= width
units in inches
*rounded to the nearest 1/8"

Based on the information summarized in Table 1, the row corresponding to the selected scale is highlighted and equal to a force scaling of 1:2.571. This scaling is equivalent to a geometric scale factor of 1:1.62, which implies that the specimen has geometric dimensions that are equal to 62% of the dimensions of the prototype connection. During the scaling process, adjustments were made to preserve the dimension of the bend radius, $16t$, which is an important characteristic of the gusset-less connection. This issue is particularly relevant because the focus of the experimental setup is on the fatigue performance of the radiused fillet welds. In addition, it is important to note that the welds at the gusset-less bridge connections are $5/8$ " fillet welds, while on the specimen, due to scaling, the weld size was set to $3/8$ ". Table 2 depicts the main differences and similarities between the gusset-less connection (prototype) and the specimen (model).

Table 2 - Summary of Main Differences and Similarities of Prototype and Model

Differences		Similarities
Prototype	Model	Same for both
Flange and web thicknesses		Fabrication company Cold-bent steel process Material Welding process (submerged arc weld) Weld type (fillet weld) Bend radius - $16t$
1 1/4"	→ 3/4"	
Fillet weld		
5/8"	→ 3/8"	
Weld passes		
4 or 5	→ 2	
Coating		
Metalized	→ Sandblasted	

2.1.2.3 Finite Element Modeling of Specimen

Several models were created in Abaqus® to aid and inform the specimen and the experimental test setup design process. The most important parameters considered include: (i) the specimen geometry and boundaries conditions and (ii) the most appropriate loading location to reproduce the stress distribution provided in the calculations from HNTB Corporation [31] when the prototype connection was exposed to the critical fatigue limit state load combination. Table 3 was

developed as a summary of the various models created as part of this study. The groups were established based on the geometry of the specimen model, within each group, load location, condition, magnitude and boundaries conditions change.

Table 3 - Summary of Models Created in Abaqus®

Group	Model Name	Model Size	Load Condition	Load Location	Load Magnitude (kips)	Boundaries Conditions			Max Stress Location	Max Stress Magnitude (ksi)	Reason for Rejection		
						Right Specimen	Left Specimen	Diagonal					
1	1.1	Full	Diagonal Y+	Centroid	30	Fixed	Free	Free	Top of left curve	2.85	Stress distribution not as desired		
	1.2		Diagonal Y-						Under right curve	2.85			
	1.3		Bottom Chord X-						Free	Under left curve	0.35	Compression in the diagonal	
	1.4										Fixed		0.35
	1.5										Pinned		0.35
	1.6										Free		1.18
2	2.1	Full	Bottom Chord X-	Centroid	30	Fixed	Free	Fixed	Under left curve	0.36	Increases the size of the specimen, similar results from Group 1		
3	3.1	Full	Bottom Chord X-	Centroid	50	Fixed	Free	Free	Under left curve	0.69	Compression in the diagonal		
4	4.1	Full	Bottom Chord X-	Centroid	100	Fixed	Free	Free	Under left curve	1.75	Magnitude of stresses are too small compared to allowable stresses		
	4.2			Eccentricity +0.5"						1.88			
	4.3			Eccentricity +1.5"						2.16			
	4.4			Eccentricity +2.5"						2.43			
	4.5									2.56			
	4.6									2.58	Negligible difference from model 4.5		
	4.7			Eccentricity +3.0"	2.55					Same model as 4.6 with a 0.2" mesh. Negligible difference.			
	4.8				2.48					Same model as 4.6 with a 0.5" mesh. Negligible difference.			
	4.9				2.23					Magnitude of stresses are too small compared to allowable stresses			
	4.10			Eccentricity +6.0"	2.94								
	4.11			Eccentricity +10.0"	3.88								
	4.12			Eccentricity +14.0"	4.82								
5	5.1	Full	Bottom Chord X-	Centroid	100	Fixed	Free	Free	Under left curve	2.12	The height of the fixed end is bigger compared to models of Group 4, requiring a bigger support		
	5.2			Eccentricity +3.0"						3.90			
	5.3			Eccentricity +5.0"						5.08			
6	6.1	Scale	Bottom Chord X-	Centroid	35	Fixed	Free	Free	Under left curve	1.56	Size of the actuator would not fit at that height location		
	6.2			Eccentricity +8.875"						2.91	Magnitude of stresses are small compared to the target magnitude		
	6.3			Eccentricity +11.625"						4.02			
	6.4									5.14			
	6.5									7.34			
	6.6									10.27			
	6.7			Eccentricity +14.375"	90					13.21	Magnitude of stresses are close to the target, but the model still needs refinement, add plate as part of the setup		
	6.8				100					14.67			
	6.9			Distributed load at the vertical plate, simulating the actuator area (equivalent to +14.375" eccentricity)	90					15.34	Plate is ok, it needs the welds		
	6.10									14.06	Welds are ok, need more appropriate loading location, at holes at the plate		
	6.11			Distributed load at the nut area (equivalent to +14.375" eccentricity)						Weld in the vertical plate	24.92	Maximum stress are not at the curve, it needs to model the actuator	
	6.12			Distributed load at the nut area (equivalent to +14.375" eccentricity)						Under left curve	14.14	Magnitude of stresses are close to the target, but can still be increased	
	6.13			Distributed load at the nut area (equivalent to +17.125" eccentricity)							18.9	FINAL MODEL	

Figure 8 explains the nomenclature used in Table 3. The first models were developed with the full size of the connection (Groups 1 to 5), with different geometries. It was immediately evident that significant scaling would have to take place to achieve the desired stress levels given the 90 kips load limit set for the actuator. Several iterations took place until a model with the final dimensions highlighted in Table 1 was generated. An important decision was to apply the load on the bottom chord section of the specimen, parallel to the longitudinal axis of the bottom chord but above the centroid of the cross-section. An eccentricity was necessary to induce the target levels of stress in the region of interest. In addition, the actual bottom chord of a Memorial Bridge truss experiences both axial loads and strong-axis bending. Thus, the equivalent axial load in the elements would act with an eccentricity with respect to the centroidal axis of the bottom-chord elements.

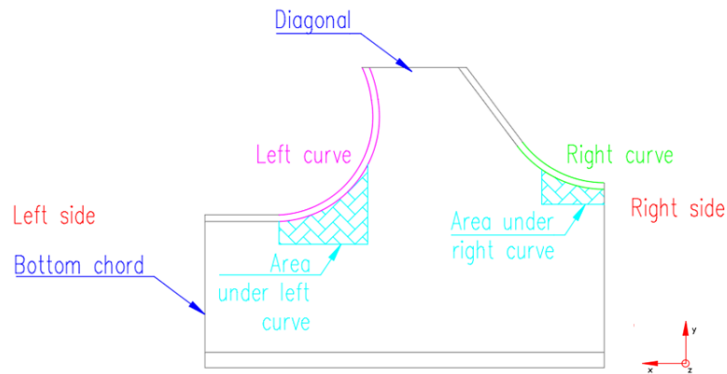


Figure 8 - Specimen Nomenclature Explanation

The sensitivity of the stress magnitude and distribution to the boundary conditions of the specimens was also evaluated. The final decision was to assign a fixed support to one side of the specimen and a free end at the location where the load is applied (Figure 9).

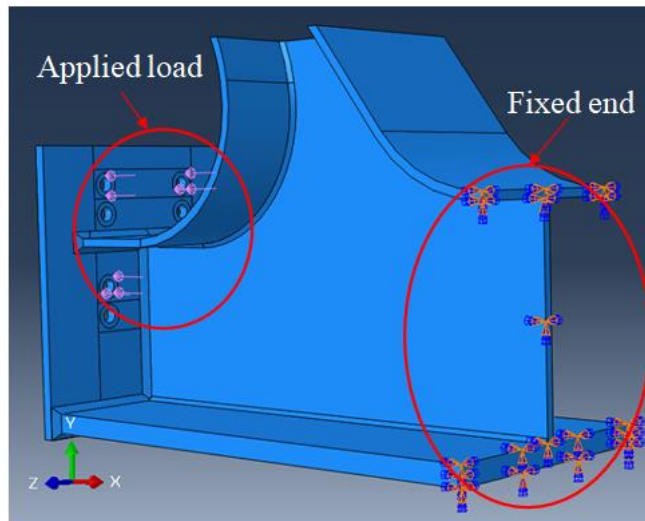


Figure 9 - Graphical Representation of Abaqus® Model

In Abaqus®, the fixed end is visually represented by individual points, but, the entire surface of the element is fixed. Subsequently, the Abaqus® model was further refined by explicitly modeling the welds and an end plate, as part of the setup, to be used to transfer more uniformly the load from

the actuator to the specimen cross-section so that the load transfer is closer to reality (model 6.11). Furthermore, the sensitivity of the stress distribution to the mesh size was also investigated. The basic element type chosen for this application was a linear hexahedral element, called C3D8R in Abaqus®. This type of element has eight nodes and three translational degrees of freedom per node.

Another important parameter in the model was the type of constraint enforced between element surfaces (e.g., weld-to-flange or weld-to-web regions). For instance, tie constraints [29] were used. The FE model was also used to determine the frequency of the applied load during the fatigue test in order to induce strain rates (change in strain with respect to time) that were consistent with a static test. Figure 10 shows that the strain rate for static test of steel specimens ranges approximately from 10^{-5} to 10^{-2} (s^{-1}). Therefore, the model was also run with different loading frequencies and the strain rate was calculated at various locations in the region of interest.

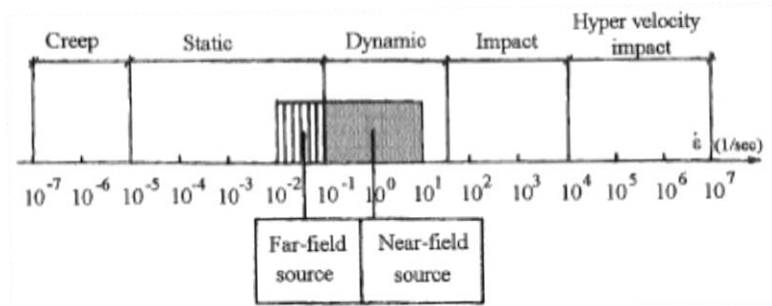


Figure 10 - Strain Rates for Different Loading Conditions [32]

2.1.2.4 Specimen Fabrication

Simplified fabrication drawings for the specimens are shown in Figure 11. The fabrication process was done by the CANAM Bridge Corporation, who fabricated the gusset-less connections for the Memorial Bridge. The same material and fabrication process were used for the specimens, including the welds along the curved region of the connection. Important characteristics associated with the bridge fabrication process were replicated for the specimen fabrication.

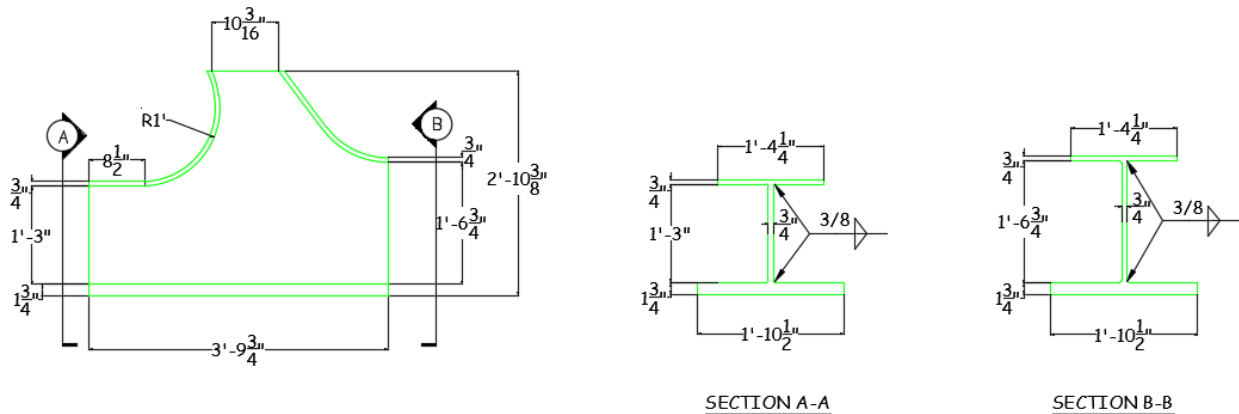


Figure 11 - Simplified Specimen Shop Drawings

The Memorial Bridge connections incorporate cold-bent steel. This manufacturing process is based on bending the steel at ambient temperature, which is different from the most common method, hot-rolled steel, where high temperatures are needed to shape the different steel components [33]. Secondly, welding techniques were developed for the prototype gusset-less connections to make an automatic weld under the curvature. This technique involves using a tracker with wheels with a magnetic base, doing the submerged arc welding while keeping a constant speed at all parts of the connection. The objective was to create a smooth and uniform weld.

The first difference between the gusset-less connection specimen and its prototype is its coating. In the Memorial Bridge, the connection is metalized [34] while the test specimen was only sandblasted because it is easier to prepare the uncoated surface for instrumentation placement. It should be noted that in the Memorial Bridge, the metalizing is applied at a temperature that is not expected to affect metallurgical properties. A second difference relates to the size of the electrode used in the welding process because of differences in the fillet weld size between the specimen and the prototype, i.e., $\frac{3}{8}$ " and $\frac{5}{8}$ ", respectively. The number of weld passes is different from the connection to the specimen; four or five passes were necessary for a $\frac{5}{8}$ " weld in the prototype while only two passes were needed for the $\frac{3}{8}$ " fillet weld in the specimen. Hence, the micro structure of the weld could reasonably be expected to behave differently. However, when conducting fatigue assessment to replicate the behavior of the prototype, there are many other influential variables to be considered when scaling is performed such as, the influence of the heat affected zone (HAZ) due to the thickness of the plate, the heat input during welding, the potential presence of weld defects, among others. All the aforementioned variables should be given due consideration when conducting the fatigue assessment using the experimental setup designed as part of this work. For instance, studies have shown that given the same material and weld size, when the number of passes is increased, the HAZ (measured from the surface at the end of the weld to the heat-affected area) also increases [35]. In addition, there might be additional micro structural differences in the weld, which should also be evaluated.

In consultation with the NHDOT, keeping the weld size as close as possible to that of the prototype while maintaining the same geometric scaling for the various steel plates was deemed to be important criteria. The most important specimen design criterion was keeping the bend radius the same as the one in the prototype: $16t$. Moreover, the welding process was performed as closely as possible to the one used in the Memorial Bridge connections. For fillet welds, visual inspection was performed to check that the weld did not have defects or imperfections. The same weld inspection process was performed as that of the prototype connection. Moreover, the same welding specialist responsible for the connection at the Memorial Bridge was also assigned to the welding procedure of each of the two specimens fabricated.

2.2 Specimen Photos, Instrumentation Plan and Final Model

This section illustrates the final characteristics of the fabricated specimens, including a description of the initial instrumentation plan. In addition, sample model results for static loading conditions are also presented.

Figure 12 shows the first specimen to be tested. The dimensions shown in Figure 12 include the width of the transfer plate (between the actuator connector-swivel and the specimen) as part of the setup.

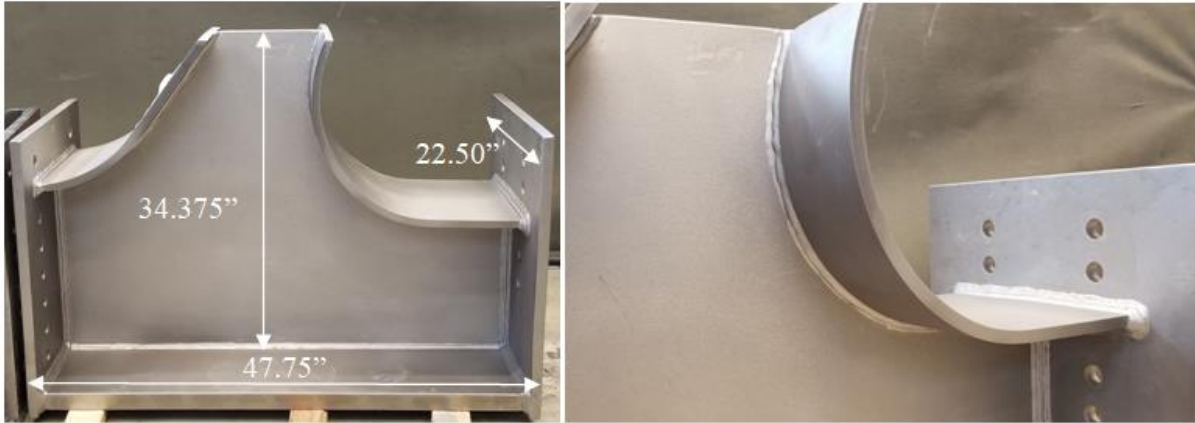


Figure 12 - Fabricated Specimen of the Gusset-less Connection

At the stage shown in Figure 12, the specimen was available for surface preparation and installation of the instrumentation. The instrumentation plan to evaluate the fatigue performance of the radiused fillet welds includes the use of uniaxial strain gauges, strain rosettes, and non-contact measurements (digital image correlation). The location of the gauges was decided based on two criteria: (i) FE model results, focusing on the ones approximately 1” close to the weld along the curved region of the connection, and (ii) the placement of gauges at selected connections in the Memorial Bridge. The bridge is physically instrumented with strain rosettes and accelerometers (Figure 13). Field data, experimental data using the setup developed in this study, and data from numerical simulations can be combined to develop a protocol to assess the condition and predict the remaining life of the gusset-less truss connections used at the Memorial Bridge [36].

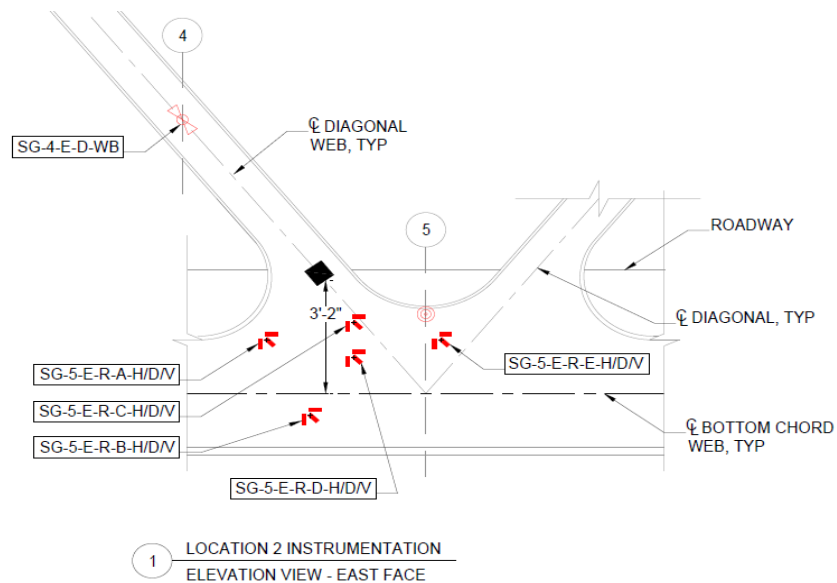


Figure 13 - Memorial Bridge Instrumentation Plan – Lower chord connection [37]

Since the goal of the test is the fatigue evaluation of the radiused fillet weld, strain rosettes were also added at the bottom of the flange, in alignment with the strain rosette on the web, so that additional information about the weld, and its surrounding region, can be collected. Figure 14

shows the location of gauges for one side of the specimen at the web, and, a photo of the strain rosettes after installation.

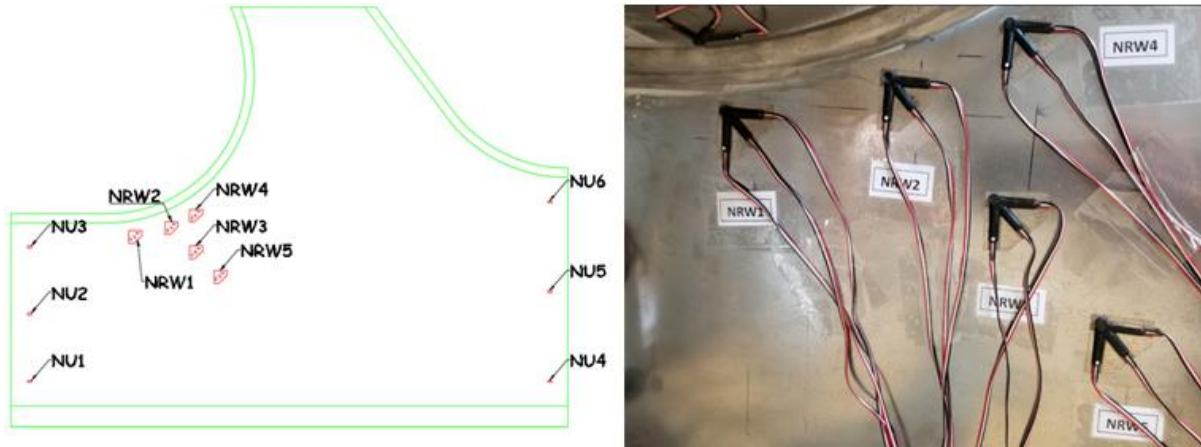


Figure 14 - Instrumentation of North Side of the Scale Model of the Gusset-less Connection

In addition, close to the ends of the specimen, uniaxial strain gauges were placed in order to gather more information about load transfer. The collection of data to better understand and characterize the behavior of the supports and their associated degrees of restraint is particularly important. Additional gauges were placed on the other side (south side) of the specimen to verify the loading symmetry, provide additional measurement redundancy, and approximately estimate the influence of three-dimensional effects. Figure 15 presents the absolute maximum principal stress contours when 90 kips is applied in tension to the final specimen design and the actuator is positioned at its highest location. Therefore, the maximum location of principal stresses is near the radiused fillet weld closer to the point of load application, as desired, with an estimated magnitude of 18.9 ksi. The numerical model used in this study was later updated by other members of the research team due to an error in modeling constraints between the vertical plate and the actuator. This issue was found to be local, as it only affected the stress magnitude and distribution on the vertical plate and not on the rest of the numerical model.

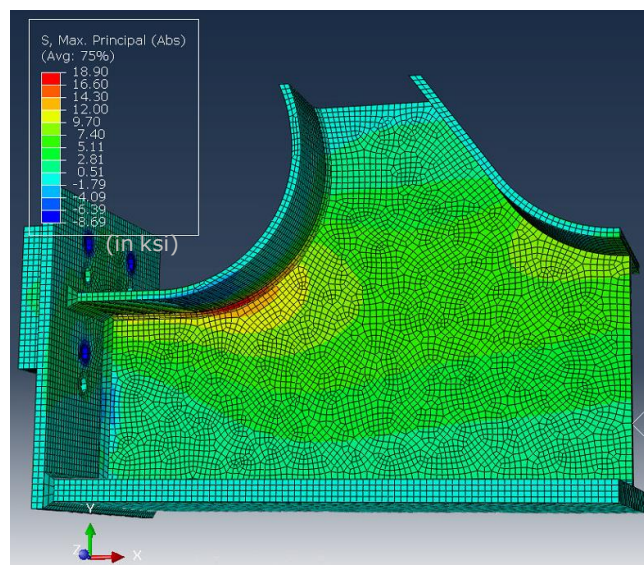


Figure 15 - Absolute Maximum Principal Stresses

In order to determine the frequency of load application for the fatigue test, the strain rate was analyzed as described in section 2.1.2.3 FE Modeling of Specimen. Figure 16 shows the strain rate plots from the most stressed element according to the model, which is located close to the radiused fillet weld in the region of interest, when a maximum load of 110 kips in tension is applied to the model. The data is for loading rates of 2 and 4 Hz, respectively, with a total duration of one second.

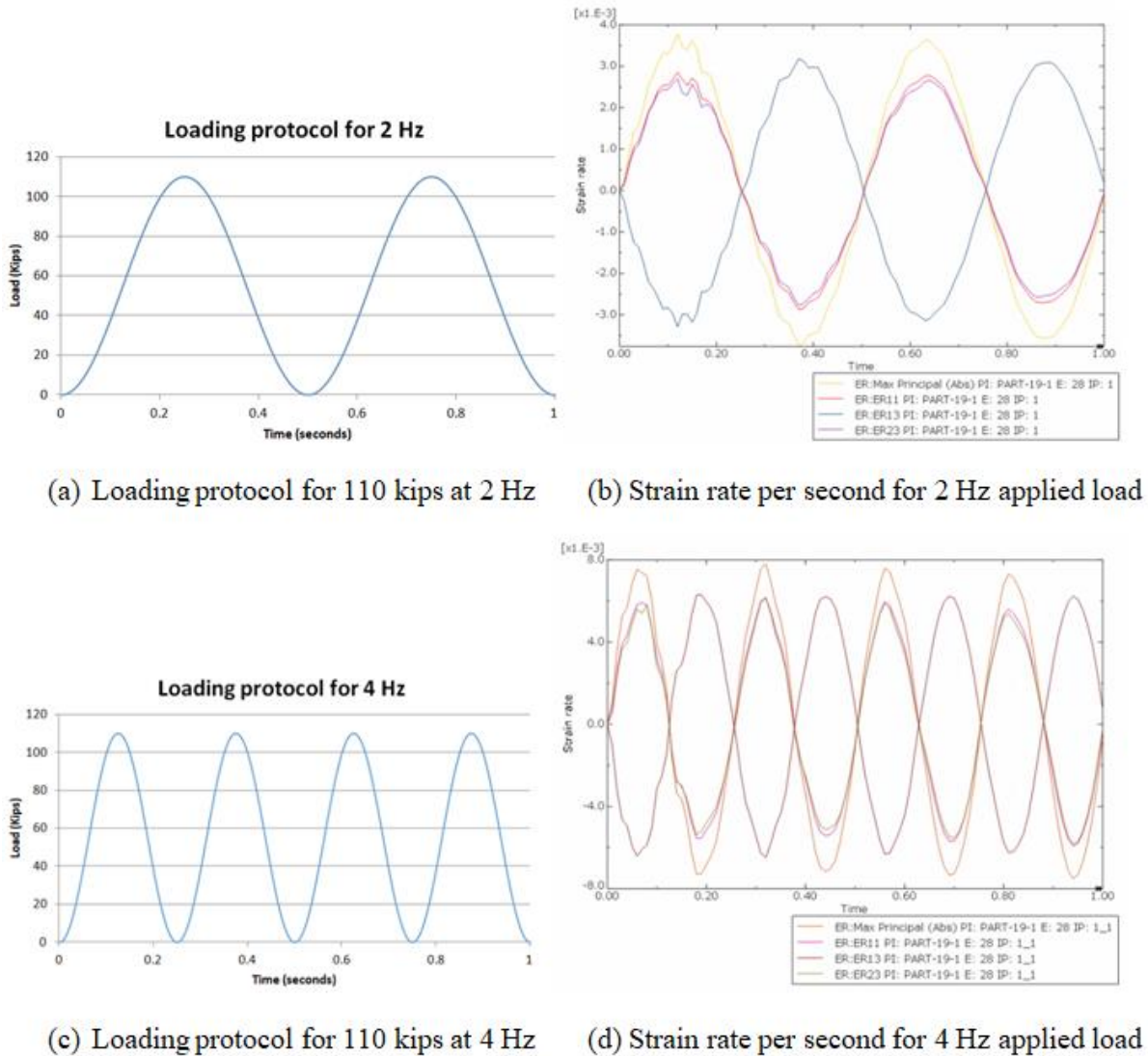


Figure 16 - Simulated Strain Rate Histories

In order to minimize the total test duration (by increasing the frequency), and still keeping static test conditions, a loading frequency of 3.5 Hz was selected for the fatigue testing. This frequency was chosen based on the results from Figure 16, where 2 Hz approximately achieved 4×10^{-3} strain per second, and 4 Hz, almost 8×10^{-3} strain per second. Based on the literature (Figure 10), for a static test, the strain rate should be between 10^{-5} and 10^{-2} s^{-1} . Thus, 4 Hz would still be appropriate for this loading configuration, but to add more conservatism, a frequency rate of 3.5 Hz was selected.

3. DESIGN OF EXPERIMENTAL SETUP FOR FATIGUE TESTING AT THE UNH STRUCTURAL ENGINEERING LABORATORY

This chapter deals with a description of the design of the experimental setup for fatigue testing at the UNH Structural Engineering Laboratory (“High Bay”). The basic experimental setup design objective is to build a robust and reliable system that would allow (i) the application of the required fatigue loading to the gusset-less connection specimen while (ii) maintaining the structural integrity of all other components of the system (i.e., specimen supports, support attachments, and hydraulic actuator). Detailed calculations relevant to the information discussed in this chapter are provided in Appendix A.

3.1 Design Constraints

The UNH Structural Laboratory has a variety of testing capabilities but for this unique, large-scale, fatigue test some additional infrastructure was needed. The most relevant design constraints were related to the current infrastructure in the High Bay, located at S106, Kingsbury Hall, UNH, Durham, NH. An evaluation of existing capabilities was conducted to determine the most appropriate path forward. For instance, two alternatives were considered. First, the potential use of the UNH Structural Testing Frame (“Green Frame”) to provide support to the actuator as part of the fatigue-testing setup was evaluated. This structure consists of a frame designed to apply vertical loads to specimens. Figure 17 shows a schematic of the Green Frame that shows the minimum height for which the fully retracted actuator used as part of this study could be attached.

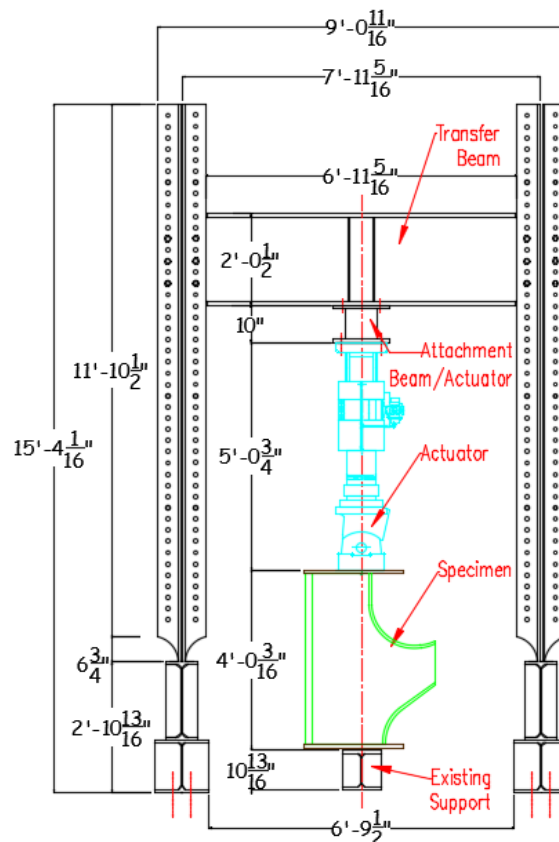


Figure 17 - Front view of Green Frame from the University of New Hampshire’s Structural High Bay, Kingsbury S106

The main concern with the current setup was the possibility of transferring a horizontal force to the loading beam when it is located at a height at least equal to the one shown in Figure 17. Nganyi Imbembe, as part of his semester project report for CEE 995 – Experimental Structural Dynamics (Spring 2017) [38], evaluated the feasibility of using the Green Frame to conduct the fatigue testing of the gusset-less connection specimen given geometric and loading constraints. Imbembe concluded that the Green Frame was not sufficiently rigid both in plane and out of plane to safely transfer the required loading to the strong floor. He proposed a re-design of the frame, which resulted to be at this point financially prohibitive.

Given the limitations associated with the Green Frame and the fact that the High Bay does not have an alternative system (e.g., a reaction wall), there was a need to design a complete system that would fulfil the objectives of the fatigue testing. Therefore, the second setup design alternative required the design of components anchored to the strong floor in which every single component had to be designed and fabricated. Some of the major constraints associated with this second alternative included the size of the specimen and actuator, the hole pattern of the strong floor, and the pullout capacity of the anchors. The High Bay strong floor consists of a reinforced concrete slab 48” thick with anchor holes, which are composed of steel threads where threaded rods can be placed and fixed with a nut. The strong-floor hole pattern is shown in Figure 18.

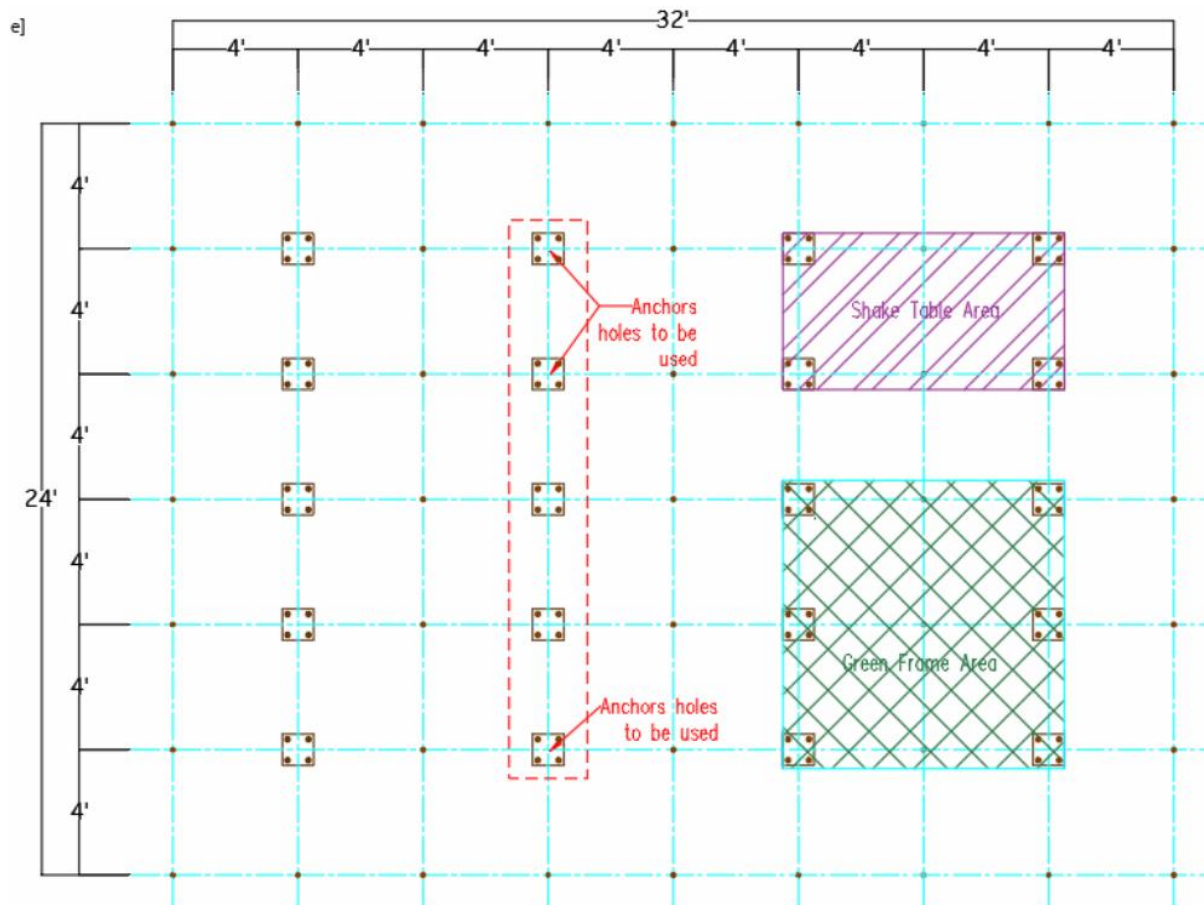


Figure 18 - University of New Hampshire Structural High Bay, Kingsbury S106, Strong Floor Tie-down Hole Pattern with General Dimensions and Location of Experimental Setup

A study was performed to design supports for both the specimen and the actuator. Given the geometric constraints associated with the size of the specimen, the actuator, and the hole pattern, it was determined that one support would engage four anchor points, and the other one eight (see Figure 18). Other configurations were evaluated, including placing the setup diagonally instead of parallel or orthogonally to the girder formed by the anchor holes used. It was concluded that given the aforementioned constraints, the most efficient placement of components (i.e., to maximize the number of anchor points while minimizing fabrication costs) was the one shown in Figure 18.

Another constraint was the characteristics of the anchors at the strong floor. These were designed primarily for pullout resistance and not necessarily for shear (or tension-shear interaction). A final geometric constraint was the hole pattern of the actuator pedestal. The influence of this constraint is specifically discussed in the next section.

3.2 Experimental Setup for Fatigue of Gusset-less Connection Specimen

The main goal was to design an experimental setup system capable of supporting the specimen on one side and the actuator on the other. The actuator would be positioned horizontally (i.e., parallel to the strong floor), attached to the specimen at the swivel end and as close as possible to the strong floor. The first option evaluated was to create two identical reinforced-concrete reaction blocks (one at the end of the specimen and another one at the base of the actuator), which was not feasible due to the holes pattern on the strong floor (see Figure 18). Therefore, the second option included a steel bracket to support the specimen and a reaction block to support the actuator, which are shown later in this section.

Both the steel bracket and the reaction block need to resist and to be able to safely transfer to the anchors a load of 90 kips (maximum load planned for the test) in tension. On the actuator side, the area of load application is smaller because it is equal to the area of the pedestal of the actuator, which is held by four bolts (see Figure 19). On the specimen side, the forces could be distributed throughout a larger area and hence more bolts could be used. Therefore, the support structure on the actuator side (reaction block) at the point of load application needed to be stiffer than on the specimen side.

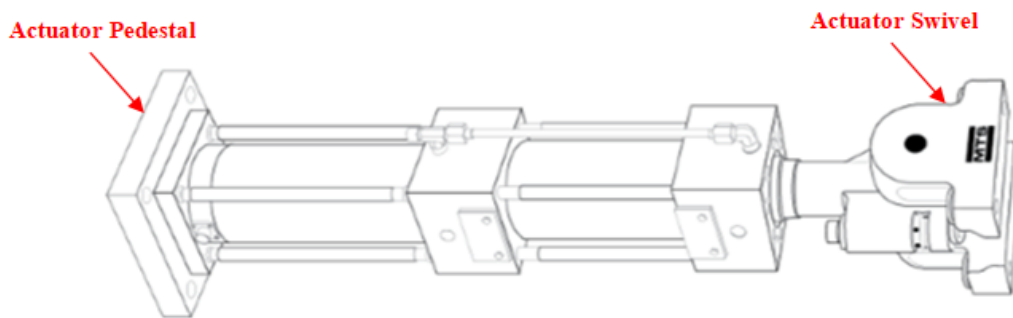


Figure 19 - MTS Actuator Model 244.41 Drawing [39]

The reinforced-concrete reaction block was designed to include threaded rods for the anchors (vertical direction) and for the actuator (horizontal direction) as shown in Figure 20a. The main issue with this option was that, given the strong floor hole pattern and the location of the holes in the actuator's pedestal, enough space was unavailable to prevent threaded rods from interfering with one another. Alternative designs were evaluated, as shown in Figure 20b, in which the

actuator would be attached to a thick steel plate that could be embedded into the reinforced concrete block. This option was also discarded because of cost considerations.

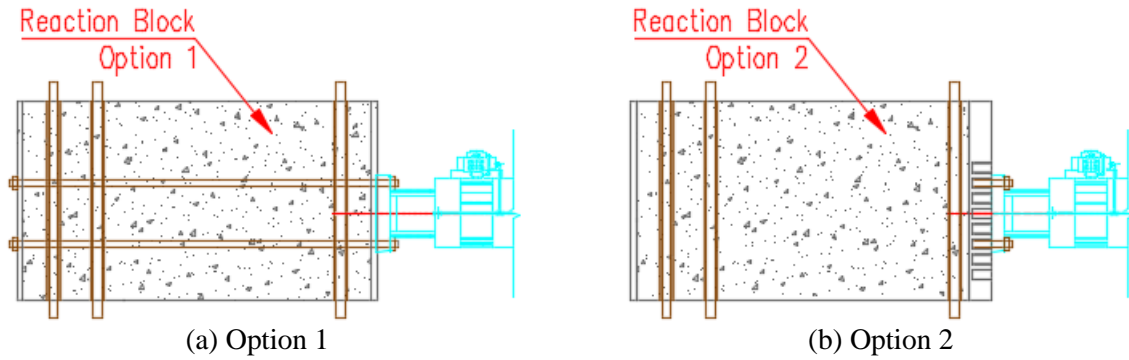


Figure 20 - Reaction Block Options During Fatigue Testing Setup Design Process

To solve the problems related to Option 1 in Figure 20, the final version of the reaction block was composed of two steel brackets with a horizontal plate at the bottom, and steel pipes running between the vertical plates (see Figure 21). In addition, Figure 22 shows a picture of the steel bracket and the reaction block while Figure 23 is a photo of the setup already assembled. The rigidity and the restoring-moment capabilities of the configuration shown in Figure 22a was increased by pouring concrete as shown later in Figure 29.

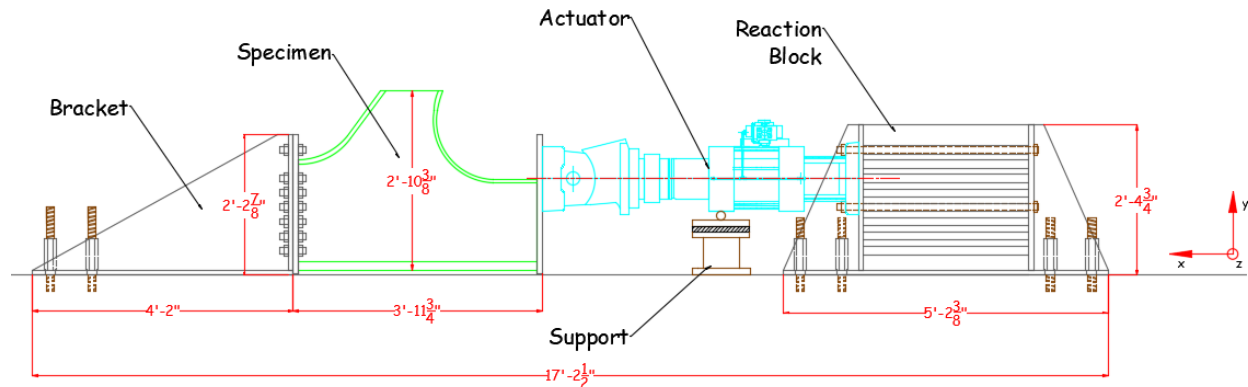
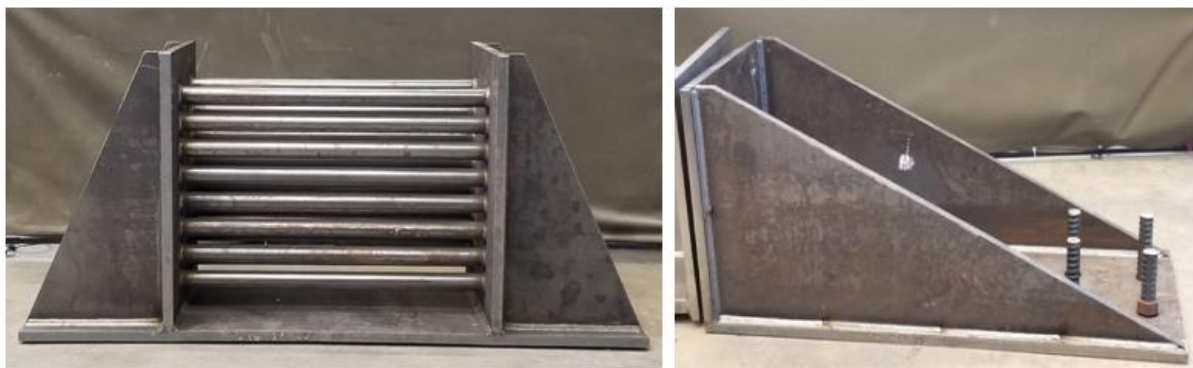


Figure 21 - Fatigue Testing Setup Drawing From South View



(a) Reaction block

(b) Steel bracket

Figure 22 - Structural Supports



Figure 23 - Assembled Experimental Setup (without concrete poured on the reaction block)

As shown in Figure 22a, the reaction block has eight lines of steel pipes running through the brackets. This allows shifting the actuator down from the top location (shown in Figure 23) to change the stresses in the specimen, if needed. This criterion was deemed to be important to allow flexibility in this test configuration not only for the fatigue tests but also for future use of the setup.

3.3 Actuator and Mounting Bolts Specifications

A drawing of the MTS actuator, model 244.41 is presented in Figure 24. According to MTS, this actuator is a “double-acting, double-ended, heavy-duty actuator that operates under precision servovalve in MTS closed-loop servohydraulic systems” [39]. The actuator has a pressure rating of 3000 psi, force rating of 110 kip, and a dynamic stroke of 6 in. In addition, it can work in displacement- and force-control mode, and it is fatigue rated. During the design process, the specified length of the actuator was consistent with the actuator at its mid-stroke position (i.e., allowing displacements of +/- 3 in.) to permit adjustments during the setup assembly, if needed.

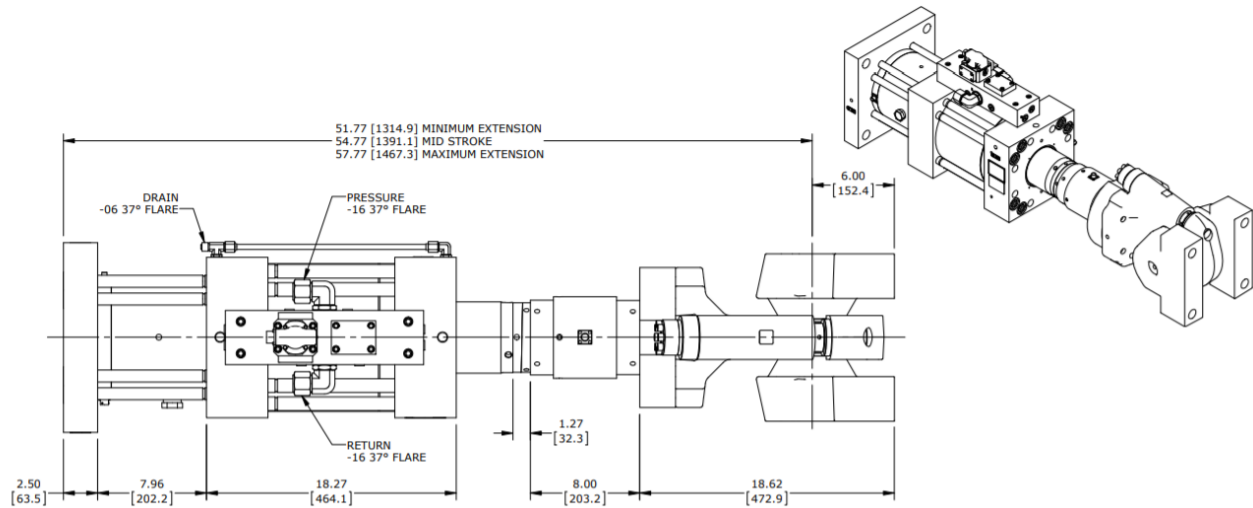


Figure 24 - Schematic of the MTS actuator Used for the Fatigue Testing [40]

Furthermore, the actuator is connected to the specimen on its swivel end. This swivel model, MTS model 249xx.500, allows for adjustment of its angle in two directions, called swivel angle and tilt angle, as shown in Figure 25. This adjustment can be made by loosening, adjusting and re-tightening the torque-nut at the swivel. The torque-nut is tightened to the recommended clamping bolt torque (see Figure 25) of 45 lbf-ft.

Figure 26 depicts the recommended mounting bolt specification for various actuator models. The red rectangle highlights the specifications for the actuator used in this setup. Because the design of the reaction block required the use of threaded rods that run through the pipes shown in Figure 22a, these same threaded rods were used to attach the pedestal of the actuator to the reaction block. The rods followed the same size and thread's specification as the mounting bolts. Detailed design calculations for the various components of the experimental setup described in this chapter are shown in Appendix A. Appendix B contains the shop drawings for fabrication of the supports, including dimensions and material properties for all elements of the setup

Operation Specifications (Base & Rod End)

MODEL	TILT ANGLE* (α)	SWIVEL ANGLE (β)	Clamping Bolt Torque†	
			N·M	LBF-FT
249xx.M25	$\pm 7^{\circ}$ **	$-90^{\circ}, +90^{\circ}$	34	25
249xx.M70	$\pm 17^{\circ}$	$-75^{\circ}, +90^{\circ}$	110	84
249xx.M160	$\pm 17^{\circ}$	$-80^{\circ}, +90^{\circ}$	380	280
249xx.M340	$\pm 14^{\circ}$	$-75^{\circ}, +90^{\circ}$	780	680
249xx.M500	$\pm 6^{\circ}$	$-30^{\circ}, +90^{\circ}$	62	45
249xx.M730	$\pm 7^{\circ}$ **	$-30^{\circ}, +90^{\circ}$	62	45
249xx.M1000	$\pm 8^{\circ}$	$-30^{\circ}, +90^{\circ}$	62	45
249xx.M1775	$\pm 8^{\circ}$	$-30^{\circ}, +90^{\circ}$	285	210

†Models 249xx.M500 through 249xx.M1775 use Superbolt® torque nut. Each jackbolt in the torque nut is torqued to the values shown.

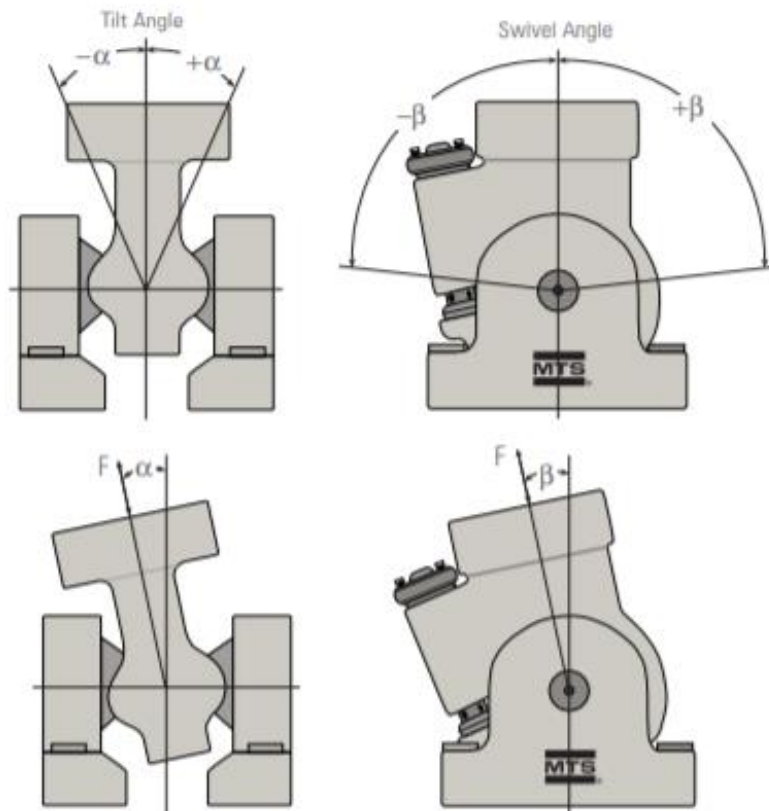


Figure 25 - MTS Actuator Swivel Operation Specifications [41]

Pedestal Base Mounting Bolt Specifications						
Model	Recommended Mounting Bolt Size		Mounting Bolt Torque		Recommended Bolt Grade	
	mm	UNC	N-m	lbf-ft	ISO	SAE
244.11	M12 x 1.75	1/2-13	93	84	12.9	8
244.12	M12 x 1.75	1/2-13	93	84	12.9	8
244.21	M16 x 2.00	5/8-11	230	160	12.9	8
244.20	M16 x 2.00	5/8-11	230	160	12.9	8
244.22	M16 x 2.00	5/8-11	230	160	12.9	8
244.23	M16 x 2.00	5/8-11	230	160	12.9	8
244.31	M20 x 2.50	7/8-9	450	454	12.9	8
244.41	M30 x 3.50	1 1/4-7	1600	1400	12.9	8
244.51	M42 x 4.50	1 1/2-6	3200	2400	12.9	8

Figure 26 - MTS Recommended Bolts Specification for Actuator Attachment [39]

3.4 Additional modifications of the test specimen

After installation of the supports and test specimen, some initial static load tests were performed to characterize the behavior of the system (i.e. system identification). Specifically, the strain in the area of interest and at the boundary conditions, as well as the displacements in key locations along the test setup were investigated. These measurements led to four key observations made about the test setup in its initial state;

1. There was significant support motion in both the reaction block and the support bracket, causing undesirable actuator motion.
2. The vertical plate connecting the specimen and the actuator, also referred to as the specimen tip, was displacing significantly in the vertical direction.
3. The specimen tip was rotating significantly out of plane about the horizontal loading axis.
4. There was a high strain reading (2000 $\mu\epsilon$) in the vertical direction on the vertical plate connecting the specimen and the actuator.

Based on these observations, some modifications to the test setup were needed in order to further control the behavior of the test setup. Specifically, the modifications were intended to ensure the desired loading was applied to the fatigue specimen while protecting the hydraulic actuator from undesirable side loading [42]. The first modification was creating a new boundary condition at the specimen tip, hereby referred to as the “shim support”, in order to restrain the vertical displacement as well as the rotation of the test specimen. This was accomplished using multiple steel shims, shown in Figure 27, wedged under the tip of the specimen at two locations, on either side of the specimen tip. This support acts as a roller in the plane of loading because the steel shims can slide against each other while restricting motion in the vertical direction. It should be noted that this only restrains the vertical motion while applying a tensile load, which causes the specimen to

displace downward. Due to the discretization of the shims, at either ends of the specimen tip, the rotation about the plane of loading is also restrained. In addition to the shims at the tip of the specimen, shims were added under the reaction block and bracket to increase the contact with the floor and decrease rotations at the supports.

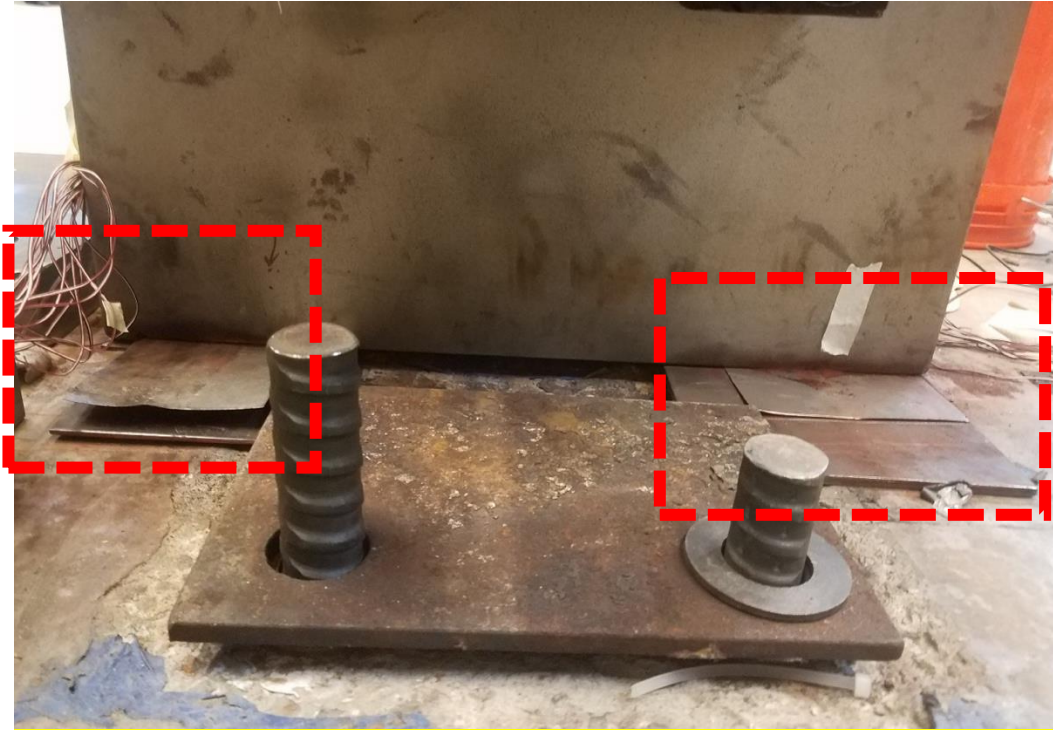


Figure 27 - Location of Shim Support at Specimen Tip for the Fatigue Test

Another major modification was the addition of concrete between the two vertical plates of the reaction block to increase the overall stiffness. Specifically, the rotation of the base plate of the reaction block caused significant rotation of the vertical plate where the actuator is connected to the reaction block. This rotation was due to the portion of the base plate between the two vertical plates being essentially unrestrained. This was identified as the source of the undesirable actuator motion. Figure 28 shows the added reinforcement in the reaction block and the reaction block with the additional concrete.

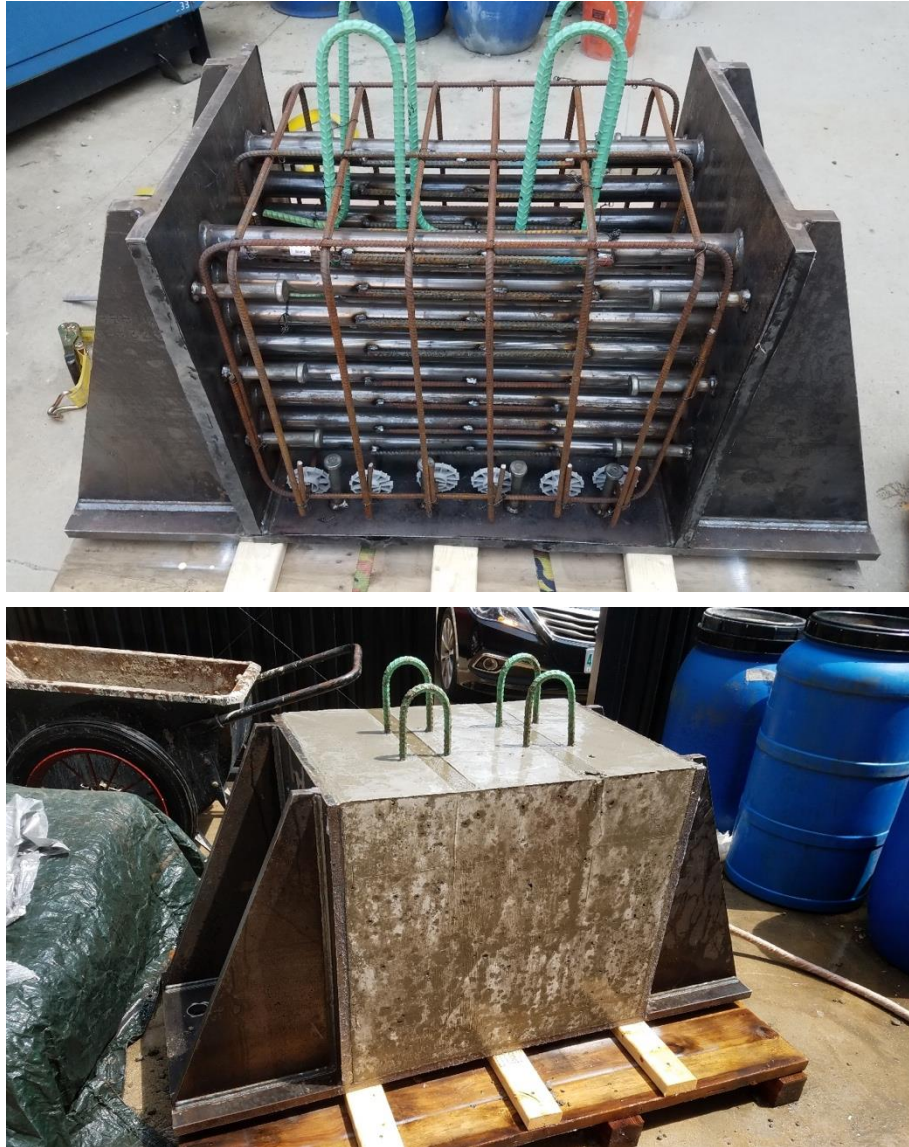


Figure 28 - Reaction Block Reinforcement and Reaction Block with Concrete

The final modification was the change in actuator position to prevent a stress concentration on the vertical plate attaching the specimen to the actuator. During installation, it was noted that the vertical plate had a significant bend, most likely due to the welding process. When the actuator was in its original, highest, position and the bolts were tightened, this bend was removed due to the force from the bolts. The straightening of this plate caused the strain in the plate close to the weld to exceed the yield strain of the material, creating a point in the test setup that would be prone to fatigue damage due to the magnitude of the strain applied. Since this location was not the area of interest, it was decided to lower the actuator to the next position, which resulted in a significant reduction in the strain at the location. With the modifications to the test setup made, additional tests were performed, and the structural response was measured and found to be acceptable. The test setup in its final state is shown in Figure 29. This configuration consists of the reaction block, the actuator, the fatigue specimen, the shim support, and the bracket.



Figure 29 - System Components - Overall Test Setup, Reaction Block (a), Bracket Support (b), Specimen (c), and Shim Support (d)

In addition to the physical test setup, a loading protocol was also developed for this test. The loading protocol can be divided into three main sections;

1. The pre-cyclic loading
2. The cyclic fatigue loading
3. The post-cyclic loading

The loading protocol is implemented using MTS Multi-Purpose Testware software to apply either loads or displacements to the MTS 244.41 hydraulic actuator. In this specific loading protocol, the commands are given in terms of force measured on the load cell, a device to measure the force applied, of the actuator. The loading procedures were coded in the MPT Procedure Editor in the form of force commands.

The pre-cyclic loading consists of two ramp functions in which the load is brought from 0 kip to 40 kip in 10 seconds, then from 40 kip to 20 kip in 5 seconds and occurs before the cyclic fatigue loading. The purpose of this ramp loading is to create some unique peaks in the measured response that will be used to synchronize the data sets from different measurement methods. The post-cyclic loading consists of three ramp functions in which the load is brought to 40 kip in 7.5 seconds, then 60 kip in 5 seconds, and finally 0 kip in 7.5 seconds. The post-cyclic loading occurs after the cyclic fatigue loading and serves as a second point of synchronization for the post-processing.

The cyclic fatigue loading, which is implemented after the pre-cyclic loading and before the post-cyclic loading, that is being used in this test is a pulsating tensile loading, in which, the actuator is cycling in force control as a sinusoidal signal in tension. The loading specifications are as follows:

- Mean axial load applied: 55 kip
- Cyclic amplitude: ± 50 kip
- Cyclic frequency: 3.5 Hz
- Applied function: Sine wave
- Cycles per Test Session: Variable.

The level of loading was limited by the capacity of the actuator load cell, which is 110 kip, while maximizing the applied tensile stress range, would increase the chances of fatigue failure. With this level of loading, the endurance limit of a category C fatigue detail, which was the design assumption, would be exceeded according to the numerical models. The pulsating tensile loading is used to be representative of the conditions on the Memorial Bridge, where the bottom-chord will be in tension under the service loads. It is also important to note that the test was performed in ambient temperature in a controlled lab environment. The frequency of loading was limited to ensure the test was performed in with “quasi-static” loading. A sample of the cyclic loading is shown in Figure 30, and a sample of the overall loading protocol is provided graphically in Figure 31 below. Figure 32 shows a schematic of the loading.

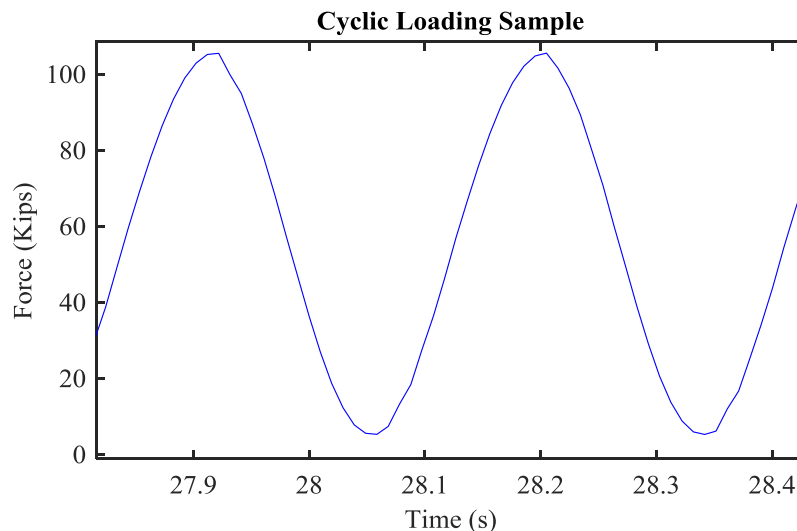


Figure 30 - Cyclic Loading Sample

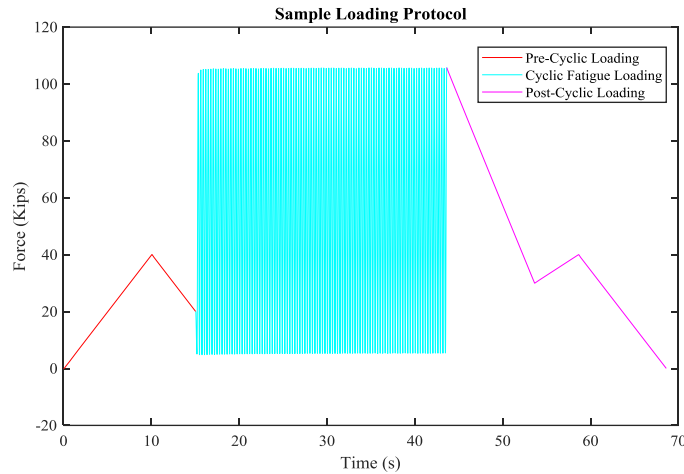


Figure 31 - Sample Loading Protocol

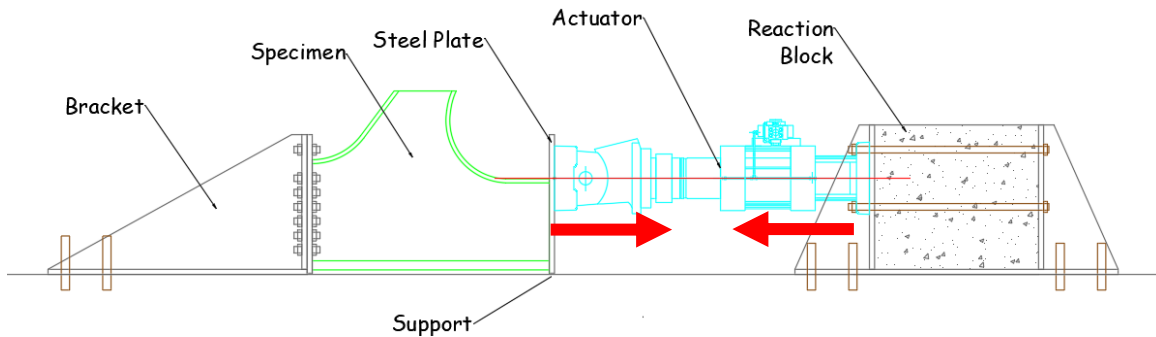


Figure 32 - Loading Schematic

In addition to the development of the loading procedures, the tuning parameters as well as the limits for the actuator were selected. The tuning of the actuator refers to adjusting the inputs, in terms of a proportional-integral-derivative (PID) control loop. The specific methods for tuning this control loop were obtained from the MTS user manual [43]. The goal of tuning the actuator controls was to ensure that the command being input, in terms of force and frequency, matched the actual measured output of the actuator. Additionally, with a poorly tuned actuator, especially when using force-controlled testing, the system is susceptible to instability in which the measured force can rapidly deviate from the command in terms of magnitude and frequency. This is one of the main reasons for the limits being implemented. The limits refer to an upper and lower force limit that, if the actuator load cell reading exceeds, will interlock the hydraulics and stop pressure from reaching the actuator. The upper limit, set to approximately 107 kip, is in place to prevent the actuator load cell from reaching the 110 kips limit, while the lower limit, set to approximately -2 kip (compression), is in place to prevent the specimen from being loaded in compression. Therefore, in the case of instability, the limits will be exceeded, and the hydraulics will quickly cease pressure to the actuator.

3.5 Instrumentation

The objectives of the experiment must be considered prior to determining the location and type of sensors. Each sensor should provide a needed piece of information to fulfill these objectives. For this experiment, the bridge owner was interested in (1) investigating the design assumption of fatigue category C [20] for the gusset-less truss connection, which implies infinite fatigue life under service conditions, and (2) collecting data useful for providing guidance for fatigue-focused visual inspection procedures of the gusset-less connection through the service life of the bridge. An additional research interest was verifying the structural model of the gusset-less connection and evaluating the dissipation of strain with distance from the weld toe. In order to accomplish these goals, the experimental setup, including boundary condition and component interface, must be categorized and fully understood for both fatigue assessment and structural model verification.

The measurements techniques and sensors that are utilized for the scale model laboratory fatigue experiment are Digital Image Correlation (DIC), Linear Variable Differential Transformers (LVDTs), and strain gauges (uniaxial and rosettes), which are used to measure displacements, rotations and strains. The instrumentation used can broadly be categorized as contact (LVDTs and strain gauges) and non-contact (DIC) measurements.

Strain gauges and LVDTs are two of the most traditional contact tools for obtaining structural response measurements. These sensors function by maintaining contact with the specimen, through contact in the case of the LVDT, or bonding (epoxy or spot-weld), in the case of the strain gauge. These tools tend to be the most commonly used due to their cost, availability, reliability, and accuracy of structural response measurements. Although strain gauges are the most frequently used sensors, there are some significant drawbacks and limitations to their use and applicability. One of the most significant drawbacks for the strain gauges is the installation procedure, which generally consists of the following:

1. Surface preparation consisting of abrasion (sanding or grinding) followed by a thorough cleaning of the surface to remove particles and oils which could weaken the adhesive bond.
2. Positioning of the gauge to define the measurement direction(s).
3. Application of accelerant to prepare the gauge for adhesion.
4. Application of adhesive and bonding of the gauge.
5. Positioning of the lead wires and soldering if necessary.
6. Connection to strain measuring device and data recording.

Strain gauges are limited to relatively smooth and preferably flat surfaces that allow complete bonding of the gauge to the specimen. Additionally, the locations where the strain gauges and LVDTs can be installed are limited to locations that can be physically accessible with sufficient space to perform all the steps necessary for installation. Another major drawback to these contact measurements is the amount of surface preparation required for adequate installation. Not only is surface preparation a significant amount of work but it also has the potential to interact and affect the specimen behavior. Specifically, if there is any coating or outer layer of environmental protection on a specimen, the surface preparation requires coating removal, while this is not an issue for laboratory specimens exposed to indoor environmental conditions, it can adversely impact field application. Further, strain gauges and LVDTs only provide discrete measurements at the point of installation.

The amount of measurements needed to fully characterize the response of a specimen is significant. To capture all the required measurements, many sensors are necessary, which is costly in terms of

number of sensors and installation time. To a lesser extent, the size of these sensors may also provide important limitations, especially when localized strain measurements are needed very close to one another. The DIC measurements fall under the non-contact measurements category since contact is not present between the cameras and the specimen. DIC identifies and tracks the movement of groups of pixels captured via a speckle pattern on the area of interest. Using a correlation algorithm, the translation vectors for each pixel grouping are calculated and the movement is computed relative to the location of the pixel groupings of an undeformed reference image. A mathematical background of the DIC analysis method is provided in Appendix C. Although DIC is not as widely used as other more traditional measurement methods, it is becoming more popular as digital image technology advances become more cost-effective and the post-processing technology improves. DIC measurements, while not being as consistently accurate as traditional methods, given the impact of image collection conditions and camera capability, excels in many other aspects. One of the largest benefits of DIC compared to other forms of instrumentation is its ease of installation. DIC requires very little installation time depending on the type of equipment used and the environment where the measurements are collected. The general installation procedure is as follows:

1. Application of a suitable tracking pattern to the measurement area of interest. Typically, this is done with a black on white speckle pattern or the inverse.
2. Placement of camera(s) to focus on the measurement area. If 2-D DIC is being used, the cameras need to be perpendicular to the area of interest. When 3-D DIC is being used, a minimum of two cameras will be in a stereo configuration, typically at an angle of 30 degrees with respect to each other.
3. Adjustment of camera(s) settings to optimize focus, lighting, and resolution. These parameters should be optimized uniquely for the test setup and the hardware used.
4. Image capturing. Typically, a commercial program is used to control the capture settings/timings, especially in the case of 3-D DIC in order to synchronize the multiple cameras.

An experienced user can record measurements with DIC in a relatively short time without difficulty. The other major benefit is that the DIC measurements can be used to characterize a large area where applying multiple gauges would not be feasible. With the correct setup and equipment, it is possible to obtain a full-field characterization of the area of interest. One major drawback for the DIC is the computational effort, which is much more significant than evaluating results from strain gauges or LVDTs. This is due to the differences in data, with the strain gauges and LVDTs resulting in direct measurements without post-processing needed. For DIC, indirect measurements are obtained because pixel movements should be converted into displacements and strains mathematically. Lastly, the initial cost of the DIC equipment can be high, but it is a tool that can be reused and applied to a variety of situations, which has the potential to mitigate long-term costs. The strain gauge instrumentation plan for the specimen is shown in Figure 33. The naming convention for the gauges are as follows;

- Specimen side; N = on the North face of the specimen, S = on the South face of the specimen, VP = on the vertical plate of the specimen.
- Type; R = Rosette type strain gauge, U = Uniaxial type strain gauge.
- Location; W = web of specimen. FB = Flange (bottom-side). FT = Flange (top-side).
- Number; the number corresponding to specific gauge of a specific type.
- Example; NRW1 = Rosette number one on the North face of the specimen web.

In this study, a total of 12 strain rosettes and 10 uniaxial strain gauges are being used to characterize the strains throughout the specimen. The uniaxial strain gauges used were CEA-06-125UW-120 gauges while the rosettes used were EA-XX-125BZ-350, all of which were wired in a quarter bridge configuration [2]. The device used to connect the strain gauges to a data acquisition computer was the NI cDAQ™-9178 chassis with NI 9219 Universal Analog Input Modules, and the data acquisition software was LabVIEW 2017. The capture frequency chosen for all strain gauges was 60 Hz, which was sufficient enough to characterize the response given the input frequency, while maintaining a reasonable sized data set from each testing period. The strains were chosen to be recorded continuously throughout the entire loading protocol, as opposed to incrementally, to ensure that if there was a change in behavior, it would be captured through the strain measurements. Lastly, it is important to note that the strain gauges were calibrated, or zeroed, while the specimen was not attached to the test setup, meaning that the strains from the installation, mainly the bolt loading and gravity loads, are present in the measured strains. Since the main factor is strain range, the range for each of the gauges during the fatigue loading is of interest, but the mean strain is also important for characterizing the fatigue performance.

As previously mentioned, the strain field near the radiused fillet weld at the web-flange intersection is the area of interest for this fatigue study. For this reason, strain rosettes are installed on both sides of the specimen web at three locations along the curved geometry (NRW1/SRW1, NRW2/SRW2, NRW4/SRW4 in Figure 33) and aligned at three distances from the toe of the weld (NRW2/SRW2, NRW3/SRW3, NRW5 in Figure 33) to capture the strain distribution in the web. Additionally, three rosettes are placed on the top flange; two on the underside (NRFB1/SRFB1) and one on the topside (SRFT1) to characterize the strain in the flange. The uniaxial gauges are placed on the specimen close to the interface between the specimen and its boundary conditions, specifically the actuator and the bracket support (NU1 to NU6; SU2, SU5; VP1, VP2 in Figure 33.) These uniaxial gauges are in place to measure the structural response at the interfaces and provide data useful for characterization of boundary condition effects.

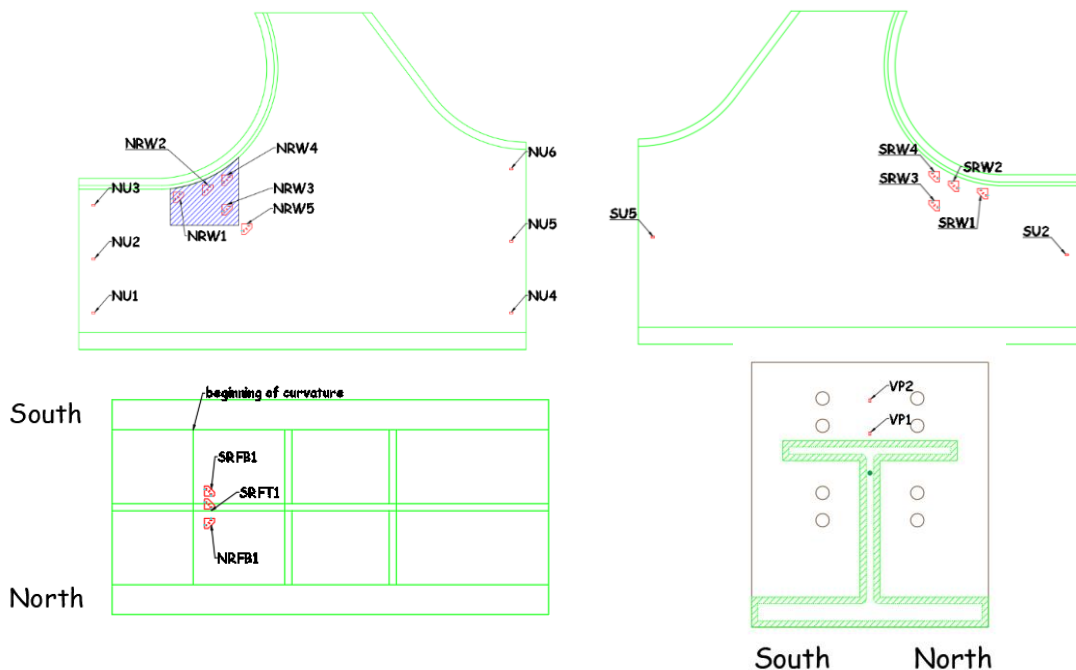


Figure 33 - Instrumentation of Gusset-less Fatigue Specimen

In addition to the strain gauges, DIC is used to measure strains and displacements in the area of interest, shown with shading in Figure 33. In this study, 2-Dimensional DIC is being used. The camera used in this study is the Grasshopper 5.0 MP Mono FireWire 1394b with a 2448x2048 resolution. For image capturing, the VIC-Snap software from Correlated Solutions is used. The images are taken in 30 second intervals, spaced 20 minutes apart, at a capture frequency of 12.5 Hz during the capture period. The 30 second capture, followed by 20 minutes of no recording is chosen to reduce the total number of images due to the significant processing time required. The 12.5 Hz capture frequency, within that 30 second capture window, is chosen as the highest capture frequency possible given the hardware used in this setup. A schematic, as well as a picture of the DIC setup used in the test is shown in Figure 34.

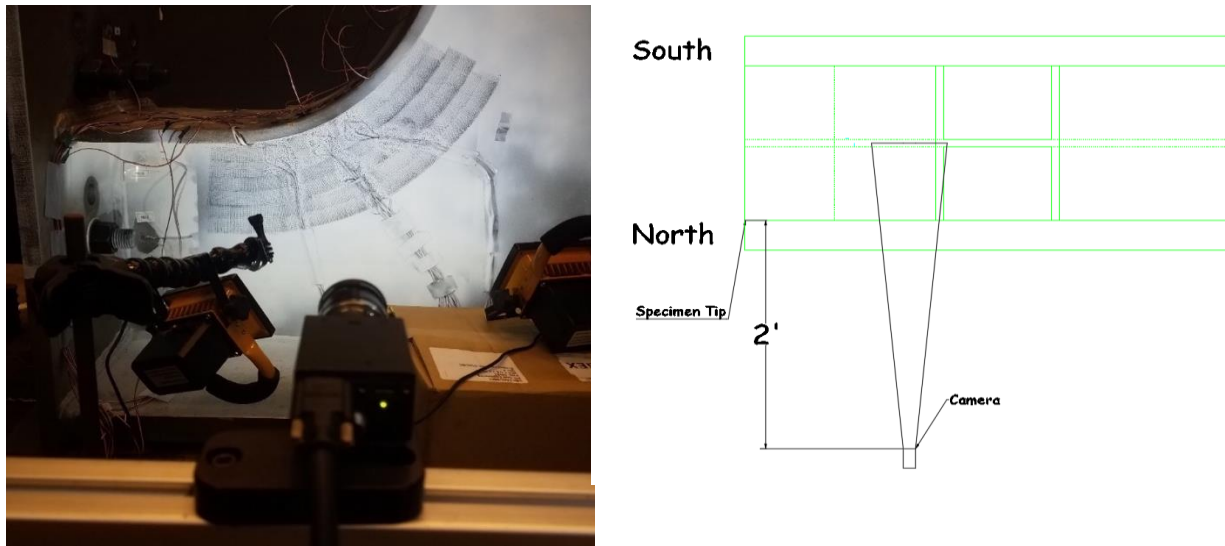


Figure 34 - DIC Schematic and Setup for the Fatigue Testing

The area depicted by the blue hatch pattern in Figure 33 represents the field of view that is captured with the DIC via a speckle pattern. The speckle pattern was applied with an ink roller supplemented by permanent marker to produce a high-quality pattern. A sample of the pattern is shown in Figure 35. These DIC measurements serve as verification for the strain rosettes as well as a full-field characterization in this region at locations in which strain rosettes are not present. The combination of all the measurements from DIC as well as the strain gauges can also be used as a comparison to the numeric model of the test setup.

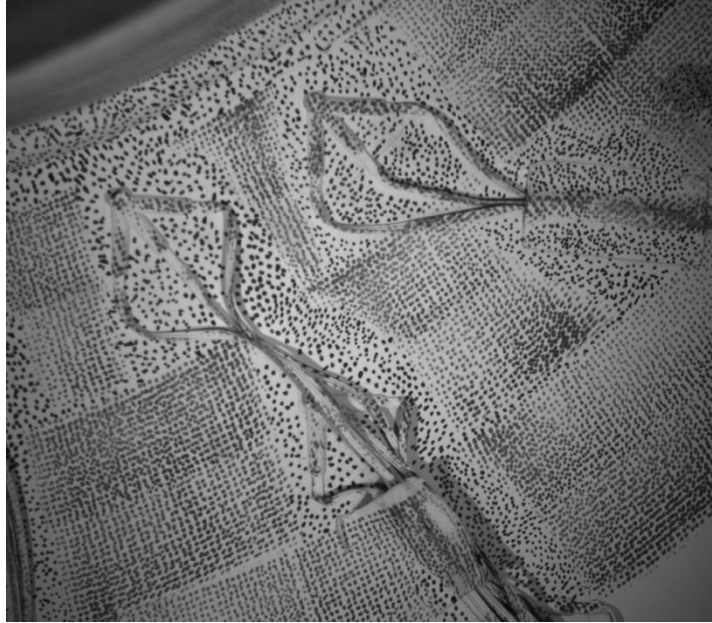


Figure 35 - Sample Speckle Pattern

4. FATIGUE TEST MONITORING

This chapter will introduce the developed fatigue test monitoring protocol specific to this test. After this introduction, the System Identification (System ID) that has been performed will be explained in detail and the results of the System IDs performed are presented. Finally, the force-displacement relationship of the actuator is discussed, specifically its value as reliable quantitative representation of the behavior of the system.

4.1 Fatigue Test Monitoring Protocol

Ensuring consistent behavior in a high-cycle fatigue test is important, especially when the test must be performed in multiple smaller testing intervals in which the loading is paused and later resumed. There is added complexity in this study related to potential changes in the test setup due to the fatigue loading. Specifically, the shims under the specimen tip as well as all the bolted connections in the test setup have the potential for degradation, in the case of the shims, or loosening in the case of the bolted connections. In this scenario, it is critical to develop a protocol to systematically monitor the structural response of the system and use this data to identify any changes in behavior throughout the high-cycle fatigue test. Additionally, a monitoring protocol aids in identifying potential fatigue damage or failure in the specimen. For these reasons, a test monitoring protocol was developed for this study in order to maintain a consistent structural behavior throughout this test. A graphical representation of the monitoring protocol is shown in the form of a flowchart in below Figure 36.

The flowchart developed for monitoring the high-cycle fatigue test is specific to this research, but the general concept can be applied while the specific monitoring details can be altered to be used in another test.

The start point of this monitoring protocol is equivalent to day zero of fatigue testing, meaning that the specimen is mounted in the test setup and is properly instrumented for the fatigue test, but no fatigue testing has been performed on the specimen. Advancing from the start position in this

protocol, the next step is to inspect the instrumentation used in the test. This is one of the most critical steps, specifically because the monitoring protocol revolves around making data-driven decisions using the measured structural response from the instrumentation. Therefore, it is extremely important to ensure that the measurements that are being used are not compromised. During the instrumentation inspection, the following components are checked

1. Strain gauges, both rosettes and uniaxial gauges, are checked for debonding from the specimen surface. Additionally, the wiring is inspected for any damage. This check is in place to ensure that there has not been any physical change to the gauges. Specifically, due to the location and length of the wires connecting the strain gauges to the measurement system, there is a significant risk that the wires become damaged due to foot traffic in the laboratory.
2. A gauge test, in the form of recording strains for ~10 seconds, is performed to check the strain values being recorded by the gauges. This test will quantitatively indicate any erroneous strain measurements as well as allow the user to quickly identify which, if any, strain gauges need to be inspected further. One example of this is if a strain gauge wire is damaged due to foot-traffic, an abnormally high strain will be shown in the gauge test.
3. The LVDT's are tested in a similar fashion to the gauges. They are visually inspected to ensure that the required contact to the specimen is made and the direction of the LVDT is still consistent with the measurement in the direction of interest. Additionally, the displacements are recorded for ~10 seconds to check for any measurement errors.
4. Lastly the DIC system is assessed. First the camera is turned on and the lens cap removed. The two LED lights are turned on and positioned to illuminate the area of interest. Next the camera is inspected for perpendicularity to the surface in which the area of interest is located on. The saturation of the light is checked in the VIC-Snap software and adjusted to the optimal level through adjustments to the exposure timing. Lastly, images are recorded for ~10 seconds to check for any errors in the recording software. One specific example of an error in this study was that the cameras would sometimes not record at the specified frequency, so adjustments had to be made before testing.

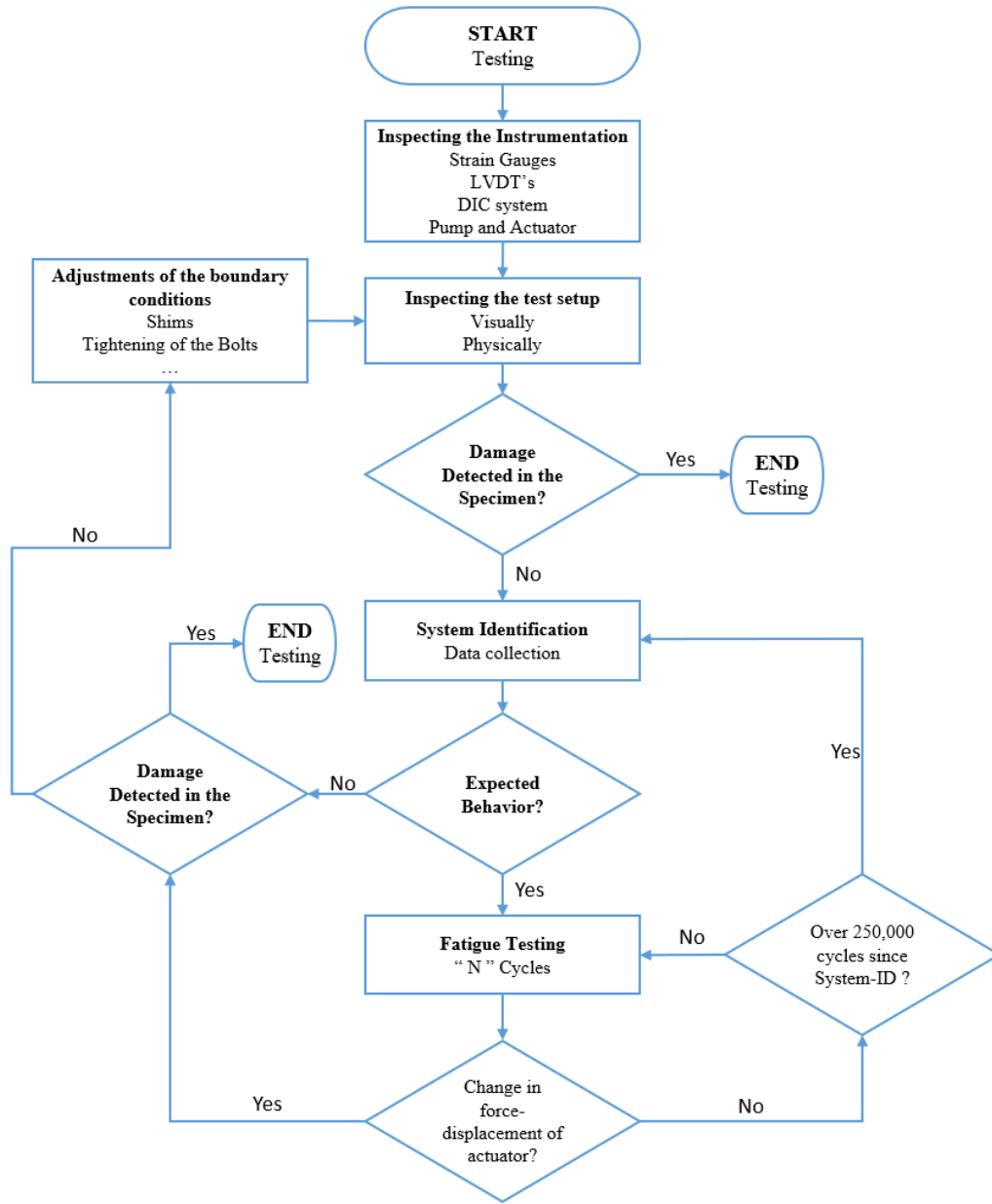


Figure 36 - Monitoring Protocol Flowchart

Once the instrumentation has been inspected, ensuring that it is functioning as expected, the specimen and the test setup are inspected visually and physically. This inspection is in place to check for any visual damage in terms of cracking (fatigue related or otherwise), movement of the shim supports, any unexpected wear in the test setup, and any loosening of the bolts. Figure 37 shows an example of shim support which has been rotated and shifted. If there is damage detected at this point, the testing does not progress, and the damage is investigated further, but if there is no damage detected in the specimen or test setup a System Identification is performed.



Figure 37 - Shim Support Movement

The System Identification, as defined in this project, is a full characterization of the structural response of the test setup through measurements at key points in the test setup while it is being subjected to a short version of a testing interval using the fatigue loading protocol. A detailed explanation of the System Identification and the measurements taken is provided in Section 4.2. The response captured with the System Identification is used as baseline behavior to assess future System Identifications. Once the System Identification is performed and the data is processed, the research team compares the observed structural behavior to the previous System Identification or a theoretical behavior in the case of the first System Identification. Specifically, in this study, the first measurements were compared to a numerical model of the test setup. At this point, the behavior is evaluated, and a decision is made on whether the behavior is as expected or if a significant difference exists between the expected and the measured response.

If the response is significantly different than expected, adjustments must be made to the system to modify and correct the behavior. Some examples of how this is accomplished are; adjusting the shim supports, re-torquing the anchor bolts, and re-torquing the bolts connecting the different parts of the test setup. Once the modifications have been made, another inspection is performed followed by the System Identification, if there is no damage detected during the inspection. This process forms an iterative loop until the behavior is within acceptable limits, at which point the fatigue testing can begin.

The fatigue testing is performed in testing intervals with a set number of cycles per interval. The intervals used in this research ranged from 2 hours (~26000 load cycles) up to 12 hours (~155000 load cycles), but due to the likelihood of data acquisition errors occurring, the test intervals were typically 2-2.5-hours. These intervals resulted in the least amount of data acquisition errors while maximizing the cycles performed in a given testing interval.

After each fatigue test interval, regardless of duration, the actuator force-displacement hysteresis is examined, specifically the slope, or stiffness of the response. This measurement was identified as a representative measurement for the system response, meaning that if there is a change in the system response, there will be a change in the behavior of the actuator force-displacement hysteresis. This representative measurement is discussed in greater detail in Section 4.3. The hysteresis provides a quick way to determine if the behavior of the system has changed without having to perform a full System Identification after every testing interval. If there is a change in behavior between two test periods, adjustments should be made to the test setup and a System Identification should be performed, iterating until the behavior is corrected. In the case that there is no change in behavior, an additional check is in place to ensure that long intervals do not elapse without characterization of the test setup. In this study, if there has been no change in behavior after a cumulative 250,000 cycles since the last System Identification occurred, a System Identification should be performed. This is essentially a safeguard to ensure that if there was a change in behavior, but the hysteresis did not reflect that change, the behavior would periodically be characterized.

In summary, there is a protocol in place to inspect the test setup and track the structural response periodically, or as needed. In addition to a full characterization, a representative measurement has been identified and used to quickly evaluate potential changes in behavior. Using a systematic approach as described above ensures that consistent conditions are kept throughout the duration of a high-cycle fatigue test performed across multiple testing intervals.

4.2 System Identification

As previously mentioned, the System Identification (S-ID) refers to a full characterization of the structural response of the test setup while it is being subjected to a short version of a testing interval using the fatigue loading protocol. The S-ID serves two purposes: (1) ensuring the test is producing measurements in the expected range, and (2) monitoring and verifying the consistency of the structural behavior throughout the fatigue test prior to specimen damage.

In the current high-cycle fatigue experiment, due to the estimated cycles to failure, the test is completed over multiple testing periods. The test is performed under constant loading (force) amplitude and it is expected that the specimen will experience a consistent range of stress, which can be verified, for example, by evaluating the strain history measurements collected during the test. The stability and consistency of the testing environment and boundary conditions is critical during the test. Consequently, it is imperative to characterize the behavior prior to the test. Any changes in the test setup during the test could result in system responses that are inconsistent. Using the S-ID, a reference set of measurements is generated to serve as benchmark for future characterizations of the system. Using this benchmark as reference, the test setup is periodically checked against previous characterizations to ensure that the behavior is consistent between fatigue testing intervals.

One of the key features of the S-ID used in this study is its ability to identify behavior at key locations. This is achieved using many sensors and data acquisition devices, namely;

- 2-Dimensional Digital Image Correlation (2-D DIC)
- Linear Variable Differential Transformers (LVDTs)
- Strain Gauges

The background on the measurement devices has been provided in Section 3.4. There are two significant changes between the instrumentation plan for the fatigue test and the instrumentation used in the S-ID. The first is the use of GoPro cameras to capture 2-D DIC measurements at additional locations along the test setup. The second is the use of LVDTs as verification points for the DIC measurements.

The locations of the additional measurements using the GoPro cameras are shown as red hatched areas in Figure 38. Each location was chosen to characterize the boundaries between different portions of the test setup as well as the relative behavior of each component of the test setup. The LVDTs used in this study correspond to model LVDT-01-030 from BDI, the data acquisition software used is STS-LIVE, and the capture frequency is 100 Hz. The locations of the LVDTs are not shown in Figure 38, but are always present in the S-ID. Typically, there are two or four LVDTs used during the S-ID depending on availability. The reason they are not depicted is due to the variability in their location along the test setup. Since the LVDTs are the easiest measurement device to relocate and use to take measurements, the location of the measurements taken with the LVDTs is varied to verify different DIC locations or take measurement where the DIC is not implemented. It is important to note that all measurements are taken simultaneously during each S-ID operation.

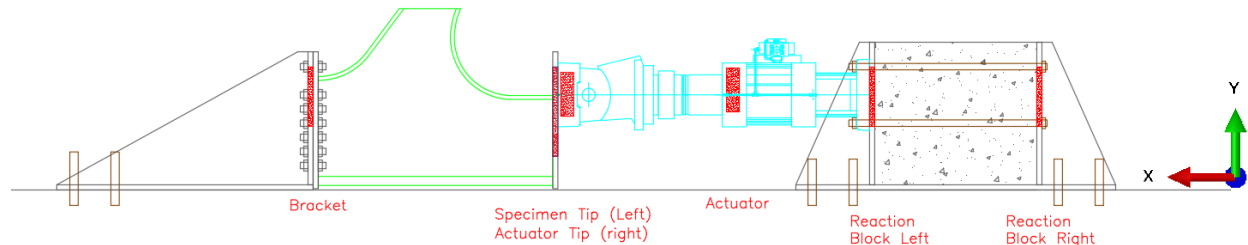


Figure 38 - System Identification - DIC Measurement Locations

The following figures are results from two selected S-IDs performed at different instances throughout the overall fatigue test. Additional S-ID results are shown in Appendix C. The first S-ID shown was performed on July 24, 2018, which was after approximately 260,000 fatigue loading cycles and the second S-ID was performed on October 23, 2018, after approximately 1,510,000 fatigue loading cycles. Between these two testing windows, the test setup underwent minor changes in the form of maintenance to the test setup. The primary adjustments were made in the form of replacing shims that were being worn through, and re-torquing bolts throughout the test setup. The results from the S-IDs are labeled by the date they were performed, either in the figure title or the legend when the results from both dates are plotted together. Figure 39 and Figure 40 show the loading history for both S-IDs, note that the loading protocol is the same except for the duration of the cyclic portion of the loading. In the test performed on July 24, 2018 the cyclic portion was approximately double that of the second test shown. The reduction in cyclic duration was done to reduce the overall processing time of the data from each S-ID.

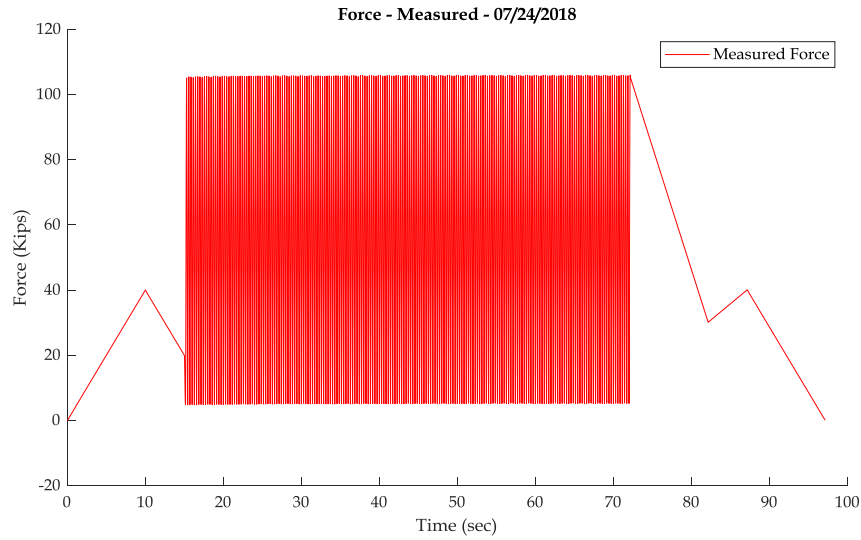


Figure 39 - Force Time-History of the Fatigue Specimen Collected on July 24, 2018

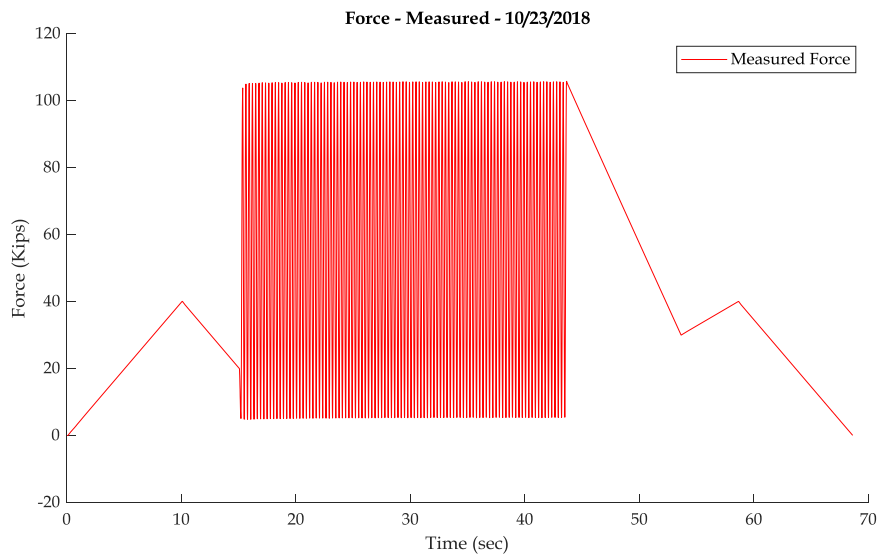


Figure 40 - Force Time-History of the Fatigue Specimen Collected on October 23, 2018

Figure 41 shows an example of the cross-verification between the measurements with the 2-D DIC and an LVDT. In this case the location is the tip of the actuator and the measurement taken is the horizontal displacement. As the graph shows, the measurements match closely, it should be noted that this is raw data with no post-processing or adjustments.

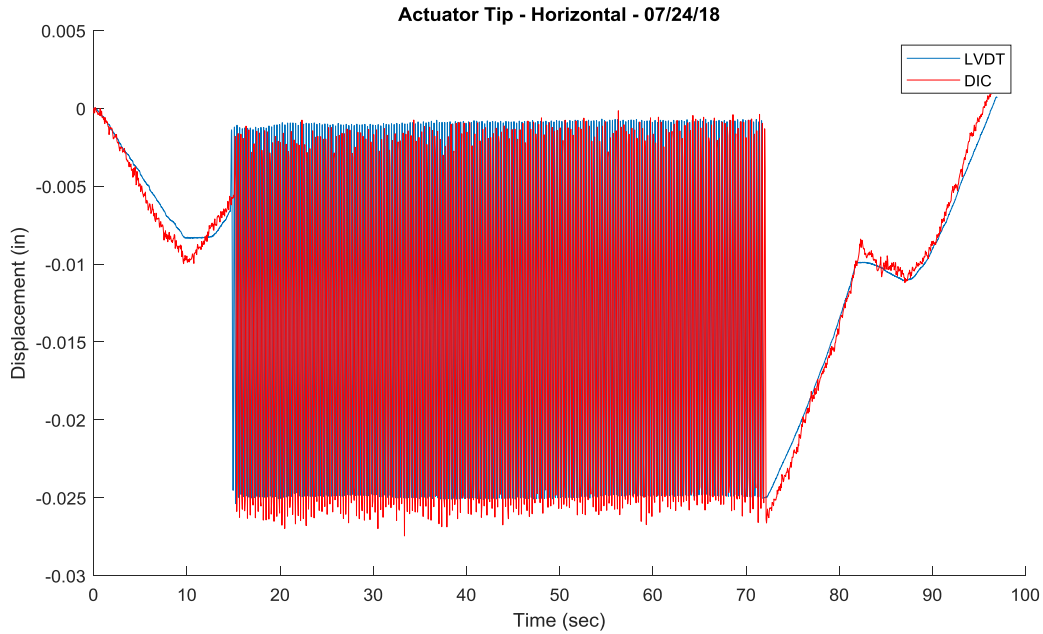


Figure 41 - DIC and LVDT Verification of the Fatigue Testing Collected on July 24, 2018

Since the duration of the cyclic portions of the loading across the two testing periods are different, the following figures will be limited to a 2-second window during the cyclic loading to compare the same measurements from the two different test windows. Figure 42 shows the horizontal displacement of the right side of the reaction block from both test periods.

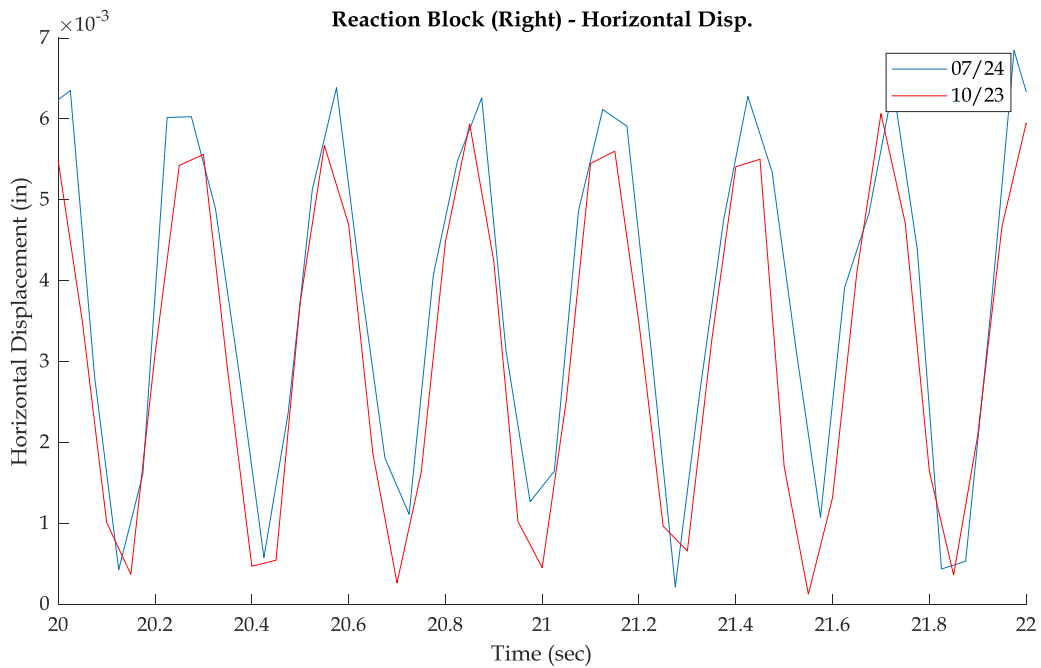


Figure 42 - Reaction Block (Right) - Horizontal Displacement Comparison between July 24, 2018 and October 23, 2018

It should be noted that this data is raw, unadjusted, data output from the 2-D DIC. For this reason, some truncations can be noted in the measured response due to the sampling frequency of the cameras used. Since the frequency was not high relative to the loading frequency, the peaks of the response were not always captured. Based on the output, a cyclic range of displacement, in the vertical and horizontal directions, was measured for each of the two data sets and the percent difference was calculated based on these cyclic ranges. This was done for the displacement at each of the measurement locations along the test setup and is shown below in Table 4.

Table 4 - Fatigue Speciment System Identification Comparison from July 24, 2018 and October 23, 2018

Location	Date	Cumulative Fatigue Cycles	Horizontal Displacement Range (in)	Vertical Displacement Range (in)
Reaction Block (Right)	07/24/18	260375	0.00583	0.00349
	10/23/18	1546414	0.00570	0.00309
	Difference	1286039	2.4%	11.5%
Reaction Block (Left)	07/24/18	260375	0.00528	0.000690
	10/23/18	1546414	0.00558	0.000700
	Difference	1286039	5.6%	1.3%
Actuator	07/24/18	260375	0.00862	0.00322
	10/23/18	1546414	0.00873	0.00336
	Difference	1286039	1.3%	4.3%
Actuator Tip	07/24/18	260375	0.0247	0.01137
	10/23/18	1546414	0.0257	0.01019
	Difference	1286039	4.3%	10.4%
Specimen Tip	07/24/18	260375	0.0233	0.00993
	10/23/18	1546414	0.0240	0.00979
	Difference	1286039	2.8%	1.4%
Bracket	07/24/18	260375	0.01026	0.001572
	10/23/18	1546414	0.01121	0.001627
	Difference	1286039	9.3%	3.5%

Based on Table 4 some slight differences can be seen throughout the comparison across the two testing periods. It is important to note the scale of these measurements when making the comparison, the difference between the two displacement measurements are often less than 1/1000th of an inch. This resolution alone leads to potential measurement errors based on the way the 2-D DIC is calibrated for scale, if there is a slight error in defining the proper scale for the analysis, the measurements will be off slightly. One other potential source of error, as previously mentioned, is the minor adjustments between the shim supports, as well as the torquing of the

bolts. Overall, the differences ranged from 1%-11% with an average difference of 4.84% between the two measurement dates.

4.3 Representative Measurement

Ensuring consistent behavior in a prolonged test is important but performing a full System Identification, detailed in Figure 36, before every testing period would be cumbersome and would add a significant delay between testing due to the processing time required to analyze the S-ID measurements. Hence, it is important to have the availability of benchmark measurements during the fatigue test that could be used as reference measurements to identify potential undesirable changes in the structural response of the system. Having such measurements allows the test to be monitored between S-ID intervals and can be used as a tool to decide when an additional (unscheduled) S-ID needs to be performed.

In this project, the measurement that is being used as a representative characterization of the system is the force-displacement relationship of the actuator. This is measured through the actuator LVDT, with respect to the displacement, and the actuator load cell for the force. The force-displacement relationship is an indicative measurement because if a consistent force is applied (force-controlled test), any change in a stable system, for example boundary conditions, will be reflected in this measurement. For example, if the attachment bolts are not tightened at the specimen-bracket interaction, the actuator will end up displacing a further distance to reach the same level of force compared to if the bolts were completely tightened. Therefore, if there is a noticeable change in the force-displacement hysteresis of the actuator, the test setup ought to be evaluated for changes in the supports, any loosening of bolts, or any noticeable damage. If the source of the change is not visible, a full characterization is required in the form of the S-ID process. These steps create a systematic approach for maintaining a consistent structural response throughout the fatigue test.

Throughout this project, a history of the force-displacement relationship was monitored to create a benchmark measurement and use this benchmark to assess the presence of changes in the system. Figure 43 through Figure 47 show an overall history of the force-displacement relationship of the actuator throughout the setup and testing phases of this project. Each of the data sets shown, labeled by the date in which the test was performed, are approximately 50 seconds of the cyclic loading protocol close to the end of the respective testing interval. Taking a data window close to the end of the testing period ensures that the maximum number of cycles occurs between the comparisons of the data sets. This is desirable to ensure that the changes that occurred during that testing period are reflected on the measurement before the next testing period occurs.

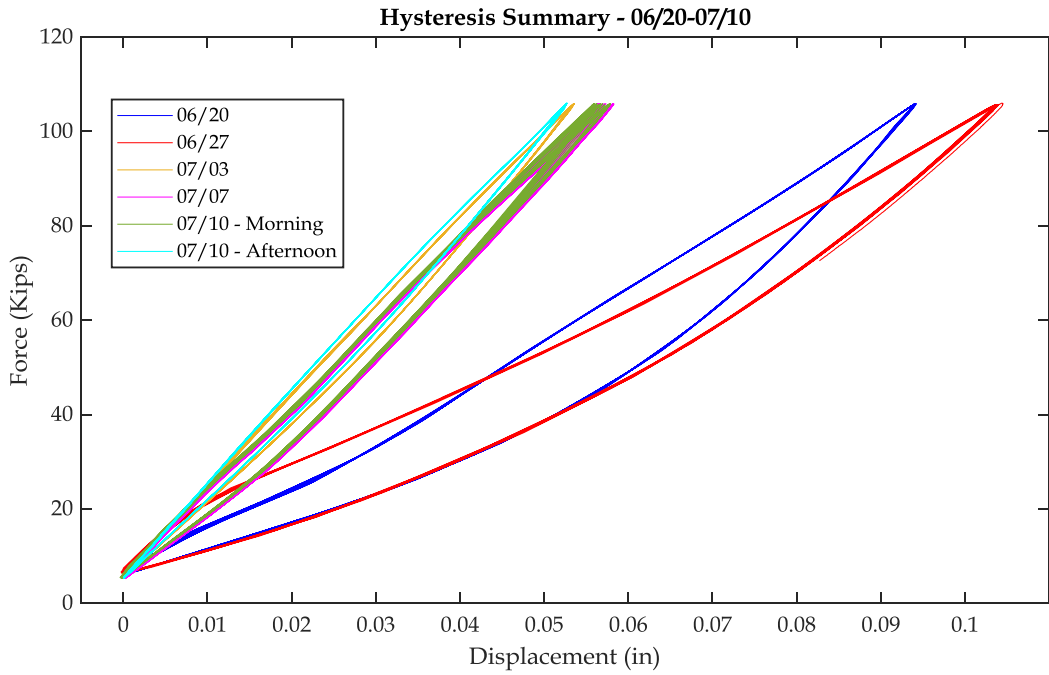


Figure 43 - Hysteresis Loop Recorded During Fatigue Testing on June 20, 2018 and July 10, 2018

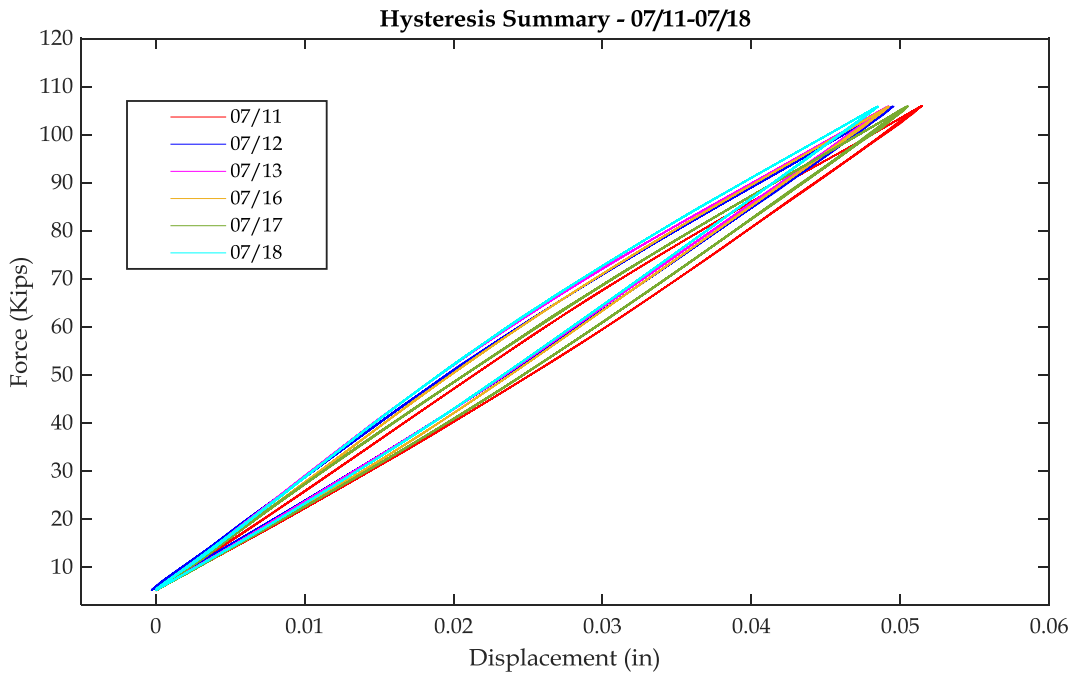


Figure 44 - Hysteresis Loop Recorded During Fatigue Testing on July 11, 2018 and July 18, 2018

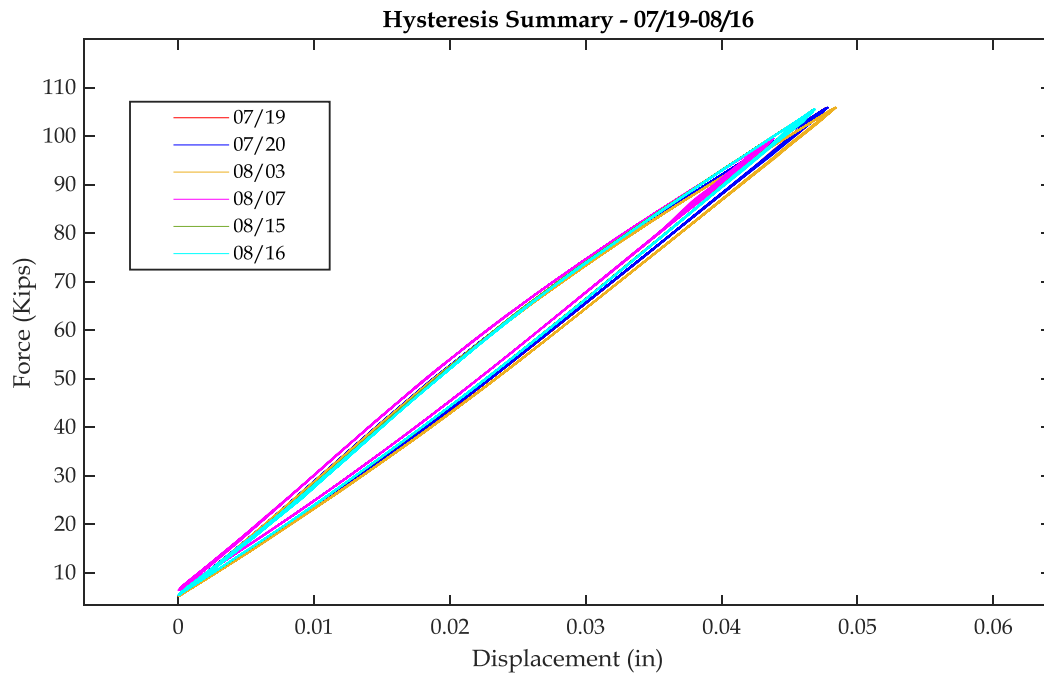


Figure 45 - Hysteresis Loop Recorded During Fatigue Testing on July 19, 2018 and August 16, 2018

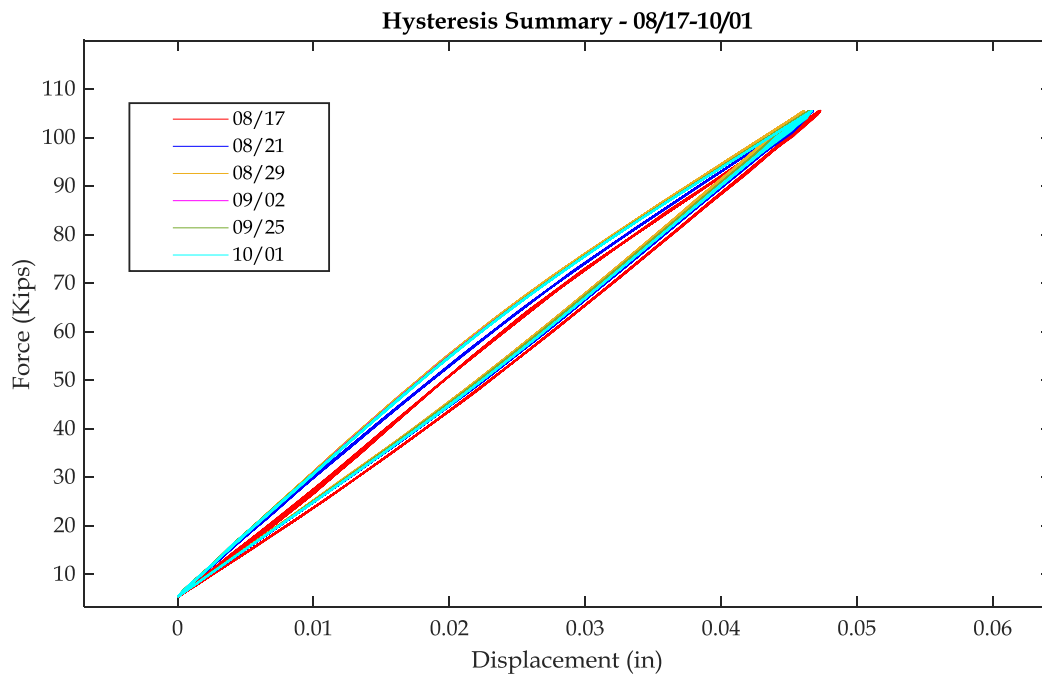


Figure 46 - Hysteresis Loop Recorded During Fatigue Testing on August 17, 2018 and October 1, 2018

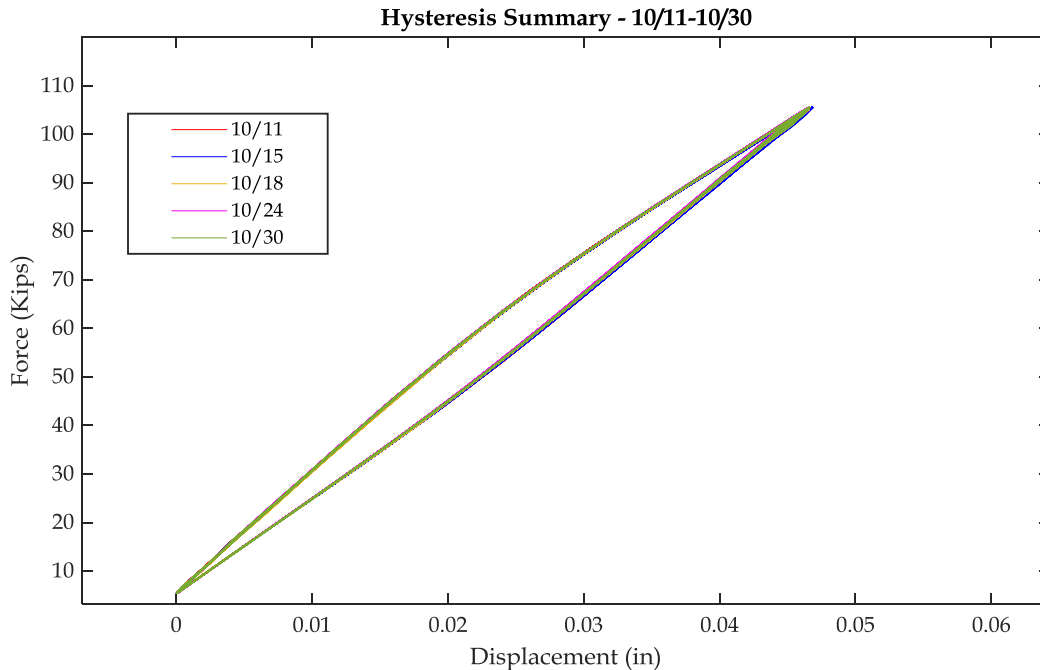


Figure 47 - Hysteresis Loop Recorded During Fatigue Testing on October 11, 2018 and October 30, 2018

As Figures 43-47 show, besides the initial hysteresis shown in Figure 43, there is a consistent force-displacement relationship across the different testing periods. This indicates that over the time frame between July 11, 2018 to October 30, 2018, the behavior of the test setup was consistent according to this measure. To be able to use this measurement as an indicator, as this project has, it was important to verify that any changes in the test setup would be reflected in this force-displacement relationship. The justification for defining the hysteresis as the representative measurement for the system behavior comes from the observed behavior during the first few test periods, namely June 20, 2018, June 27, 2018, July 3, 2018, and July 10, 2018. Each of these data sets shows the effect of different changes to the test setup and how they are reflected in the force-displacement.

The first behavior that should be highlighted can be seen in Figure 48, which shows the force-displacement relationship from test periods on June 20, 2018 and June 27, 2018. The first data set, June 20, 2018, was the first fatigue test period. After inspecting the test setup, minor grinding of the concrete floor was observed under the vertical attachment plate to the actuator. Therefore, the supports were modified from narrow steel channels to flat aluminum shims to mitigate this grinding. The objective of this change was to increase the surface area of the support to distribute the force and allow for the shims to slide on each other rather than having the channel grinding against the concrete floor. The change in the force-displacement relationship between June 20, 2018 and June 27, 2018 shows a significant reduction in the slope from the previous test, which is attributed to the change from the steel channel to the aluminum shims. With this change, the specimen was able to displace further under the same load since the aluminum support was much more flexible. Although this change was subtle, with a change of approximately 0.01 inches of displacement, it was clearly captured with the force-displacement relationship.

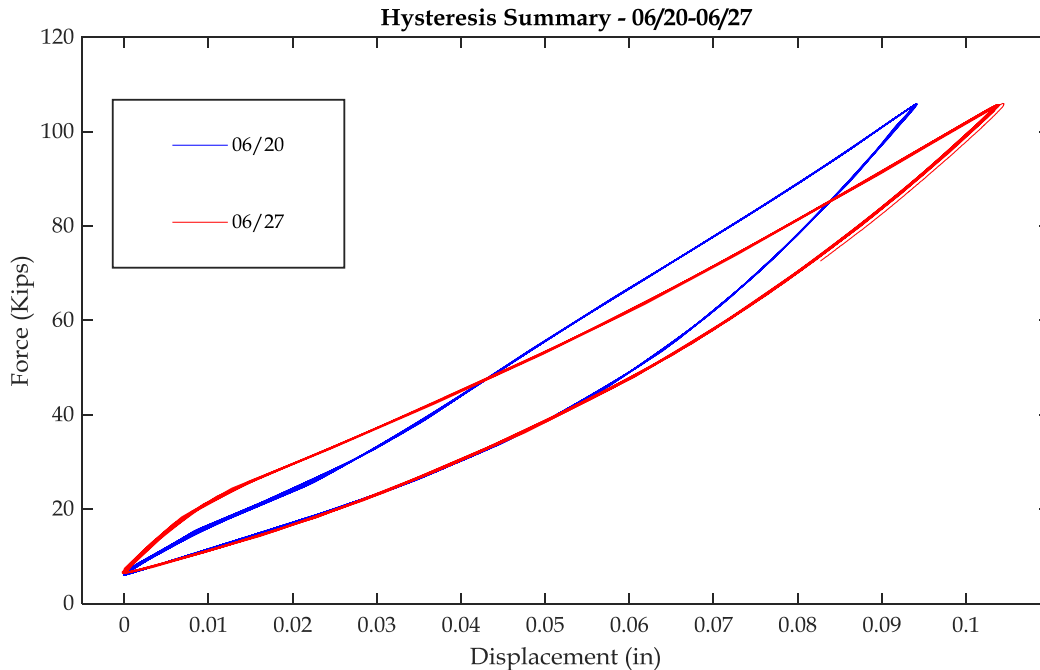


Figure 48 - Hysteresis Loop Recorded During Fatigue Testing on June 20, 2018 and June 27, 2018

The next change in behavior is much more drastic relative to the overall behavior and can be seen in Figure 49. This plot shows the change in the force-displacement relationship between the June 27, 2018 test period and the July 3, 2018 test period. During the June 27, 2018 test session, it was noted that the reaction block was rotating about the z-direction and had significant horizontal movement, so a decision was made to increase the torque applied to the anchors that clamp the reaction frame to the floor. This change is reflected in the change in slope between June 27, 2018 and July 3, 2018, where the increase in clamping force added significant stiffness to the overall system. This is due to the actuator previously having to displace more to achieve the same level of force, therefore, when the support was sufficiently restrained to the floor, the actuator did not have to compensate for any additional movement. As Figure 49 shows, the change in torque to the anchor bolts is clearly reflected in the force-displacement relationship.

The last behavioral change that should be highlighted is very subtle and is shown in Figure 50. Data from July 3, 2018 compared to July 10, 2018 shows a slight loss of stiffness in the force-displacement relationship. During the July 10, 2018 testing period the shim supports under the vertical plate became dislodged from their initial location. The test was stopped before reaching the desired level of cycles to adjust the support and improve the boundary conditions. This dislodging is reflected by the loss of stiffness as well as the fact that there is a change in behavior even across the short number of cycles shown in this plot. A zoomed in view, Figure 51, shows that while the shim is dislodging, the relationship is changing. This change in behavior was critical to prove that the force-displacement relationship is an effective measurement tool to identify undesirable changes in the system

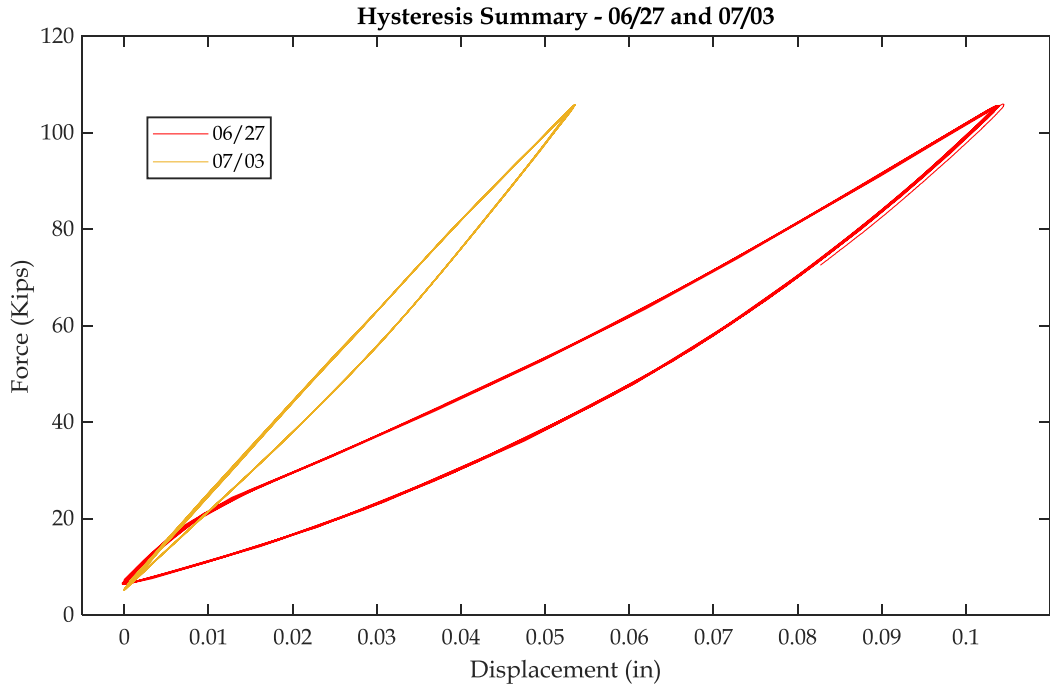


Figure 49 - Hysteresis Loop Recorded During Fatigue Testing on June 27, 2018 and July 3, 2018

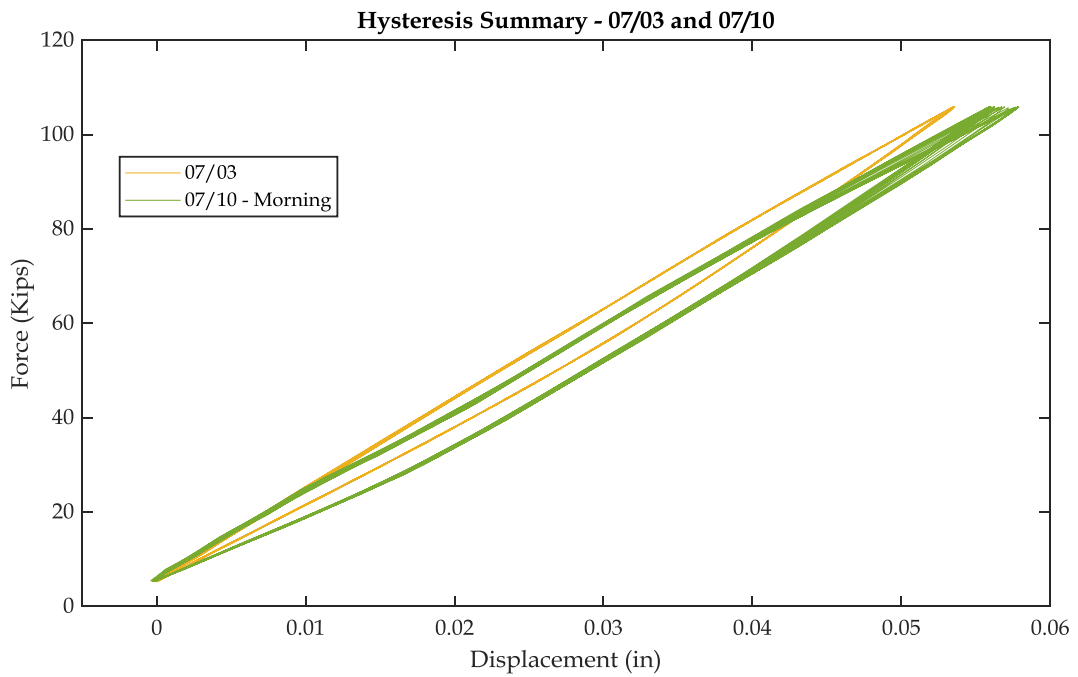


Figure 50 - Hysteresis Loop Recorded During Fatigue Testing on July 3, 2018 and July 10, 2018

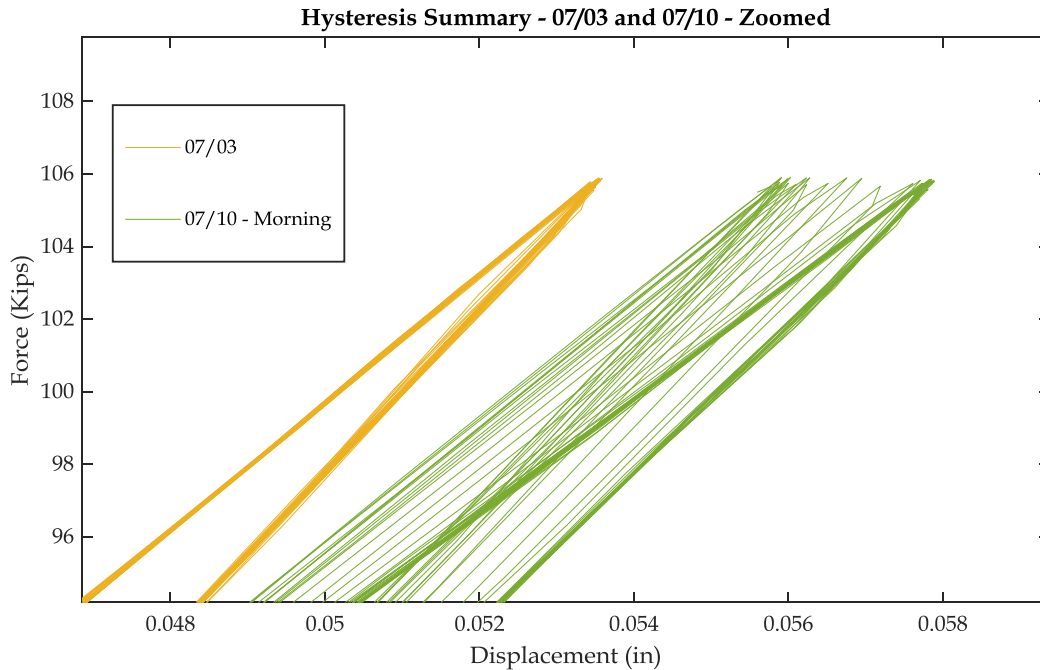


Figure 51 - Close up View of Hysteresis Loop Recorded During Fatigue Testing on July 3, 2018 and July 10, 2018

4.4 Summary

With a large-scale experimental setup, particularly one designed for fatigue testing, it is critical to ensure that there is consistency during the testing. In this study, this was accomplished using a systematic monitoring protocol to monitor the entire test setup. This protocol was developed with the design goals of consistency, reliability, and efficiency. For these reasons the characterization and structural monitoring of the test setup was done in two ways, a detailed, full characterization, in the form of the S-ID, and a representative measurement, in the form of the actuator force-displacement hysteresis.

The results from the S-ID characterized the structural response of the entire test setup at critical locations. From this characterization, the behavior of the test setup was monitored and periodically checked for changes. Although there were slight differences between each characterization, the overall behavior was consistent throughout the test.

The force-displacement relationship was used as a fast way to detect changes in the behavior of the test setup. It was found that the physical changes to the test setup had a clear effect on the force-displacement relationship. These changes justify the use of this measure as a representative, quantitative, measurement of the overall system. After some initial changes near the beginning of the overall fatigue test, the force-displacement relationship reflected the consistency of the test setup over the time frame between July 11, 2018 and October 30, 2018.

5. FINITE ELEMENT MODELING

This chapter further discusses the need for finite element modeling of the fatigue test and setup. The chapter introduces the developed model of the test setup and discusses the modeling technique and assumptions made. Lastly, the results from the numerical analysis are introduced and briefly discussed.

5.1 Finite Element Modeling

The use of finite element modeling was a powerful tool to estimate behaviors and structural responses of various components such as the specimen and test setup used in this project. A numerical model might not be a perfect representation of an actual test due to the idealistic conditions assumed in modeling, but it can still be used as a way to estimate structural behavior. With such a geometrically complex test specimen, it is important to be able to have a theoretical comparison point for the measurements being recorded. Additionally, understanding the stress distribution in this complex specimen is critical in order to maximize the efficiency of the instrumentation of the test setup. Lastly, numerical models can be used to investigate the effect of different changes to boundary conditions in the test setup and aid in decision making in terms of potential modifications to the test setup.

Although there are many benefits to having a numerical model, the results must be examined with caution. It is important to be able to distinguish whether or not the numerical results are true, or a close representation of reality. Often times, a complex numerical model contains sharp geometries and transitions which can result in spurious results in the form of stress concentrations. For this reason, engineering judgement must be used when using numerical models for analysis.

5.2 Fatigue Test Specimen Finite Element Model

In this project, multiple finite element models (FEM) of the specimen as well as portions of the test setup were developed and refined using ABAQUS® CAE/2017 [29]. The models were created in order to estimate stresses and strains in the specimen as well as the overall structural response of the test setup. As noted in Section 3.5, the original model of the specimen was used to estimate the overall stress contours to determine the locations of interest for the instrumentation. In this chapter, the model is expanded to include a more detailed model of the welds in the specimen, the actuator swivel, the support bracket, the rigid floor, and the bolts throughout the test setup. The goal of this more detailed model is to create a numerical model of the test setup and understand the true behavior of the boundary conditions not just the specimen. The results of the finite element analysis (FEA) are compared to the actual measurements from the test in Section 6.2 to verify the structural response of the model.

The FEM, shown in Figure 52, consists of four main parts: actuator swivel, specimen, bracket, and rigid floor. The connection specimen consists of a vertical attachment plate on the actuator side, the front-top flange, the web, the bottom flange, the back-top flange, and the vertical attachment plate on the bracket side, and welds between all of these parts. The geometry of the fabricated parts are the same as those shown in Figure 11.

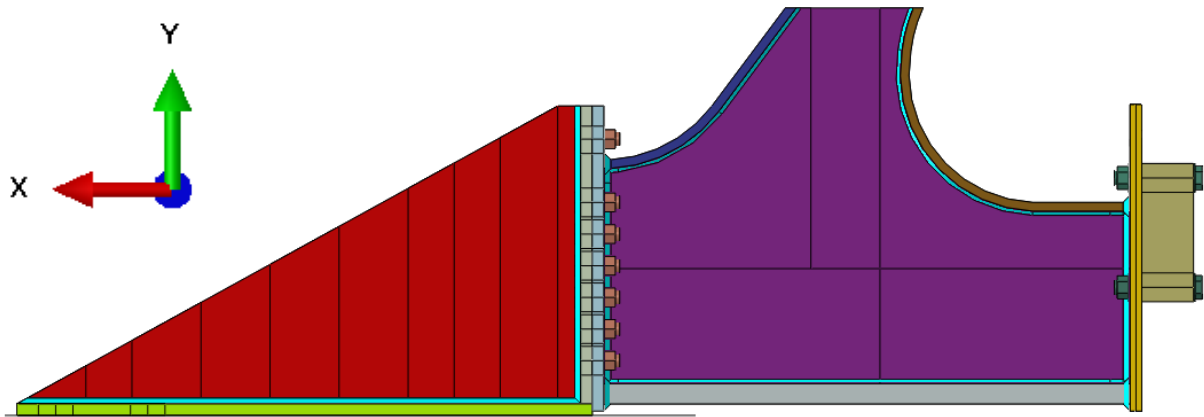


Figure 52 - Finite Element Model of Experimental Test Setup in Abaqus

The interaction between the different components was chosen carefully to give a realistic response. The specimen components are connected by the weld surfaces with a tie constraint. This means that the parts are not bonded to each other directly, but the weld is bonded to each of the individual parts. In addition to this, the only interaction between the individual parts is modeled with surface-to-surface contact. These interactions were chosen to simulate the most realistic transfer of stresses through the specimen, which would be through the weld itself or via contact between the various components of the model at their intersections. This modeling technique also allows for a better estimate of the stress distribution through the weld geometry. The same approach was taken when modeling the support bracket, all forces are transferred through the welds or through part to part contact.

Further, the bolted connection of the specimen to the actuator swivel, as well of the specimen to the bracket, are simulated in the numerical model. Each bolt is modeled as a single solid part consisting of the bolt (shaft and hex-head), one washer on either end, and the hex-nut. The bolt's interactions with each individual component are modeled as surface-to-surface contact using the washer surfaces as the contact surface to the individual parts. This interaction was chosen to simulate the interaction between parts including their potential separation or loss of contact, whereas the tie constraint would simulate the components working as a unit. The last modeled interaction is between the bottom of the support bracket and the rigid floor. This interaction is modeled as a frictionless "hard" contact between the bottom surface of the support bracket and the top surface of the rigid floor. The frictionless "hard" contact interaction allows the bracket to press against the rigid floor without penetrating it or having any frictional force generated between the two surfaces.

The boundary conditions of the FEM were chosen to be representative of those present in the experimental test setup. Boundary conditions are applied at four locations in this FEM; the swivel's center of rotation, the bottom surface of the vertical attachment plate on the actuator side, the surface of the rigid floor, and the locations of the anchor holes in the bracket.

The actuator swivel is restrained from rotation about the X, Y, and Z directions and allowed to translate in the X, Y, and Z directions. These restraints were selected to simulate the swivel, which has its orientation locked in place, preventing any rotations during loading. This boundary was

applied by coupling a reference point, located at the center of rotation of the swivel geometry, with the swivel, and restraining the rotations of this reference point, but allowing it to translate freely.

The bottom surface of the vertical attachment plate on the actuator side is restrained from rotation about the Z direction and restrained from translations in the Y direction. These restraints are representative of the metal shim supports that are under this vertical plate, these shims slide on top of each other while restraining any vertical (Y direction) movement and preventing rotation. This boundary was applied by coupling a reference point to the bottom surface of the vertical attachment plate and restricting the rotation about the Z direction and the translations in the Y direction of the reference point.

The bracket is restrained from translations and rotations at the location of the anchors. This is meant to simulate the near fixed-end condition created by the four anchors at the end of the bracket. This was accomplished by coupling the inner surfaces of the anchor holes to reference points located in the center of the circular holes and restraining all translations and rotations.

Lastly, the rigid floor is restrained in all directions against translations and rotations to simulate the actual floor under the test setup. This was applied by coupling a reference point to the entire bottom surface of the rigid floor and restraining all translations and rotations.

The loading protocol is implemented in the numerical model in two steps; the pre-tensioning step, and the static loading step. The pre-tensioning step is created to simulate the application of the bolt loads generated from tightening the bolts that connect the various components together, as discussed previously, while the static loading step is meant to simulate the fatigue loading. These two steps were created to give a better approximation of the behavior of the test setup, including the behavior during installation (pre-tensioning step), and not just the specimen under idealized initial conditions and fatigue loading. Additionally, since the instrumentation, namely the strain gauges, are calibrated when the specimen is uninstalled, this approach provides a more representative comparison to the measured data.

As mentioned, the pre-tension step occurs first. In this step a pre-tension load is applied to the bolts, creating a clamping force on the two components that the bolt is connecting. This is meant to be consistent with the actual axial force applied to these bolts. This force was estimated by converting an applied torque of 800 ft-lb to an axial force which was then applied to each bolt in the FEM through the bolt-load option in Abaqus. The way that the bolt-load applies a force is by pulling the bolt-head and nut towards the center of the bolts, simulating a tension force on the bolt which causes it to clamp the parts that it is in contact with. Once the pre-tensioning of the bolts is completed, the static loading step is performed.

In the static loading step, a 100 kip ramp tensile load in the X direction, is applied to the actuator swivel. The load applied is equivalent to the loading range applied to the specimen during a fatigue test, from a minimum of 5 kip to maximum of 105 kip. The load is applied by applying a point load of 100 kip to a reference point coupled to the swivel. The forces are then transferred from the swivel to the bolts and finally into the specimen.

The overall meshed model is shown in **Error! Reference source not found.** In this model, three element types were used throughout the assembly depending on the geometry and part type. The three elements used were the following; linear hexahedral elements – C3D8R, quadratic tetrahedral elements – C3D10, and linear quadrilateral elements – R3D4.

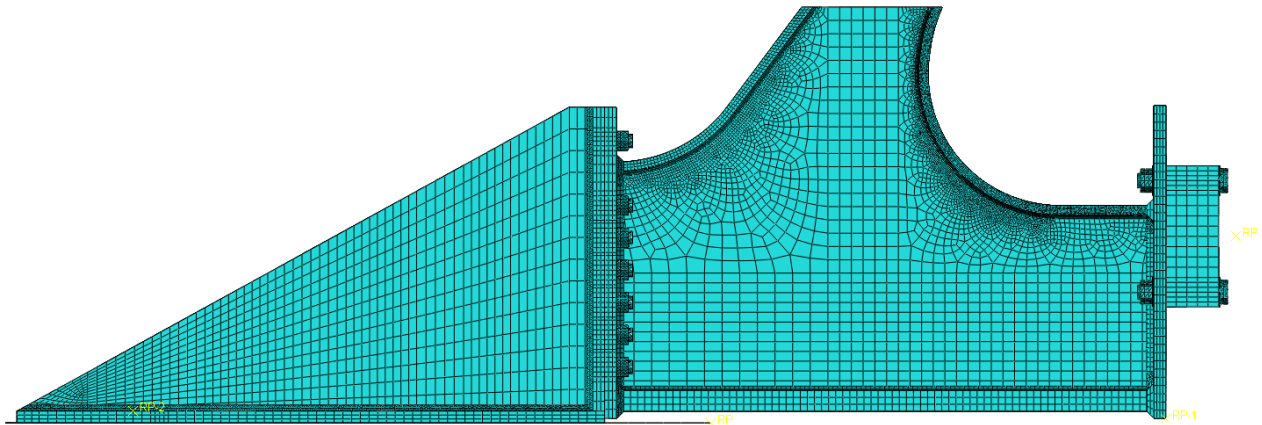


Figure 53 - Meshing of Entire Model in Abaqus

The most commonly used element was the C3D8R element, totaling at 226,228 elements. This element was used as the default element where the geometry was compliant with the restrictions of the Abaqus mesh generation. This element is a linear hexahedral element with eight nodes, each node having three translational degrees of freedom. Generally, the model was partitioned in such a way to allow transitions from regions of fine mesh sizes to larger sizes. Additionally, the partitions serve to manipulate the geometry and change the mesh type in a region. The second most commonly used element was the C3D10 element, totaling at 38,525 elements. This element was primarily used in regions of complex geometry where the hexahedral mesh would not work. This element is a quadratic tetrahedral element with 10 nodes, each node having three translational degrees of freedom. Lastly, 6,240 R3D4 elements were used to model the rigid floor. This element is a rigid linear quadrilateral element with four nodes. In total, the current model has 270,993 elements and the total analysis time was approximately 90 minutes using a direct solver. This mesh was the result of a meshing sensitivity analysis in which many mesh sizes and types were used to find a balance between resolution, accuracy, and analysis time.

5.3 Results from the Finite Element Model of the Fatigue Specimen and Test Setup

The finite element model used in this project required several levels of refinement prior to achieving an acceptable representation of the fatigue specimen and test set up. It should be noted that calibration of the numerical model was not within the scope of this project. The fatigue test and modeling were performed simultaneously and separately, meaning the model used was a blind analysis.

The following figures will show the results from the numerical analysis using the previously described loading protocol. Figure 54 shows the overall displaced shape of the model, and Figure 55 shows the deflected shape of just the specimen portion of the model. Both deflected shaped are visually magnified by a factor of 100, for display.

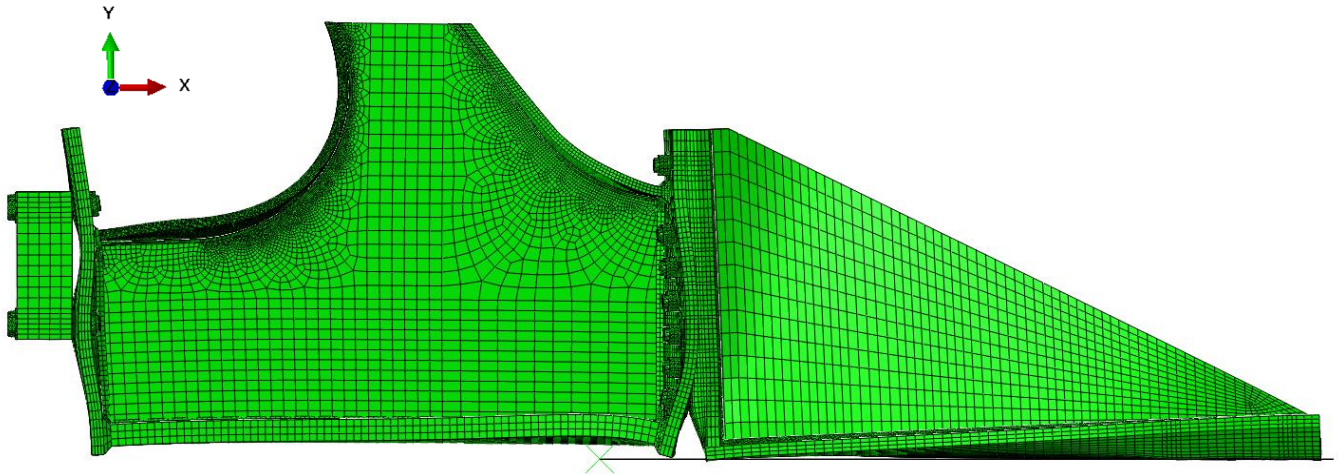


Figure 54 - Predicted Deflected Shape of the fatigue specimen and test set-up

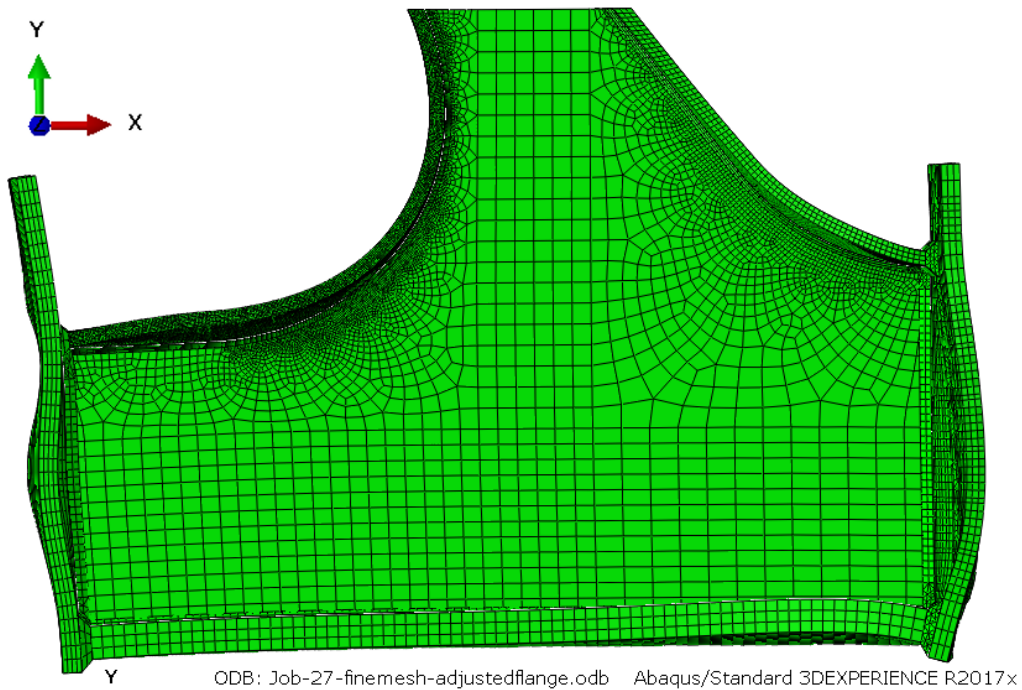


Figure 55 - Predicted Specimen Deflected Shape of the Fatigue Specimen

As a comparison, the principal stress contour of the web portion of the numerical model used in this study is shown in Figure 57 and the contour developed by HNTB Corporation during the design of the Memorial Bridge is shown in Figure 56. The magnitudes of the stresses are different, but the general shape of the contours is noted as similar.

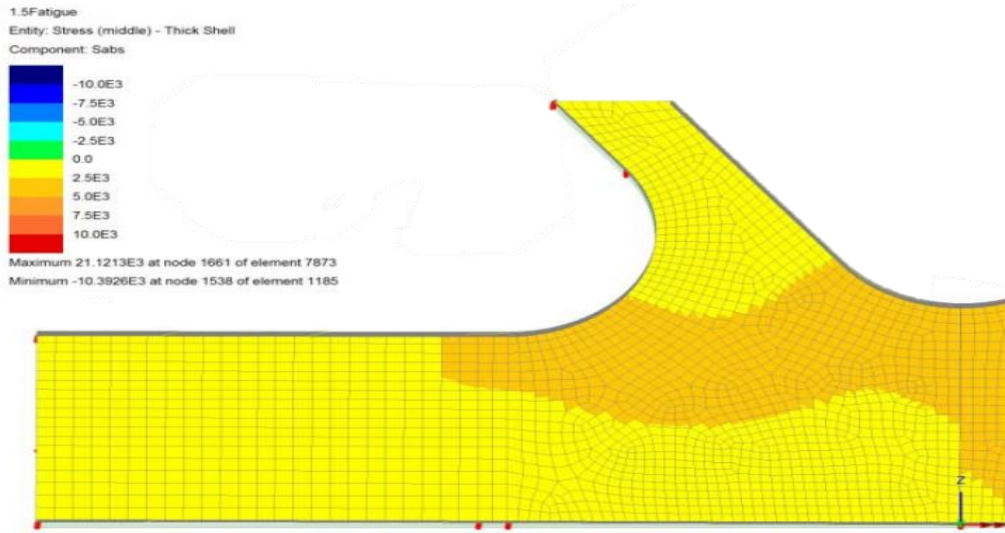


Figure 56 - Design Stress Contour for the Gusset-less Connection at the Memorial Bridge from HNTB Corporation

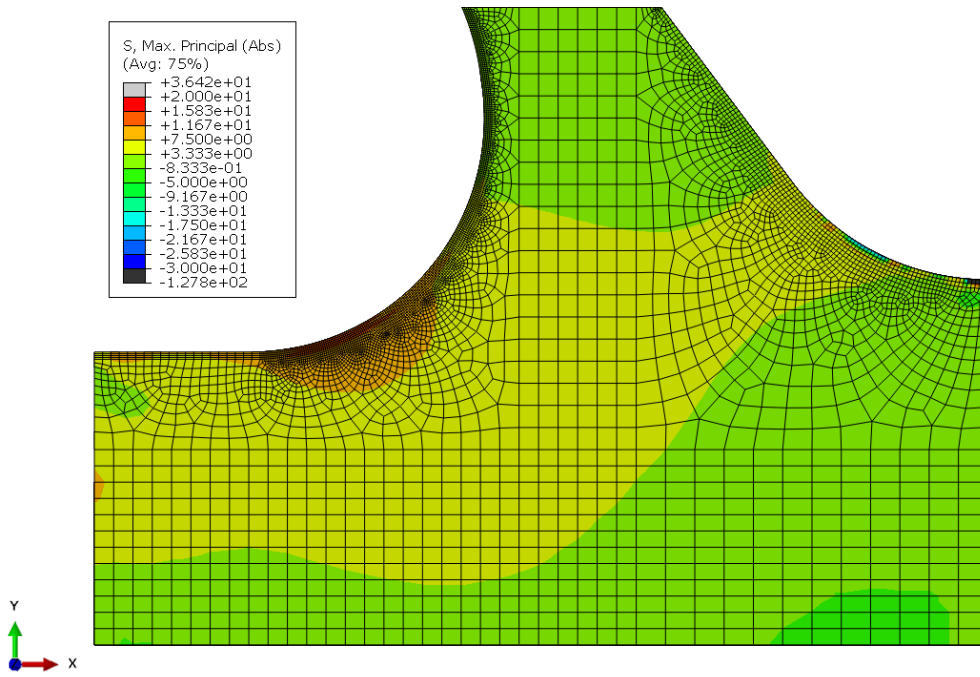


Figure 57 - Predicted Web Max Principal Stress (Absolute) for the Gusset-less Connection at the Memorial Bridge

Figure 58 and Figure 59 show the absolute maximum principal stress contour in the test specimen portion of the model and the area of interest (AOI) respectively. It should be noted that some stress concentrations were located away from the area of interest, for this reason the stress contour was limited to -25 ksi to 25 ksi to show the relative contour without the effect of the stress

concentrations in Figure 58. Additionally, the stress ranges for each of the two figures are different in magnitude despite having the same color scheme.

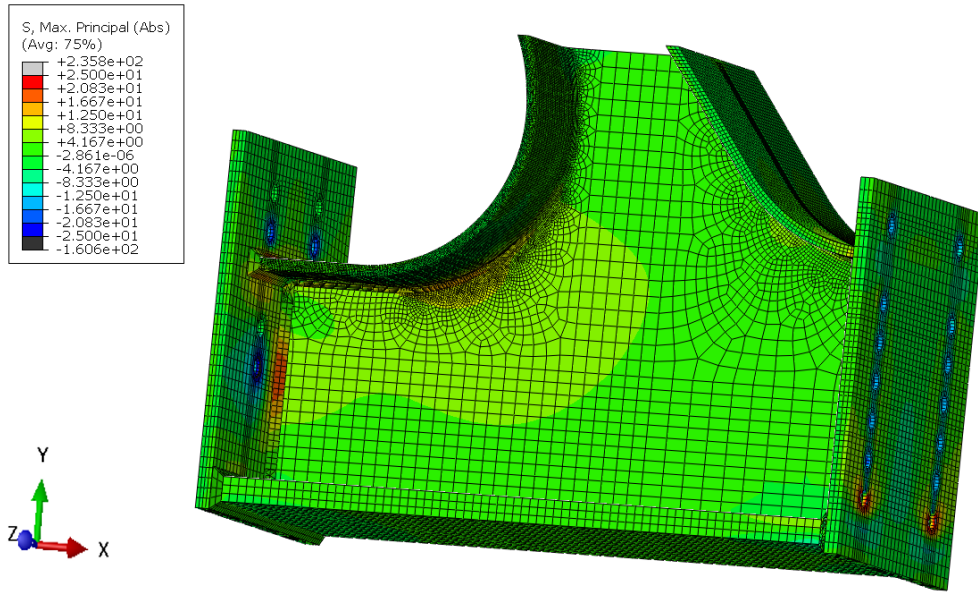


Figure 58 - Predicted Specimen Max Principal Stress (Absolute) Under Laboratory Loading Conditions of the Fatigue Specimen

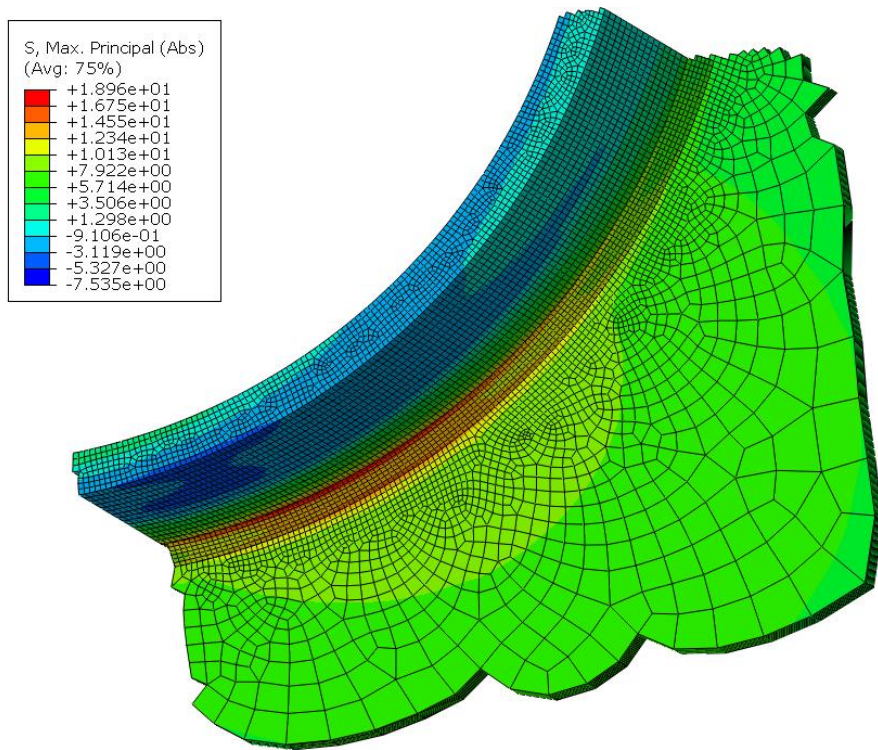


Figure 59 - Predicted AOI Max Principal Stress (Absolute) Under Laboratory Loading Conditions of the Fatigue Specimen

Figure 60 and Figure 61 show the elastic strain contours in the x-direction of the overall specimen model and the area of interest respectively. In a similar fashion to the previous contours, the contour limits were set to ignore the concentrations present in areas away from the AOI in the specimen figure.

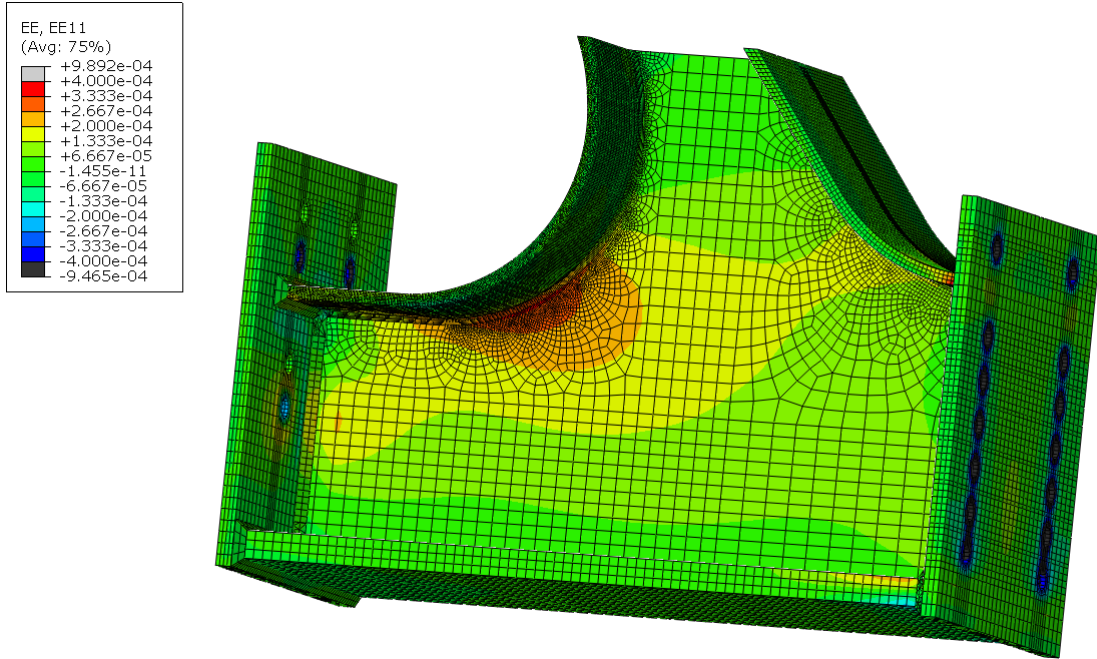


Figure 60 – Predicted Specimen Horizontal Strain Under Laboratory Loading Conditions of the Fatigue Specimen

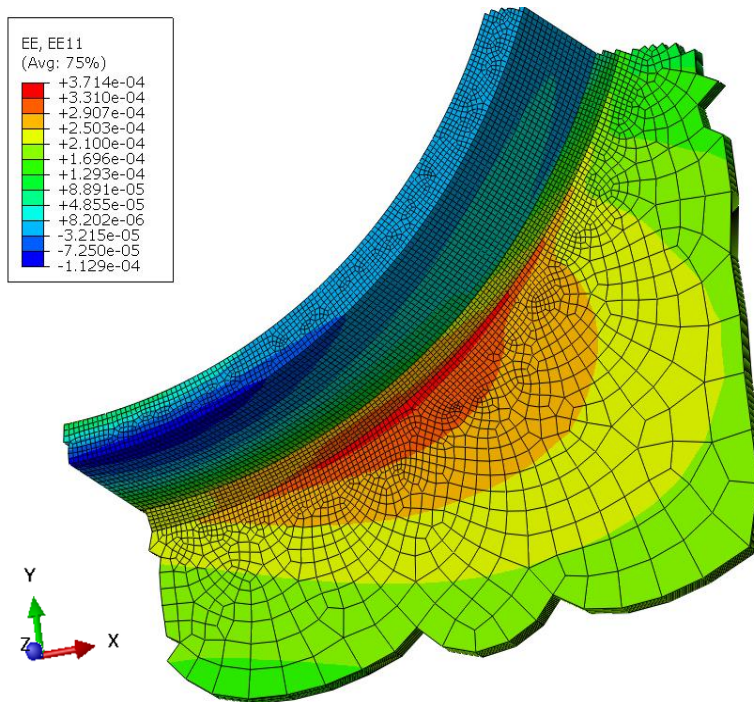


Figure 61 – Predicted AOI Horizontal Strain Under Laboratory Loading Conditions of the Fatigue Specimen

Finally, Figure 62 and Figure 63 show the elastic strain contours in the y-direction of the overall specimen model and the area of interest respectively, with the same caveat of limiting the contours for the specimen model to avoid concentrations.

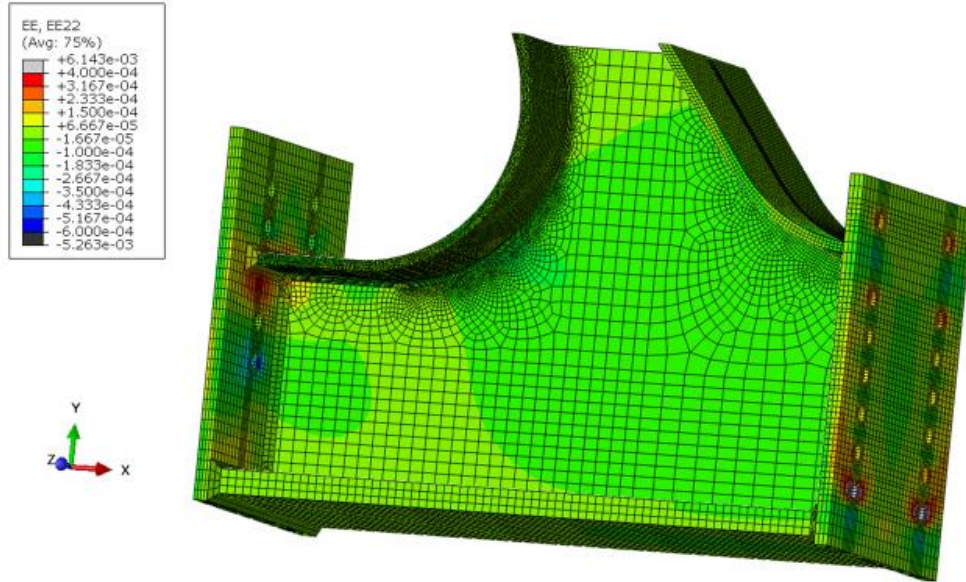


Figure 62 – Predicted Specimen Vertical Strain Under Laboratory Loading Conditions of the Fatigue Specimen

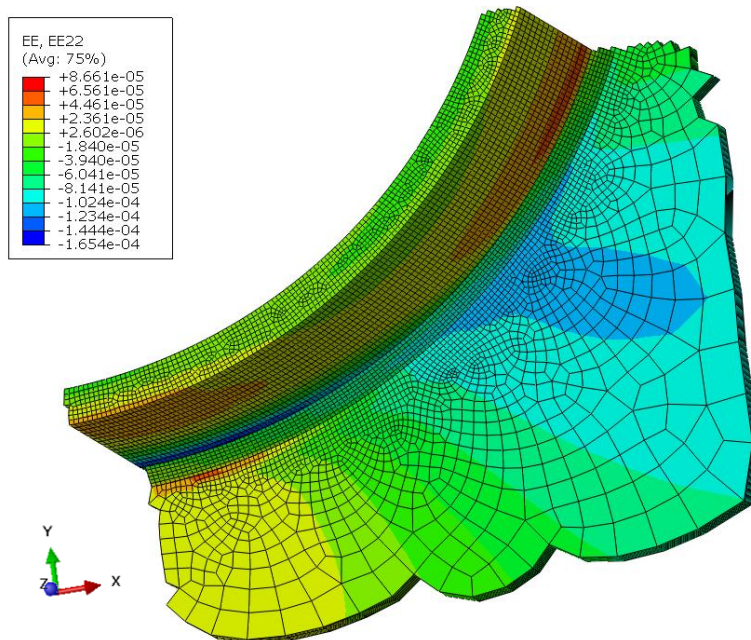


Figure 63 – Predicted AOI Vertical Strain Under Laboratory Loading Conditions of the Fatigue Specimen

5.4 Recommendation for Gusset-less Connection Inspection

Based on the results of the finite element model, the critical areas for visual inspection of the gusset-less connection are shown in Figures 59, 61, and 63. These areas, which are all focused in the region of the radiused weld as expected, are predicted to experience the highest level of stress. The weld at these locations should be visually inspected and periodically inspected with nondestructive evaluation techniques, such as magnetic particle. Given the performance of the fatigue test specimen, presented in Chapter 6, the period and frequency of any nondestructive evaluation assessment could exceed ten years without concern of fatigue performance of the connection but should be ultimately determined based on the judgement of the NHDOT.

5.5 Summary

The strains obtained from the numerical model can be compared to the measurements from the experimental fatigue test. This comparison will provide insight into how closely this model represents reality. Once the model has been verified, it can be used to estimate stresses and strains in and around the radiused fillet weld itself. This analysis will help supplement the information obtained from measurements as only strain data adjacent to the weld can be obtained experimentally.

6. FATIGUE TESTING RESULTS

This chapter will briefly reintroduce the fatigue loading protocol and reiterate the design criteria for the connection. Performance expectations are also discussed. Next, the results from the fatigue test, in terms of measured strains from the strain gauges and the 2-D DIC in the area of interest, are introduced and discussed. Lastly, a comparison between the measured response and the theoretical response from the numerical model is evaluated.

6.1 Introduction

The objective of the fatigue testing was to investigate the fatigue performance of the gusset-less truss connection used in the Memorial Bridge. Since the connection has such a unique geometry, there was no specific category for the critical fatigue location, which was the radiused weld connecting the curved top flange to the web. For this reason, a design assumption was made to conservatively categorize the region of interest as fatigue category C. With this assumption, and the calculated stresses from the controlling fatigue load combination for the Memorial Bridge, the gusset-less connection is expected to have infinite life because the design stresses, approximately 4 ksi, are well below the endurance limit of 10 ksi for fatigue category C [1]. Therefore, to investigate this assumption, it was critical induced stresses to the fatigue specimen that were greater than those experienced by gusset-less connections in the Memorial Bridge.

The cyclic loading protocol used in this fatigue test was previously described in Section 3.4, but is repeated here for convenience;

- Mean axial load applied: 55 kip
- Cyclic amplitude: ± 50 kip
- Cyclic frequency: 3.5 Hz
- Applied function: Sine wave

With the applied loading, the numerical model predicts principal stresses of approximately 14 ksi close to the toe of the weld. Although this stress is higher than the endurance limit for the fatigue category C, the stress predicted is better described as a hot-spot stress due to its proximity to the weld toe. Therefore, the comparison of a hot-spot stress to the S-N curves derived using nominal stresses, is considered conservative. Using this “hot-spot” stress at the weld toe and applying it to the S-N curve for the design category, the expected cycles to failure would be 1,600,000 fatigue cycles. At the time of this preparing this section of the report, the specimen has undergone a total of 1,602,300 fatigue cycles.

6.2 Strain Gauge Results

This section presents the results from the fatigue testing in terms of recorded strains in the area of interest. The strain gauge results presented will be measurements from three testing sessions spaced over the course of the overall fatigue test. The goal of showing the results in this manner is to make a comparison of the cyclic strain range applied to the specimen throughout the fatigue test. The testing periods will be labeled by the date on which they were performed;

- Test period 1: July 17, 2018, Cumulative fatigue cycles; 178,831
- Test period 2: August 29, 2018, Cumulative fatigue cycles; 880,014
- Test period 3: October 30, 2018, Cumulative fatigue cycles; 1,602,287

In terms of fatigue testing, the strain of interest is the maximum principal strain. For this reason, all comparisons to the S-N curve were performed using the principal strains calculated from the rosettes or obtained from the DIC. Just for the sake of comparison, with respect to each other, the strain gauge results are shown in terms of the horizontal, diagonal, and vertical strain components. Before the comparison between different test periods takes place, the overall structural response of the specimen in the area of interest is assessed. Figure 64 shows the horizontal strain measurements of the gauges NRW1, NRW2, and NRW4. These rosettes are the gauges that are placed along the curved weld, close to the toe of the weld. As the figure shows, the horizontal strain range increases as the measurement is taken along the length of the weld. In other words, NRW1 had the smallest strain range while NRW4 had the largest, with a 35% increase in the measured horizontal strain range between the two rosettes.

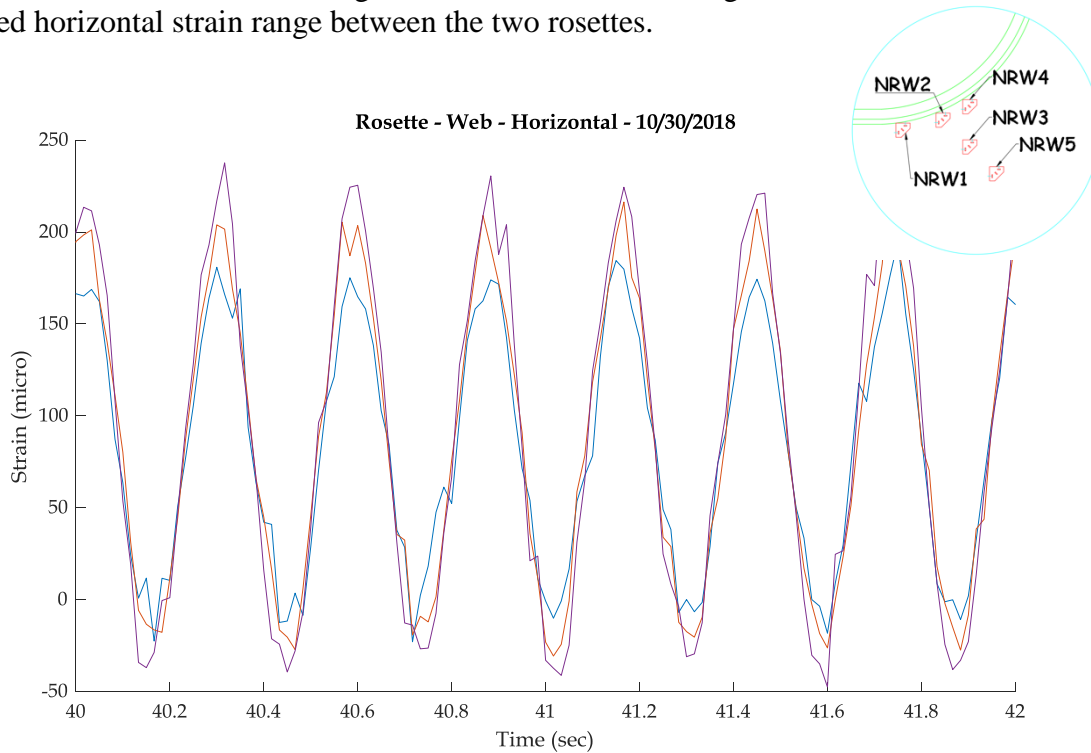


Figure 64 - Horizontal Strain Pattern Along Weld Toe

Similarly, Figure 65 shows the horizontal strain components of the gauges NRW2, NRW3, and NRW5. These gauges are placed on the same line perpendicular to a tangent at the weld toe, at varying distances from the toe of the curved weld. These measurements show that as the distance from the weld toe increases, the strain range measured decreases. In this case, the reduction in the measured horizontal strain range from NRW5 compared to NRW2 is approximately 33%. Based on the observed patterns, the critical location, in terms of the discrete measurements taken from the rosettes, for fatigue is NRW4. This gauge shows the highest strain range measured, as well as the highest mean strain compared to the other gauges in the area of interest. It is important to note, that this is also confirmed from the supplementary rosettes located on the South-face of the specimen. Of these rosettes, SRW4, corresponding to the same geometric location as NRW4, is the critical strain gauge. It should also be noted that there are slight differences in the mean stress levels between the strain gauges located on the North and South faces of the specimen.

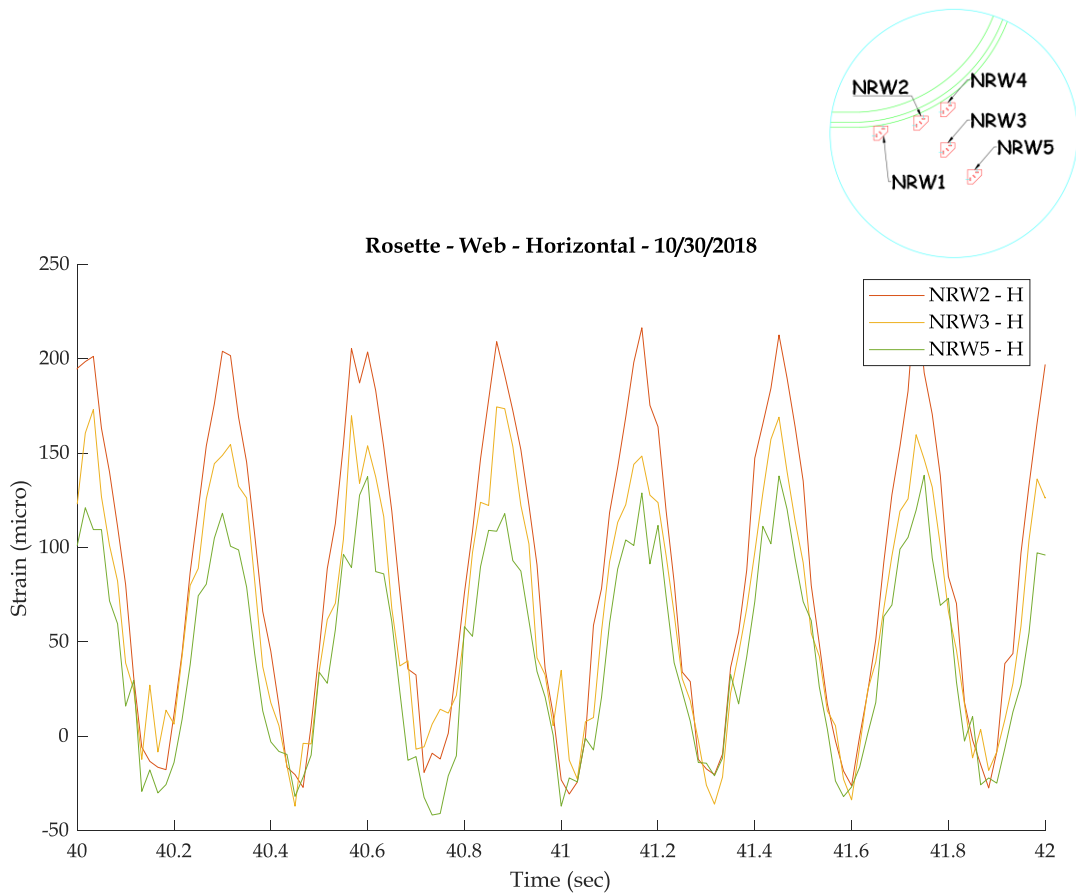


Figure 65 - Horizontal Strain Pattern Recorded Away from Weld Toe from the Fatigue Specimen on October 30, 2018

Figure 66 shows a comparison between the horizontal strain component of NRW4 and SRW4. As the figure shows, the magnitude of the strains measured are approximately 70 micro-strain different, with the South side rosette being higher. An important consideration is that the strain range is approximately identical for both gauges; there just appears to be a shift in the response based on the side that the rosette is located on. A similar pattern exists for the other rosette comparisons between the two sides, with the shift ranging from 60 to 90 micro-strain but the range staying approximately the same.

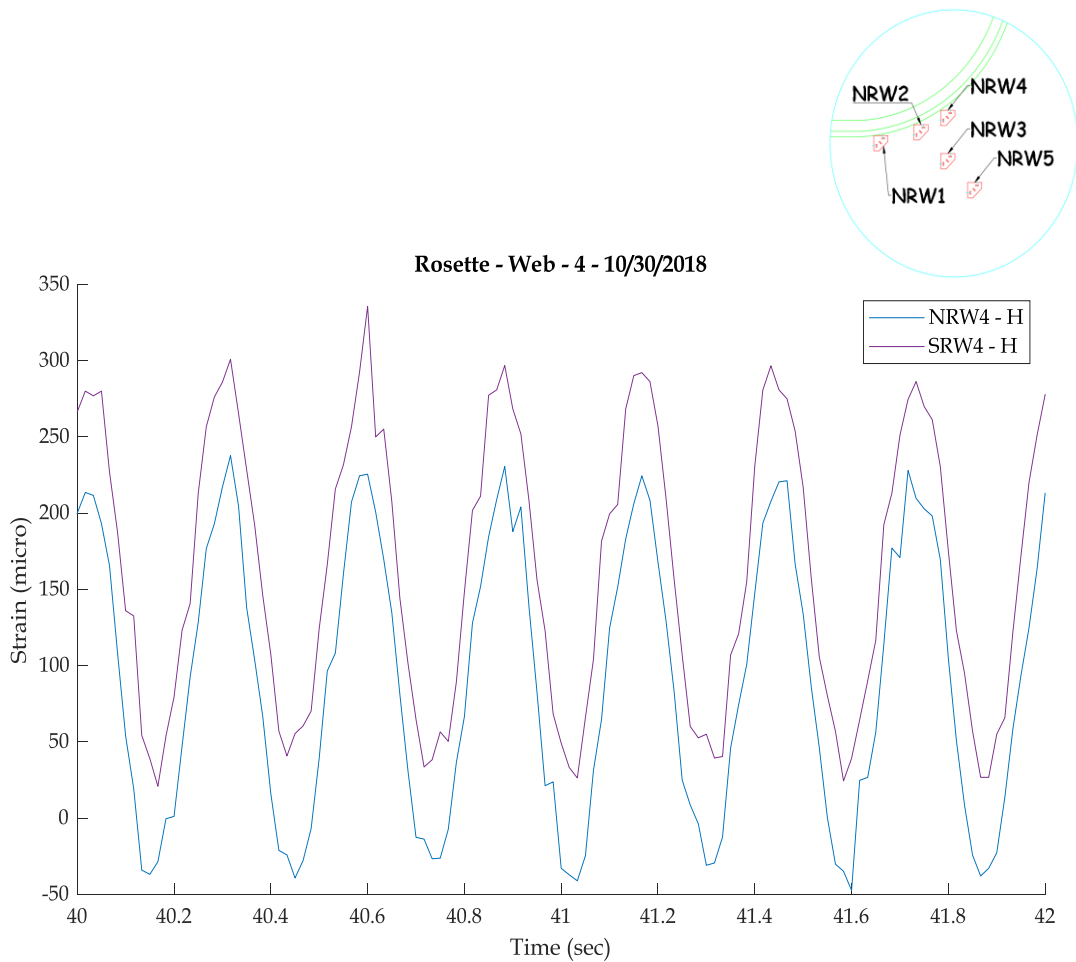


Figure 66 - Horizontal Strain Recorded at the Web of Both Faces of the Fatigue Specimen on October 30, 2018

Knowing that the critical location corresponds to NRW4, the comparison between test dates will focus on the results from this strain gauge. Figure 67 shows the horizontal strain component of NRW4 at the three previously mentioned testing intervals. As the figure shows, the results from the first two test intervals (July 17, 2018 and August 29, 2018) match closely, while the data from the final interval (October 30, 2018) is slightly offset from the previous. This offset is approximately 65 micro-strain, and across all horizontal components of the rosettes, the average decrease is 38 micro-strain. The average change in the range of horizontal strains is approximately 1 micro-strain, which is at the level of noise. A similar pattern can be seen in Figure 68, which shows the vertical strain component of NRW4 at the three testing intervals. The vertical strain measured is approximately 40 micro-strain less on the final interval compared to the previous two. Across all rosettes, the average decrease in the vertical strain component is 54 micro-strain, with an average change in the vertical strain range of 6 micro-strain. This shows that there is a clear shift in the response, but the range of strains is still consistent between the tests. The pattern is similar in the final, diagonal, component of NRW4, which across all rosettes has an average shift of 42 micro-strain and an average change in the strain range of 6 micro-strain. Overall, there is a clear shift in the response across all the rosettes, but the range of applied strains are still consistent.

In fatigue, as previously mentioned, the most influential parameter is the applied stress range, so it is very important to consistently apply the same stress range across all testing periods.

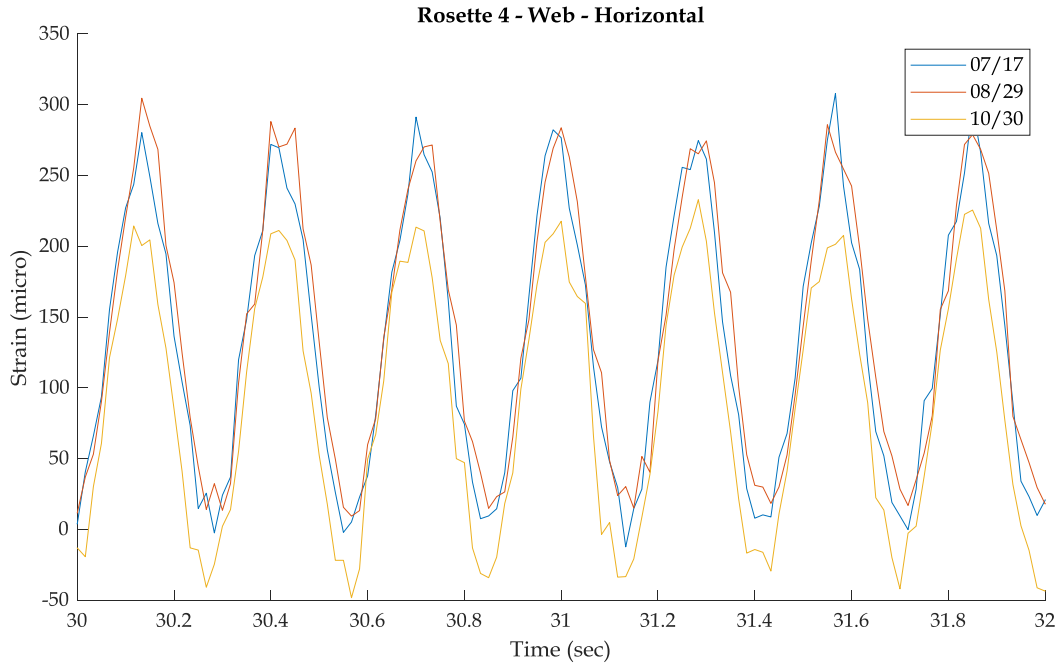


Figure 67 - Horizontal Strain Comparison Recorded from the Fatigue Specimen on July 17, 2018, August 29, 2018 and October 30, 2018

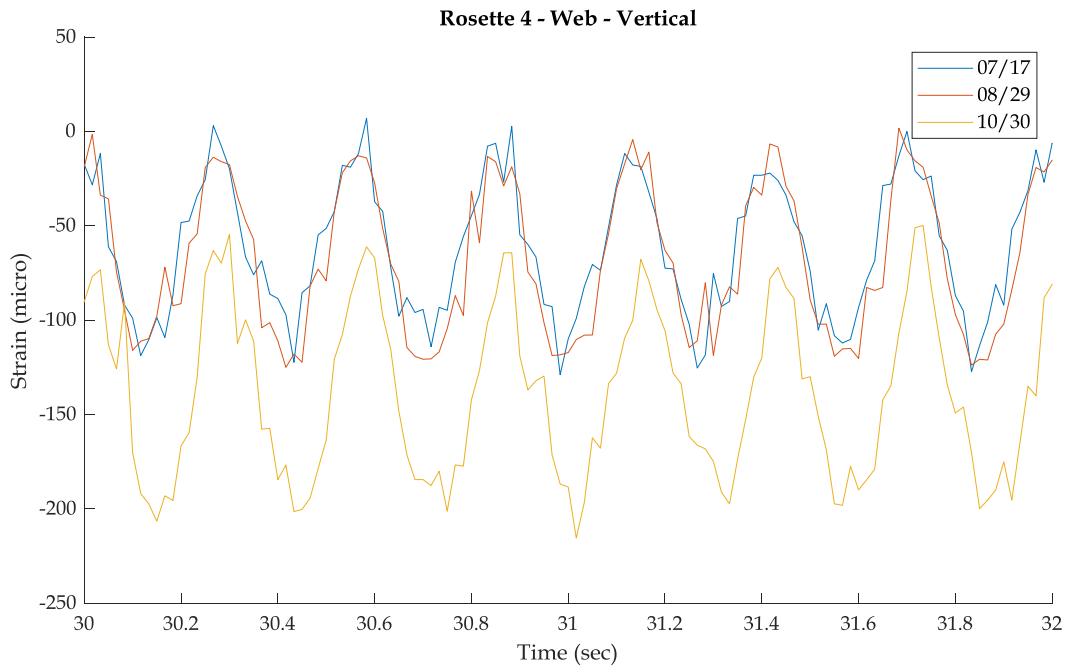


Figure 68 - Vertical Strain Comparison Recorded from the Fatigue Specimen on July 17, 2018, August 29, 2018 and October 30, 2018.

Table 5 through Table 9 summarize the results from the five rosettes in the area of interest across the three test periods.

Table 5 - NRW1 – Test Interval Comparison

Measure ($\mu\epsilon$)	NRW1			
	Date			
	07/17/18	08/29/18	10/30/18	Average
Max. Horizontal Strain	232	243	196	224
Min. Horizontal Strain	19	32	-15	12
Horizontal Strain Range	213	211	211	212
Mean Horizontal Strain	125	138	90	118
Max. Vertical Strain	14	2	-28	-4
Min. Vertical Strain	-60	-51	-96	-69
Vertical Strain Range	74	53	68	65
Mean Vertical Strain	-23	-24	-62	-36
Max. Diagonal Strain	186	189	140	171
Min. Diagonal Strain	-25	-19	-54	-33
Vertical Diagonal Range	211	207	193	204
Mean Diagonal Strain	80	85	43	69

Table 6 - NRW2 - Test Interval Comparison

Measure ($\mu\epsilon$)	NRW2			
	Date			
	07/17/18	08/29/18	10/30/18	Average
Max. Horizontal Strain	254	262	232	249
Min. Horizontal Strain	-9	9	-31	-10
Horizontal Strain Range	263	253	263	260
Mean Horizontal Strain	123	135	101	120
Max. Vertical Strain	2	0	-58	-19
Min. Vertical Strain	-67	-70	-128	-88
Vertical Strain Range	69	70	70	70
Mean Vertical Strain	-32	-35	-93	-53
Max. Diagonal Strain	179	166	140	162
Min. Diagonal Strain	-28	-39	-69	-45
Vertical Diagonal Range	207	205	208	207

Mean Diagonal Strain	76	64	36	58
----------------------	----	----	----	----

Table 7 - NRW3 - Test Interval Comparison

NRW3				
Measure ($\mu\epsilon$)	Date			
	07/17/18	08/29/18	10/30/18	Average
Max. Horizontal Strain	207	223	185	205
Min. Horizontal Strain	-10	10	-30	-10
Horizontal Strain Range	216	213	215	215
Mean Horizontal Strain	99	117	77	97
Max. Vertical Strain	20	34	-45	3
Min. Vertical Strain	-31	-22	-104	-52
Vertical Strain Range	50	56	59	55
Mean Vertical Strain	-6	6	-74	-25
Max. Diagonal Strain	178	187	157	174
Min. Diagonal Strain	-18	-14	-41	-24
Vertical Diagonal Range	197	201	199	199
Mean Diagonal Strain	80	87	58	75

Table 8 - NRW4 - Test Interval Comparison

NRW4				
Measure ($\mu\epsilon$)	Date			
	07/17/18	08/29/18	10/30/18	Average
Max. Horizontal Strain	291	305	233	276
Min. Horizontal Strain	-2	17	-44	-10
Horizontal Strain Range	293	288	277	286
Mean Horizontal Strain	145	161	95	133
Max. Vertical Strain	7	-4	-48	-15
Min. Vertical Strain	-114	-120	-179	-138
Vertical Strain Range	121	116	131	123
Mean Vertical Strain	-54	-62	-114	-76
Max. Diagonal Strain	108	129	71	103
Min. Diagonal Strain	-34	-29	-78	-47
Vertical Diagonal Range	142	158	149	150
Mean Diagonal Strain	37	50	-3	28

Table 9 - NRW5 - Test Interval Comparison

Measure ($\mu\epsilon$)	NRW5			
	Date			
	07/17/18	08/29/18	10/30/18	Average
Max. Horizontal Strain	181	177	151	170
Min. Horizontal Strain	7	9	-28	-4
Horizontal Strain Range	174	168	179	174
Mean Horizontal Strain	94	93	61	83
Max. Vertical Strain	23	54	-14	21
Min. Vertical Strain	-39	-13	-83	-45
Vertical Strain Range	62	67	69	66
Mean Vertical Strain	-8	20	-49	-12
Max. Diagonal Strain	195	234	147	192
Min. Diagonal Strain	-19	13	-58	-21
Vertical Diagonal Range	213	222	205	213
Mean Diagonal Strain	88	124	44	85

Additional plots of the strain gauge responses are shown in Appendix F.

6.3 Digital Image Correlation Displacement Measurements

This section will introduce and discuss the measurements obtained from the 2-D DIC applied to the area of interest. Unlike the previous section, only one testing period is shown and comparisons to the strain gauge measurements are conducted. Before presenting the measurements from the post-processed images, a brief overview of the methodology used, and the parameters selected for post-processing will be provided. Firstly, the software used for the post-processing of the raw image files in this study was VIC-2D 2009 [44]. Within this software there are a few key variables that must be chosen to provide a consistent and accurate correlation. The first is the subset size, or the area used to track the pixel movement across successive images. The size of the subset is directly related to the spatial resolution of the analysis, in which as the subset size increases, spatial resolution is lost due to the averaging effect of the subset tracking. Additionally, the step size factors into the resolution and run-time because it controls how often, in terms of pixels, the correlation is performed. If a higher step-size is chosen, the correlation will be performed less often. Next, the correlation options must be chosen in terms of interpolation, correlation criterion, and subset weights. A higher order interpolation provides more accurate results at the cost of analysis time. The correlation criterion is the statistical method to determine a match for the tracking, the default of normalized squared differences is suggested due to its stability with respect to changes in lighting. The subset weights determine how the movement within a subset is weighted for the analysis, either uniformly across the subset, meaning that each pixel has the same effect, or center-weighted, meaning as the pixels get closer to the edge of the subset their

movement has less effect on the overall movement. Lastly, the strain tensor is chosen along with the filter size and type. The strain tensor defines the calculation type, while the filter options how the data is averaged and over what area. The key parameters used in this study were determined through a sensitivity analysis and are as follows;

- Subset-size – 69,
- Step-size – 8,
- Interpolation – Optimized 8-tap
- Correlation criterion – Normalized squared differences
- Subset weights – Gaussian weights (center-weighted)
- Strain tensor – Lagrange
- Strain filter size – 33
- Strain filter type – Decay filter

Figure 69 shows the defined area of interest, shaded in green, in the VIC-2D software. Note that the area of interest that was selected covers the area on or around the strain gauges and their wires. For this reason, care must be taken in extracting data away from these regions to avoid any false measurements stemming from loose wires or out-of-plane geometry caused by the raised surfaces of the strain rosettes, their coating and backing plates.

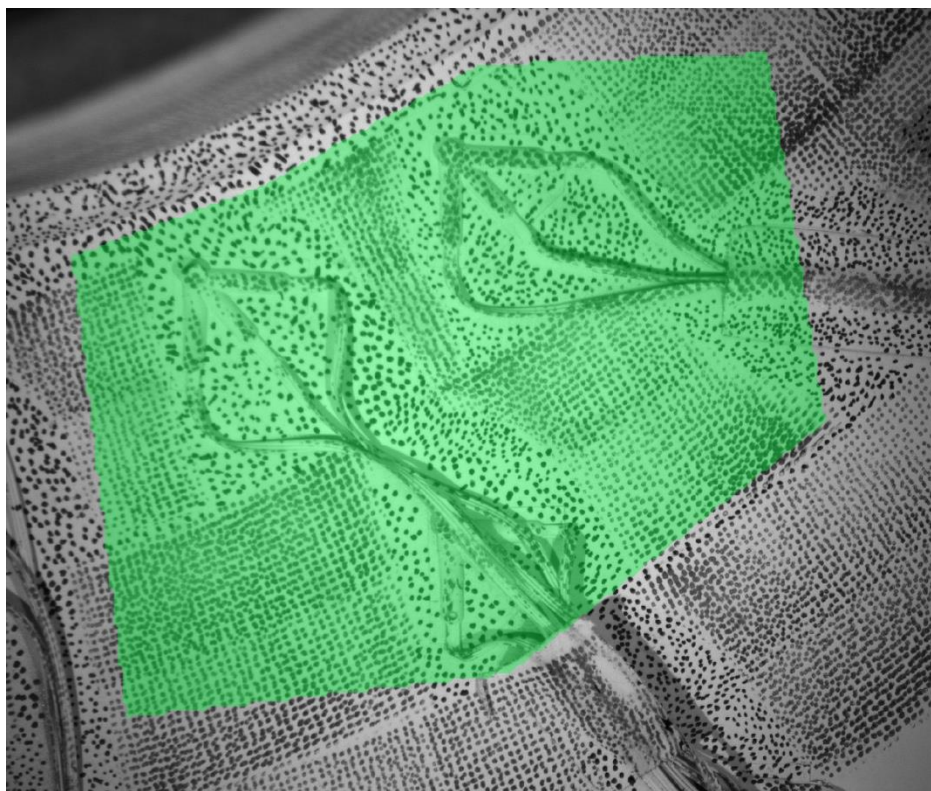


Figure 69 - Analysis Area of Interest – DIC on the Fatigue Specimen

Figure 70 shows a sample contour, in this case the horizontal displacement from an image during the cyclic loading. Note the point on the strain gauge wire in which the contour has a discontinuity. This is likely due to the out-of-plane geometry of the wire as well as the lack of speckle pattern applied to the wire. This causes the program to be unable to accurately track that area. Figure 72

shows the locations of extraction points DIC 1 through DIC 5 along the curved weld and Figure 71 shows the plots principal strain at each location. These locations will be used for comparison between the DIC and the finite element model in Section 6.4.

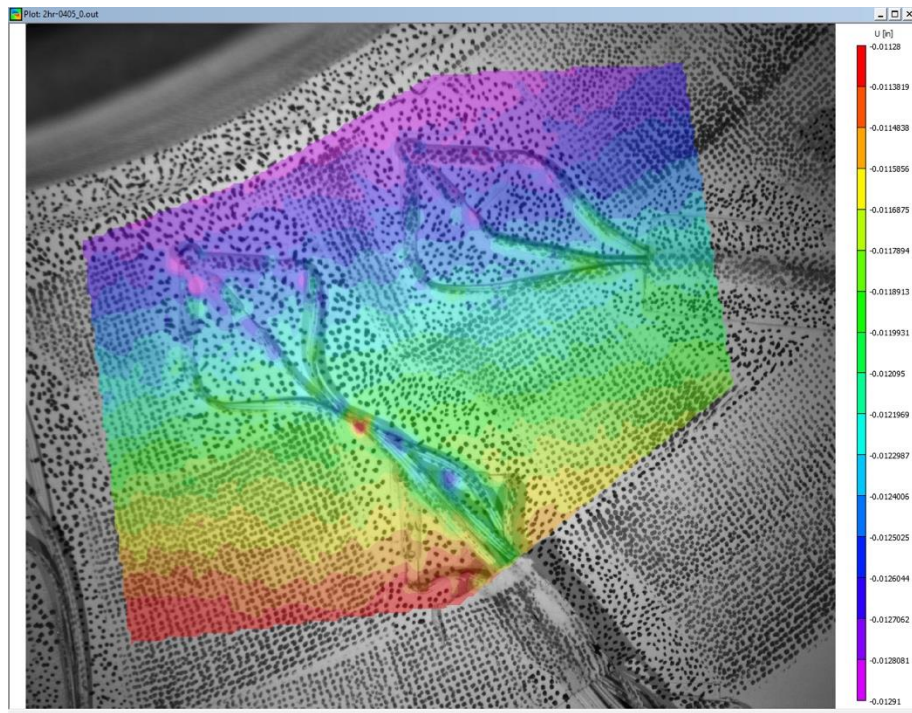


Figure 70 - Horizontal Displacement Contour Recorded Via Digital Image Correlation During Fatigue Testing

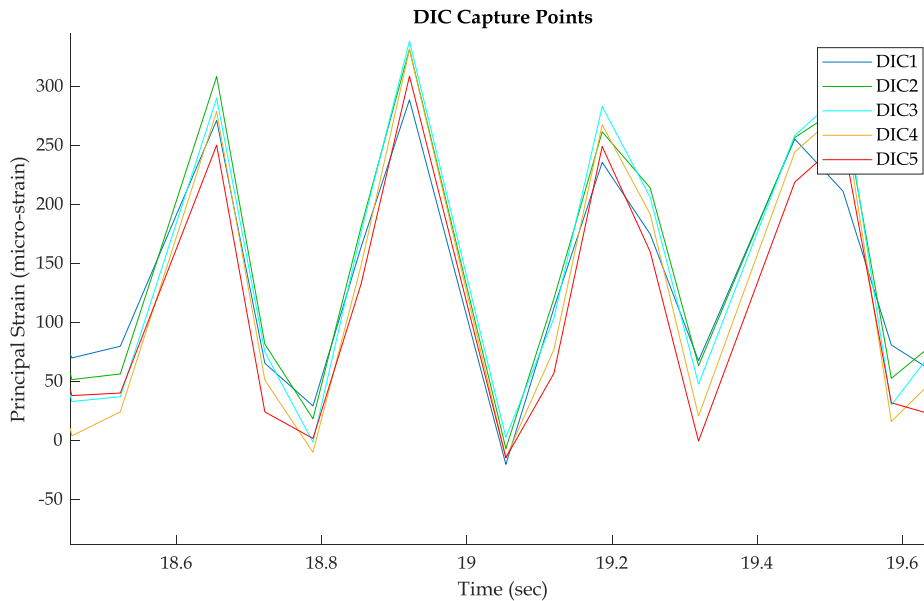


Figure 71 - Strain Response Recorded Via Digital Image Correlation at Locations Shown in Figure 72 from the Fatigue Specimen

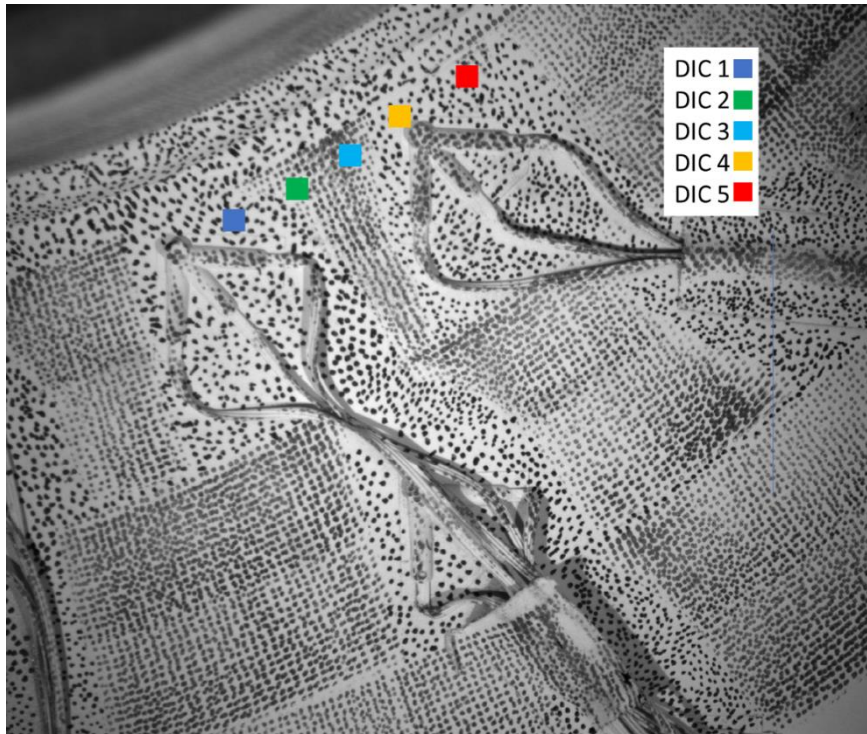


Figure 72 - Locations of Recorded Digital Image Correlation Data

6.4 Measurement Comparison

This section presents the comparison between the measured response from the 2-D DIC and two of the relevant strain gauges. This comparison is provided to verify the two measurements against one another, but mainly to verify the strain measurements from the 2-D DIC since the strain gauges generally provide a more reliable (and direct) measurement. If the DIC data matches closely the data from the strain gauges, it shows that the measured response of the DIC is accurate. Additionally, comparisons between both measured responses, from the DIC and the strain gauges, are evaluated with respect to the results of the numerical model. Table 10 shows the comparison of principal strains measured from strain gauges NRW2 and NRW4, and points from the DIC analysis near the base of the rosette. As the table shows, the DIC measurements match the strain gauge measurements well. It should be noted that the verification using NRW3 was not done due to the wires obstructing the base of the rosette where the DIC measurement would be taken.

Table 10 - Structural Response Comparison between Digital Image Correlation and Strain Gauge Measurements

	Data Source	Max Principal Strain ($\mu\epsilon$)
NRW2	DIC	249
	NRW2	268
	Difference	7.6%
NRW4	DIC	296
	NRW4	301
	Difference	1.6%

The next comparison is between the numerical model and the strain rosettes, shown in Table 11. The locations of the strain rosettes were identified in the numerical model and the principal strain of the surface element corresponding to that location was captured. The table shows that there is some variability in the comparison, but the overall measured response matches the FEA results, with an average difference of 6.4%. It should also be noted that this model has not been calibrated to match the response, as previously mentioned, it is a blind model.

Table 11 - Structural Response Comparison between Strain Gauge Measurements and Model Predictions

Location	Data Source	Max Principal Strain ($\mu\epsilon$)	Equivalent Stress (ksi)
NRW1	Strain Gauge	236	6.84
	FEA	250	7.26
	Difference	6.2%	-
NRW2	NRW2	268	7.76
	FEA	296	8.59
	Difference	10.7%	-
NRW3	NRW3	236	6.84
	FEA	242	7.02
	Difference	2.6%	-
NRW4	NRW4	301	8.72
	FEA	298	8.65
	Difference	0.8%	-
NRW5	NRW5	227	6.57
	FEA	200	5.80
	Difference	11.8%	-

The final comparison is between the DIC locations 1-5, and the FEA results. Using the same method as the strain gauge comparison, the locations of the DIC points were identified in the numerical model and the principal strain was extracted. Table 12 shows that there is some variability, but results obtained using DIC match closely the numerical results, with an average difference of 3.7%.

Table 12 - Structural Response Comparison between Digital Image Correlation and Model Predictions

Location	Data Source	Max Principal Strain ($\mu\epsilon$)	Equivalent Stress (Ksi)
DIC 1	DIC	309	8.96
	FEA	317	9.20
	Difference	2.7%	-
DIC 2	DIC	315	9.13
	FEA	320	9.28
	Difference	1.7%	-
DIC 3	DIC	335	9.73
	FEA	316	9.15
	Difference	5.9%	-
DIC 4	DIC	338	9.81
	FEA	312	9.05
	Difference	7.8%	-
DIC 5	DIC	307	8.90
	FEA	305	8.86
	Difference	0.5%	-

6.5 Summary and Discussion

In summary, the two experimental results were compared to one another and were found to have a similar behavior. It should be noted that since the comparison was limited to two strain rosette locations, it is difficult to draw conclusions about the measurements compared to one another. Comparisons were also made between the FEA and the strain rosettes. This comparison showed that there was some variation between the calculated response of the FEA and the measured response from the strain rosettes, but the overall difference was 6.4% on average. Lastly, a comparison between the DIC measurements and the FEA was performed. This comparison showed a relatively close match between the two, with an average difference of 3.7%.

In terms of fatigue testing results, the measured strain in the specimen indicates that the corresponding stresses are below the theoretical endurance limit for the assumed design fatigue category (i.e. C) as expected. Since the model is matching the response well, the stresses can be extrapolated to the weld using the numerical results. Based on this extrapolation, the maximum principal stress applied near the toe of the weld is approximately 14 ksi. As previously mentioned, the predicted fatigue life of this specimen, considering the design assumptions and the 14 ksi applied stress, was 1,600,000 cycles. In terms of damage, in this study, fatigue failure, or damage, is defined as a visible crack. These cycles have been applied and no damage has been detected in the specimen. A conclusion from this work is that the design assumption of a category C fatigue

detail was conservative, and the endurance limit of the actual fatigue specimen may be higher than expected.

7. SUMMARY, CONCLUSIONS, AND FUTURE WORK

This chapter summarizes the work discussed in this report including the results from the fatigue testing. Next, overall conclusions are listed, and future work is discussed.

7.1 Summary

The objective of this research was to investigate the fatigue performance of the gusset-less truss connection used in place on the Memorial Bridge, particularly the radiused fillet welds. To investigate the performance, a scale-model of the connection was designed and fabricated. Fabrication was performed by CANAM Bridge Corporation, i.e., the same steel fabricator of the Memorial Bridge connections, using the same fabrication process. In addition to the scaled-connection, a test setup for an experimental fatigue test was designed given the current limitations of the University of New Hampshire (UNH) Structural Engineering Laboratory. Adjustments were made to the original test setup to correct undesirable behaviors. These adjustments were in the form of providing additional rigidity to the reaction block by adding concrete and adding a steel shim support under the tip of the specimen to restrain vertical movement. Modifications were also made to the original instrumentation plan with the addition of 2-Dimensional Digital Image Correlation (DIC).

Given that the infrastructure available for this fatigue test was limited, the test setup was not traditional. With that, there were concerns about ensuring consistency across multiple testing periods in a high-cycle fatigue test. For this reason, an approach to monitoring the response of the fatigue test specimen and the overall setup was developed in this work. The protocol that was presented is a systematic method that combines visual and physical inspections, along with periodic, full quantitative characterizations of the structural response of the test setup through a System Identification (S-ID). The S-ID method used in this project captures the structural response at key locations along the test setup using DIC measurements along with LVDTs. In addition to the periodic characterization provided by the System ID, the actuator force-displacement relationship was used to quickly and reliably detect potential changes in the overall response of the system.

In this work several finite element models (FEM) of the test setup were developed and refined. The final model used in this study is a detailed, blind, model able to capture the structural response of not only the fatigue specimen, but the test setup as well. This model underwent a mesh sensitivity study and was refined until the response was acceptable.

During this work, the gusset-less fatigue specimen was tested with the presented fatigue loading. The structural response was recorded through strain gauges and DIC measurements. These measured responses were also compared to numerical responses to check the validity of the model. In terms of loading the specimen in fatigue, a fatigue-life prediction was estimated using the design assumptions and the specimen was loaded to the expected number of cycles to failure, which was 1,600,000 cycles. No damage was detected in the test specimen.

7.2 Observations

Based on the works completed as part of the project and include in this report, there are some observation that are noteworthy

- System Identification (S-ID) was used to characterize the response at key locations along the test setup. The responses across different testing periods were compared, and the average change in response was approximately 5%. [Section 4.2]
- The actuator force-displacement relationship was used as an indicative measurement between S-IDs in this project. It was found that this relationship could reliably detect relevant changes in the test setup. [Section 4.3]
- Based on the results from the S-IDs, supplemented by the actuator force-displacement relationship, it was shown that the overall response of the test setup was consistent throughout the various intervals of the high-cycle fatigue test. [Section 4.4]
- The principal strains measured with DIC matched closely with the measurements from the strain gauges, but the comparison was limited to two strain gauges. [Section 6.4]
- Comparisons between all forms of measurement were performed. The displacements measured with DIC matched closely with the LVDT responses as part of the S-ID. [Section 4.2]
- The principal strains measured with DIC and the strain gauges were compared to those obtained from the numerical model. It was found that the average difference between strains obtained from the DIC and the model was approximately 3.7%. The average difference between the strains recorded using strain gauges and those from the model was approximately 6.4%. This suggests that the model is matching the measured response relatively well, but further numerical model refinement might be needed. [Section 6.4]

7.3 Conclusions

Based on the work presented in this report, the following conclusions can be drawn;

- The monitoring protocol developed in this study provides a reliable way to ensure consistent behavior across a high-cycle fatigue test in which the test is performed in multiple testing intervals. [Section 4.1]
- Structural response measurement, collected from both contact and non-contact methods, were consistent. All collected structural response measurement collected from the test specimen reasonably agreed with the predicted structural response from the finite element model.
- Under the most conservative assumptions, using a hot-spot stress of 14 ksi at the toe of the weld, the AASHTO S-N curve, and a category C fatigue detail, experimental results showed that the design assumptions were reasonable. As a reference, the highest stress measured to date at the gusset-less connection on the Memorial Bridge during in-service conditions is approximately equal to 6 ksi; therefore, in the absence of significant weld defects, the radiused fillet welds in the Memorial Bridge are indeed expected to have infinite fatigue life. [Section 6.5]
- Based on the finite element model predictions and the fatigue test results, visual inspections of the gusset-less connection at the Memorial Bridge should focus on the web-to-flange interface, as shown in Figures 59, 61 and 63.

- Given the assumptions regarding the fatigue life, further research is needed to appropriately categorize the gusset-less connection in terms of fatigue details to be able to apply the S-N curves and estimate fatigue life. [Section 6.5]

7.4 Future Work

The following recommendations are presented for future work relating to this project;

- Additional research is needed to categorize, or develop a fatigue category, based on a curved weld loaded for fatigue.
- Energy-based indicators, derived from strain gauges in the critical fatigue area, should be quantified and monitored to better assess damage in the area.
- The numerical model used in this study should be calibrated to match the measured response from the experiment more closely.
- Once the model is calibrated, multiple damage scenarios to the weld could be modeled to see the response of a damaged weld (or a weld with significant defects).
- Damage could be induced, based on the results of the modeling, to the fatigue specimen to create a more severe fatigue detail.
- Once damage is induced, the specimen should be tested to failure and crack propagation, stress redistribution, and remaining fatigue life should be evaluated.

REFERENCES

1. Contractors, H.C.A.W., *Portsmouth Memorial Bridge Replacement: An Exploration of Truss Design without Gusset Plates*. 2013: New York.
2. Instruments, N. *Measuring Strain with Strain Gages*. White Papers 2016; Available from: <http://www.ni.com/white-paper/3642/en/#top>.
3. Group, V.P., *Fatigue Characteristics of Micro-Measurements Strain Gages*, in *Tech Note*. 2010.
4. D. A. Skolnik, W.J.K., J. W. Wallace, *Instrumentation For Structural Health Monitoring: Measuring Interstory Drift*, in *World Conference on Earthquake Engineering*. 2008: Beijing, China.
5. Instruments, N. *Measuring Position and Displacement with LVDTs*. White Papers 2018; Available from: <http://www.ni.com/white-paper/3638/en/>.
6. Bing, P., et al., *Two-dimensional digital image correlation for in-plane displacement and strain measurement: a review*. *Measurement Science and Technology*, 2009. **20**(6): p. 062001.
7. Aktan, A.E., et al., *Structural identification for condition assessment: experimental arts*. 1997. **123**(12): p. 1674-1684.
8. F. Catbas, T.K.-C., A Emin Aktan, *Structural Identification of Constructed Systems*, in *Structural Identification of Constructed Systems*, T.K.-C. F. Catbas, A Emin Aktan, Editor.
9. Pan, Q., *System identification of constructed civil engineering structures and uncertainty*. Vol. 68. 2007: Citeseer.
10. Dutt, A., *Effect of Mesh Size on Finite Element Analysis of Beam*. Vol. 2. 2015.
11. *Abaqus/CAE User's Guide*, ed. D. Systèmes. 2011, Providence, RI, USA.
12. Choi, C.K. and H.G. Kwak, *The effect of finite element mesh size in nonlinear analysis of reinforced concrete structures*. *Computers & Structures*, 1990. **36**(5): p. 807-815.
13. Liu, Y., *Effects of Mesh Density on Finite Element Analysis*. Vol. 2. 2013.
14. *Fatigue (Material)*. 2018 [cited 2018; Available from: [https://en.wikipedia.org/wiki/Fatigue_\(material\)](https://en.wikipedia.org/wiki/Fatigue_(material))].
15. Campbell, F.C., *Elements of Metallurgy and Engineering Alloys*. 2008: ASM International.
16. Transportation, O.D.O., *Structure Project Manager Seminar - Fatigue Analysis*. 2005.
17. Dong, P., *A structural stress definition and numerical implementation for fatigue analysis of welded joints*. *International Journal of Fatigue*, 2001. **23**(10): p. 865-876.
18. Fisher, J. and B. T. Yen, *fatigue strength of steel members with welded details*. Vol. 14. 1977. 118-129.
19. Fisher, J.W., *evaluation of typical welded bridge details for fatigue design* 1973.
20. *AASHTO LRFD bridge design specifications*. 2008: Fourth edition with 2008 interim revisions. Washington, D.C. : American Association of State Highway and Transportation Officials, [2008] ©2007.
21. Socie, D.F., *Fatigue of Welds*. 2014: efatigue.com.
22. Kamaya, M. and M. Kawakubo, *Mean stress effect on fatigue strength of stainless steel*. *International Journal of Fatigue*, 2015. **74**: p. 20-29.
23. Kumbhar, S. and R. Tayade, *A Case Study on Effect of Mean Stress on Fatigue life*. 2014.
24. Susmel, L., R. Tovo, and P. Lazzarin, *The mean stress effect on the high-cycle fatigue strength from a multiaxial fatigue point of view*. *International Journal of Fatigue*, 2005. **27**(8): p. 928-943.
25. Wehner, T. and A. Fatemi, *Effects of mean stress on fatigue behaviour of a hardened carbon steel*. *International Journal of Fatigue*, 1991. **13**(3): p. 241-248.

26. Fatemi, A., *Fatigue Tests and Stress-Life (S-N) Approach*. 2014: efatigue.com.
27. University, I.S., *Fatigue Life Evaluation*.
28. Fatemi, A., *Residual Stresses and Their Effects On Fatigue Resistance*. 2014: efatigue.com.
29. Corp., D.S., *ABAQUS*. 2013.
30. Shehadeh, M., Y. Shennawy, and H.J.A.E.J. El-Gamal, *Similitude and scaling of large structural elements: Case study*. 2015. **54**(2): p. 147-154.
31. Contractors, H.C.A.W., *Portsmouth Memorial Bridge Replacement: An Exploration of Truss Design without Gusset Plates*. . New York, 2013.
32. Gioncu, V., Mazzolani, F. M. , *Ductility of Seismic Resistant Steel Structures*. New York: Spon Press, 2002.
33. Nawale, S.S., S. Chalukya, and S. Admane, *Comparative Analysis and Bending Behavior of Cold form Steel with Hot Rolled Steel Section*.
34. CanamBridges. *Metallizing: A Choice Solution for Corrosion Protection of Steel* 16 April 2015; Available from: <https://www.canambridges.com/metallizing-a-choice-solution-for-corrosion-protection-of-steel>.
35. Taiwade, R.V., et al., *Effect of welding passes on heat affected zone and tensile properties of AISI 304 stainless steel and chrome-manganese austenitic stainless steel*. 2013. **53**(1): p. 102-109.
36. Mashayekhizadeh, M., E. Santini-Bell, and T. Adams. *Instrumentation and Structural Health Monitoring of a Vertical Lift Bridge*. in *26th ASNT Research Symposium*. 2017.
37. BDI, "University of New Hampshire Monitoring of the Memorial Bridge in Portsmouth, NH." Boulder, 09 December 2016.
38. Nganyi Imbembe, J.B., "Memorial Bridge Connection - Test set up: Effects of out of plane load on the Green Frame." Class Semester Project Report. 2017.
39. Corporation, M.S., "Series 244 Actuators Product Information." 2013.
40. Corporation, M.S., "ACTR ASSY-244.21, 150MM, 15GPM, PED." August 2016.
41. Corporation, M.S., "Series 249 and 249N Swivels." Minesota, 2014.
42. Corporation, M.S., *Series 244 Hydraulic Actuators*.
43. Corporation, M.S., *MTS Series 793 Tuning and Calibration*.
44. Solutions, C., *VIC-2D 2009*. 2009.
45. Inc, P., *PTC Mathcad Prime 3.1*. 2015.
46. MicroMeasurements, *General Purpose Strain Gages - Linear Pattern*. 2018.
47. Correlated Solutions, I., *Minimizing Noise and Bias in 3-D DIC*.
48. Simonsen, M., *Strain Tensors and Criteria in Vic*. 2018, Correlated Solutions, Inc.: Correlated Solutions Knowledge Base.

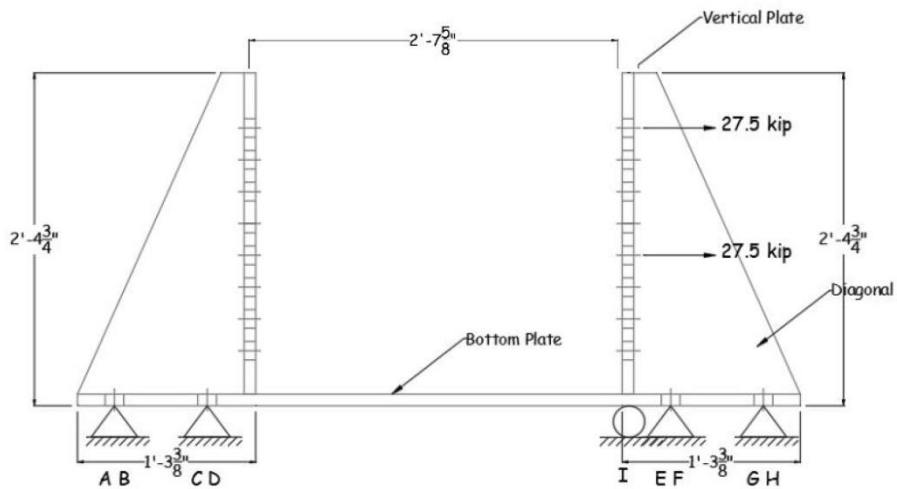
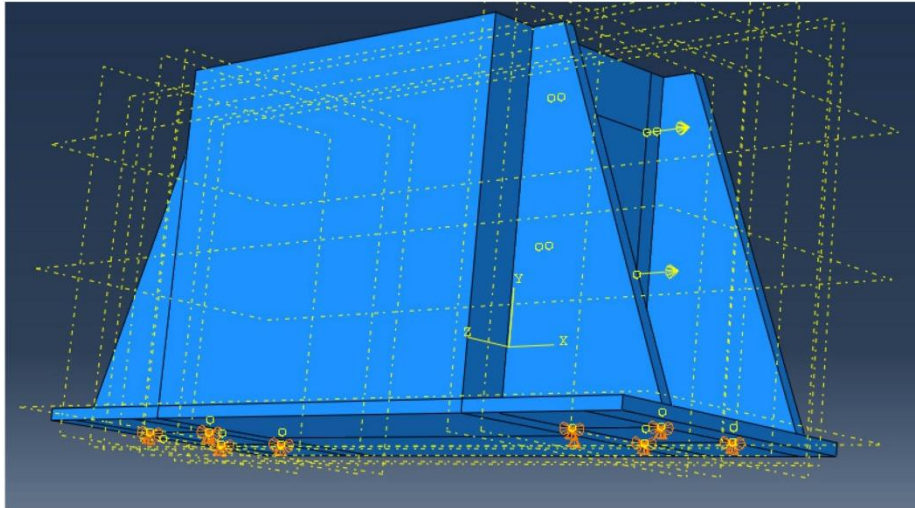
APPENDICES

APPENDIX A – SETUP DESIGN CALCULATIONS

This appendix includes the design calculations for the reaction block, and the steel bracket. All calculations were done using MathCad [45].

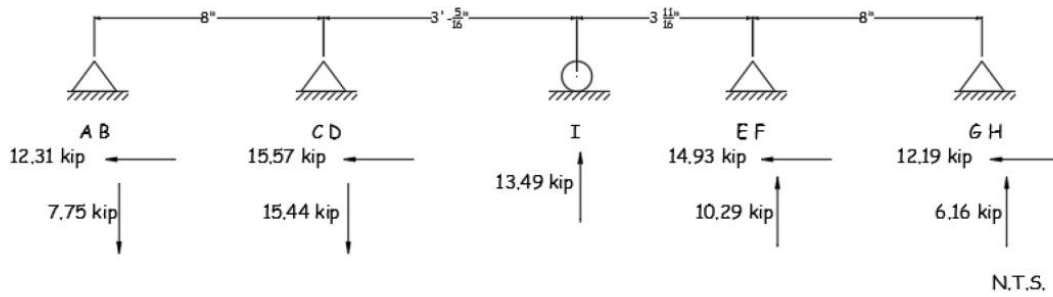
Fernanda Fischer

January 16th 2018



Note: the picture only shows one line of bolts/holes, there are 4 in total total of 110 kips. Also I is a roller located at the midpoint of the width, and A and B are in the anchors in line, as well as C and D, E and F and G and H. Anchors are pin supports.

Non-Commercial Use Only



Load at Anchors

$$n_{anchors} := 8$$

$$V_{ut} := 110 \text{ kip}$$

$$V_u := 15.57 \text{ kip}$$

(From Abaqus)

$$w := 24 \text{ in} \quad \text{width}$$

$$l := 31.625 \text{ in} \quad \text{length}$$

$$d := 27.75 \text{ in} \quad \text{depth}$$

$$V_c := w \cdot l \cdot d = 21062.3 \text{ in}^3 \quad \text{volume}$$

$$\gamma := 150 \text{ pcf}$$

$$Weight_{concrete} := V_c \cdot \gamma = 1.8 \text{ kip}$$

$$Plate_{bottom} := 1 \text{ in} \cdot 62.375 \text{ in} \cdot 24 \text{ in} = 1497 \text{ in}^3$$

$$Bracket := 24 \text{ in} \cdot 27.75 \text{ in} \cdot 1 \text{ in} + 2 \cdot 1 \text{ in} \cdot 226.93 \text{ in}^2 = 1119.9 \text{ in}^3$$

$$V_s := (Plate_{bottom} + 2 \cdot Bracket) = 3736.7 \text{ in}^3$$

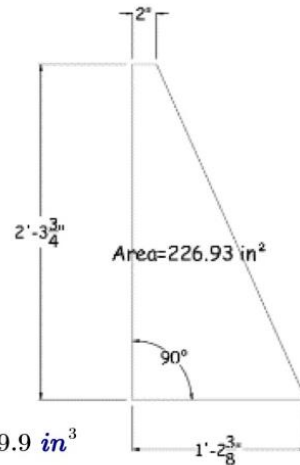
$$\gamma := 490 \text{ pcf}$$

$$Weight_{steel} := V_s \cdot \gamma = 1.1 \text{ kip}$$

$$Weight_{total} := Weight_{concrete} + Weight_{steel} = 2.9 \text{ kip}$$

$$N_u := 15.44 \text{ kip}$$

(From Abaqus)



Non-Commercial Use Only

Anchors Capacity

From ACI 318-11 Appendix D

According to Ap D, steel elementes for adhesive anchors include threaded rods. So, anchor type = adhesive anchor

$d_a := 1.61 \text{ in}$ outside diameter of the rod #11 carbon-steel

$A := \pi \cdot \left(\frac{d_a}{2}\right)^2 = 2.036 \text{ in}^2$ area of the rod

$nt := 1.5 \text{ in}^{-1}$ number of threads per inch (measured)

Steel strength of anchor in shear

$A_{sev} := \frac{\pi}{4} \cdot \left(d_a - \frac{0.9743}{nt}\right)^2 = 0.725 \text{ in}^2$ effective cross-sectional area of an anchor in shear (D-28)

$f_{ya} := 75000 \text{ psi}$ specified yield strenght of anchor steel, Grade 75

$f_{uta} := \min(1.9 \cdot f_{ya}, 125000 \text{ psi}) = 125000 \text{ psi}$

$V_{sa} := 0.6 \cdot A_{sev} \cdot f_{uta} = 54.3 \text{ kip}$ (D-28)

Concrete breakout strenght of anchor in shear

Use Case 3 as the conservative approach. Case 3 is shown on Fig. RD.6.2.1 (b), where $s < c_{a1,1}$, applu the entire shear load V to the front anchor. This case does not apply for anchors welded to a common plate. For the calculation of concrete breakout, c_{a1} is taken as $c_{a1,1}$

Because of the strong floor, all distances to edge of concrete are assumed to be 100 in

$h_a := 48 \text{ in}$ thickness of member in which an anchor is located. In this case it is the strong floor

$c_{a1} := 100 \text{ in}$ distance from center of an anchor to the edge of concrete

$A_{vc} := 2 \cdot (1.5 \cdot c_{a1}) \cdot h_a = 14400 \text{ in}^2$ projected concrete failure area of a single anchor or group of anchors, for calculation of strength in shear. Fig. RD.6.1 (b)

$$A_{vco} := 4.5 \cdot c_{a1}^2 = 45000 \quad in^2 \quad (D-32)$$

$$h_{ef} := 3 \quad in$$

effective embedment depth of anchor.
Conservatively estimated base on 3 in
measured

$$l_e := h_{ef} \quad in$$

(D.6.2.2 - for anchors with a constant
stiffness over the full length of embedded
section, such as headed studs and post-
intalled anchors with one tubular shell over
full length of the embedment depth)

$$d_a := d_a \cdot \frac{1}{in} = 1.61$$

unit adjustment

$$\lambda := 1.0$$

normal weight concrete (uniteless)

$$\lambda_a := 1 \cdot \lambda = 1$$

D.3.6 - no lightweight concrete

$$f'c := 3000 \quad psi$$

assuming a low value for concrete of strong
floor

$$V_{b1} := \left(7 \cdot \left(\frac{l_e}{d_a} \right)^{0.2} \cdot \sqrt{d_a} \right) \cdot \lambda_a \cdot \sqrt{f'c} \cdot (c_{a1})^{1.5} = 550973.5 \quad lb \quad (D-33)$$

$$V_{b2} := 9 \cdot \lambda_a \cdot \sqrt{f'c} \cdot (c_{a1})^{1.5} = 492950.3 \quad lb \quad (D-34)$$

$$V_b := \min(V_{b1}, V_{b2}) = 492950.3 \quad lb$$

$$c_{a2} := 100 \quad in$$

distance between resultant shear load on
group of anchors loaded in shear in the
same direction, and the centroid of the
group of anchors loaded in shear in the
same direction.

$$e_v := 0$$

$$\psi_{ecv} := \frac{1}{\left(1 + \frac{2 \cdot e_v}{3 \cdot c_{a1}} \right)} = 1 \quad (D-36)$$

$$\psi_{edv} := \left\| \begin{array}{l} \text{if } c_{a2} \geq 1.5 \cdot c_{a1} \\ \quad \left\| \begin{array}{l} \text{"}\psi_{edv} = \text{equation D-37"} \\ \text{else} \\ \quad \left\| \begin{array}{l} \text{"}\psi_{edv} = \text{equation D-38"} \end{array} \right. \end{array} \right. \\ \end{array} \right\| = \text{"}\psi_{edv} = \text{equation D-38"}$$

$$\psi_{edv} := 1 \quad (D-37)$$

$$\psi_{edv} := 0.7 + 0.3 \cdot \frac{c_{a2}}{1.5 \cdot c_{a1}} = 0.9 \quad (D-38)$$

$$\psi_{cv} := 1.0$$

D.6.2.7 for anchors in cracked concrete without supplementary reinforcement or with edge reinforcement smaller than a #4 bar. Conservative approach

$$\psi_{hw} := \sqrt{\frac{1.5 \cdot c_{a1}}{h_a}} = 1.768 \quad (D-39)$$

it should not be taken less than 1.0

$$V_{cbg1} := \frac{A_{vc}}{A_{vco}} \cdot \psi_{ecv} \cdot \psi_{edv} \cdot \psi_{cv} \cdot \psi_{hw} \cdot V_b = 250969.3 \text{ lb} \quad (D-31)$$

$$V_{cbg} := \frac{V_{cbg1} \cdot 1 \text{ kip}}{1000} = 251 \text{ kip} \quad \text{units adjustment}$$

Concrete pryout strength of anchor in shear

$$k_{cp} := 2$$

for hef greater than 2.5in (D.6.3.1)

$$c_{amin} := 100 \text{ in}$$

$$\tau_{uncr} := 1000 \text{ psi}$$

Table D.5.5.2

$$c_{na} := 10 \cdot d_a \cdot \sqrt{\frac{\tau_{uncr}}{1100}} = 15.351 \text{ in} \quad (D-21)$$

projected distance from center of an anchor shaft on one side of the anchor required to develop the full bond strength

$$c_{a1} := 100 \text{ in}$$

distance from the center of an anchor shaft to the edge of concrete in one direction

$$c_{a2} := 100 \text{ in}$$

distance from the center of an anchor shaft to the edge of concrete perpendicular to ca1

$$s_1 := 8 \text{ in}$$

$$s_2 := 8 \text{ in}$$

Non-Commercial Use Only

$$A_{na} := (c_{na} + s_1 + c_{a1}) \cdot (c_{na} + s_2 + c_{a2}) = 15215.4 \text{ in}$$

Figure RD.5.5.1

$$A_{nao} := (2 \cdot c_{na})^2 = 942.6 \text{ in}^2$$

(D-20)

Center of load from EF and GH loads

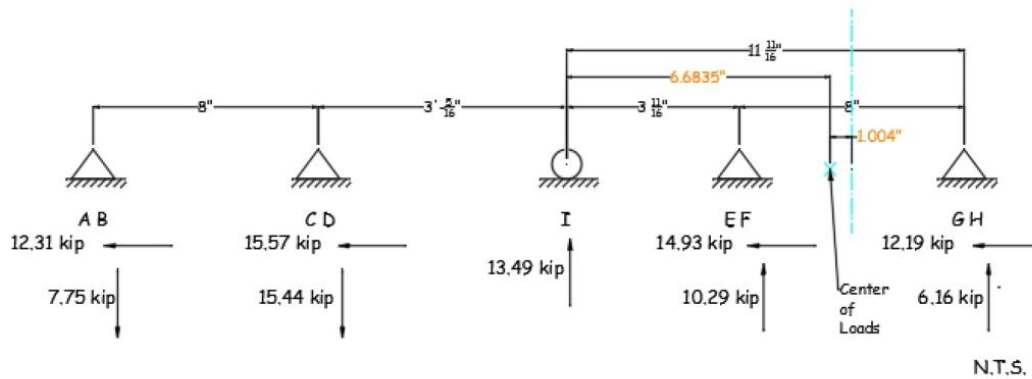
$$x_{cl} := \frac{10.29 \cdot -4 + 6.16 \cdot 4}{10.29 + 6.16} = -1.004$$

$$distance := 6.6835$$

Distance center of loads to point of rotation (I)

$$e_n := distance = 6.684$$

distance between resultant tension load on group of anchors loaded in tension and the centroid of the group of anchors loaded in tension



$$\psi_{ecna} := \frac{1}{\left(1 + \frac{e_n}{c_{na}}\right)} = 0.7$$

(D-23)

$$\psi_{edna} := 1$$

(D-24)

$$c_{ac} := 2 \cdot h_{ef} = 6$$

D.8.6 for adhesive anchors

$$\psi_{cpna} := 1$$

(D-26)

$$\tau_{cr} := 300 \text{ psi}$$

Table D.5.5.2

$$N_{ba} := \lambda_a \cdot \tau_{cr} \cdot \pi \cdot d_a \cdot h_{ef} \cdot 1 \text{ lbf} = 4.6 \text{ kip}$$

(D-22)

(D-19)

$$N_{ag} := \frac{A_{na}}{A_{nao}} \cdot \psi_{ecna} \cdot \psi_{edna} \cdot \psi_{cpna} \cdot \psi_{hv} \cdot N_{ba} = 90.5 \text{ kip}$$

Bonded strength of adhesive anchor in tension unit adjustment

$$A_{nc} := (c_{a1} + s_1 + 1.5 \cdot h_{ef}) \cdot (c_{a2} + s_2 + 1.5 \cdot h_{ef}) = 12656.3$$

Figure RD.5.2.1

$$A_{nco} := 9 \cdot h_{ef}^2 = 81 \text{ in}^2$$

(D-5)

$$\psi_{ecn} := \frac{1}{\left(1 + \frac{2 \cdot e_n}{3 \cdot h_{ef}}\right)} = 0.4$$

(D-8)

$$\psi_{edn} := 1$$

(D-9, $c_{amin} \geq 1.5 \cdot h_{ef}$)

$$\psi_{cn} := 1.4$$

D.5.2.6 for post installed anchors

$$\psi_{cpn} := 1$$

(D-11, $c_{amin} \geq c_{ac}$)

$$k_c := 17$$

for post installed anchors

$$N_b := k_c \cdot \lambda_a \cdot \sqrt{f'_c} \cdot h_{ef}^{1.5} = 4838.3 \text{ lb}$$

(D-6)

$$N_{cbg} := \frac{A_{nc}}{A_{nco}} \cdot \psi_{ecn} \cdot \psi_{edn} \cdot \psi_{cn} \cdot \psi_{cpn} \cdot N_b \cdot 1 \text{ lbf} = 425.9 \text{ kip}$$

(D-4)
unit adjustment

$$N_{cpg} := \min(N_{ag}, N_{cbg}) = 90.5 \text{ kip}$$

$$V_{cpg} := k_{cp} \cdot N_{cpg} = 181 \text{ kip}$$

(D-41)

$$V_n := \min(V_{sa}, V_{cbg}, V_{cpg}) = 54.3 \text{ kip}$$

$$\phi := 0.65$$

governed by strength of a ductile steel element - shear loads (D.4.3)

$$\phi V_n := \phi \cdot V_n = 35.3 \text{ kip}$$

Non-Commercial Use Only

$$Shear.capacity_{anchors} := \left\| \begin{array}{l} \text{if } V_u \leq \phi V_n \\ \quad \left\| \begin{array}{l} \text{"OK"} \\ \text{else} \\ \quad \left\| \begin{array}{l} \text{"Not OK"} \end{array} \right\| \end{array} \right. \\ \end{array} \right\| = \text{"OK"}$$

Steel strength of anchor in tension

$$A_{sen} := A_{sev} = 0.725 \text{ in}^2$$

effective cross-sectional area of an anchor in tension

$$N_{sa} := A_{sen} \cdot f_{uta} = 90.6 \text{ kip}$$

futa equation on page 3 (D-2)

$$\psi_{cp} := 1$$

Np is not checked for adhesive anchor

D.5.3.6 (conservative)

$$N_n := \min(N_{sa}, N_{cbg}, N_{ag}) = 90.5 \text{ kip}$$

$$\phi := 0.75$$

governed by concrete pryout - condition A - tension loads (D.4.3)

$$\phi N_n := \phi \cdot N_n = 67.9 \text{ kip}$$

$$Tension.capacity_{anchors} := \left\| \begin{array}{l} \text{if } N_u \leq \phi N_n \\ \quad \left\| \begin{array}{l} \text{"OK"} \\ \text{else} \\ \quad \left\| \begin{array}{l} \text{"Not OK"} \end{array} \right\| \end{array} \right. \\ \end{array} \right\| = \text{"OK"}$$

Interaction of tensile and shear forces (D.7)

$$V_{ua} := V_u = 15.57 \text{ kip}$$

$$N_{ua} := N_u = 15.4 \text{ kip}$$

$$Total.capacity_{anchors} := \left\| \begin{array}{l} \text{if } \frac{N_{ua}}{\phi N_n} + \frac{V_{ua}}{\phi V_n} \leq 1.2 \\ \quad \left\| \begin{array}{l} \text{"OK"} \\ \text{else} \\ \quad \left\| \begin{array}{l} \text{"Not OK"} \end{array} \right\| \end{array} \right. \\ \end{array} \right\| = \text{"OK"}$$

From AISC 14th Ed, J9: "The anchor rods shall be designed in accordance with the requirements for threaded parts in Table J3.2. And satisfy the requirements of ACI 318.

From Table J3.2, Nominal Tensile Strength (F_{nt}) is:

$$F_u := 100 \text{ ksi}$$

$$F_{nt} := 0.75 \cdot F_u = 75 \text{ ksi}$$

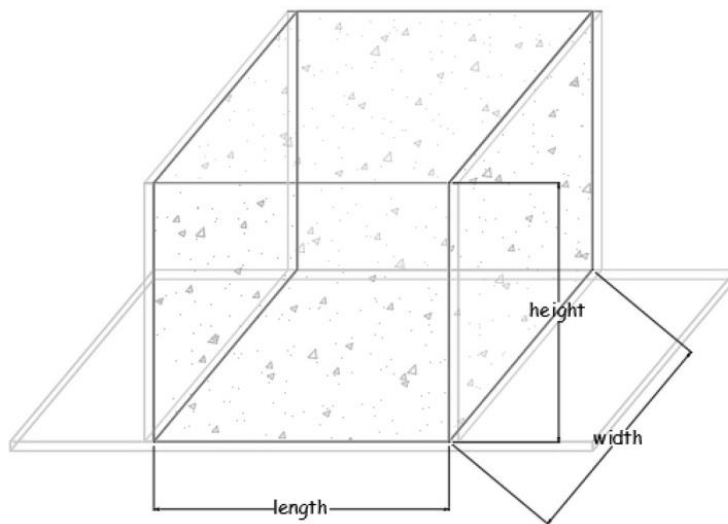
$$\text{Stress.check} := \left\| \begin{array}{l} \text{if } \frac{N_u}{A_{sev}} \leq F_{nt} \\ \quad \left\| \begin{array}{l} \text{"OK"} \\ \text{else} \\ \text{"Not OK"} \end{array} \right\| \\ \end{array} \right\| = \text{"OK"}$$

Ultimate Tensile Stress for
Grade 75 Thread Rebar.
(online source)

Block Design

$$\text{Crane.capacity} := 22.5 \text{ kip}$$

$$\text{Capacity} := \left\| \begin{array}{l} \text{if } \text{Crane.capacity} > \text{Weight}_{total} \\ \quad \left\| \begin{array}{l} \text{"OK"} \\ \text{else} \\ \text{"Not OK"} \end{array} \right\| \\ \end{array} \right\| = \text{"OK"}$$



$$f'_c := 3000 \text{ psi}$$

minimum required compressive strength

Non-Commercial Use Only

Shear as a deep beam

$$b_w := w = 24 \text{ in}$$

$$cover := 1.5 \text{ in}$$

$$d_{eff} := l - cover - \frac{0.375 \text{ in}}{2} = 29.9 \text{ in}$$

$$f_y := 60000 \text{ psi}$$

$$\lambda := 1 \text{ psi}$$

$$V_c := 2 \cdot \lambda \cdot (\sqrt{f'_c}) \cdot b_w \cdot d_{eff} = 78.7 \text{ kip}$$

$$\phi_{shear} := 0.75$$

$$f_{yt} := 60000 \text{ psi}$$

Transverse Steel

$$n_{stirups} := 6$$

$$s_{max} := \min\left(\frac{d_{eff}}{5}, 12 \text{ in}\right) = 6 \text{ in}$$

$$diam_{bar3} := 0.375 \text{ in}$$

$$s_{transv} := \frac{(l - 2 \cdot cover - diam_{bar3})}{n_{stirups} - 1} = 5.7 \text{ in}$$

$$spacing_{transv} := \begin{cases} \text{if } s_{transv} \leq s_{max} \\ \quad \text{“OK”} \\ \text{else} \\ \quad \text{“Not OK”} \end{cases} = \text{“OK”}$$

$$A_{minv} := 0.0025 \cdot b_w \cdot s_{transv} = 0.3 \text{ in}^2$$

$$A_{bar3} := \pi \cdot \left(\frac{diam_{bar3}}{2}\right)^2 = 0.11 \text{ in}^2$$

cast-in-plane cover 7.7.1c (ACI 318-11)

assume #3 bar longitudinal

Grade 60 Rebar

normal weight concrete (uniteless)

shear reduction factor 9.3.2.3 (ACI 318-11)

spacing center to center of bars

11.7.4.1 (ACI 318-11)

Area of shear reinforcement perpendicular to the longitudinal axis of the beam

$$A_{vt} := n_{stirups} \cdot A_{bar3} \cdot 2 = 1.3 \text{ in}^2$$

$$A_{steeltransv} := \begin{cases} \text{if } A_{vt} \geq A_{minv} \\ \quad \text{"OK"} \\ \text{else} \\ \quad \text{"Not OK"} \end{cases} = \text{"OK"}$$

Use 6 (six) #3 stirups for transverse steel

$$f_{yt} := 60000 \text{ psi}$$

Grade 60 steel

$$V_s := \frac{A_{vt} \cdot f_{yt} \cdot d_{eff}}{s_{transv}} = 421.4 \text{ kip}$$

Eq 11-15 (ACI 318-11)

$$V_t := V_s + V_c = 500.1 \text{ kip}$$

$$V_{u1} := 110 \text{ kip}$$

$$V_{u2} := \phi_{shear} \cdot 10 \cdot \sqrt{f'c} \cdot b_w \cdot d_{eff} \cdot 1 \text{ psi} = 295.2 \text{ kip} \quad \text{11.7.3 (ACI 318-11)}$$

(psi added for units match)

$$V_u := \begin{cases} \text{if } V_{u1} \leq V_{u2} \\ \quad \text{"OK"} \\ \text{else} \\ \quad \text{"Not OK"} \end{cases} = \text{"OK"}$$

$$Shear_{capacity} := \begin{cases} \text{if } V_{u1} \leq V_t \\ \quad \text{"OK"} \\ \text{else} \\ \quad \text{"Not OK"} \end{cases} = \text{"OK"}$$

Longitudinal Steel (minimum)

$$n_{bars} := 6$$

$$plate_{thickness} := 1 \text{ in}$$

$$s_{long} := \frac{(d - 2 \cdot cover - diam_{bar3})}{n_{bars} - 1} = 4.9 \text{ in}$$

spacing center to center of bars

$$spacing_{long} := \left\| \begin{array}{l} \text{if } s_{long} \leq s_{max} \\ \quad \left\| \begin{array}{l} \text{"OK"} \\ \text{else} \\ \text{"Not OK"} \end{array} \right\| \end{array} \right\| = \text{"OK"}$$

$$A_{minvh} := 0.0025 \cdot b_w \cdot s_{long} = 0.3 \text{ in}^2$$

11.7.4.2 (ACI 318-11)

Area of shear reinforcement parallel to the longitudinal axis of the beam

$$A_{bar3} := \pi \cdot \left(\frac{diam_{bar3}}{2} \right)^2 = 0.11 \text{ in}^2$$

$$A_{vl} := n_{bars} \cdot A_{bar3} \cdot 2 = 1.3 \text{ in}^2$$

$$A_{steeltransv} := \left\| \begin{array}{l} \text{if } A_{vl} \geq A_{minvh} \\ \quad \left\| \begin{array}{l} \text{"OK"} \\ \text{else} \\ \text{"Not OK"} \end{array} \right\| \end{array} \right\| = \text{"OK"}$$

Use 6 (six) #3 bars for longitudinal steel

There are 16 1 1/2" steel pipes with a cross section area of 0.8 in² each. The pipes are used as transverse reinforcement. Thus, #3 rebar top and bottom to form the cage of reinforcement are needed .

LIFTING

Flexure Capacity

$$M_u := \frac{1}{8} \cdot \frac{Weight_{total}}{l} \cdot l^2 = 11.4 \text{ kip}\cdot\text{in}$$

$$f_y := 60000 \text{ psi}$$

Grade 60 steel

$$\phi_{flexure} := 0.9$$

tension reduction factor 9.3.2.1 (ACI 318-11)

$$A_s := \frac{A_{vt}}{4} = 0.3 \text{ in}^2$$

considering only bottom layer

$$ima := \frac{d}{4} = 6.9 \text{ in}$$

rule of thumb for estimating ima for rectangular sections

$$\phi M_n := 0.9 \cdot f_y \cdot A_s \cdot ima = 124.1 \text{ kip}\cdot\text{in}$$

Non-Commercial Use Only

$$Moment := \left\| \begin{array}{l} \text{if } \phi M_n \geq M_u \\ \quad \left\| \begin{array}{l} \text{"OK"} \\ \text{else} \\ \quad \left\| \begin{array}{l} \text{"Not OK"} \end{array} \right\| \end{array} \right\| \end{array} \right\| = \text{"OK"}$$

Shear Capacity

$$V_u := \frac{1}{2} \cdot Weight_{total} = 1.4 \text{ kip}$$

$$f'_c := 3000 \text{ psi}$$

minimum required compressive strength

$$cover := 1.5 \text{ in}$$

$$d_{eff} := d - cover - \frac{0.375 \text{ in}}{2} = 26.1 \text{ in}$$

cast-in-plane cover 7.7.1c (ACI 318-11)
assume #3 bar longitudinal

$$b_w := w = 24 \text{ in}$$

$$f_y := 60000 \text{ psi}$$

$$\lambda := 1 \text{ psi}$$

normal weight concrete (unitless)

$$V_c := 2 \cdot \lambda \cdot (\sqrt{f'_c}) \cdot b_w \cdot d_{eff} = 68.5 \text{ kip}$$

$$\phi_{shear} := 0.75$$

shear reduction factor 9.3.2.3 (ACI 318-11)

Check shear for beam considering longitudinal reinforcement of deep beam

$$A_{vmin1} := 0.75 \cdot \sqrt{f'_c} \cdot \frac{b_w \cdot s_{transv}}{f_y} = 0.09 \text{ in}^2$$

Eq 11-13 (ACI 318-11)

$$A_{vmin2} := 50 \cdot b_w \cdot \frac{s_{transv}}{f_y} = 0.1 \text{ in}^2$$

$$A_v := \max(A_{vmin1}, A_{vmin2}) = 0.1 \text{ in}^2$$

$$A_s := \left\| \begin{array}{l} \text{if } \frac{A_{vl}}{3} \geq A_v \\ \quad \left\| \begin{array}{l} \text{"OK"} \\ \text{else} \\ \quad \left\| \begin{array}{l} \text{"Not OK"} \end{array} \right\| \end{array} \right\| \end{array} \right\| = \text{"OK"}$$

considering only bottom layer of longitudinal steel

$$f_{yt} := 60000 \text{ psi}$$

Grade 60 steel

$$V_s := \frac{A_{vt} \cdot f_{yt} \cdot d_{eff}}{s_{transv}} = 366.8 \text{ kip}$$

Eq 11-15 (ACI 318-11)

$$V_t := V_s + V_c = 435.3 \text{ kip}$$

$$\text{Shear}_{capacity} := \begin{cases} \text{if } V_u \leq V_t \\ \text{“OK”} \\ \text{else} \\ \text{“Not OK”} \end{cases} = \text{“OK”}$$

ANCHOR CAPACITY

Design of Bolts for Lifting

Design Guide 1

$$f'_c := 3 \text{ ksi}$$

$$d := 0.625 \text{ in}$$

$$L := 18 \text{ in}$$

bolt diameter

hook length

$$\varphi_t := 0.75$$

resistance factor for tension

$$F_u := 58 \text{ ksi}$$

minimum tensile strength for A36 bar

$$A_g := \pi \cdot \left(\frac{d}{2}\right)^2 = 0.307 \text{ in}^2$$

$$T_n := 0.75 \cdot \varphi_t \cdot F_u \cdot A_g = 10 \text{ kip}$$

bolt tensile capacity according to cross section

$$T_{nh} := \frac{0.7 \cdot f'_c \cdot d \cdot (L)}{2} = 11.8 \text{ kip}$$

bolt tensile capacity according to length

$$T_n := \min(T_n, T_{nh}) = 10 \text{ kip}$$

$$n_{hook} := 4$$

$$T_u := \frac{\text{Weight}_{total}}{n_{hook}} = 0.7 \text{ kip}$$

Non-Commercial Use Only

$$\text{Bearing.capacity} := \left\| \begin{array}{l} \text{if } T_n \geq T_u \\ \quad \left\| \begin{array}{l} \text{"OK"} \\ \text{else} \\ \quad \left\| \begin{array}{l} \text{"Not OK"} \end{array} \right\| \end{array} \right\| \end{array} \right\| = \text{"OK"}$$

So, use 4 lifting points, #5 bend rebars.

Design of Bolts and Rods with a Nut Design Guide 1

$$f'_c := 3000 \quad \text{ksi}$$

$$n_{bolts} := 4$$

$$P_u := 110 \quad \text{kip}$$

$$T_u := \frac{P_u}{n_{bolts}} = 27.5 \quad \text{kip}$$

$$\varphi_t := 0.75$$

$$F_u := 58 \quad \text{ksi}$$

$$A_g := \frac{T_u}{0.75 \cdot \varphi_t \cdot F_u} = 0.8 \quad \text{in}^2$$

$$A_{psf} := \frac{T_u}{4 \cdot \varphi_t \cdot \sqrt{f'_c}} \cdot \frac{1}{\text{psi}} = 167.4 \quad \text{in}^2$$

$$L_{min} := \sqrt{\frac{A_{psf}}{3.14}} = 7.3 \quad \text{in}$$

For this case,

$$L := 31.625 \quad \text{in}$$

$$\text{Lenght.check} := \left\| \begin{array}{l} \text{if } L \geq L_{min} \\ \quad \left\| \begin{array}{l} \text{"OK"} \\ \text{else} \\ \quad \left\| \begin{array}{l} \text{"Not OK"} \end{array} \right\| \end{array} \right\| \end{array} \right\| = \text{"OK"}$$

resistance factor for tension

minimum tensile strength for A36 bar

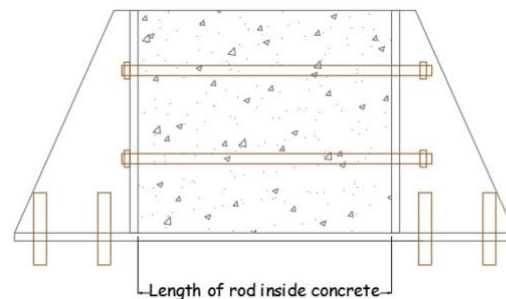
gross bolt area

required surface area

1/psi (for equation unit matching)

bolt length

Failure occurs when either the bolt fails or when a cone of concrete surrounding the bolt separates from the concrete. The cone radiates at an assumed angle of 45° (DG1)



Non-Commercial Use Only

Check bolts (rebar) capacity

From DSI America website:

DYWIDAG THREADBAR® Reinforcing Steel ASTM A615 (Grade 75 & 80)

THREADBAR® Designation	Maximum THREADBAR® Diameter			Minimum Yield Stress (f _y)		Nominal Cross Section Area (A _n)		Minimum Yield Load (f _y x A _n)		Nominal Weight	
	[mm]	[in]	[mm]	[ksi]	[MPa]	[in ²]	[mm ²]	[kips]	[kN]	[lbs/ft]	[kg/m]
#6	19	0.86	22	75	517	0.44	284	33.0	147	1.50	2.23
#7	22	0.99	25	75	517	0.60	387	45.0	200	2.04	3.04
#8	25	1.12	28	75	517	0.79	510	59.3	264	2.67	3.97
#9	29	1.26	32	75	517	1.00	645	75.0	334	3.40	5.06
#10	32	1.43	36	75	517	1.27	819	95.3	424	4.30	6.40
#11	36	1.61	41	75	517	1.56	1,006	117.0	520	5.31	7.90
#14	43	1.86	47	80	552	2.25	1,452	180.0	801	7.65	11.38
#18	57	2.50	64	80	552	4.00	2,581	320.0	1,423	13.60	20.24
#20	63	2.72	69	80	552	4.91	3,168	393.0	1,748	16.70	24.85
#24	75	3.18	81	75	517	7.06	4,555	529.5	2,355	24.09	35.85
#28	90	3.68	94	75	517	9.62	6,207	721.5	3,209	32.79	48.80

Note: Maximum allowable temporary tension is 90% of yield load. Mill length is 60 ft (#6 through #24) and 53 ft for #28.

$$yield.load := 75 \text{ kip}$$

#9 threadbar

$$T_u := \frac{110 \text{ kip}}{4} = 27.5 \text{ kip}$$

$$Tensile.check := \begin{cases} \text{if } yield.load \geq T_u \\ \quad \text{“OK”} \\ \text{else} \\ \quad \text{“Not OK”} \end{cases} = \text{“OK”}$$

Use threadbar #9 as rods, 40" long

Design of Bracket

Steel Plates

For both ends of the actuator
 AISC 14th Edition
 Steel Design Guide 1 - LRFD Procedure

$$f_y := 50 \text{ ksi}$$

$$\phi_c := 0.6$$

Grade 50 steel

$$f'_c := 3000 \text{ psi}$$

Vertical Plate

Design of Axially Loaded Base Plate

$$P_u := 110 \text{ kip}$$

$$A_1 := \frac{P_u}{1.7 \cdot \phi_c \cdot f'_c} = 35.9 \text{ in}^2$$

Dimensions of actuator plate:

$$d := 13.88 \text{ in}$$

$$b_f := 13.88 \text{ in}$$

$$\Delta := 0.5 \cdot (0.95 \cdot d - 0.8 \cdot b_f) = 1 \text{ in}$$

$$N := \sqrt{A_1} + \Delta = 7 \text{ in}$$

$$B := \frac{A_1}{N} = 5.1 \text{ in}$$

$$A_2 := 4 \cdot N \cdot B = 143.8 \text{ in}^2$$

$$A_{block} := w \cdot d = 333.1 \text{ in}^2$$

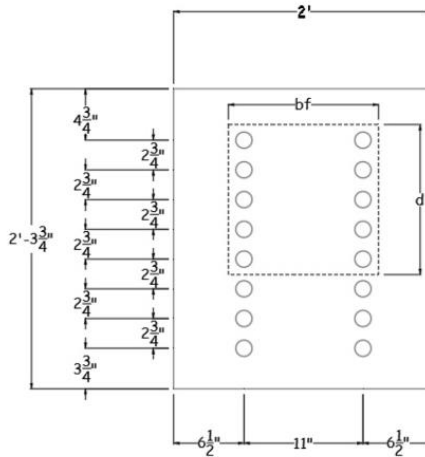
$$Check := \left\| \begin{array}{l} \text{if } A_{block} \geq A_2 \\ \quad \left\| \begin{array}{l} \text{"OK"} \\ \text{else} \\ \text{"Not OK"} \end{array} \right\| \\ \end{array} \right\| = \text{"OK"}$$

Considering the different locations needed for the actuator, the size of the base plate should be 28.75" by 24". Then:

$$N := 28.75 \text{ in}$$

$$B := 24 \text{ in}$$

$$m := \frac{N - 0.95 \cdot d}{2} = 7.8 \text{ in}$$



Pedestal dimensions

AISC Eq 14-2

AISC Eq 14-3

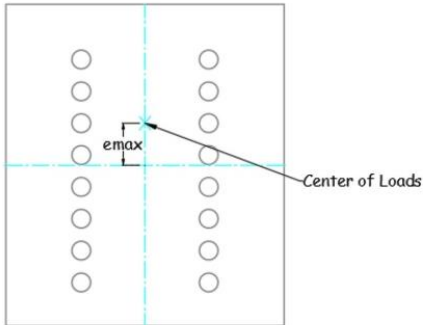
$$l := \max(m, n) = 7.8 \text{ in}$$

Non-Commercial Use Only

$$t_{axial} := l \cdot \sqrt{\frac{2 \cdot P_u}{0.9 \cdot f_y \cdot B \cdot N}} = 0.7 \text{ in}$$

AISC Eq 14-7a

Design of Base Plate with Moments



$$e_{max} := 3.69 \text{ in}$$

e_{max} is the difference of center of load at the highest location of the actuator and the center of holes

$$Eccentricity.criteria := \begin{cases} \text{if } e_{max} \leq \frac{N}{6} \\ \quad \text{"Equation 1"} \\ \text{else} \\ \quad \text{"Equation 2"} \end{cases} = \text{"Equation 1"}$$

$$M := P_u \cdot e_{max} = 405.9 \text{ kip} \cdot \text{in}$$

$$I := \frac{N \cdot B^3}{12} = 33120 \text{ in}^4$$

$$c := \frac{n}{2} = 3.224 \text{ in}$$

$$f_{12max} := \frac{P_u}{B \cdot N} + \frac{M \cdot c}{I} = 198.9 \text{ psi}$$

Equation 1- part A

$$f_{12min} := \frac{P_u}{B \cdot N} - \frac{M \cdot c}{I} = 119.9 \text{ psi}$$

Equation 1- part B

$$stress := \max(f_{12max}, f_{12min}) = 0.2 \text{ ksi}$$

Non-Commercial Use Only

$$A := 3 \cdot \left(\frac{N}{2} - e_{max} \right) = 32.1 \text{ in}$$

$$f_1 := \frac{2 \cdot P_u}{A \cdot B} = 0.3 \text{ ksi}$$

Equation 2

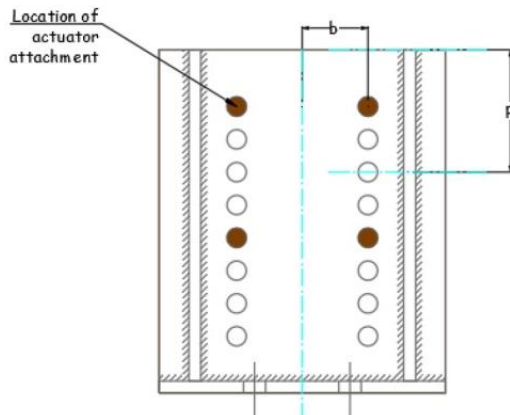
$$\phi_c := 0.6$$

$$F_p := 0.85 \cdot \phi_c \cdot f'_c \cdot \sqrt{\frac{A_2}{A_1}} = 3.1 \text{ ksi}$$

$$Capacity := \begin{cases} \text{if } F_p \geq stress \\ \quad \text{“OK”} \\ \text{else} \\ \quad \text{“Not OK”} \end{cases} = \text{“OK”}$$

Prying Action

Prying action is not needed to be consider for this case because the plate is embedded in concrete. But it was checked anyways.



$$T := 27.5 \text{ kip}$$

required strenght per bolt

$$d_b := 1.128 \text{ in}$$

bolt diameter. In this case, nominal diameter of #9 rebar

$$b := 5.5 \text{ in}$$

distance of bolt to centerline of the steel element

Non-Commercial Use Only

$$b' := \left(b - \frac{d_b}{2} \right) = 4.9 \text{ in}$$

$$p := 10.2519 \text{ in}$$

tributary length, maximum of 2b

$$F_u := 65 \text{ ksi}$$

AISC Table 2.4, minimum F_u for Grade 50 steel

$$\phi := 0.9$$

$$t_{prying} := \sqrt{\frac{4 \cdot T \cdot b'}{\phi \cdot p \cdot F_u}} = 0.95 \text{ in}$$

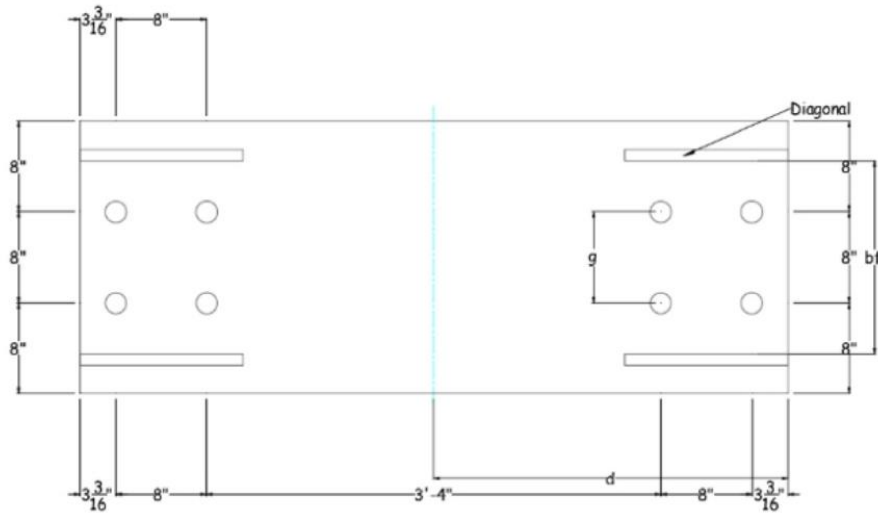
$$t_{min} := \max(t_{axial}, t_{prying}) = 0.95 \text{ in}$$

$$t_{vertical} := 1 \text{ in}$$

$$Thickness.check := \begin{cases} \text{if } t_{vertical} \geq t_{min} \\ \quad \text{"OK"} \\ \text{else} \\ \quad \text{"Not OK"} \end{cases} = \text{"OK"}$$

Bottom Plate

Adjustment of the size of the plate, accordingly with the needs.



Non-Commercial Use Only

Dimensions

$$d := 31.18 \text{ in}$$

$$b_f := 17 \text{ in}$$

$$N := 31.18 \text{ in}$$

$$B := 23.75 \text{ in}$$

$$m := \frac{N - 0.95 \cdot d}{2} = 0.8 \text{ in} \quad \text{AISC Eq 14-2}$$

$$n := \frac{B - 0.8 \cdot b_f}{2} = 5.1 \text{ in} \quad \text{AISC Eq 14-3}$$

$$l := \max(m, n) = 5.1 \text{ in}$$

$$P_u := 4 \cdot N_u = 61.8 \text{ kip} \quad \text{Maximum pullout load at anchors}$$

$$t_{axial} := l \cdot \sqrt{\frac{2 \cdot P_u}{0.9 \cdot f_y \cdot B \cdot N}} = 0.3 \text{ in} \quad \text{AISC Eq 14-7a}$$

Check for Uplift Loads
Design Guide 1 page 15

$$f_y := 50 \text{ ksi}$$

$$\phi_c := 0.6$$

$$f'_c := 3000 \text{ psi}$$

$$Uplift.criteria := \left\| \begin{array}{l} \text{if } \sqrt{2} \cdot b_f \leq d \\ \quad \left\| \begin{array}{l} \text{"Equation 1"} \\ \text{else} \\ \text{"Equation 2"} \end{array} \right\| \\ \end{array} \right\| = \text{"Equation 1"}$$

$$\phi_b := 0.9$$

$$g := 8 \text{ in}$$

$$tp_1 := \sqrt{\frac{\sqrt{2} \cdot P_u \cdot g}{4 \cdot \phi_b \cdot b_f \cdot f_y}} = 0.5 \text{ in} \quad \text{Equation 1}$$

Non-Commercial Use Only

$$t_{p2} := \sqrt{\frac{P_u \cdot g \cdot d}{\phi_b \cdot f_y \cdot (d^2 + 2 \cdot b_f^2)}} = 0.5 \text{ in}$$

Equation 2

$$t_{uplift} := t_{p1} = 0.5 \text{ in}$$

$$t_{min} := \max(t_{axial}, t_{uplift}) = 0.5 \text{ in}$$

$$t_{bottom} := 1 \text{ in}$$

$$Thickness.check := \begin{cases} \text{if } t_{bottom} \geq t_{min} \\ \quad \text{"OK"} \\ \text{else} \\ \quad \text{"Not OK"} \end{cases} = \text{"OK"}$$

Diagonal Stiffener

$$a := 15.375 \text{ in}$$

$$b := 28.75 \text{ in}$$

$$z := 1.39 - 2.2 \cdot \left(\frac{b}{a}\right) + 1.27 \cdot \left(\frac{b}{a}\right)^2 - 0.25 \cdot \left(\frac{b}{a}\right)^3 = 0.08$$

$$E := 29000 \text{ ksi}$$

$$e_{load} := 18.5 \text{ in}$$

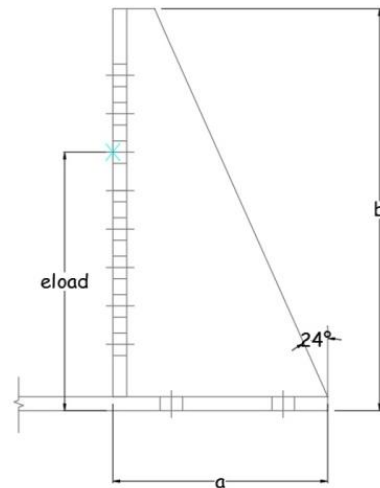
Buckling

$$P_u := 110 \text{ kip}$$

$$F_y := 50 \text{ ksi}$$

$$\phi_c := 0.85$$

$$t_b := \frac{P_u}{\phi_c \cdot F_y \cdot z \cdot b} = 1.1 \text{ in}$$



Stability Requirement

$$\text{For } 1.0 \leq b/a \leq 2.0$$

Non-Commercial Use Only

$$ratio_{bt} := 1.47 \cdot \left(\frac{b}{a}\right) \cdot \sqrt{\frac{E}{F_y}} = 66.2$$

$$t_s := \frac{b}{ratio_{bt}} = 0.4 \quad in$$

Plastic Strength method

$$e := e_{load} - \frac{b}{2} = 4.1 \quad in$$

$$s := 0.165434 \quad s = \sin^2(24)$$

$$t_p := \frac{P_u}{\phi_c \cdot F_y \cdot s \cdot \sqrt{4 \cdot e^2 + b^2} - 2 \cdot e} = 0.5 \quad in$$

$$t_{min} := \max(t_b, t_s, t_p) = 1.1 \quad in$$

$$t_{diagonal} := 1 \quad in$$

$$Thickness.check := \begin{cases} \text{if } 2 \cdot t_{diagonal} \geq t_{min} \\ \quad \text{“OK”} \\ \text{else} \\ \quad \text{“Not OK”} \end{cases} = \text{“OK”} \quad \text{There are 2 diagonals in the bracket}$$

For the diagonal stiffener, use 1" each side, for tension and compression bracket

Flexural yielding of vertical plate

$$t := \frac{t_{vertical}}{1 \quad in} = 1 \quad (\text{unit adjustment})$$

$$M_u := P_u \cdot e_{load} = 2035 \quad k-in$$

$$Z_x := \frac{t \cdot b^2}{4} = 206.6 \quad in^3$$

$$M_n := F_y \cdot Z_x = 10332 \quad k-in$$

$$\phi := 0.9$$

Non-Commercial Use Only

$$Flexure.check := \begin{cases} \text{if } \phi \cdot M_n \geq M_u \\ \quad \text{"OK"} \\ \text{else} \\ \quad \text{"Not OK"} \end{cases} = \text{"OK"}$$

Shear yielding of the plate

$$A_g := t \cdot b = 28.8 \quad in^2$$

$$R_n := 0.6 \cdot F_y \cdot A_g = 862.5 \quad kip$$

$$\phi := 0.9$$

$$Shear.check := \begin{cases} \text{if } \phi \cdot R_n \geq P_u \\ \quad \text{"OK"} \\ \text{else} \\ \quad \text{"Not OK"} \end{cases} = \text{"OK"}$$

Welds

Weld in vertical plate

For 50 ksi steel

Preliminary trial

$$a_{maxeff} := \frac{t}{1.49} = 0.67$$

use 3/4" welds

Try thickness of 3/4"

Defining the length of weld

$$\phi R_n := 1.392 \cdot \frac{\frac{3}{4}}{\frac{1}{16}} = 16.7 \quad \frac{kip}{in}$$

$$Length_{weld} := \frac{P_u}{\phi R_n} = 6.6 \quad in$$

use minimum of 7 inches for length of weld.

Because the length of weld is bigger than the minimum, try 1/2" weld

Try thickness of 1/2"

$$F_{exx} := 70 \text{ ksi}$$

$$F_{nw} := 0.6 \cdot F_{exx} = 42 \text{ ksi}$$

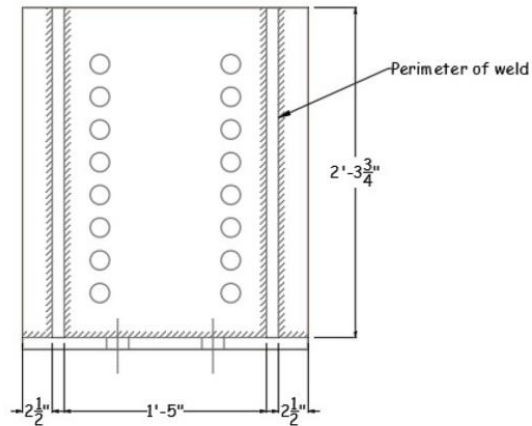
$$A_{we} := 0.5 \cdot 133 = 66.5 \text{ in}^2$$

$$R_n := F_{nw} \cdot A_{we} = 2793 \text{ kip}$$

$$\phi := 0.75$$

$$P_u := 110 \text{ kip}$$

$$Capacity.check := \begin{cases} \text{if } \phi \cdot R_n \geq P_u \\ \quad \text{"OK"} \\ \text{else} \\ \quad \text{"Not OK"} \end{cases} = \text{"OK"}$$



Cross section of weld (in^2)
133 in^2 is the perimeter of weld

Bottom weld parallel to the load

$$a := 0.5 \text{ in}$$

$$t_e := 0.707 \cdot a = 0.354 \text{ in}$$

effective throat dimension

$$R_n := t_e \cdot F_{nw} = 14.8 \text{ kip}$$

$$\phi := 0.75$$

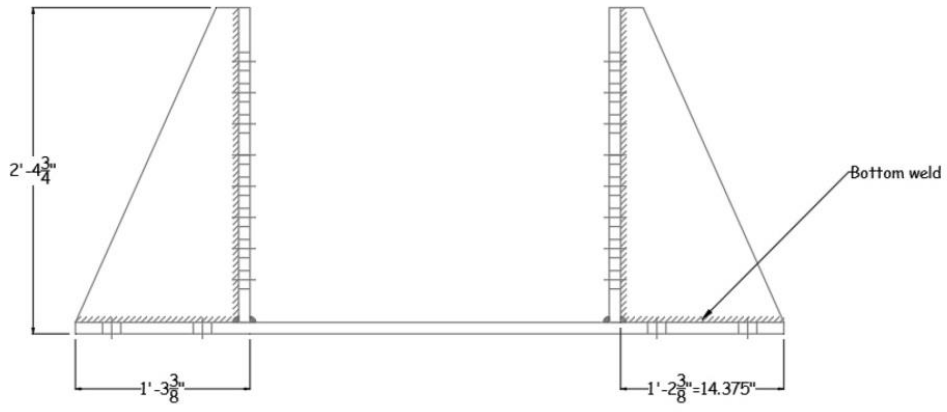
shear strength

$$\phi R_n := \phi \cdot R_n = 11.1 \frac{\text{kip}}{\text{in}}$$

$$Length_{weldrequired} := \frac{P_u}{\phi R_n} = 9.9 \text{ in}$$

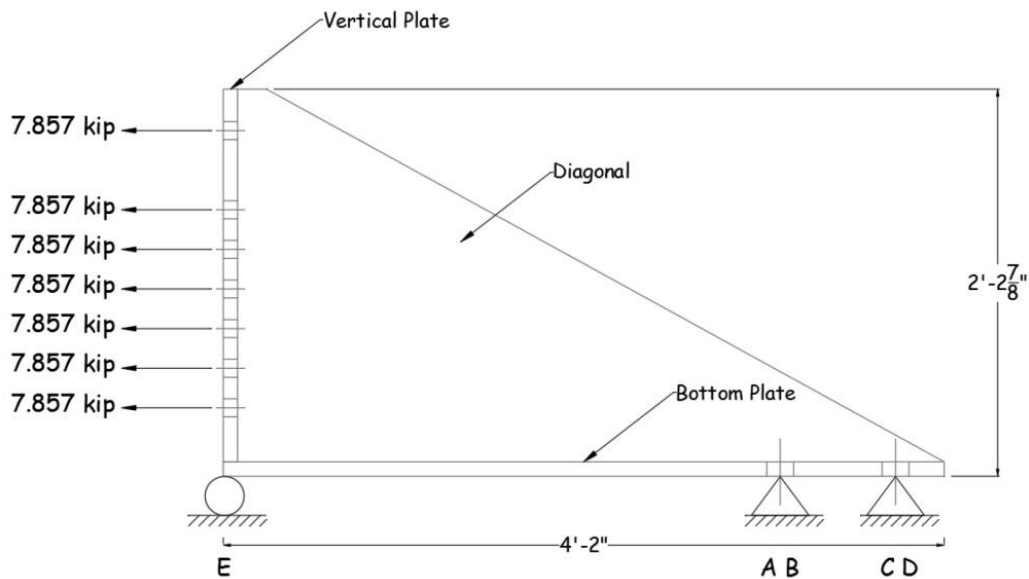
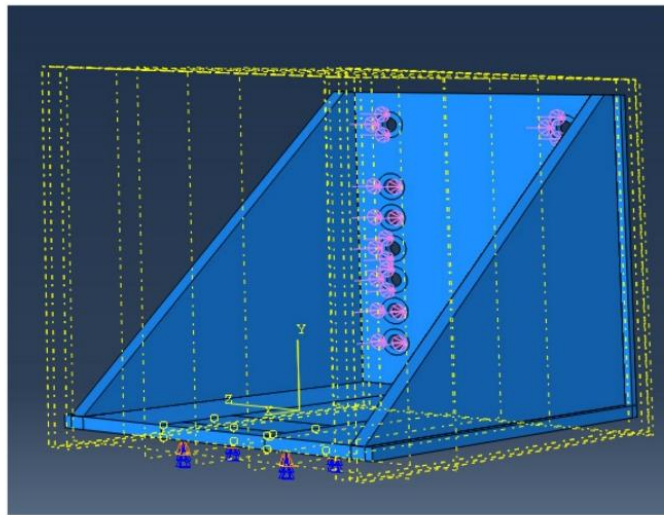
$$Length_{weld} := 14.375 \text{ in}$$

conservative approach, it it only considering one side of the diagonal, there are a total of 4 parts of the same length



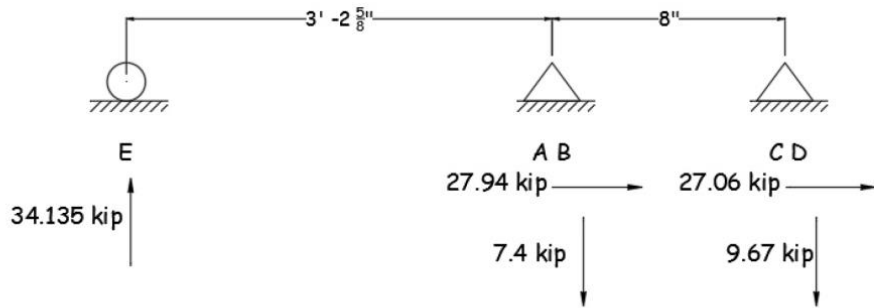
Capacity.check := $\begin{cases} \text{if } Lenght_{weld} \geq Lenght_{weldrequired} \\ \quad \text{"OK"} \\ \text{else} \\ \quad \text{"Not OK"} \end{cases} = \text{"OK"}$

Use 1/2" filled weld



The load applied at each nut is a total of 7.857 kip, as shown in the picture. This total load is distributed in the nut area. Note: the picture only shows one line of bolts/nut, there are 14 in total, totalizing 110 kips. Also E is a roller located at the midpoint of the width, and A and B are in the anchors in line, as well as C and D. Anchors are pin supports.

Non-Commercial Use Only



N.T.S.

Load at Anchors

$$n_{anchors} := 4$$

$$V_{ut} := 110 \text{ kip}$$

$$V_u := 27.9 \text{ kip}$$

(From Abaqus)

$$Plate_{bottom} := 1 \text{ in} \cdot 50 \text{ in} \cdot 23.75 \text{ in} = 1187.5 \text{ in}^3$$

$$Plate_{vertical} := 23.75 \text{ in} \cdot 25.875 \text{ in} \cdot 1 \text{ in} = 614.5 \text{ in}^3$$

$$Bracket := 1 \text{ in} \cdot 659.82 \text{ in}^2 = 659.8 \text{ in}^3$$

$$V_s := (Plate_{bottom} + Plate_{vertical} + 2 \cdot Bracket) = 3121.7 \text{ in}^3$$

$$\gamma := 490 \text{ pcf}$$

$$Weight_{steel} := V_s \cdot \gamma = 0.9 \text{ kip}$$

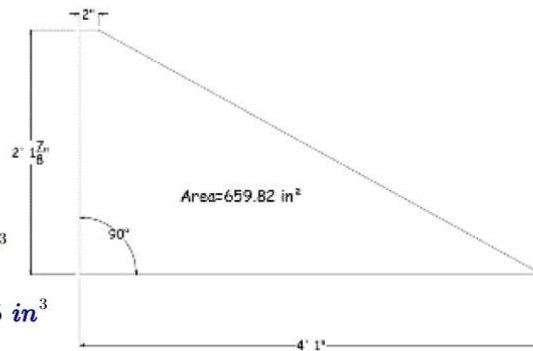
$$N_u := 9.67 \text{ kip}$$

(From Abaqus)

Anchors Capacity

From ACI 318-11 Appendix D

According to Ap D, steel elementes for adhesive anchors include threaded rods. So, anchor type = adhesive anchor



Non-Commercial Use Only

$d_a := 1.61 \text{ in}$ outside diameter of the rod #11 carbon-steel

$A := \pi \cdot \left(\frac{d_a}{2}\right)^2 = 2 \text{ in}^2$ area of the rod

$nt := 1.5 \text{ in}^{-1}$ number of threads per inch (measured)

Steel strength of anchor in shear

$A_{sev} := \frac{\pi}{4} \cdot \left(d_a - \frac{0.9743}{nt}\right)^2 = 0.7 \text{ in}^2$ effective cross-sectional area of an anchor in shear (D-28)

$f_{ya} := 75000 \text{ psi}$ specified yield strength of anchor steel, Grade 75

$f_{uta} := \min(1.9 \cdot f_{ya}, 125000 \text{ psi}) = 125000 \text{ psi}$

$V_{sa} := 0.6 \cdot A_{sev} \cdot f_{uta} = 54.3 \text{ kip}$ (D-28)

Concrete breakout strength of anchor in shear

Use Case 3 as the conservative approach. Case 3 is shown on Fig. RD.6.2.1 (b), where $s < c_{a1,1}$, apply the entire shear load V to the front anchor. This case does not apply for anchors welded to a common plate. For the calculation of concrete breakout, c_{a1} is taken as $c_{a1,1}$

Because of the strong floor, all distances to edge of concrete are assumed to be 100 in

$h_a := 48 \text{ in}$ thickness of member in which an anchor is located. In this case it is the strong floor

$c_{a1} := 100 \text{ in}$ distance from center of an anchor to the edge of concrete

$A_{vc} := 2 \cdot (1.5 \cdot c_{a1}) \cdot h_a = 14400 \text{ in}^2$ projected concrete failure area of a single anchor or group of anchors, for calculation of strength in shear. Fig. RD.6.1 (b)

$A_{vco} := 4.5 \cdot c_{a1}^2 = 45000 \text{ in}^2$ (D-32)

$h_{ef} := 3 \text{ in}$ effective embedment depth of anchor. Conservatively estimated base on 3 in measured

$$l_e := h_{ef} \text{ in}$$

(D.6.2.2 - for anchors with a constant stiffness over the full length of embedded section, such as headed studs and post-installed anchors with one tubular shell over full length of the embedment depth)

$$d_a := d_a \cdot \frac{1}{\text{in}} = 1.6$$

unit adjustment

$$\lambda := 1.0$$

normal weight concrete (uniteless)

$$\lambda_a := 1 \cdot \lambda = 1$$

D.3.6 - no lightweight concrete

$$f'c := 3000 \text{ psi}$$

assuming a low value for concrete of strong floor

$$V_{b1} := \left(7 \cdot \left(\frac{l_e}{d_a} \right)^{0.2} \cdot \sqrt{d_a} \right) \cdot \lambda_a \cdot \sqrt{f'c} \cdot (c_{a1})^{1.5} = 550973.5 \text{ lb} \quad (\text{D-33})$$

$$V_{b2} := 9 \cdot \lambda_a \cdot \sqrt{f'c} \cdot (c_{a1})^{1.5} = 492950.3 \text{ lb} \quad (\text{D-34})$$

$$V_b := \min(V_{b1}, V_{b2}) = 492950.3 \text{ lb}$$

$$c_{a2} := 100 \text{ in}$$

distance between resultant shear load on group of anchors loaded in shear in the same direction, and the centroid of the group of anchors loaded in shear in the same direction.

$$e_v := 0$$

$$\psi_{ecv} := \frac{1}{\left(1 + \frac{2 \cdot e_v}{3 \cdot c_{a1}} \right)} = 1$$

(D-36)

$$\psi_{edv} := \left\| \begin{array}{l} \text{if } c_{a2} \geq 1.5 \cdot c_{a1} \\ \quad \left\| \begin{array}{l} \text{"}\psi_{edv}=\text{equation D-37"} \\ \text{else} \\ \text{"}\psi_{edv}=\text{equation D-38"} \end{array} \right\| \\ \end{array} \right\| = \text{"}\psi_{edv}=\text{equation D-38"}$$

$$\psi_{edv} := 1 \quad (\text{D-37})$$

$$\psi_{edv} := 0.7 + 0.3 \cdot \frac{c_{a2}}{1.5 \cdot c_{a1}} = 0.9 \quad (\text{D-38})$$

Non-Commercial Use Only

$$\psi_{cv} := 1.0$$

D.6.2.7 for anchors in cracked concrete without supplementary reinforcement or with edge reinforcement smaller than a #4 bar. Conservative approach

$$\psi_{hv} := \sqrt{\frac{1.5 \cdot c_{a1}}{h_a}} = 1.8$$

(D-39)

it should not be taken less than 1.0

$$V_{cbg1} := \frac{A_{vc}}{A_{vco}} \cdot \psi_{ecv} \cdot \psi_{edv} \cdot \psi_{cv} \cdot \psi_{hv} \cdot V_b = 250969.3 \text{ lb} \quad (\text{D-31})$$

$$V_{cbg} := \frac{V_{cbg1} \cdot 1 \text{ kip}}{1000} = 251 \text{ kip}$$

units adjustment

Concrete pryout strength of anchor in shear

$$k_{cp} := 2$$

for hef greater than 2.5in (D.6.3.1)

$$c_{amin} := 100 \text{ in}$$

$$\tau_{uncr} := 1000 \text{ psi}$$

Table D.5.5.2

$$c_{na} := 10 \cdot d_a \cdot \sqrt{\frac{\tau_{uncr}}{1100}} = 15.4 \text{ in}$$

(D-21)

projected distance from center of an anchor shaft on one side of the anchor required to develop the full bond strength

$$c_{a1} := 100 \text{ in}$$

distance from the center of an anchor shaft to the edge of concrete in one direction

$$c_{a2} := 100 \text{ in}$$

distance from the center of an anchor shaft to the edge of concrete perpendicular to c_{a1}

$$s_1 := 8 \text{ in}$$

$$s_2 := 8 \text{ in}$$

$$A_{na} := (c_{na} + s_1 + c_{a1}) \cdot (c_{na} + s_2 + c_{a2}) = 15215.4 \text{ in}^2$$

Figure RD.5.5.1

$$A_{nao} := (2 \cdot c_{na})^2 = 942.6 \text{ in}^2$$

(D-20)

Non-Commercial Use Only

$$x_{cl} := \frac{7.4 \cdot -4 + 9.67 \cdot 4}{7.4 + 9.67} = 0.53$$

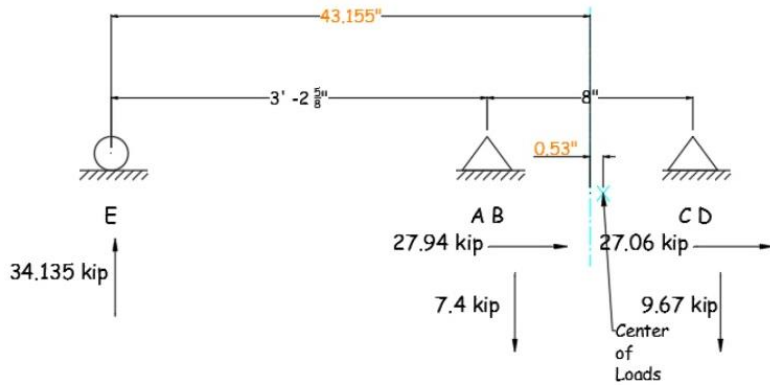
$$distance := 43.155 \quad in$$

$$e_n := distance = 43.2 \quad in$$

Center of load from AB and CD loads

Distance center of loads to point of rotation (I)

distance between resultant tension load on group of anchors loaded in tension and the centroid of the group of anchors loaded in tension



N.T.S.

$$\psi_{ecna} := \frac{1}{\left(1 + \frac{e_n}{c_{na}}\right)} = 0.3$$

(D-23)

$$\psi_{edna} := 1$$

(D-24)

$$c_{ac} := 2 \cdot h_{ef} = 6$$

D.8.6 for adhesive anchors

$$\psi_{cpna} := 1$$

(D-26)

$$\tau_{cr} := 300 \quad psi$$

Table D.5.5.2

$$N_{ba} := \lambda_a \cdot \tau_{cr} \cdot \pi \cdot d_a \cdot h_{ef} \cdot 1 \quad lbf = 4552.2 \quad lbf$$

(D-22)

$$N_{ag} := \frac{A_{na}}{A_{nao}} \cdot \psi_{ecna} \cdot \psi_{edna} \cdot \psi_{cpna} \cdot \psi_{hv} \cdot N_{ba} = 34.1 \quad kip$$

(D-19)

Bonded strength of adhesive anchor in tension unit adjustment

Non-Commercial Use Only

$$A_{nc} := (c_{a1} + s_1 + 1.5 \cdot h_{ef}) \cdot (c_{a2} + s_2 + 1.5 \cdot h_{ef}) = 12656.3 \quad \text{Figure RD.5.2.1}$$

$$A_{nco} := 9 \cdot h_{ef}^2 = 81 \quad \text{in}^2 \quad (\text{D-5})$$

$$\psi_{ecn} := \frac{1}{\left(1 + \frac{2 \cdot e_n}{3 \cdot h_{ef}}\right)} = 0.1 \quad (\text{D-8})$$

$$\psi_{edn} := 1 \quad (\text{D-9, } c_{amin} \geq 1.5 \cdot h_{ef})$$

$$\psi_{cn} := 1.4 \quad \text{D.5.2.6 for post installed anchors}$$

$$\psi_{cpn} := 1 \quad (\text{D-11, } c_{amin} \geq c_{ac})$$

$$k_c := 17 \quad \text{for post installed anchors}$$

$$N_b := k_c \cdot \lambda_a \cdot \sqrt{f'_c} \cdot h_{ef}^{1.5} = 4838.3 \quad \text{lb} \quad (\text{D-6})$$

$$N_{cbg} := \frac{A_{nc}}{A_{nco}} \cdot \psi_{ecn} \cdot \psi_{edn} \cdot \psi_{cn} \cdot \psi_{cpn} \cdot N_b \cdot 1 \quad \text{lb} = 99.9 \quad \text{kip} \quad (\text{D-4})$$

unit adjustment

$$N_{cpg} := \min(N_{ag}, N_{cbg}) = 34.1 \quad \text{kip}$$

$$V_{cpg} := k_{cp} \cdot N_{cpg} = 68.2 \quad \text{kip} \quad (\text{D-41})$$

$$V_n := \min(V_{sa}, V_{cbg}, V_{cpg}) = 54.3 \quad \text{kip}$$

$$\phi := 0.65$$

governed by strength of a ductile steel element - shear loads (D.4.3)

$$\phi V_n := \phi \cdot V_n = 35.3 \quad \text{kip}$$

$$\text{Shear.capacity}_{anchors} := \begin{cases} \text{if } V_u \leq \phi V_n \\ \quad \text{“OK”} \\ \text{else} \\ \quad \text{“Not OK”} \end{cases} = \text{“OK”}$$

Steel strength of anchor in tension

Non-Commercial Use Only

$$A_{sen} := A_{sev} = 0.7 \text{ in}^2$$

effective cross-sectional area of an anchor in tension

$$N_{sa} := A_{sen} \cdot f_{uta} = 90.6 \text{ kip}$$

futa equation on page 3 (D-2)

$$\psi_{cp} := 1$$

N_p is not checked for adhesive anchor

D.5.3.6 (conservative)

$$N_n := \min(N_{sa}, N_{cbg}, N_{ag}) = 34.1 \text{ kip}$$

$$\phi := 0.75$$

governed by concrete pryout - condition A - tension loads (D.4.3)

$$\phi N_n := \phi \cdot N_n = 25.6 \text{ kip}$$

$$Tension.capacity_{anchors} := \left\| \begin{array}{l} \text{if } N_u \leq \phi N_n \\ \quad \left\| \begin{array}{l} \text{"OK"} \\ \text{else} \\ \quad \left\| \begin{array}{l} \text{"Not OK"} \end{array} \right\| \end{array} \right. \\ \end{array} \right\| = \text{"OK"}$$

Interaction of tensile and shear forces (D.7)

$$V_{ua} := V_u = 27.9 \text{ kip}$$

$$N_{ua} := N_u = 9.7 \text{ kip}$$

$$Total.capacity_{anchors} := \left\| \begin{array}{l} \text{if } \frac{N_{ua}}{\phi N_n} + \frac{V_{ua}}{\phi V_n} \leq 1.2 \\ \quad \left\| \begin{array}{l} \text{"OK"} \\ \text{else} \\ \quad \left\| \begin{array}{l} \text{"Not OK"} \end{array} \right\| \end{array} \right. \\ \end{array} \right\| = \text{"OK"}$$

From AISC 14th Ed, J9: "The anchor rods shall be designed in accordance with the requirements for threaded parts in Table J3.2. And satisfy the requirements of ACI 318.

From Table J3.2, Nominal Tensile Strength (F_{nt}) is:

$$F_u := 100 \text{ ksi}$$

Ultimate Tensile Stress for Grade 75 Thread Rebar. (online source)

$$F_{nt} := 0.75 \cdot F_u = 75 \text{ ksi}$$

$$Stress.check := \left\| \left\| \begin{array}{l} \text{if } \frac{N_u}{A_{sev}} \leq F_{nt} \\ \quad \left\| \begin{array}{l} \text{"OK"} \\ \text{else} \\ \text{"Not OK"} \end{array} \right\| \end{array} \right\| = \text{"OK"}$$

Check crane capacity

$$Crane.capacity := 22.5 \text{ kip}$$

$$Capacity := \left\| \left\| \begin{array}{l} \text{if } Crane.capacity > Weight_{steel} \\ \quad \left\| \begin{array}{l} \text{"OK"} \\ \text{else} \\ \text{"Not OK"} \end{array} \right\| \end{array} \right\| = \text{"OK"}$$

Check capacity of bolts located between the vertical plate and the plate of the specimen

From AISC Table 7-2 (Available Tensile Strength of Bolts), for nominal bolt area of 1.23 in^2 (nominal bolt diameter of 1.25 in), Group A307 (lowest capacity)

$$\phi r_n := 41.4 \text{ kip}$$

$$T_u := \frac{110 \text{ kip}}{14} = 7.9 \text{ kip}$$

$$Tensile.check := \left\| \left\| \begin{array}{l} \text{if } \phi r_n \geq T_u \\ \quad \left\| \begin{array}{l} \text{"OK"} \\ \text{else} \\ \text{"Not OK"} \end{array} \right\| \end{array} \right\| = \text{"OK"}$$

Use UNC 1 1/8-7 bolts

$$Weight_{actuator} := 1242 \text{ lbf}$$

weight of actuator based on information provided by MTS drawings in Specifications

$$d_{bolt} := 1.25 \text{ in}$$

$$F_{ybolt} := 150000 \text{ psi}$$

Non-Commercial Use Only

$$\phi_{vbolt} := 0.6$$

$$Strenght.shear := \phi_{vbolt} \cdot F_{ybolt} \cdot \left(\pi \cdot \frac{d_{bolt}^2}{4} \right) = 110.4 \text{ kip}$$

Strenght of the bolt in single shear

$$Shear.check := \left\| \begin{array}{l} \text{if } Strenght.shear \geq \frac{1}{2} Weight_{actuator} \\ \quad \left\| \begin{array}{l} \text{"OK"} \\ \text{else} \\ \text{"Not OK"} \end{array} \right\| \\ \end{array} \right\| = \text{"OK"}$$

Design of Bracket

Steel Plates

AISC 14th Edition

Steel Design Guide 1 - LRFD Procedure

$$f_y := 50 \text{ ksi} \quad \text{Grade 50 steel}$$

$$\phi_c := 0.6$$

$$f'_c := 3000 \text{ psi}$$

Vertical Plate

Design of Axially Loaded Base Plate

$$P_u := 110 \text{ kip}$$

$$A_1 := \frac{P_u}{1.7 \cdot \phi_c \cdot f'_c} = 35.9 \text{ in}^2$$

Dimensions of hole pattern

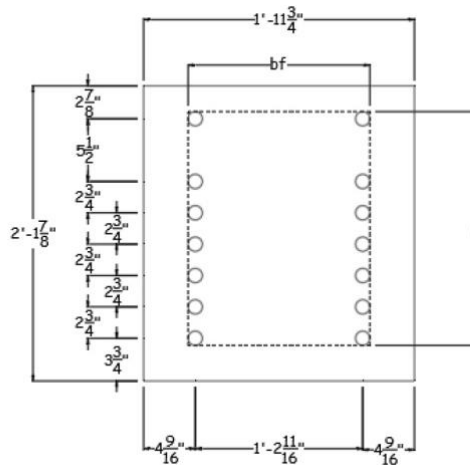
$$d := 20.5 \text{ in}$$

$$b_f := 15.95 \text{ in}$$

$$\Delta := 0.5 \cdot (0.95 \cdot d - 0.8 \cdot b_f) = 3.4 \text{ in}$$

$$N := \sqrt{A_1} + \Delta = 9.4 \text{ in}$$

$$B := \frac{A_1}{N} = 3.8 \text{ in}$$



Non-Commercial Use Only

$$A_2 := 4 \cdot N \cdot B = 143.8 \text{ in}^2$$

Adjustment of the size of the plate, accordingly with the needs.

$$N := 26.875 \text{ in}$$

$$B := 23.75 \text{ in}$$

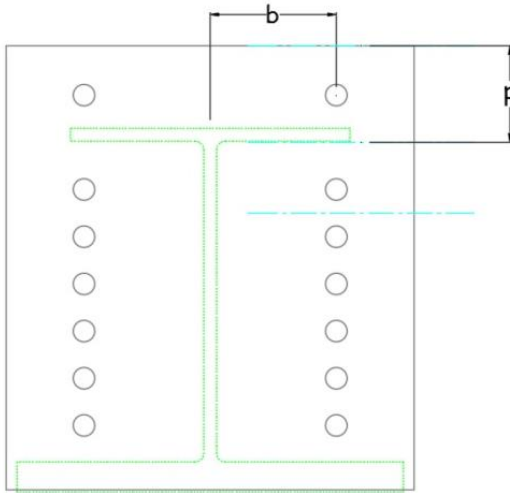
$$m := \frac{N - 0.95 \cdot d}{2} = 3.7 \text{ in} \quad \text{AISC Eq 14-2}$$

$$n := \frac{B - 0.8 \cdot b_f}{2} = 5.5 \text{ in} \quad \text{AISC Eq 14-3}$$

$$l := \max(m, n) = 5.5 \text{ in}$$

$$t_{axial} := l \cdot \sqrt{\frac{2 \cdot P_u}{0.9 \cdot f_y \cdot B \cdot N}} = 0.5 \text{ in} \quad \text{AISC Eq 14-7a}$$

Prying Action



$$T := 7.857 \text{ kip}$$

required strength per bolt

$$d_b := 1.125 \text{ in}$$

bolt diameter

Non-Commercial Use Only

$$b := 7.34 \text{ in}$$

distance of bolt to centerline of the steel element

$$b' := \left(b - \frac{d_b}{2} \right) = 6.8 \text{ in}$$

$$p := 5.625 \text{ in}$$

tributary length, maximum of 2b

$$F_u := 65 \text{ ksi}$$

AISC Table 2.4, minimum F_u for Grade 50 Steel

$$\phi := 0.9$$

$$t_{prying} := \sqrt{\frac{4 \cdot T \cdot b'}{\phi \cdot p \cdot F_u}} = 0.8 \text{ in}$$

AISC 9-20a

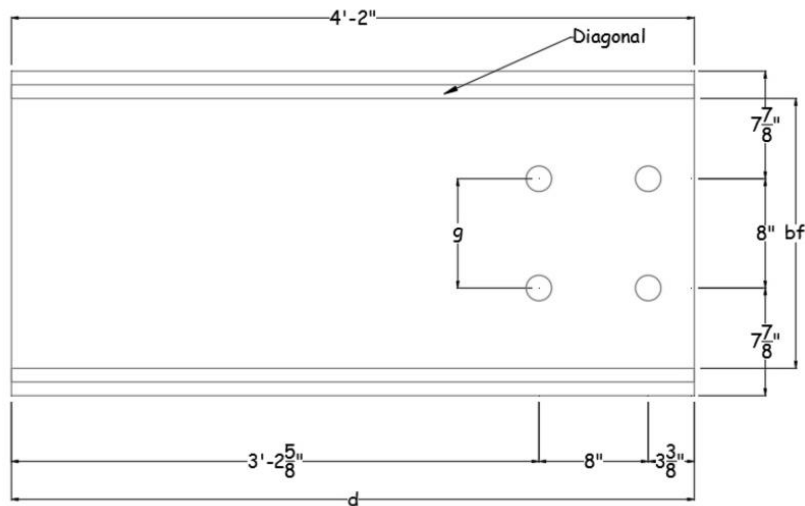
$$t_{min} := \max(t_{axial}, t_{prying}) = 0.8 \text{ in}$$

$$t_{vertical} := 1 \text{ in}$$

$$Thickness.check := \begin{cases} \text{if } t_{vertical} \geq t_{min} \\ \quad \text{"OK"} \\ \text{else} \\ \quad \text{"Not OK"} \end{cases} = \text{"OK"}$$

Bottom Plate

Adjustment of the size of the plate, accordingly with the needs.



Non-Commercial Use Only

Dimensions

$$d := 50 \text{ in}$$

$$b_f := 19.75 \text{ in}$$

$$N := 50 \text{ in}$$

$$B := 23.75 \text{ in}$$

$$m := \frac{N - 0.95 \cdot d}{2} = 1.3 \text{ in}$$

AISC Eq 14-2

$$n := \frac{B - 0.8 \cdot b_f}{2} = 4 \text{ in}$$

AISC Eq 14-3

$$l := \max(m, n) = 4 \text{ in}$$

$$P_u := 4 \cdot N_u = 38.7 \text{ kip}$$

Maximum pullout load at anchors

$$t_{axial} := l \cdot \sqrt{\frac{2 \cdot P_u}{0.9 \cdot f_y \cdot B \cdot N}} = 0.2 \text{ in}$$

AISC Eq 14-7a

Check for Uplift Loads

$$f_y := 50 \text{ ksi}$$

$$\phi_c := 0.6$$

$$f'_c := 3000 \text{ psi}$$

$$Uplift.criterion := \left\| \begin{array}{l} \text{if } \sqrt{2} \cdot b_f \leq d \\ \quad \left\| \begin{array}{l} \text{"Equation 1"} \\ \text{else} \\ \text{"Equation 2"} \end{array} \right\| \\ \end{array} \right\| = \text{"Equation 1"}$$

$$\phi_b := 0.9$$

$$g := 8 \text{ in}$$

Distance between holes, as shown on the figure above

$$t_{p1} := \sqrt{\frac{\sqrt{2} \cdot P_u \cdot g}{4 \cdot \phi_b \cdot b_f \cdot f_y}} = 0.4 \text{ in}$$

Equation 1

Non-Commercial Use Only

$$t_{p_2} := \sqrt{\frac{P_u \cdot g \cdot d}{\phi_b \cdot f_y \cdot (d^2 + 2 \cdot b_f^2)}} = 0.3 \text{ in} \quad \text{Equation 2}$$

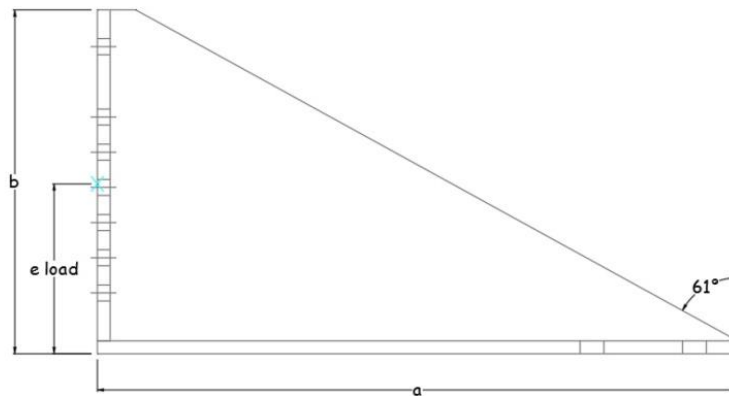
$$t_{uplift} := t_{p_1} = 0.4 \text{ in}$$

$$t_{min} := \max(t_{axial}, t_{uplift}) = 0.4 \text{ in}$$

$$t_{bottom} := 1 \text{ in}$$

$$\text{Thickness.check} := \begin{cases} \text{if } t_{bottom} \geq t_{min} & \text{= "OK"} \\ \text{"OK"} \\ \text{else} \\ \text{"Not OK"} \end{cases}$$

Diagonal Stiffener



$$a := 50 \text{ in}$$

$$b := 26.875 \text{ in}$$

$$z := 1.39 - 2.2 \cdot \left(\frac{b}{a}\right) + 1.27 \cdot \left(\frac{b}{a}\right)^2 - 0.25 \cdot \left(\frac{b}{a}\right)^3 = 0.5$$

$$E := 29000 \text{ ksi}$$

$$e_{load} := 13.4 \text{ in}$$

Buckling

Non-Commercial Use Only

$$P_u := 110 \text{ kip}$$

$$F_y := 50 \text{ ksi}$$

$$\phi_c := 0.85$$

$$t_b := \frac{P_u}{\phi_c \cdot F_y \cdot z \cdot b} = 0.2 \text{ in}$$

Stability Requirement

For $0.5 \leq b/a \leq 1.0$

$$ratio_{bt} := 1.47 \cdot \sqrt{\frac{E}{F_y}} = 35.4$$

$$t_s := \frac{b}{ratio_{bt}} = 0.8 \text{ in}$$

Plastic Strength method

$$e := \left| e_{load} - \frac{b}{2} \right| = 3.7 \cdot 10^{-2}$$

$$s := 0.794959 \quad s = \sin^2(61)$$

$$t_p := \frac{P_u}{\phi_c \cdot F_y \cdot s \cdot \sqrt{4 \cdot e^2 + b^2} - 2 \cdot e} = 0.1 \text{ in}$$

$$t_{min} := \max(t_b, t_s, t_p) = 0.8 \text{ in}$$

$$t_{diagonal} := 1 \text{ in}$$

$$Thickness.check := \begin{cases} \text{if } 2 \cdot t_{diagonal} \geq t_{min} \\ \quad \text{“OK”} \\ \text{else} \\ \quad \text{“Not OK”} \end{cases} = \text{“OK”}$$

There are 2 diagonals in the bracket

For the diagonal stiffener, use 1" each side, for tension bracket

Flexural yielding of vertical plate

$$t := \frac{t_{vertical}}{1 \text{ in}} = 1 \quad (\text{unit adjustment})$$

Non-Commercial Use Only

$$M_u := P_u \cdot e_{load} = 1474 \quad k-in$$

$$Z_x := \frac{t \cdot b^2}{4} = 180.6 \quad in^3$$

$$M_n := F_y \cdot Z_x = 9028.3 \quad k-in$$

$$\phi := 0.9$$

$$Flexure.check := \left\| \begin{array}{l} \text{if } \phi \cdot M_n \geq M_u \\ \quad \left\| \begin{array}{l} \text{"OK"} \\ \text{else} \\ \text{"Not OK"} \end{array} \right\| \end{array} \right\| = \text{"OK"}$$

Shear yielding of the plate

$$A_g := t \cdot b = 26.9 \quad in^2$$

$$R_n := 0.6 \cdot F_y \cdot A_g = 806.3 \quad kip$$

$$\phi := 0.9$$

$$Shear.check := \left\| \begin{array}{l} \text{if } \phi \cdot R_n \geq P_u \\ \quad \left\| \begin{array}{l} \text{"OK"} \\ \text{else} \\ \text{"Not OK"} \end{array} \right\| \end{array} \right\| = \text{"OK"}$$

Welds

Weld in the vertical plate

For 50 ksi steel

Preliminary trial

$$a_{maxeff} := \frac{t}{1.49} = 0.7$$

use 3/4" welds

Defining the length of weld

$$\phi R_n := 1.392 \cdot \frac{\frac{3}{4}}{\frac{1}{16}} = 16.7 \quad \frac{kip}{in}$$

$$Lenght_{weld} := \frac{P_u}{\phi R_n} = 6.6 \text{ in}$$

use minimum of 7 inches for length of weld.

Because the length of weld is bigger than the minimum, try 1/2" weld

Try thickness of 1/2"

$$F_{exx} := 70 \text{ ksi}$$

$$F_{nw} := 0.6 \cdot F_{exx} = 42 \text{ ksi}$$

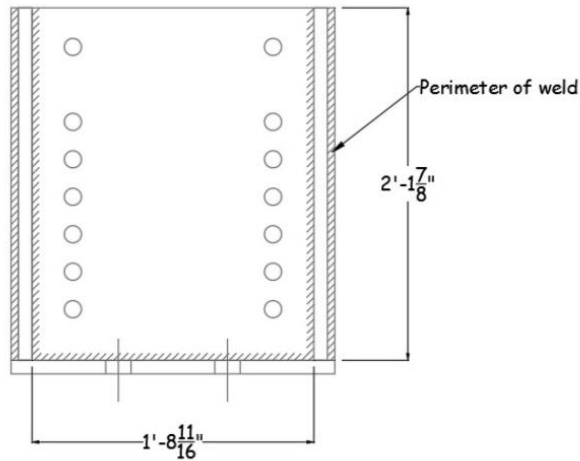
$$A_{we} := 0.5 \cdot 124 = 62 \text{ in}^2$$

$$R_n := F_{nw} \cdot A_{we} = 2604 \text{ kip}$$

$$\phi := 0.75$$

$$P_u := 110 \text{ kip}$$

$$Capacity.check := \begin{cases} \text{if } \phi \cdot R_n \geq P_u \\ \quad \text{"OK"} \\ \text{else} \\ \quad \text{"Not OK"} \end{cases} = \text{"OK"}$$



Cross section of weld (in^2). 124 in^2 is the perimeter of weld

Bottom weld pararell to the load

$$a := 0.5 \text{ in}$$

$$t_e := 0.707 \cdot a = 0.4 \text{ in}$$

effective throat dimension

$$R_n := t_e \cdot F_{nw} = 14.8 \text{ kip}$$

$$\phi := 0.75$$

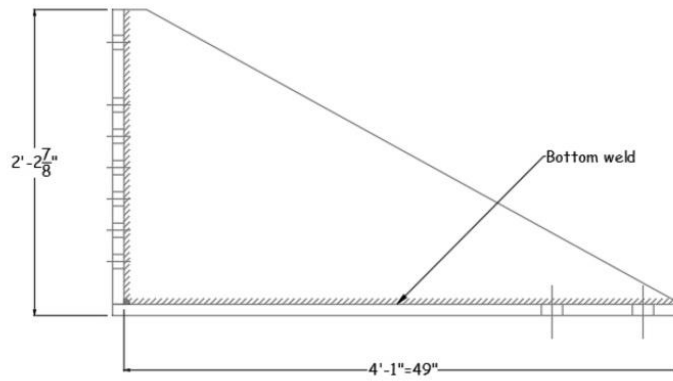
shear strenght

$$\phi R_n := \phi \cdot R_n = 11.1 \frac{\text{kip}}{\text{in}}$$

$$Lenght_{weldrequired} := \frac{P_u}{\phi R_n} = 9.9 \text{ in}$$

conservative approach, it it only considering one side of the diagonal, there are a total of 4 parts of the same length

$$Lenght_{weld} := 49 \text{ in}$$




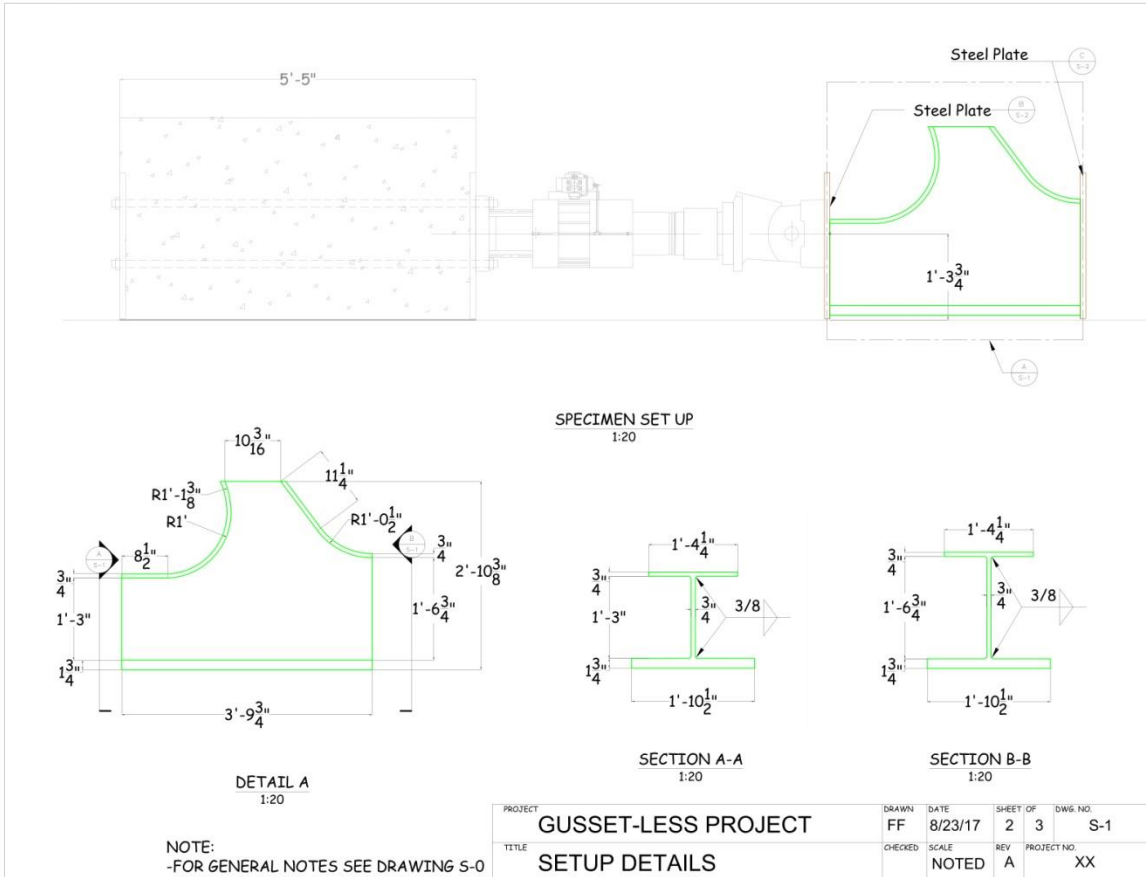
$$Capacity.check := \begin{cases} \text{if } Length_{weld} \geq Length_{weldrequired} \\ \quad \begin{cases} \text{"OK"} \\ \text{else} \\ \text{"Not OK"} \end{cases} \\ \text{"OK"} \end{cases}$$

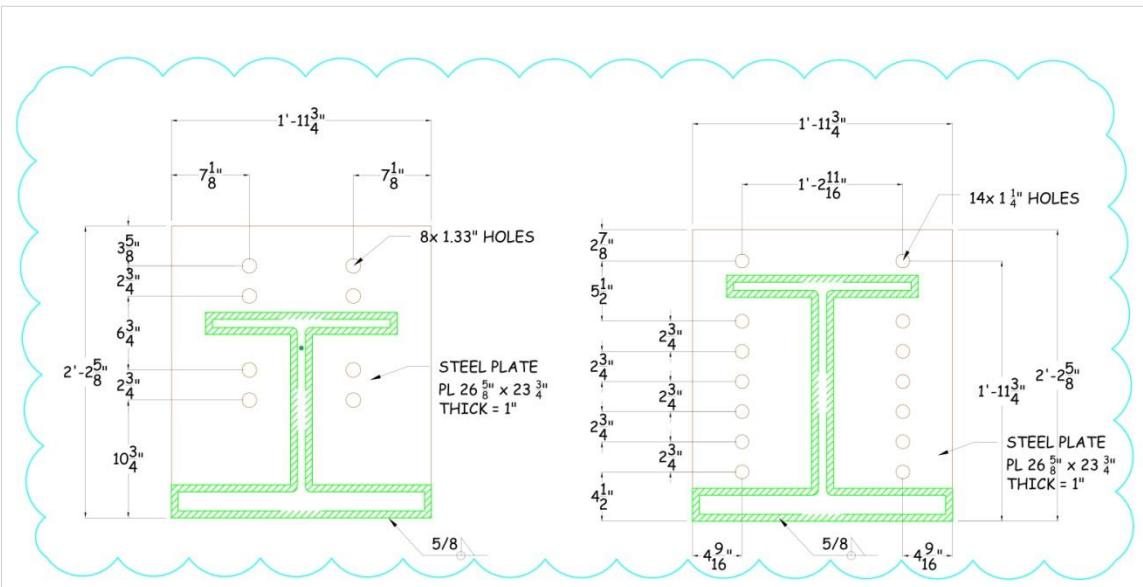
Use 1/2" filled weld

APPENDIX B – SHOP DRAWINGS

This appendix presents the shop drawings used for fabrication of the specimens and fabrication of the test setup. The first two pages are from the specimen shop drawing, sent to CANAM Bridges, and the other three pages sent to Novel Iron works for fabrication of the setup supports.

<p>GENERAL NOTES:</p> <p>CONTACT INFORMATION: DR. RICARDO MEDINA, University of New Hampshire Department of Civil Engineering, Kingsbury Hall Room W137, 33 Academic Way, Durham, NH 03824 PHONE: (603) 866-4726</p> <p>FERNANDA FISCHER University of New Hampshire Department of Civil Engineering, Kingsbury Hall Room W138, 33 Academic Way, Durham, NH 03824 Email: ff2004@wildcats.unh.edu</p> <p>DELIVERY INFORMATION: ALL PIECES SHOULD BE DELIVERED TO HIGH BAY STRUCTURES LABORATORY 1 Arts Way, Durham, NH 03824</p> <p>1. FOR CONDITIONS NOT CLEARLY UNDERSTOOD SUBMIT SKETCHES AND/OR REQUEST FOR INFORMATION TO THE DESIGN ENGINEER FOR RESOLUTION.</p> <p>2. OMISSIONS, CONFLICTS OR MISUNDERSTANDINGS BETWEEN THE VARIOUS ELEMENTS OF THE CONTRACT DOCUMENTS, IF ANY, SHALL BROUGHT TO THE ATTENTION OF THE DESIGN ENGINEER FOR RESOLUTION BEFORE PROCEEDING WITH THE WORK.</p> <p>3. VISUAL WELDING INSPECTION: VISUAL WELDING INSPECTIONS BY A QUALIFIED INSPECTOR PRIOR TO, DURING AND AFTER WELDING SHOULD BE PERFORMED AS THE PRIMARY METHOD TO EVALUATE THE CONFORMANCE OF WELDED JOINTS TO THE APPLICABLE QUALITY REQUIREMENTS. THE VISUAL INSPECTION SHOULD INCLUDE JOINTS EXAMINATION PRIOR TO THE COMMENCEMENT OF WELDING, PREPARATIONS, GAPS, ALIGNMENT AND OTHER VARIABLES; ADHERENCE TO THE WELDING PROCEDURE SPECIFICATIONS (WPS); SATISFACTORY TO THE COMPLETED WELD TO AWS D1.1.</p> <p>4. STRUCTURAL STEEL: 4.1. STRUCTURAL STEEL SHALL BE SUPPLIED, DETAILED AND ERECTED IN ACCORDANCE WITH A.I.S.C. SPECIFICATIONS LATEST EDITIONS. 4.2. MEMBER/ELEMENT SPECIFICATION a. SPECIMEN ASTM A709 GR 50 b. ALL PLATES ASTM A709 GR 50</p> <p>5. CONNECTIONS 5.1. WELDING ELECTRODES E70XX 5.2. WELDING SHALL CONFIRM TO A.W.S. SPECIFICATIONS AND BE PERFORMED BY CERTIFIED WELDERS.</p> <p>6. ERECTION SHALL BE DONE BY UNIVERSITY OF NEW HAMPSHIRE LAB PERSONAL AND GRADUATE STUDENTS.</p>						<p align="center">BILL OF MATERIALS</p> <table border="1"> <thead> <tr> <th>Item Number</th> <th>Specification</th> <th>Drawing #</th> <th>QTY</th> </tr> </thead> <tbody> <tr> <td>1</td> <td>Connection (Test Specimen)</td> <td>S-1</td> <td>2</td> </tr> <tr> <td>2</td> <td>STEEL PLATE PL 26 ^{5/8}" x 23 ^{3/4}" THICK 1"</td> <td>S-2</td> <td>2</td> </tr> <tr> <td>3</td> <td>STEEL PLATE PL 26 ^{5/8}" x 23 ^{3/4}" THICK 1"</td> <td>S-2</td> <td>2</td> </tr> </tbody> </table>						Item Number	Specification	Drawing #	QTY	1	Connection (Test Specimen)	S-1	2	2	STEEL PLATE PL 26 ^{5/8} " x 23 ^{3/4} " THICK 1"	S-2	2	3	STEEL PLATE PL 26 ^{5/8} " x 23 ^{3/4} " THICK 1"	S-2	2
Item Number	Specification	Drawing #	QTY																								
1	Connection (Test Specimen)	S-1	2																								
2	STEEL PLATE PL 26 ^{5/8} " x 23 ^{3/4} " THICK 1"	S-2	2																								
3	STEEL PLATE PL 26 ^{5/8} " x 23 ^{3/4} " THICK 1"	S-2	2																								
<p>LEGEND:</p> <p>-FILLET WELD WITH LEG SIZE α </p> <p>-THICKNESS THICK -ELEVATION ELEV.</p>																											
<p>PROJECT GUSSET-LESS PROJECT</p>		<p>DRAWN FF</p>	<p>DATE 8/23/17</p>	<p>SHEET OF 1 3</p>	<p>DWG. NO. S-0</p>																						
<p>TITLE GENERAL NOTES AND MATERIALS</p>		<p>CHECKED</p>	<p>SCALE NOTED</p>	<p>REV A</p>	<p>PROJECT NO. XX</p>																						





DETAIL B
1:10
QTY=2

DETAIL C
1:10
QTY=2

- REVISION (11/05/2017):
- DETAIL B: ADD 4 MORE HOLES
 - DETAIL C : CHANGE LOCATION OF HOLES

NOTE:
-FOR GENERAL NOTES SEE DRAWING S-0
-ALL HOLES SHOULD GO ALL THE WAY DOWN THE THICKNESS OF THE PLATE

PROJECT	GUSSET-LESS PROJECT		DRAWN	FF	DATE	8/23/17	SHEET OF	3 3	DWS. NO.	S-2
TITLE	SETUP DETAILS		CHECKED		SCALE	NOTED	REV	A	PROJECT NO.	XX

GENERAL NOTES:

CONTACT INFORMATION:

DR. RICARDO MEDINA,
University of New Hampshire Department of Civil Engineering,
Kingsbury Hall Room W137, 33 Academic Way, Durham, NH 03824
PHONE: (603) 866-4726

FERNANDA FISCHER

University of New Hampshire Department of Civil Engineering,
Kingsbury Hall Room W138, 33 Academic Way, Durham, NH 03824
Email: ff2004@wildcats.unh.edu

DELIVERY INFORMATION:

ALL PIECES SHOULD BE DELIVERED TO HIGH BAY STRUCTURES LABORATORY
1 Arts Way, Durham, NH 03824

1. FOR CONDITIONS NOT CLEARLY UNDERSTOOD SUBMIT SKETCHES AND/OR
REQUEST FOR INFORMATION TO THE DESIGN ENGINEER FOR RESOLUTION.

2. OMISSIONS, CONFLICTS OR MISUNDERSTANDINGS BETWEEN THE VARIOUS
ELEMENTS OF THE CONTRACT DOCUMENTS, IF ANY, SHALL BROUGHT TO THE
ATTENTION OF THE DESIGN ENGINEER FOR RESOLUTION BEFORE PROCEEDING WITH
THE WORK.

3. VISUAL WELDING INSPECTION:

VISUAL WELDING INSPECTIONS BY A QUALIFIED INSPECTOR PRIOR TO, DURING AND
AFTER WELDING SHOULD BE PERFORMED AS THE PRIMARY METHOD TO EVALUATE
THE CONFORMANCE OF WELDED JOINTS TO THE APPLICABLE QUALITY
REQUIREMENTS. THE VISUAL INSPECTION SHOULD INCLUDE JOINTS EXAMINATION
PRIOR TO THE COMMENCEMENT OF WELDING, PREPARATIONS, GAPS, ALIGNMENT AND
OTHER VARIABLES; ADHERENCE TO THE WELDING PROCEDURE SPECIFICATIONS
(WPS); SATISFACTORY TO THE COMPLETED WELD TO AWS D1.1.

4. STRUCTURAL STEEL:

4.1. STRUCTURAL STEEL SHALL BE SUPPLIED, DETAILED AND ERECTED IN
ACCORDANCE WITH A.I.S.C. SPECIFICATIONS LATEST EDITIONS.
4.2. MEMBER/ELEMENT SPECIFICATION
a. ALL PLATES ASTM A709 GR 50

5. CONNECTIONS

5.1. WELDING ELECTRODES E70XX
5.2. WELDING SHALL CONFIRM TO A.W.S. SPECIFICATIONS AND BE PERFORMED BY
CERTIFIED WELDERS.

6. CONCRETE = 3 KSI STRENGTH

7. ERECTION SHALL BE DONE BY UNIVERSITY OF NEW HAMPSHIRE LAB PERSONAL
AND GRADUATE STUDENTS.

BILL OF MATERIALS

Item Number	Specification	Drawing #	QTY
1	Concrete Reinforced Block	S-2	1
2	Bottom Steel Plate	S-3	1
3	Side Steel Plates	S-3	2
4	Diagonal Bracket Steel Plates	S-3	4
5	Bottom Steel Plate	S-4	1
6	Vertical Steel Plate	S-4	1
7	Diagonal Bracket Steel Plates	S-4	2

Steel Pipes:

- Nominal dimension 1 1/2"
- Actual dimensions, O.D = 1.9" diameter, I.D. = 1.61" diameter, wall thickness = 0.145"

The steel pipes should be welded to both plates.

LEGEND:

-FILLET WELD WITH LEG SIZE a

-THICKNESS THICK
-ELEVATION ELEV.

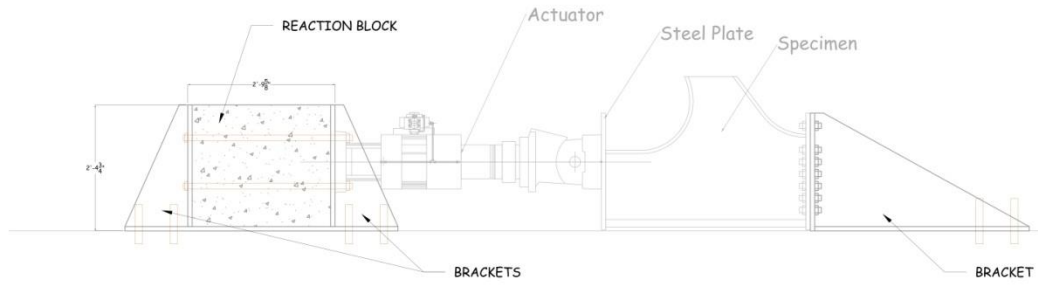


NOTE:

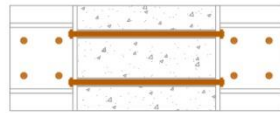
PRELIMINARY DESIGN ONLY FOR QUOTE PURPOSES

PLEASE QUOTE ALL PLATES, STEEL PIPES AND WELDING ONLY.

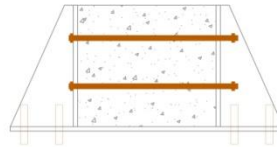
PROJECT	GUSSET-LESS PROJECT		DRAWN	DATE	SHEET OF	DWG. NO.
TITLE	GENERAL NOTES AND MATERIALS		FF	11/01/17	1 5	S-0
	CHECKED	SCALE	REV	PROJECT NO.		
		NOTED	A	XX		



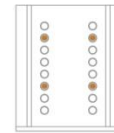
TOP VIEW



FRONT VIEW



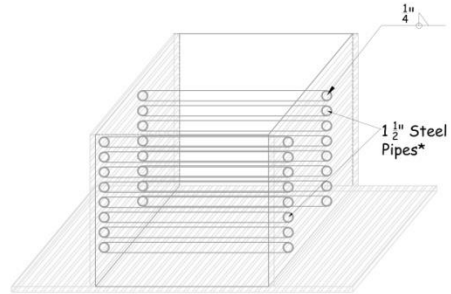
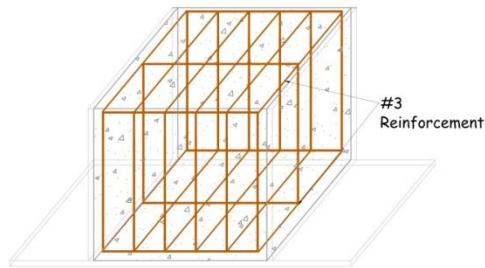
SIDE VIEW



SPECIMEN SET UP
1:25

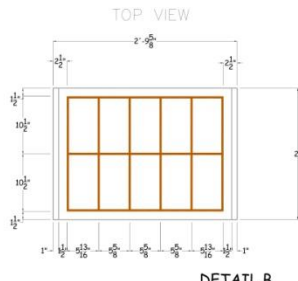
NOTE:
-PRELIMINARY DESIGN
-FOR GENERAL NOTES SEE DRAWING S-0

PROJECT	GUSSET-LESS PROJECT		DRAWN	DATE	SHEET OF	DWG. NO.
TITLE	GENERAL DRAWING		FF	11/01/17	2 5	S-1
	CHECKED	SCALE	REV	PROJECT NO.		
		NOTED	A	XX		



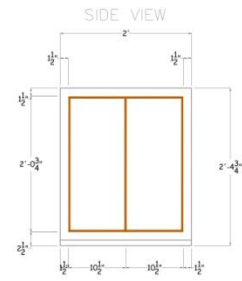
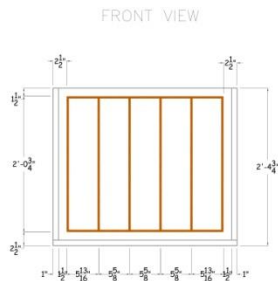
DETAIL A
1:20

NOTE:
-FOR 3D VIEWS, BRACKETS ARE NOT SHOWN

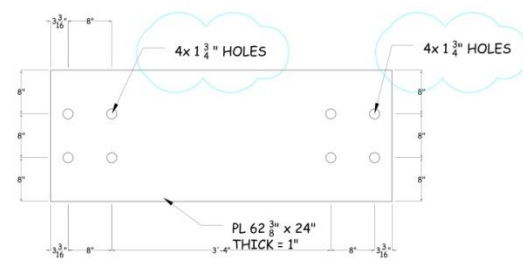
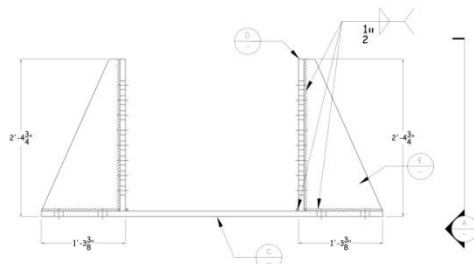


DETAIL B
1:20

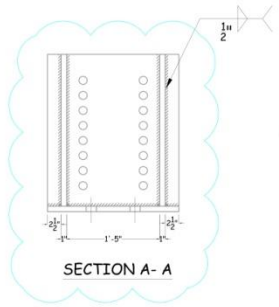
NOTE:
-PRELIMINARY DESIGN
-FOR GENERAL NOTES SEE DRAWING S-0
* Nominal dimensions for steel pipe, actual dimensions in page S-0



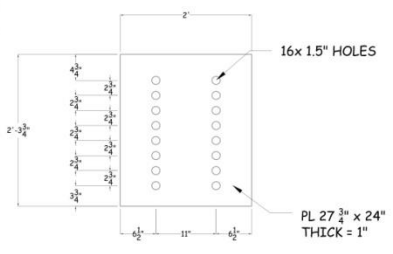
PROJECT	GUSSET-LESS PROJECT				DRAWN	DATE	SHEET OF	DWG. NO.
TITLE	BLOCK REINF. DETAILS				FF	11/01/17	3 5	S-2
CHECKED	SCALE	REV	PROJECT NO.		NOTED	A	XX	



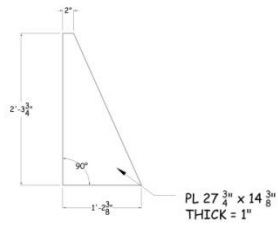
DETAIL C
QTY = 1



SECTION A-A



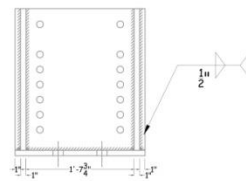
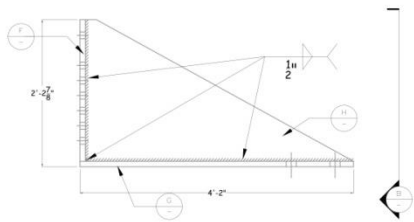
DETAIL D
QTY = 2



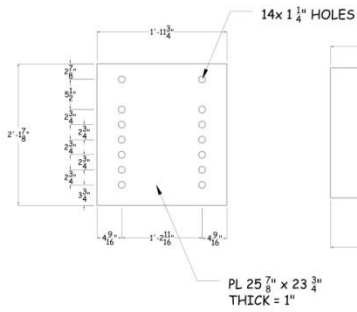
DETAIL E
QTY = 4

NOTE:
-FOR GENERAL NOTES SEE DRAWING S-0
MODIFICATIONS:
01/22/2018 - SECTION A-A: Dimensions added
Detail C - dimensions of holes from 1 7/8" to 1 3/4"

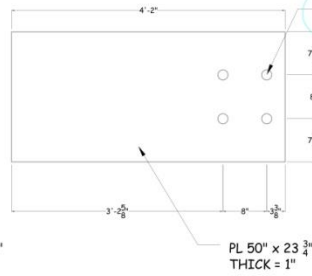
PROJECT	GUSSET-LESS PROJECT				DRAWN	DATE	SHEET OF	DWG NO
TITLE	BRACKET DETAILS				FF	01/11/18	4 5	S-3
	CHECKED	SCALE	REV	PROJECT NO	NOTED	A	XX	



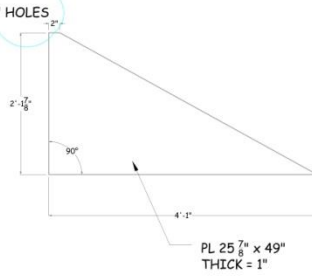
SECTION B-B



DETAIL F
QTY = 1



DETAIL G
QTY = 1



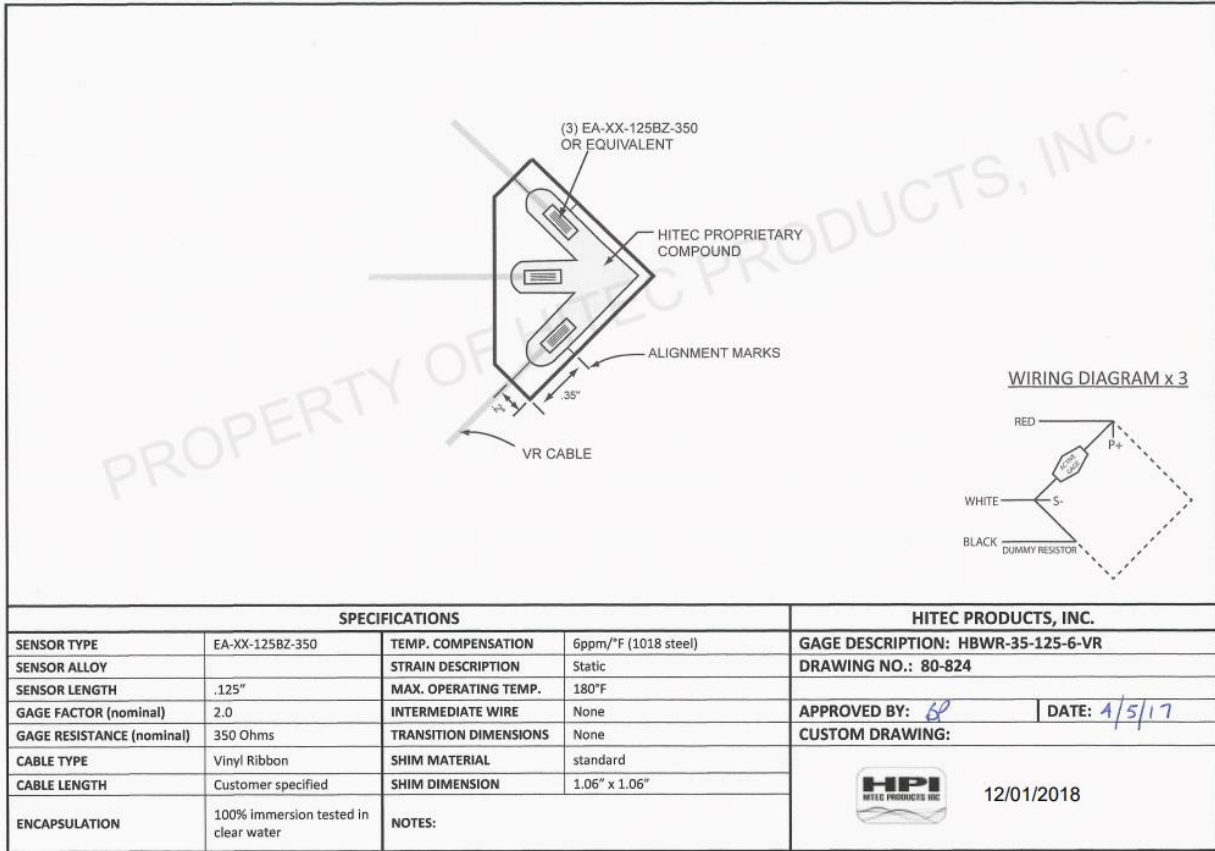
DETAIL H
QTY = 2

NOTE:
-FOR GENERAL NOTES SEE DRAWING S-0
MODIFICATIONS:
01/22/2018 - Detail G - dimensions of holes from 1 7/8" to 1 3/4"

PROJECT	GUSSET-LESS PROJECT				DRAWN	FF	DATE	01/11/18	SHEET	5	OF	5	DWG. NO.	S-4
TITLE	BRACKET DETAILS				CHECKED		SCALE	NOTED	REV	A	PROJECT NO.		XX	

APPENDIX C – INSTRUMENTATION

This appendix will provide additional information regarding the instrumentation. This will include the data sheets [46] for the strain gauges used and a mathematical background on the digital image correlation.



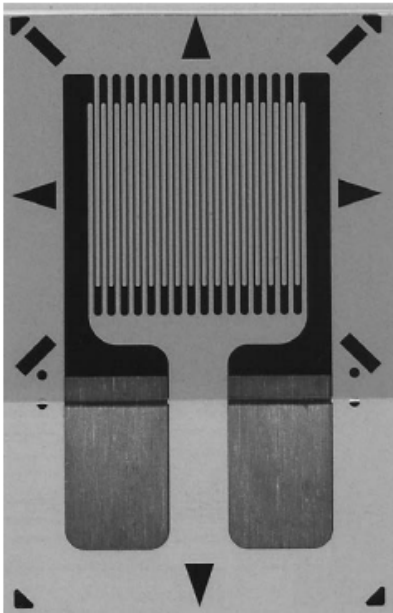


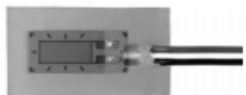

9/16/2016 3:40 PM

PRODUCT DRAWING FORM CODE 70 & 80

ENG-100 REV 0 3/14/2011

Figure 73 - Strain Rosette Data Sheet

General Purpose Strain Gages – Linear Pattern

GAGE PATTERN DATA					
		GAGE DESIGNATION See Notes 1, 2		RESISTANCE (OHMS) See Note 3	OPTIONS AVAILABLE
		CEA-XX-125UW-120 CEA-XX-125UW-350 W2A-XX-125UW-120 W2A-XX-125UW-350		120 ±0.3% 350 ±0.3% 120 ±0.6% 350 ±0.6%	P2, SP35 P2, SP35
 actual size		DESCRIPTION General-purpose gage. Exposed solder tab area 0.10 x 0.07 (2.5 x 1.8 mm). See also 125UN pattern.			 RoHS* COMPLIANT
		GAGE DIMENSIONS			Legend ES = Each Section CP = Complete Pattern S = Section (S1 = Section 1) M = Matrix
Gage Length	Overall Length	Grid Width	Overall Width	Matrix Length	Matrix Width
0.125	0.325	0.180	0.180	0.42	0.27
3.18	8.26	4.57	4.57	10.7	6.9
GAGE SERIES DATA — See Gage Series datasheet for complete specifications					
Series	Description	Strain Range	Temperature Range		
CEA	Universal general-purpose strain gages.	±5%	-100° to +350°F (-75° to +175°C)		
W2A IPX8S Rated	For water-exposure applications. Based on the CEA Series with Option P2 pre-attached cables, W2A strain gages are fully enclosed with a silicone rubber coating and tested to 10 GΩ insulation resistance, 1 meter water depth, 30 minutes duration. Other requirements can be addressed on demand.	±3%	-60° to +180°F (-50° to +80°C)		
		Example of the W2A construction: IPX8S Rated			

Note 1: Insert desired S-T-C number in spaces marked XX.

Note 2: W2A leadwires are attached with lead-free solder and are RoHS compliant.

* CEA gages with Option P2 are not RoHS compliant.

Technical Data References: SEARCH our website using the document number.

11506 – Gage Series; 11507 – Optional Features

Figure 74 - Uniaxial Strain Gauge Data Sheet [40]

The following section will provide a mathematical background on the DIC correlation. In VIC-2D the first step in measurement is dividing the image into a grid of subsets. The subsets serve to divide the image and create unique blocks of pixels used for tracking. Within the subset, a gray value for each of the pixels is assigned as a value from 0 (black) to 100 (white) based on the speckle pattern captured. Once the gray values are assigned for the subsets on the reference image, the correlation can begin on the successive images.

The correlation attempts to track the movement of the subsets in the deformed images compared to the reference image. This is done through a correlation function which used a statistical relationship, one example of which is the sum of squared differences. What the correlation function does is compare the gray values of each pixel within the subset of the reference image against the image that has been displaced by a value of u and v , which correspond to the horizontal and vertical displacements. This comparison is repeated at multiple u and v values until the difference in the gray values are minimized according to the sum of squared differences, or whatever correlation criterion are selected. Figure 75 is the generalized equation for the tracking performed in the DIC program VIC-2D [47]. Once the displacement is calculated, the strain can be derived assuming various tensors. The choices in VIC-2D are Lagrange, Hencky, Euler-Almansi, and Log Euler-Almansi. The default, and the tensor used in this study was the Lagrange strain tensor. Figure 76 [48] shows the equations used to calculate the strain using the Lagrange strain tensor. With the directional strain calculated, the principal strains are derived using the Mohr's circle relationship.

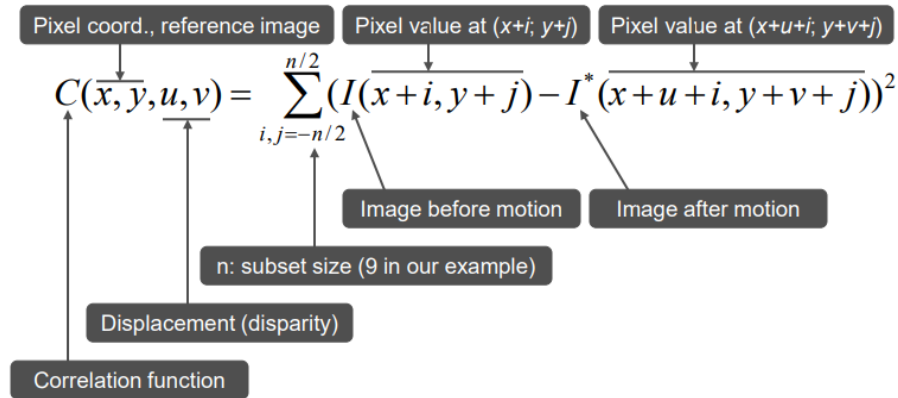


Figure 75 - DIC Correlation [41]

$$e_{xx} = \frac{\partial u}{\partial x} + \frac{\left(\frac{\partial u}{\partial x}\right)^2 + \left(\frac{\partial v}{\partial x}\right)^2}{2}$$

$$e_{yy} = \frac{\partial v}{\partial y} + \frac{\left(\frac{\partial u}{\partial y}\right)^2 + \left(\frac{\partial v}{\partial y}\right)^2}{2}$$

$$e_{xy} = \frac{\frac{\partial u}{\partial y} + \frac{\partial v}{\partial x} + \frac{\partial u}{\partial x} \frac{\partial u}{\partial y} + \frac{\partial v}{\partial x} \frac{\partial v}{\partial y}}{2}$$

Figure 76 - Lagrange Strain Equations [42]

APPENDIX D – TEST TRACKING

This appendix will present a data table of all the tests run during the work of this report. Additionally, a data sheet used to monitor the fatigue test will be shown and some examples of filled out data sheets will be presented.

Table 13 - Test Tracking History

Date	Session	Time Started	Time Ended	Test Cycles	Cumulative Cycles	System ID performed?	Test Description	Notes
6/20/2018	Night	-	-	5000	5000	No	Short initial test to gather data for DOT meeting	
6/21/2018	Afternoon	-	-	5000	10000	No	Demonstration test for DOT meeting	
7/3/2018	Night	-	-	25200	35200	No	2-hour test	No significant change noted from start to finish
7/7/2018	Afternoon	-	-	6700	41900	No	Planned 4-hour test, stopped early	Specimen tip support became free after 30 minutes, no instability was noted. The test was stopped to reevaluate the setup. The temperature interlock activated after the pressure was released in the pump. The DIC software also closed after starting the test.
7/10/2018	Morning	-	-	14444	56344	Yes	Planned 4-hour test, stopped early	Support under specimen tip moved significantly in the opposite direction as last noted. The test was stopped when one of the supports was close to coming out.
7/10/2018	Afternoon	-	-	10368	66712	No	Planned 4-hour test, stopped early	The pump interlocked due to the temperature limit. The test lasted for 49 minutes and the final temperature was 137F.
7/11/2018	Afternoon	-	-	25782	92494	No	Planned 2-Hour test	Test ran for full 2-hours, the temperature was close to the limit at the end of the test. Shims under South side of specimen tip were moving vertically, steel shims will be added for the next test.
7/12/2018	Morning	-	-	13582	106076	No	Planned 2-Hour test, stopped early	Temperature interlock was activated after 1 hour. The shims on the South side were very stable with minimal vertical movement. The shims on the North side will be replaced with steel shims.
7/13/2018	Morning	10:02	-	21191	127267	No	Planned 2-Hour test, stopped early	Temperature interlock after 1 hour 41 minutes. The temp. started at 88F and ended at 134F
7/16/2018	Morning	10:24	12:28	25782	153049	No	Planned 2-Hour test	Test ran for full 2-hours. Temp started at 97F and ended at 130F. The temperature seemed to stagnate at 130F since around 1 hour into the test all the way until the end. It was noted that the water temp. was lower than normal (60F compared to 70F as "normal").

7/17/2018	Morning	10:11	12:15	25782	178831	Yes	Planned 2-hour test	Test ran full 2 hours. South side shim became loose and was adjusted after 16minutes of testing. There was visible twisting at the tip and the shim will need to be adjusted for the next test. Temperature was stable at 130F with a water temp of 60F
7/18/2018	Morning	10:14	14:20	51610	230441	No	4-hour test	Test ran full 4-hours. Temperature was stabil around 130F for the majority of the test. The water temp. started at 65F and stabilized at 60F for the majority of the test.
7/19/2018	Morning	07:05	08:26	17054	247495	No	Planned 8-hr test	Test ran 1hr and 20 minutes. Water temp started at 65F and fluctuated between 65F and 69F. The oil temp. was 135F when the pump interlocked.
7/20/2018	Morning	-	-	12880	260375	No	Planned 8-hr test	Test ran for just over 1 hour. The water temp started at 65 and fluctuated between 69F and 75F during the test. The oil temp. was 135F when the pump interlocked.
8/3/2018	Morning	-	-	2182	262557	No	Planned 8-hr test	Temp interlock after 10 minutes
8/8/2018	Morning	-	-	1462	264019	No	Planned 8-hr test	Stopped test for tuning purposes.
8/10/2018	Afternoon	-	-	15000	279019	No	Tuning of Actuator	Tuned actuator to fix odd behavior due to lowering pressure. Pressure increased to 3000 PSI at the pump.
8/15/2018	Morning	10:52	12:56	25782	304801	No	2-Hour test	2-Hr test using the building cold water (75F) with a 1/2 hp pump on the inlet side. Oil temp. was stable at 111F for the duration of the test.
8/15/2018	Afternoon	13:04	17:08	51612	356413	No	4-hour test	4-Hr test using the building cold water (75F) with a 1/2 hp pump on the inlet side. Oil temp. was stable at 111F for the duration of the test.
8/16/2018	Morning	07:36	16:09	103225	459638	No	8-hour test	8-Hr test using the building cold water (75F) with a 1/2 hp pump on the inlet side. Oil temp. was stable at 111F for the duration of the test.
8/17/2018	Morning	-	-	154920	614558	No	12-Hour Test	12-hour test using building cold water. The first 6-hour interval ran smoothly but on the ramp to zero force the pump interlocked due to a lower limit. This means the specimen went into compression briefly. The test was restarted for the next 6 hour interval. The interlocked occurred again at the same point in the test. Some ringing in the bottom of the hysteresis and force-command was observed.

8/20/2018	Afternoon	-	-	51612	666170	Yes	4-hour test	4-hour test. Temp. was stable. Shims were changed before this test. One shim under the south side tip became loose after approximately 40 minutes into the test. Ringing was still present, tuning will be performed.
8/21/2018	Morning	-	-	77460	743630	No	6-Hour test	6-hour test. Shims were replaced on the south side of the specimen tip before test, this reduced the ringing and the vertical movement. No tuning was performed.
8/23/2018	Morning	-	-	6708	750338	No	4-hour test stopped early	4hr test stopped early due to shim movement
8/23/2018	Morning	-	-	51630	801968	No	4-hour test	4hr test, odd behavior on SRW1H approximately half-way through the test. The gage began fluctuating and the strain gradually increased with significant fluctuations. The gage may have had a loose wire where a previous repair was made from damaged wires.
8/28/2018	Morning	09:00	11:05	26482	828450	No	2-hour test	2-Hour test, shims were changed after the test to reduce the twisting of the specimen. An additional 700 cycles were performed while adjusting shims.
8/28/2018	Afternoon	-	-	25782	854232	No	2-hour test	2-hour test, new shims worked well. No problems during testing period.
8/29/2018	Morning	08:45	10:49	25782	880014	No	2-hour test	2-hour test, no problems during testing period.
8/29/2018	Afternoon	-	-	51630	931644	No	4-hour test	4-hour test, DIC restarted once. Some grinding of the concrete was observed under south side specimen tip shims.
9/2/2018	Morning	-	-	25782	957426	No	2-hour test	2-hour test, anchor bolts were tightened before test. Using new chilled water pump, oil temp seemed stable around 113F. SRW1-D had an offset from it's "normal" strain range, this was fixed after the test by moving the wire.
9/2/2018	Afternoon	-	-	25782	983208	No	2-hour test	2-hour test, chilled water pump used. The oil temp. rose to 123F from 113F over the course of the 2 hours, some adjustments to the pump speed should be made.
9/3/2018	Afternoon	-	-	25782	1008990	No	2-hour test	2-hour test, chilled water pump adjusted to stabilize oil temp at 113F.
9/4/2018	Morning	-	-	25782	1034772	No	2-hour test	2-hour test, normal operation
9/4/2018	Afternoon	-	-	25782	1060554	No	2-hour test	2-hour test, after test bolts were tightened. Actuator bolt was over torqued.

9/24/2018	Morning	-	-	30089	1090643	No	2.5-hour test	Actuator bolt was replaced, 2.5hr test was run. DIC computer shut down after approximately 2-hours due to problem with plug.
9/25/2018	Morning	-	-	25782	1116425	No	2-hour test	First 2-hour test of the day. No problems noted
9/25/2018	Afternoon	-	-	25782	1142207	No	2-hour test	Second 2-hour test of the day. No problems noted.
9/26/2018	Morning	-	-	30089	1172296	No	2.5-hour test	2.5-hour test run. No problems noted.
9/27/2018	Morning	-	-	25782	1198078	No	2-hour test	2-hour test. No problems noted.
10/1/2018	Morning	-	-	30090	1228168	No	2.5-hour test	2.5-hour test run. No problems noted.
10/1/2018	Afternoon	-	-	25872	1254040	Yes	2-hour test	2-hour test. Wires were moved and one of the strain gauges was offset in terms of magnitude. This will be adjusted before next test.
10/10/2018	Morning	-	-	30090	1284130	No	2.5-hour test	2.5-hour test run. SRW1-D wire was moved and caused an offset in measured strain. Adjusted back to normal after test was completed.
10/11/2018	Morning	-	-	30090	1314220	No	2.5-hour test	2.5-hour test. No problems noted.
10/11/2018	Morning	-	-	30090	1344310	No	2.5-hour test	2.5-hour test. No problems noted.
10/12/2018	Morning	-	-	25872	1370182	No	2-hour test	2-hour test. LVDT bumped at 1hour 20m. Into test, offset is present after this point.
10/15/2018	Morning	-	-	30090	1400272	No	2.5-hour test	2.5-hour test. No problems noted.
10/16/2018	Morning	-	-	30090	1430362	No	2.5-hour test	2.5-hour test. No problems noted. Horz. Bolts tightened after test.
10/17/2018	Morning	-	-	30090	1460452	No	2.5-hour test	2.5-hour test no problems noted.
10/18/2018	Morning	-	-	30090	1490542	No	2.5-hour test	2.5-hour test no problems noted.
10/18/2018	Morning	-	-	25782	1516324	Yes	2-hour test	2-hour test, the specimen tip was rocking out of plane more than normal, shim support was replaced and system ID was performed after this test.
10/24/2018	Morning	-	-	30090	1546414	No	2.5-hour test	2.5-hour test with new shim support. No problems noted.
10/26/2018	Morning	-	-	30091	1576505	No	2.5-hour test	2.5-hour test no problems noted.
10/30/2018	Morning	-	-	25782	1602287	No	2-hour test	2-hour test, no problems during testing period. Final test before damage is introduced.

Testing Checklist

Session #			Name of Inspector(s):	Uploaded <input type="checkbox"/>
Morning <input type="checkbox"/>	Afternoon <input type="checkbox"/>	Night <input type="checkbox"/>	Date:	
Start Time				
Stop Time				
Setup pictures are Taken Before the Test <input type="checkbox"/>			Expected # of Cycles:	
Setup Pictures are Taken After the Test <input type="checkbox"/>			Executed # of Cycles:	
Strain Gauges				
	Y	N	Description	
Strain Gauges File Name and Path				
Inspect Attachment				
Sampling Rate Frequency: 60 Hz				
Record strains for ~10 seconds while actuator is off to ensure gages are functioning				
DIC				
	Y	N	Description	
DIC File File Name and Path				
Lights are on and Check Saturation			Note: DIC display should NOT show red on the screen	
Lens Caps are off				
Check Cameras Locations				
Sync Mode: Auto				
VIC-3D Integration: Speckle mode				
Capture Mode: Flex Capture			30000ms=1 image 80ms=30s, 1170000ms=1 image	
Specimen (Take Pictures and Inspect)				
	Y	N	Description	
Shims				
Support at Tip				
Bolts and Anchors for Loosening or Damage				
Inspect Specimen				
Inspect Bracket				
Inspect Reaction Block				
Actuator				
	Y	N	Description	
MTS Specimen Number				
Inspect Hydraulic Lines				
Inspect for Oil Leak, and Note Temperature				
MTS Controller Software: '100Kip.cfg : Force Tuning Only-3hz'				
Check Tuning Parameters to ensure they have not been changed P-Gain:1.70 I-Gain:0.190				
Define force limits (480kN and -5kN respectively)				
Define force feedback error limits				
Open test procedure				
Check Cyclic load protocol				
Set-point: 55kip				
Cyclic Amplitude: +/- 50kip				

Figure 77 - Test Tracking Data Sheet - Front

APPENDIX E – SYSTEM ID

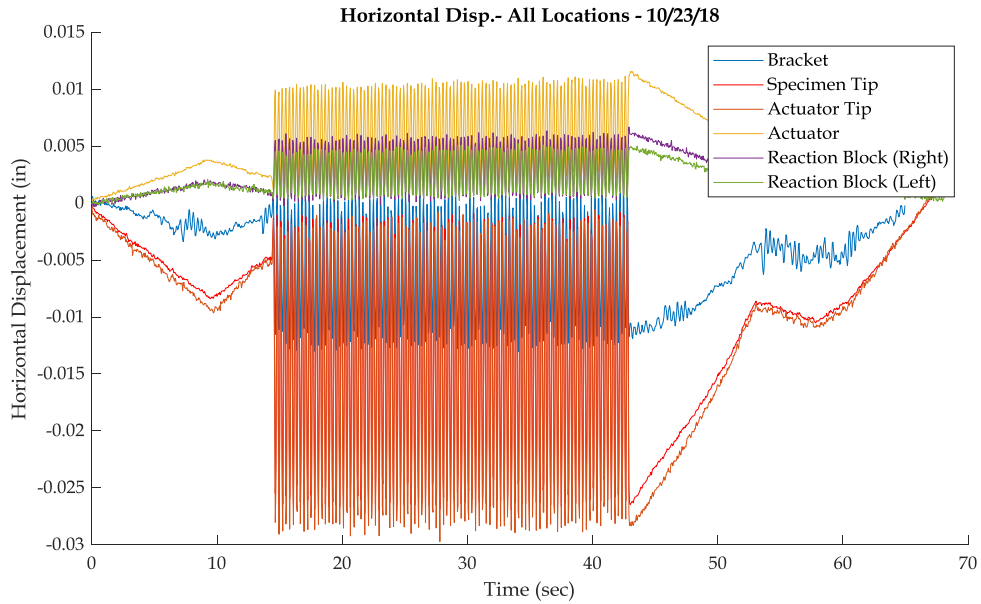


Figure 79 - Horizontal Displacements - All Locations

In this appendix, additional figures from the System ID will show the individual comparisons at each point of the System ID as well as the horizontal displacements at each location of the system relative to each other.

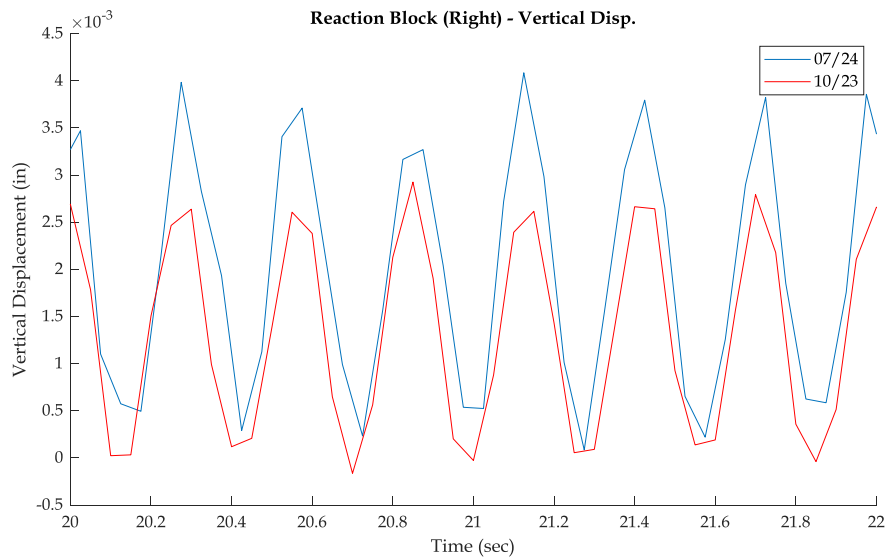


Figure 80 - Reaction Block Right - Vertical Displacement

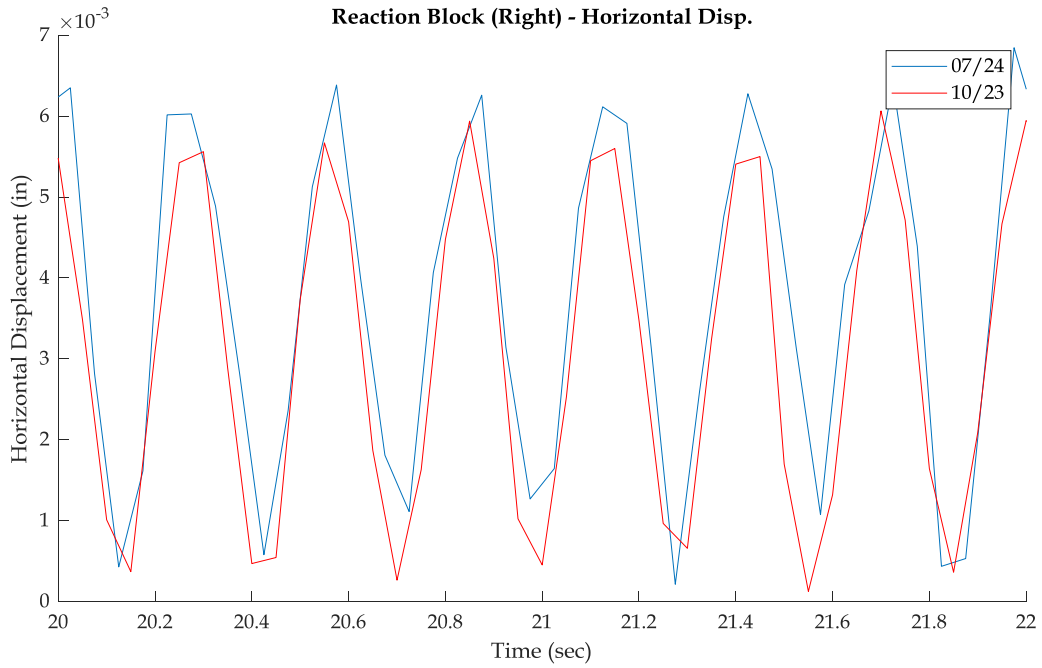


Figure 81 - Reaction Block Right - Horizontal Displacement

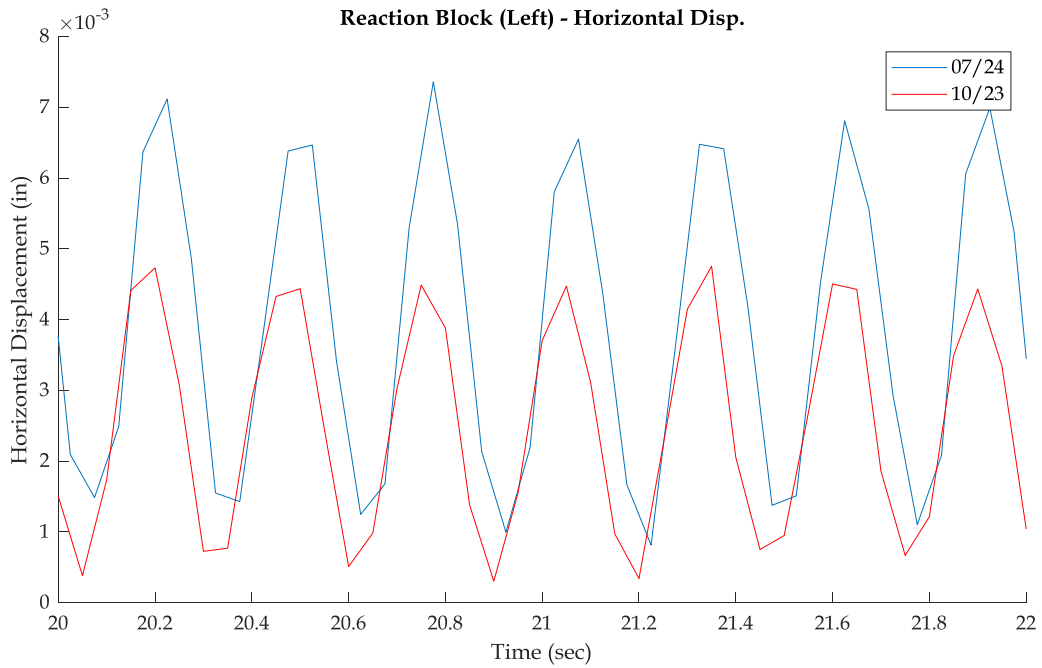


Figure 82 - Reaction Block Left - Horizontal Displacement

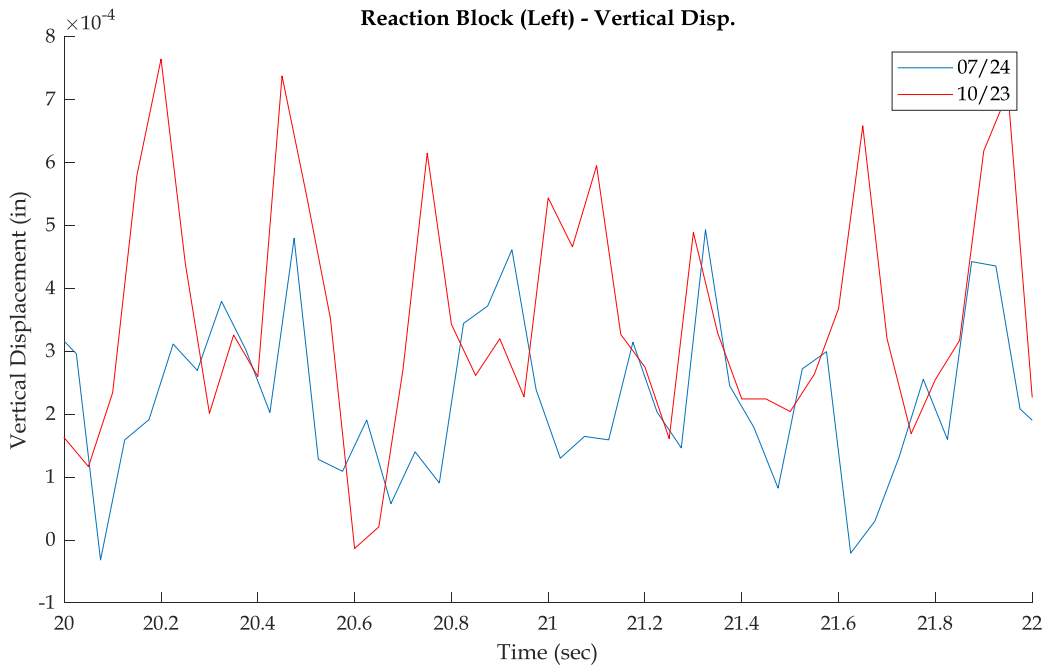


Figure 83 - Reaction Block Left - Vertical Displacement

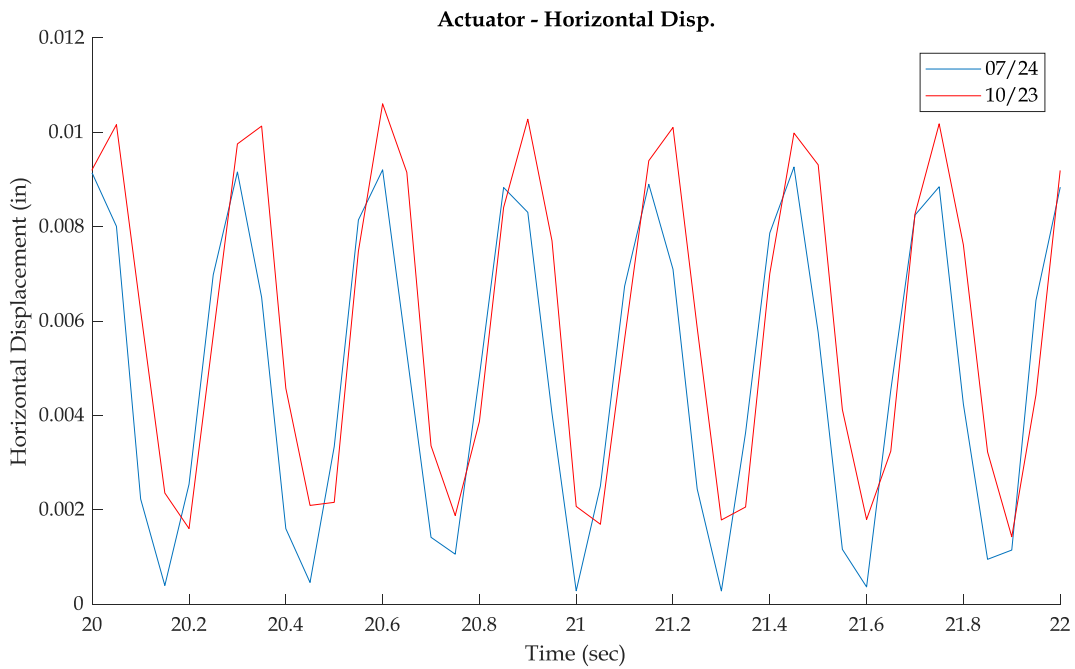


Figure 84 - Actuator - Horizontal Displacement

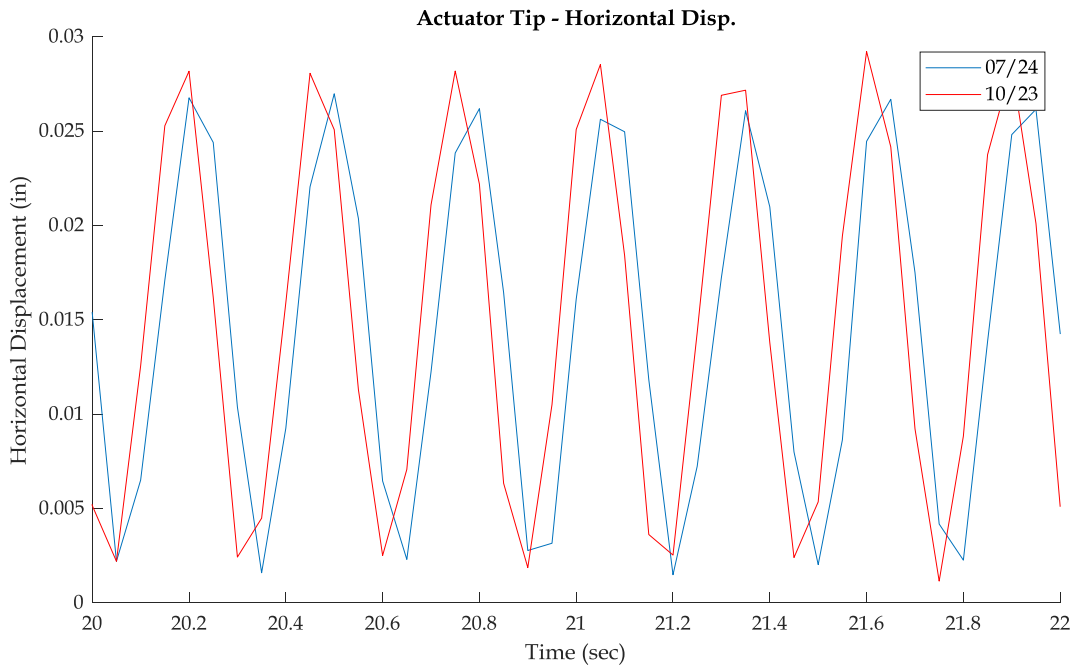


Figure 85 - Actuator Tip - Horizontal Displacement.

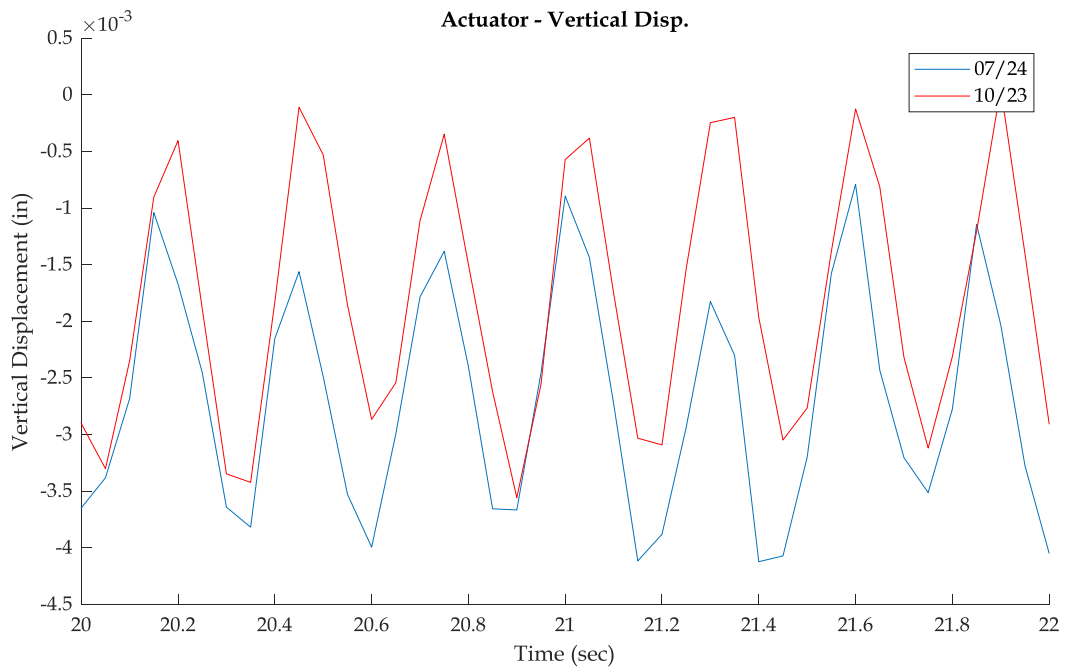


Figure 86 - Actuator - Vertical Displacement

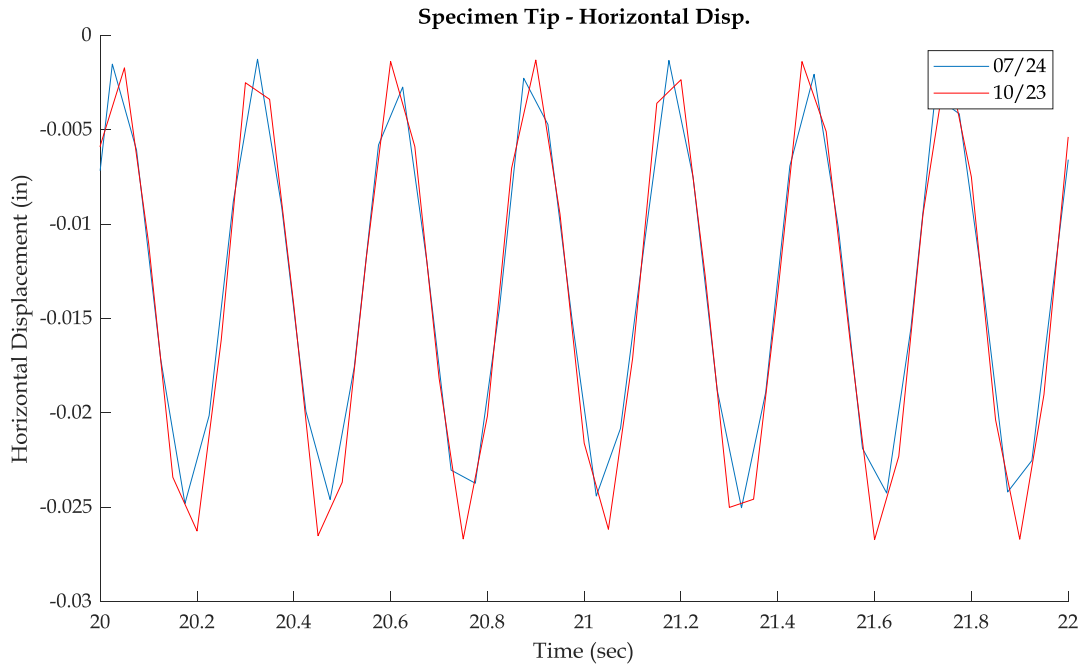


Figure 87 - Specimen Tip - Horizontal Displacement

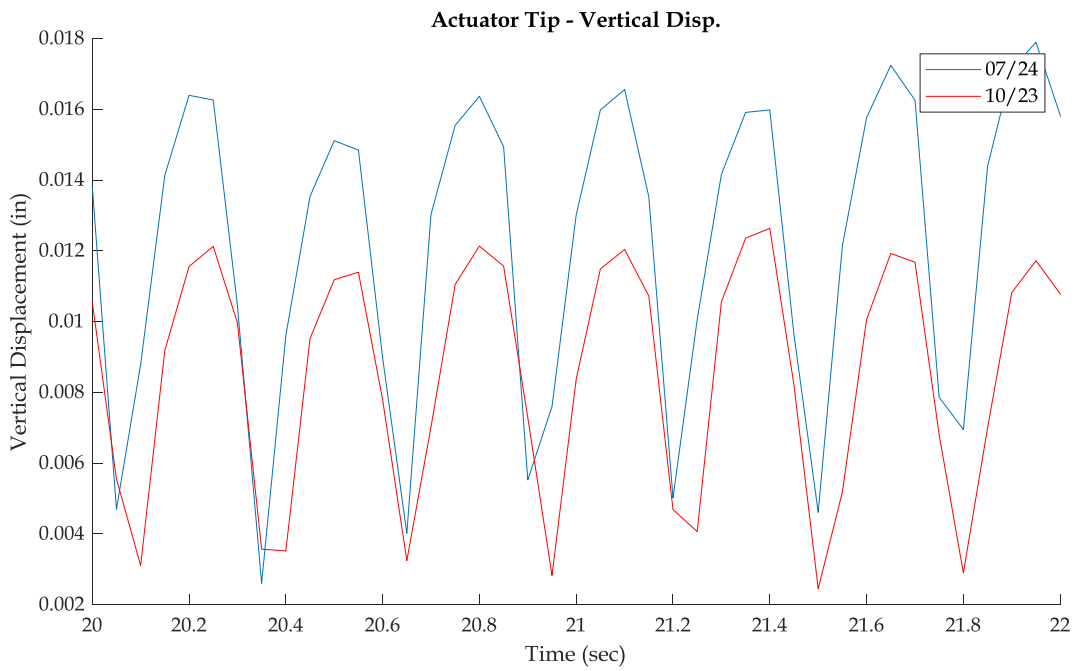


Figure 88 - Actuator Tip - Vertical Displacement

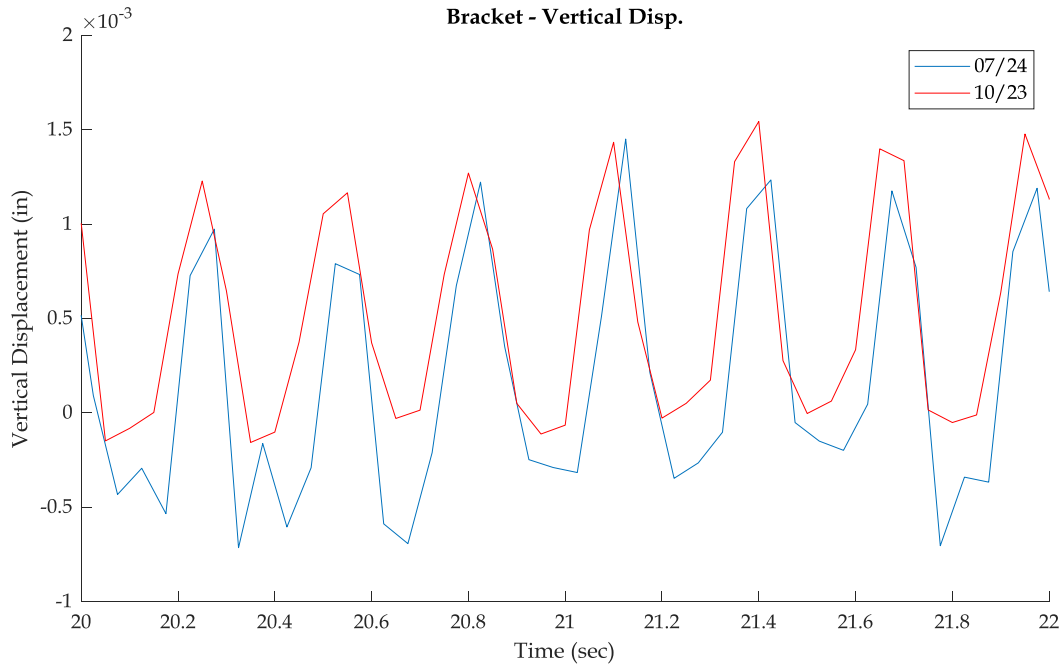


Figure 89 - Bracket - Vertical Displacement

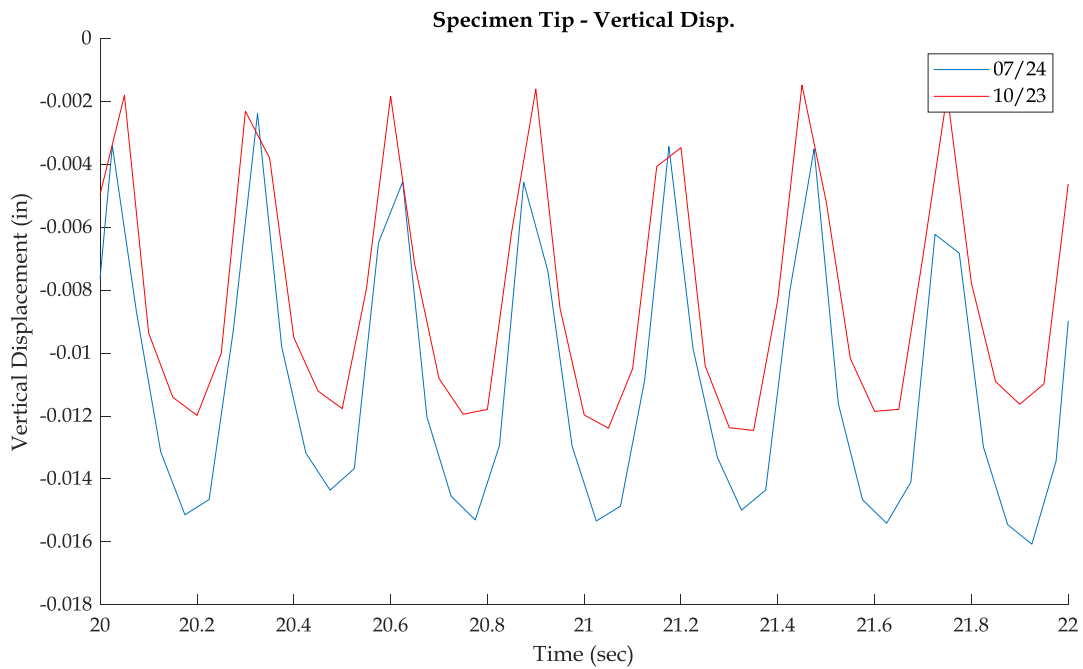


Figure 90 - Specimen Tip - Vertical Displacement

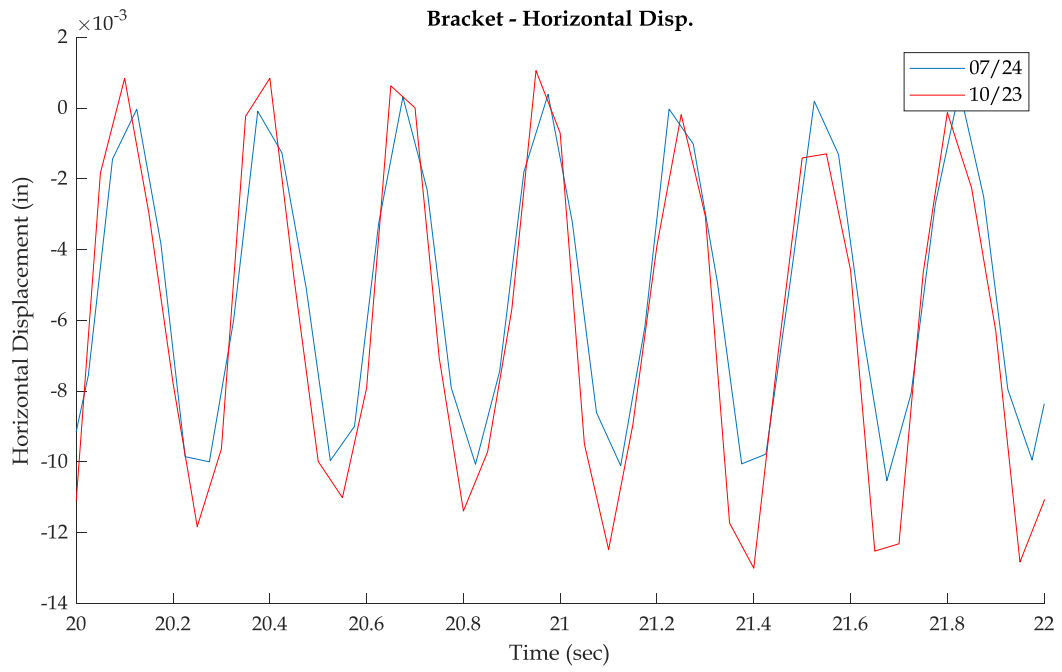


Figure 91 - Bracket - Horizontal Displacement

APPENDIX F – FATIGUE RESULTS

In this appendix, additional plots of the strain gauge response from the fatigue testing will be presented. The figures shown will show all comparisons between the three testing windows discussed in Chapter 6.

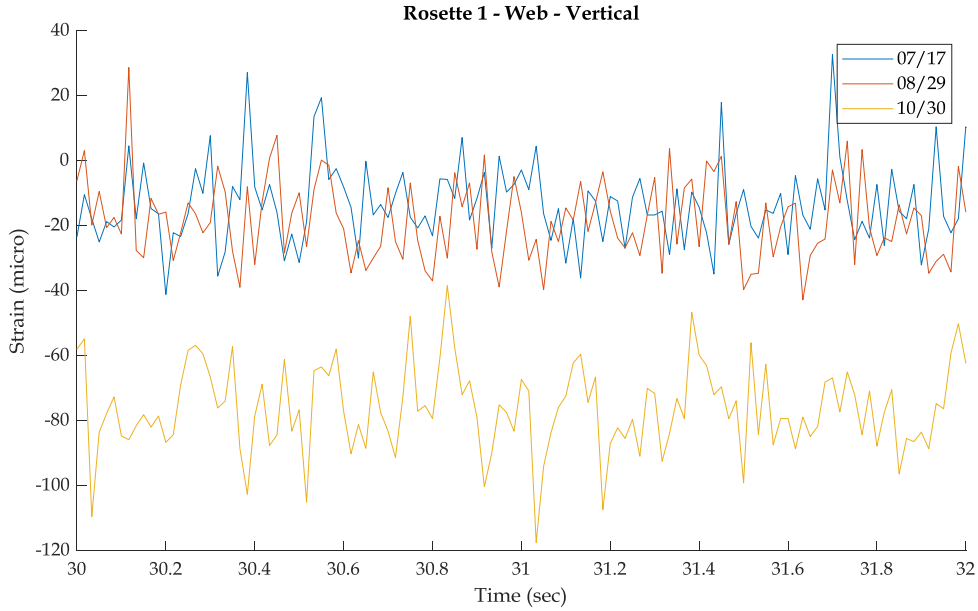


Figure 92 - NRW1 - Vertical

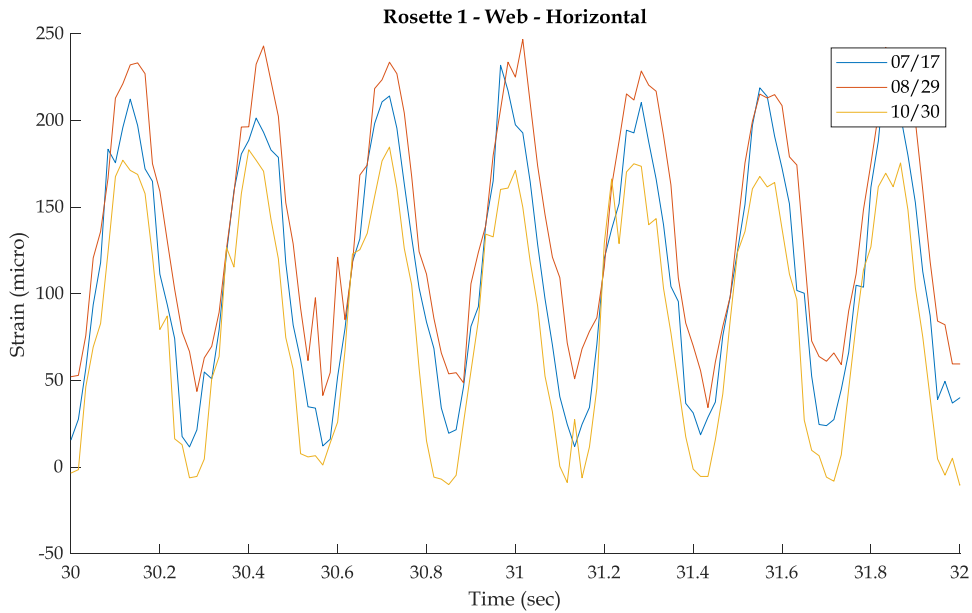


Figure 93 - NRW1 - Horizontal

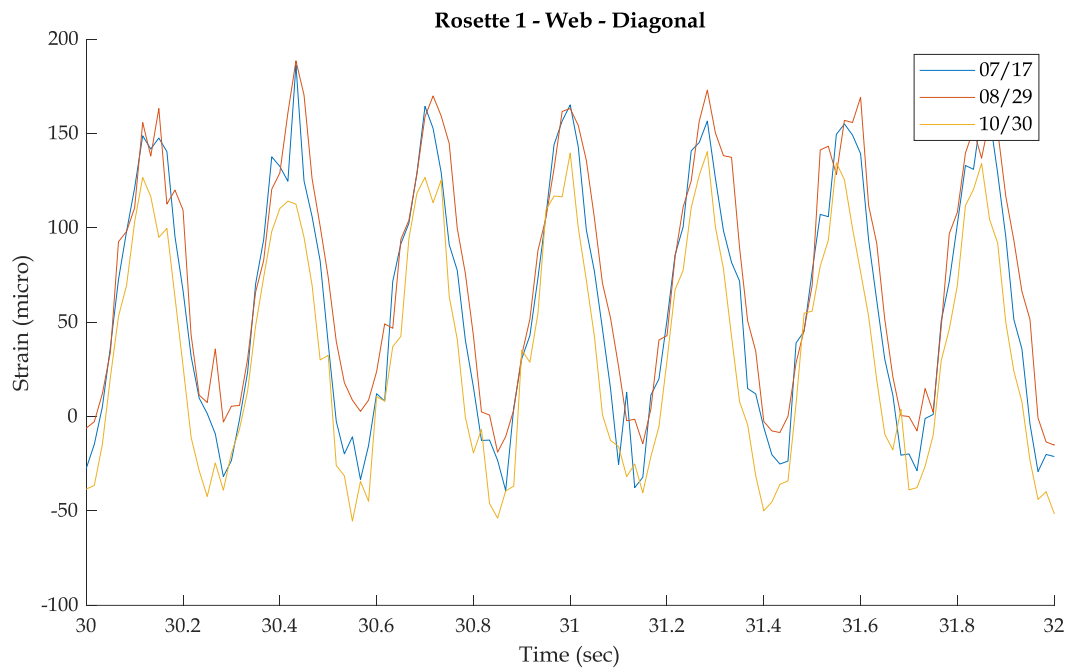


Figure 94 - NRW1 - Diagonal

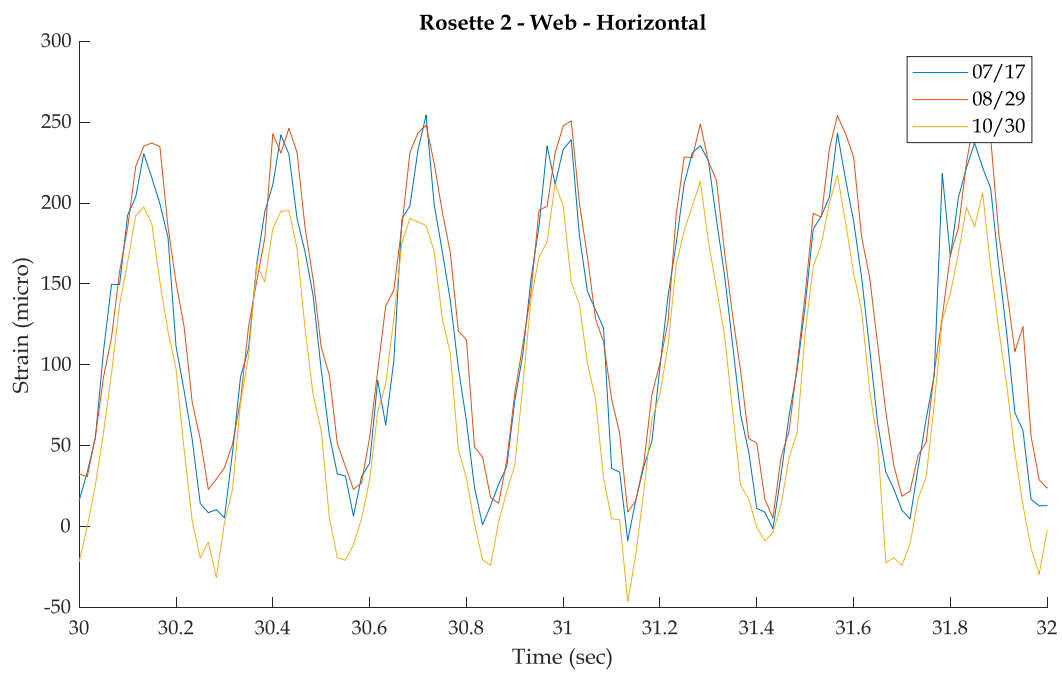


Figure 95 - NRW2 - Horizontal

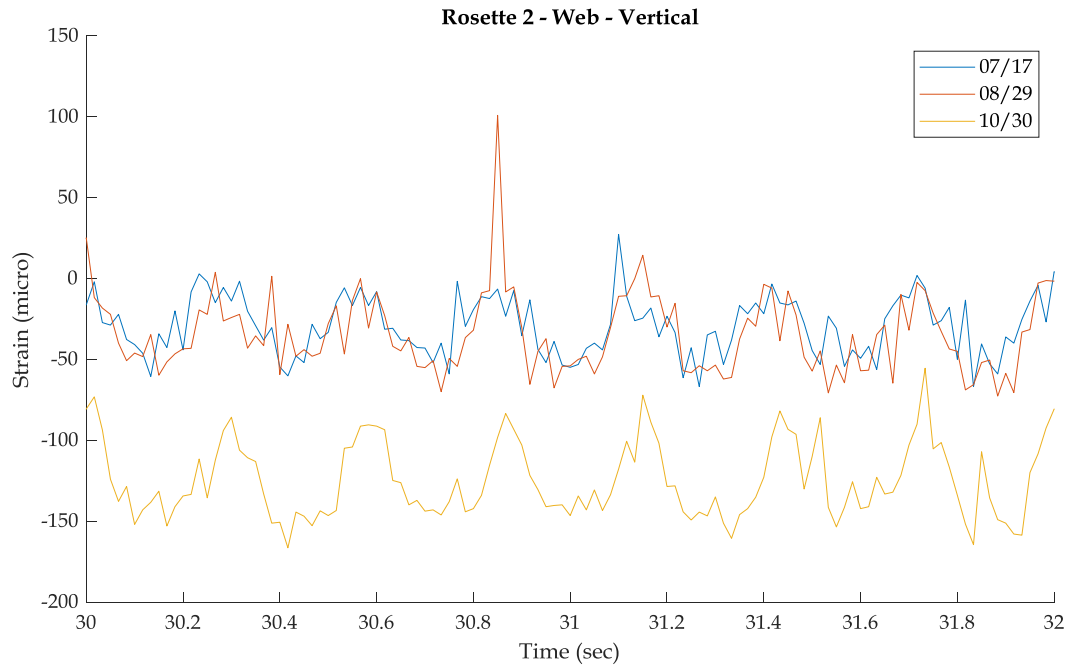


Figure 96 - NRW2 - Vertical

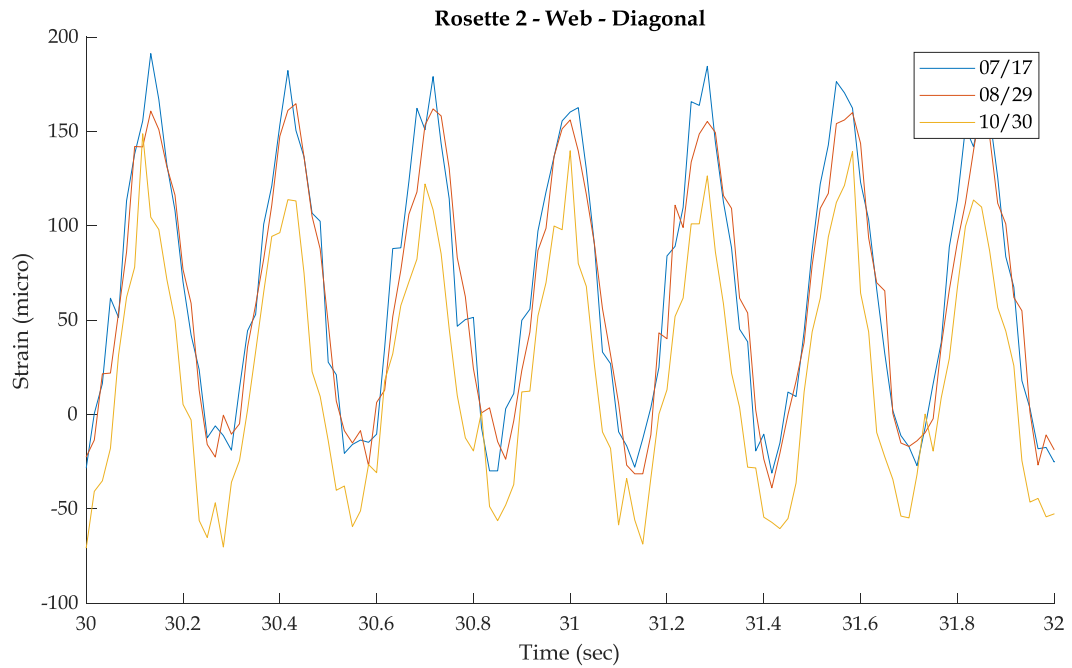


Figure 97 - NRW2 - Diagonal

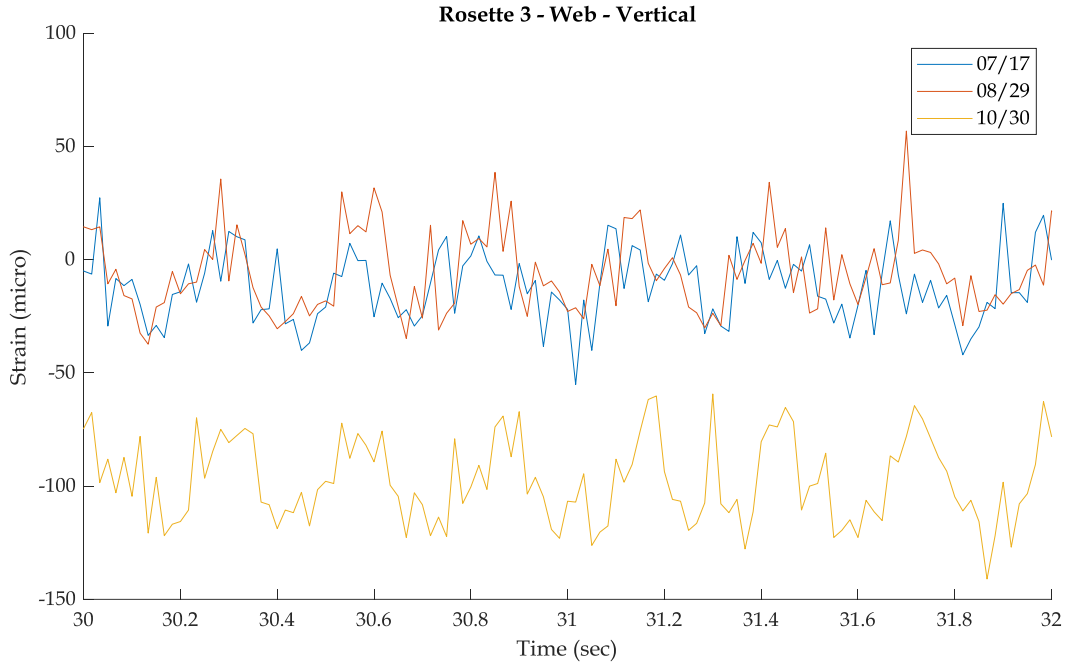


Figure 98 - NRW3 - Vertical

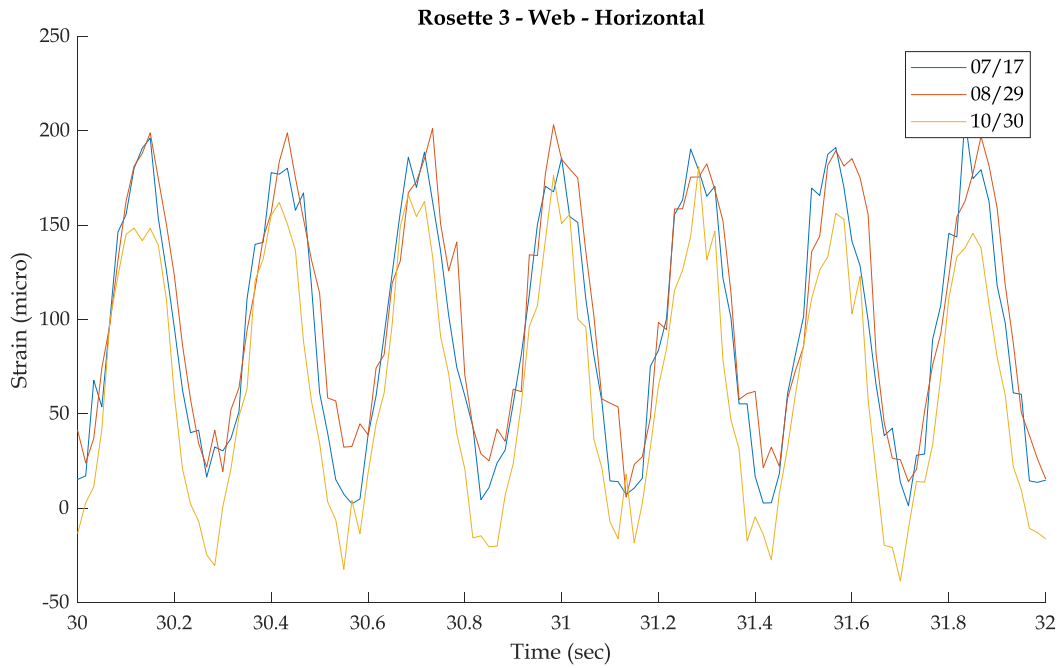


Figure 99 - NRW3 - Horizontal

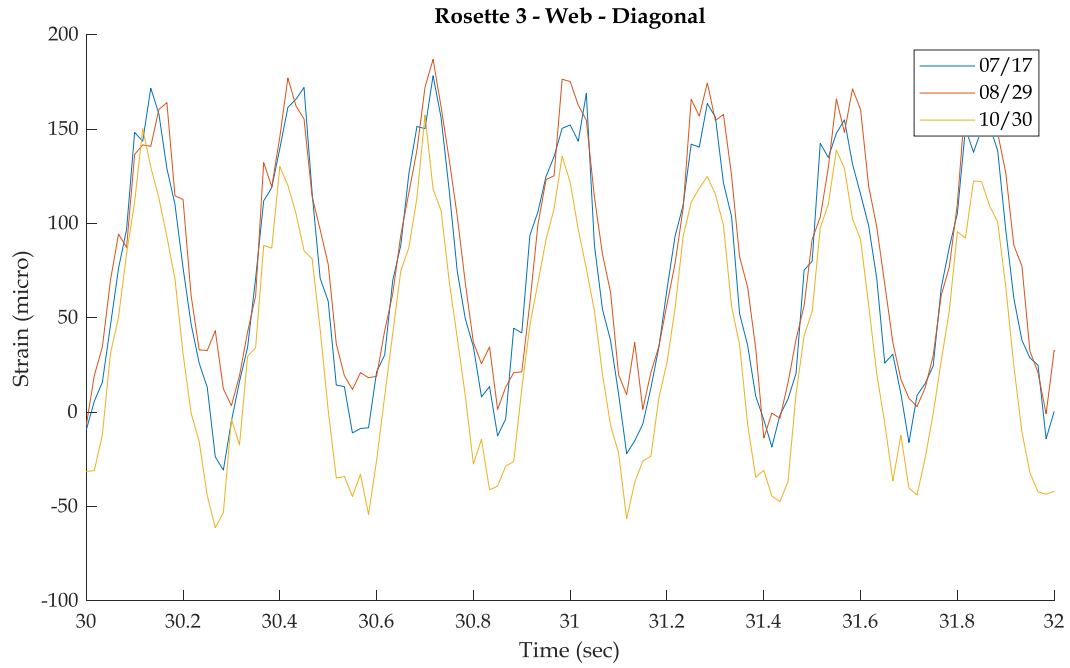


Figure 100 - NRW3 – Diagonal

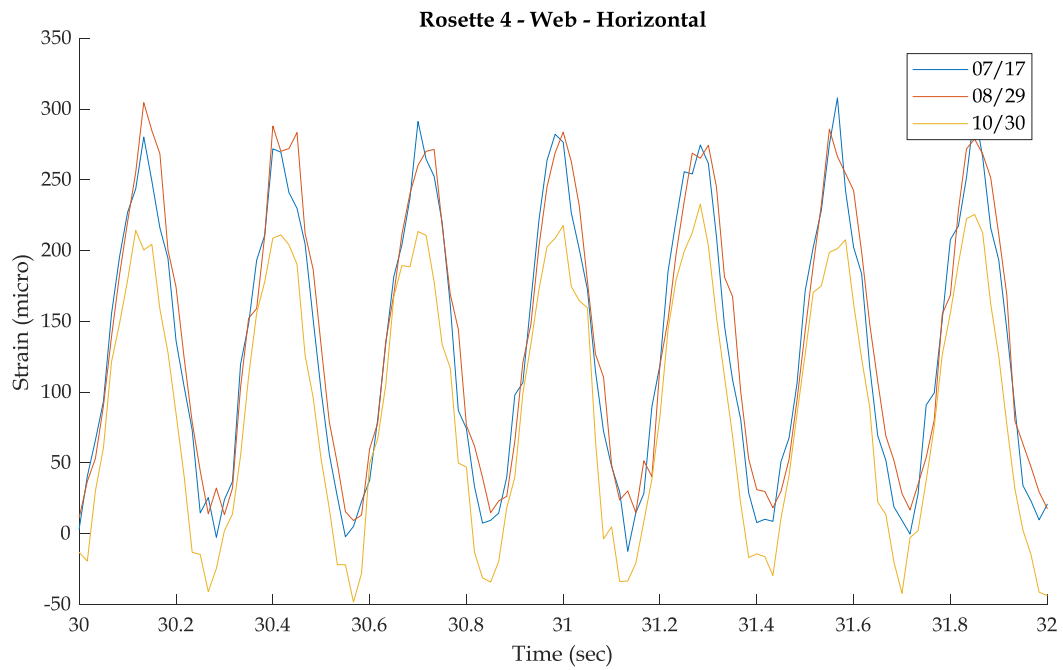


Figure 101 - NRW4 - Horizontal

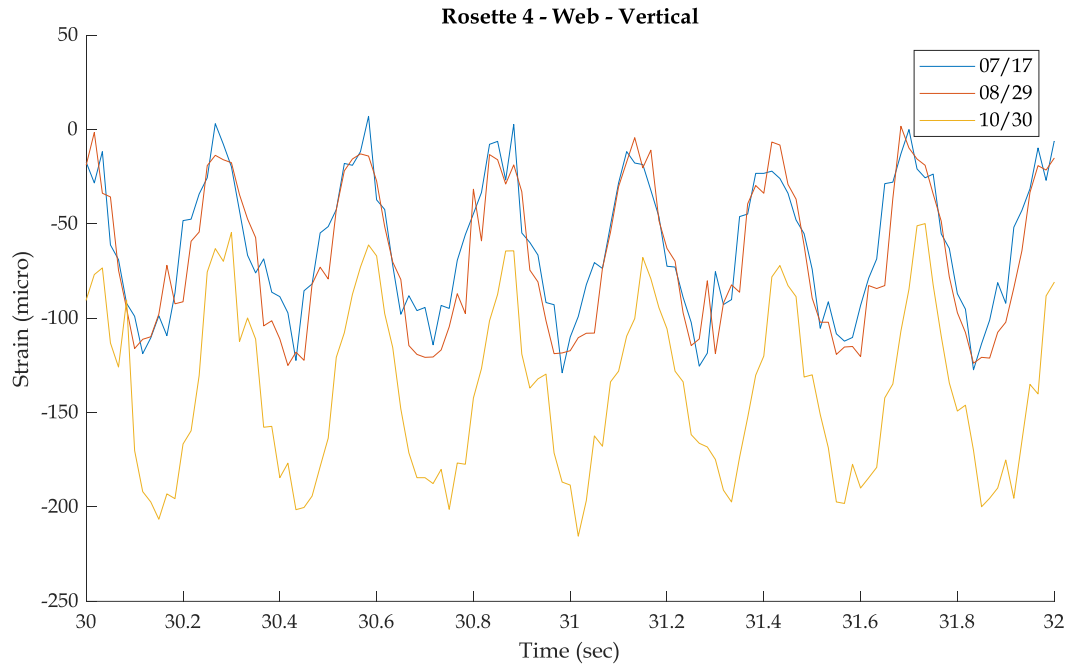


Figure 102 - NRW4 - Vertical

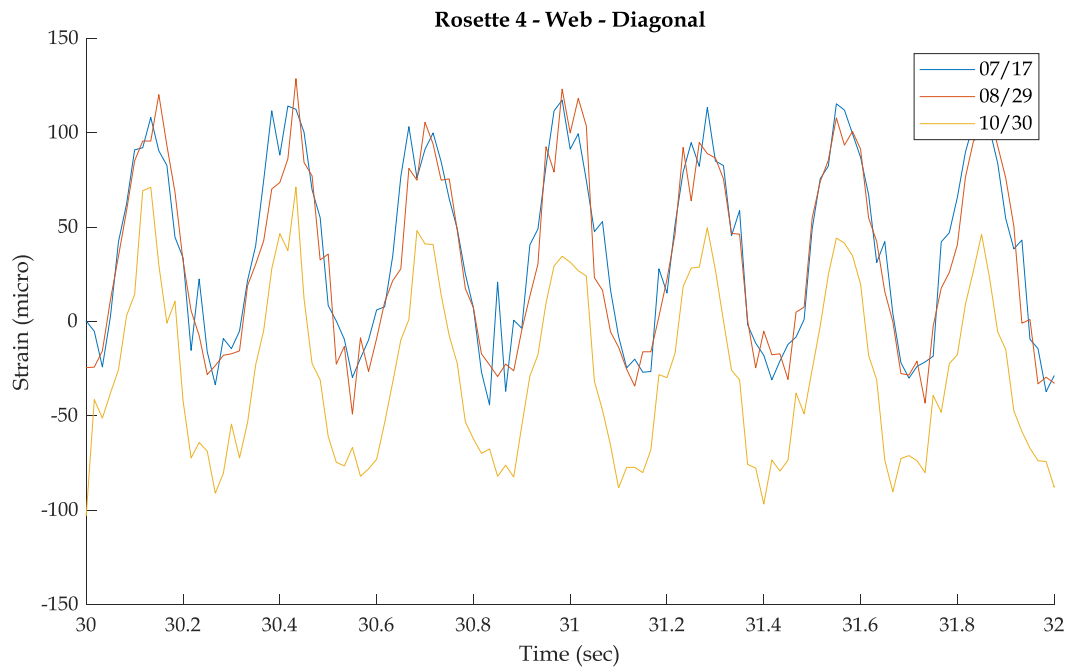


Figure 103 - NRW4 - Diagonal

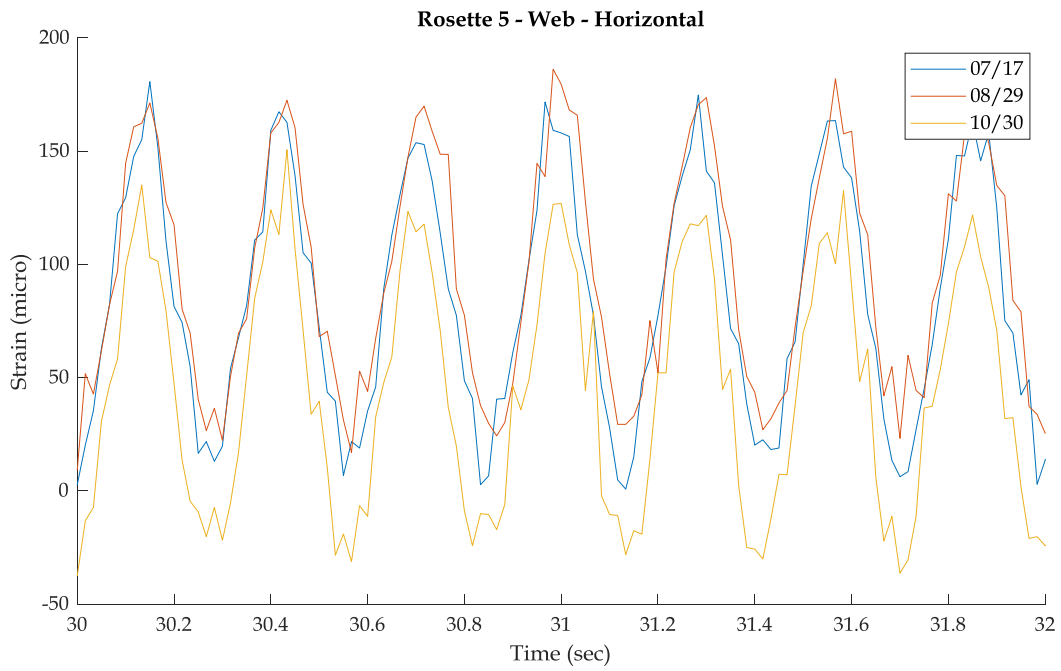


Figure 104 - NRW5 - Horizontal

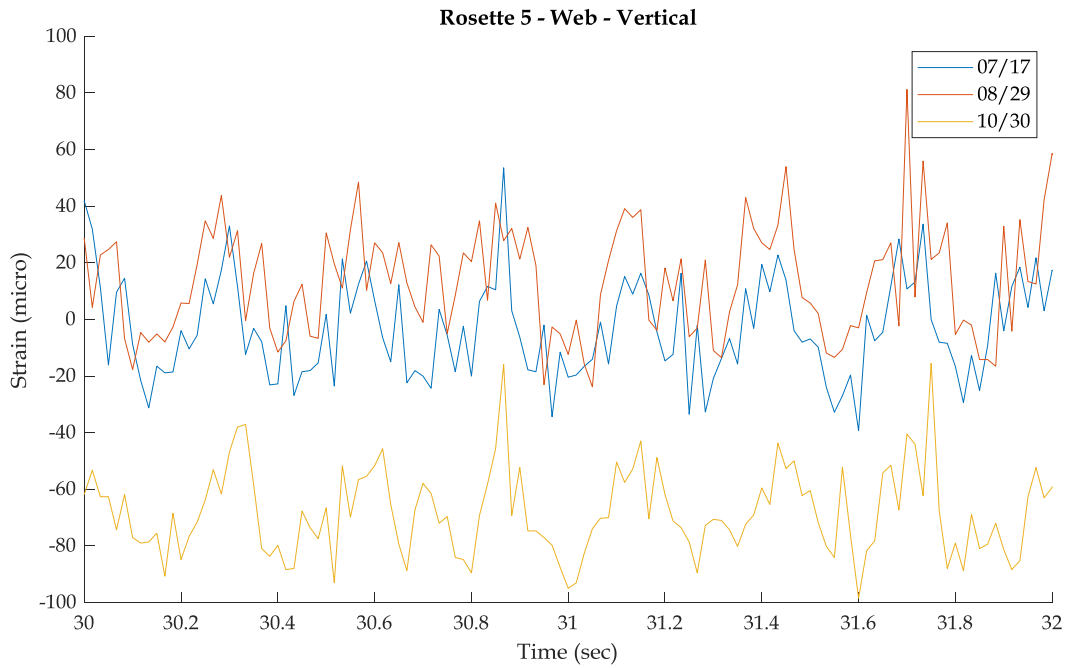


Figure 105 - NRW5 - Vertical

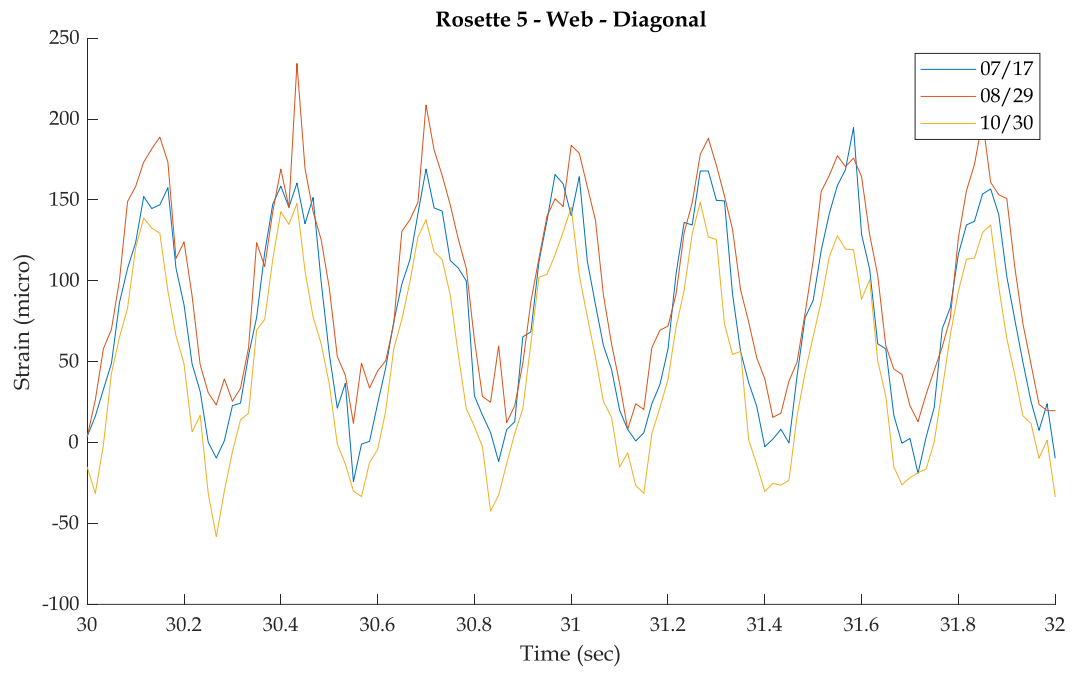


Figure 106 - NRW5 - Diagonal